Titre: Title:	Modélisation thermodynamique de systèmes contenant l'arsenic, le soufre et des métaux de transition
Auteur: Author:	Oumaima Kidari
Date:	2023
Type:	Mémoire ou thèse / Dissertation or Thesis
Référence: Citation:	Kidari, O. (2023). Modélisation thermodynamique de systèmes contenant l'arsenic, le soufre et des métaux de transition [Mémoire de maîtrise, Polytechnique Montréal]. PolyPublie. https://publications.polymtl.ca/53357/

URL de PolyPublie: PolyPublie URL:	https://publications.polymtl.ca/53357/
Directeurs de recherche: Advisors:	Patrice Chartrand
Programme: Program:	Génie des matériaux

POLYTECHNIQUE MONTRÉAL

affiliée à l'Université de Montréal

Modélisation thermodynamique de systèmes contenant l'arsenic, le soufre et des métaux de transition

OUMAIMA KIDARI

Département de génie chimique

Mémoire présenté en vue de l'obtention du diplôme de *Maîtrise ès sciences appliquées*

Génie des matériaux

Avril 2023

POLYTECHNIQUE MONTRÉAL

affiliée à l'Université de Montréal

Ce mémoire intitulé :

Modélisation thermodynamique de systèmes contenant l'arsenic, le soufre et des métaux de transition

présenté par **Oumaima KIDARI**

en vue de l'obtention du diplôme de *Maîtrise ès sciences appliquées*

a été dûment accepté par le jury d'examen constitué de :

Jean-Philippe HARVEY, président
Patrice CHARTRAND, membre et directeur de recherche
Alexandre PISCH, membre externe

DÉDICACE

À mes parents, pour l'amour et le soutien qu'ils m'ont toujours donné.

REMERCIEMENTS

Je tiens d'abord à remercier et à exprimer toute ma reconnaissance envers mon directeur de recherche, professeur Patrice Chartrand, pour m'avoir donné l'opportunité de travailler sur ce projet et qui m'a énormément guidé tout au long de la maîtrise. Ce travail n'aurait pas pu être réalisé sans son immense aide et sa disponibilité.

J'aimerais aussi remercier Christian Robelin et Paul Lafaye d'avoir toujours accepté de me rencontrer et de répondre avec grande patience à toutes mes questions. Je tiens aussi à remercier le professeur Jean-Philippe Harvey pour ses ateliers FactSage qui m'ont beaucoup appris. Je remercie également Evguenia Sokolenko pour son aide bibliographique et Aimen Gheribi pour ses nombreux encouragements. Mes sincères remerciements à tous les membres du CRCT, particulièrement à mon collègue et cher ami Minh Duc Vo pour sa disponibilité permanente et pour son énorme soutien. Nos nombreuses discussions m'ont définitivement permis de mieux avancer dans mon projet.

Enfin, je remercie ma famille pour tout le support et l'amour inconditionnels, en particulier ma sœur qui m'a aidé avec les moments les plus difficiles et solitaires de la maîtrise.

RÉSUMÉ

L'exploitation excessive des gisements de grade élevé cause progressivement leur épuisement. Cela pousse à l'extraction des minerais complexes contenant une plus forte teneur d'arsenic. La variation dans la composition des minerais cause des problèmes majeurs de contamination par l'arsenic durant leurs traitements dans les procédés de pyrométallurgie. L'utilisation de l'arsenic dans l'industrie des électroniques constitue également une source de contamination durant le recyclage des appareils contenant cet élément toxique, durant l'élimination de ces appareils par incinération ou même après leur élimination directe dans les décharges. Puisqu'il est prévu que les changements climatiques impacteront considérablement la mobilité de l'arsenic, les risques liés à son émission ne vont que s'amplifier. Quelques technologies sont employées par les industries pour diminuer leurs émissions d'arsenic, mais elles ne sont pas suffisantes pour contrôler le problème. Pour réussir à développer des technologies efficaces, il est essentiel de combler le manque dans la compréhension des interactions entre les éléments que l'on retrouve généralement associés à l'arsenic. Dans ce projet de recherche, la thermodynamique computationnelle est utilisée pour examiner le comportement de l'arsenic et de ses différentes interactions avec le soufre et quelques métaux de transition et pour développer une base de données. Les systèmes binaires et ternaires sont modélisés avec le logiciel FactSage^{TM} en utilisant la méthode CALPHAD. Le modèle Quasichimique modifié (MQM) par approximation des paires est utilisé pour modéliser les phases liquides et le *Compound Energy Formalism* (CEF) est utilisé pour modéliser les solutions solides. Les évaluations thermodynamiques et les optimisations sont effectuées pour la première fois pour les systèmes As-Cd, As-Co, Ag-As-S, As-Cd-Zn et As-Fe-S pour toutes les gammes de composition. Une réévaluation des systèmes binaires Ag-As, Ag-S, As-Fe, As-S et As-Zn est aussi réalisée, offrant des améliorations significatives par rapport aux modélisations antérieurs. Les résultats de toutes les optimisations ont permis la reproduction des propriétés thermodynamiques et des données des diagrammes de phases à l'intérieur des marges d'incertitudes expérimentales. Les résultats ont également permis la prédiction des équilibres de phases impliqués dans les systèmes étudiés. Les résultats obtenus ont aussi démontré l'intérêt d'examiner l'effet de la polymérisation de l'arsenic liquide dans le modèle. Cela impliquerait d'investiguer l'utilisation d'un modèle thermodynamique amélioré pour les phases liquides dans de prochains travaux afin de considérer les formes polymérisées de l'arsenic.

ABSTRACT

The excessive exploitation of high-grade deposits is gradually causing their depletion. This leads to the extraction of complex ores that contain high arsenic contents. This variation in composition causes major arsenic contamination problems during the processing of ores in many pyrometallurgical processes. The use of arsenic in the electronics industry also constitutes a source of contamination during the recycling of devices containing this toxic element, during the disposal of these devices by incineration or even after their direct disposal in landfills. Since it is expected that climate change will impact the mobility of arsenic, the risks associated with its emission will only increase. Some technologies are employed by the industries to reduce their arsenic emissions, but they are not sufficient to control the problem. To succeed in developing effective technologies, it is essential to fill the gap in understanding the interactions between the elements that are usually associated to arsenic. In this research project, computational thermodynamics is used to examine the behavior of arsenic and its various interactions with sulfur and some transition metals and to develop a database. Binary and ternary systems are modeled with the FactSage^{TM} software using the CALPHAD method. The Modified Quasichemical Model (MQM) by pair approximation is used to model liquid phases and the Compound Energy Formalism (CEF) is used to model the solid solutions. Thermodynamic evaluations and optimizations are performed for the first time for As-Cd, As-Co, Ag-As-S, As-Cd-Zn and As-Fe-S systems for all composition range. A reassessment of the binary systems Ag-As, Ag-S, As-Fe, As-S and As-Zn is also performed, offering significant improvements over earlier models. The results of all optimizations allowed the reproduction of thermodynamic properties and phase diagram data within experimental uncertainty limits. The results also allowed the prediction of the phase equilibria involved in the systems studied. The results obtained also demonstrated the interest of examining the effect of arsenic polymerization in the model. This would involve investigating the use of an improved thermodynamic model for the liquid phases in future work to consider polymerized forms of arsenic.

TABLE DES MATIÈRES

LISTE DES TABLEAUX

LISTE DES FIGURES

LISTE DES SIGLES ET ABRÉVIATIONS

a_i	Activité de la composante i
at. %	Pourcentage atomique
Bcc	Corps cubique centré
CALPHAD	*CALculation of PHAse Diagrams*
CEF	*Compound Energy Formalism*
C_p	Capacité calorifique molaire
DDC	Calorimétrie différentielle dynamique
DFT	Théorie de la fonctionnelle de la densité
DSC	Calorimétrie différentielle à balayage
DTA	Analyse thermique différentielle
Emf	Force électromotrice
Fcc	Cubique à faces centrées
FNN	*First-nearest-neighbor pairs*
G	Énergie de Gibbs totale
Δg_{AB}	Variation de l'énergie de Gibbs non configurationnel
$\Delta H^{\circ}_{formation}$	Enthalpie de formation standard
Hcp	Hexagonal compact
LRO	Ordre de longue distance
MQM	*Modified Quasichemical model*
n^{φ}	Nombre de moles de la phase φ
P^{sat}	Pression de saturation
PXRD	Diffraction de poudre utilisant les rayons X
$S^{\circ}_{formation}$	Entropie standard

ΔS^{config}	Variation de l'entropie configurationnelle de mélange
SRO	Ordre de courte distance
TA	Analyse thermique
T_c	Température de Curie
T_g	Température de transition vitreuse
X	Fraction molaire
x_i^{φ}	Composition d'un élément i dans la phase φ
XANES	Spectroscopie de structure près du front d'absorption de rayons X
XRD	Diffractométrie de rayons X
XRF	Spectrométrie de fluorescence de rayons X
Y	Fraction de coordination équivalente
Z	Nombre de coordination
β	Moment magnétique moyen par mole d'atomes
τ	Rapport de la température et de la température critique d'ordre magnétique
φ	Phase constituant un système

CHAPITRE 1 INTRODUCTION

L'exploitation minière est l'un des secteurs économiques majeurs au Canada. Après le ralentissement économique imposé par la pandémie de la COVID-19, les prix des métaux produits à partir de minerais ont bondi en 2021 en raison d'une très forte demande globale. Cette demande a propulsé les dépenses de l'exploration minière canadienne qui ont atteint un record de 55,5 billions de dollars canadiens [1-4]. Les projections montrent la continuité de cette tendance due aux développements anticipés dans des domaines variés. Cette tendance est également observée à l'échelle mondiale où l'exploitation des minerais est la source d'approvisionnement majeure pour produire une large gamme de métaux [5]. La forte exploitation cause un épuisement progressif des gisements traditionnels de grade élevé et pousse à l'extraction de minerais plus complexes contenant une plus forte teneur d'arsenic [6]. La variation dans la composition des minerais qui constituent la matière première des procédés métallurgiques lance des défis importants.

Les roches ignées ultrabasiques ont généralement une très faible teneur d'arsenic. L'arsenic se trouve à des concentrations plus élevées dans les roches sédimentaires contenant des minéraux sulfurés et des sulfosels [7-11]. L'arsenic a aussi une préférence pour les métaux lourds, comme le cuivre et le plomb, et peut être également associé à l'or, à l'argent, au fer, au zinc, au nickel, au cobalt et au manganèse [7, 9]. Parmi les minéraux d'arsenic les plus communs, il y a le réalgar (As_4S_4), l'orpiment (As_2S_3), le loellingite ($FeAs_2$), le cobaltite ($CoAsS$) et l'arsénopyrite ($FeAsS$). La tennantite ($Cu_{12}As_4S_{13}$) et la proustite (Ag_3AsS_3) sont aussi des sulfosels parmi les plus surgissants [9, 10].

Le traitement des minerais sulfurés est une source anthropogénique majeure de contamination par l'arsenic. Après l'extraction, la séparation des minéraux d'intérêt de la gangue durant l'étape de concentration expose les minerais à l'atmosphère. Également, le grillage et la fusion des concentrés dans les fonderies produisent des poussières et de grands volumes de gaz toxiques. Cela provoque la dispersion atmosphérique de l'arsenic et la contamination de l'environnement [11-15]. Un des cas les plus alarmants de contamination par l'arsenic au Canada a eu lieu dans la mine d'or *Giant mine* située à Yellowknife. Le traitement des minerais d'or associés au minéral arsénopyrite émettait du trioxyde d'arsenic, un sous-produit du procédé de raffinage hautement toxique. L'entreprise a partiellement réduit ses émissions grâce à l'installation de filtres en 1959, qui ont permis la collection et le stockage sous terre des poussières du trioxyde d'arsenic. Au cours des

cinquante années qui suivent l'installation des filtres, 237 000 tonnes de trioxyde d'arsenic ont été stockées. Cependant, cela n'a pas été suffisant et la poussière provenant de l'usine a continué de se disperser et de contaminer l'environnement, générant des impacts néfastes majeurs. Les opérations ont arrêté en 2004 et le site est devenu abandonné [16, 17]. Aujourd'hui, le gouvernement continue d'investir pour le projet d'assainissement de la mine et les négociations se poursuivent sur l'indemnisation et la réconciliation avec la Première Nation [18].

L'arrêt des activités de *Giant mine* était nécessaire étant donné la nature très toxique de l'arsenic et sa grande mobilité dans les zones contaminées. Les émissions d'arsenic imposent des effets nocifs graves sur divers organismes, et elles sont particulièrement dangereuses pour les populations humaines à proximité des sites d'exploitation et de traitement des minerais [12, 19]. En effet, l'arsenic est classifié comme un cancérigène humain et l'exposition chronique à de hautes concentrations affecte gravement les systèmes cardiovasculaire, neurologique, respiratoire, rénal et reproducteur humain [11, 20, 21]. À cause de ces effets préoccupants, les gouvernements à travers le monde ont établi des limites d'émission d'arsenic pour contrôler le risque de contamination.

Selon le type de procédé et le minerai utilisé, les fonderies emploient des technologies variées pour contrôler leurs émissions. Ces technologies impliquent des opérations très coûteuses et nécessitent souvent le stockage d'arsenic [22]. Mais malgré tous les efforts, les méthodes adoptées pour contrôler les émissions ne sont pas toujours suffisantes pour rencontrer les limites établies. La fonderie Horne à Rouyn-Noranda au Québec atteint une moyenne annuelle de 100 $\mu g/cm^3$, soit 33 fois plus que la limite d'arsenic autorisée fixée par le ministère de l'Environnement du Québec [23-25]. Il est estimé que les changements climatiques impacteront considérablement la mobilité de l'arsenic, amplifiant ainsi les risques liés à son exposition. Il est donc primordial d'adopter des solutions technologiques assurées pour continuer à traiter des concentrés complexes d'arsenic sans risque d'arrêt des opérations [21].

Outre le traitement des minerais sulfurés, une autre source potentielle de contamination est l'utilisation de l'arsenic dans l'industrie des électroniques. En effet, lors de la fabrication d'appareils tels que les micropuces, les circuits imprimés et les batteries, l'ajout d'une quantité contrôlée d'arsenic comme dopant additif à certains composants améliore les propriétés électroniques [26-28]. De plus, l'innovation technologique cause une utilisation plus fréquente de

semiconducteurs à base de cette impureté, comme les semiconducteurs Cd_3As_2 et Zn_3As_2 du groupe II-V qui offrent des propriétés électroniques, optiques et structurelles très intéressantes [29]. Des matériaux à base de composés d'arsenic se retrouvent ainsi dans les appareils électroniques avec d'autres métaux, typiquement l'aluminium, le cuivre, l'argent, le fer et le cobalt [28]. Lors des procédés de recyclage de ces appareils, l'arsenic cause des problèmes majeurs en formant l'arsine (AsH_3) qui est un gaz très toxique [27, 30, 31]. Pour certains appareils, les technologies de recyclage sont encore sous-développées et en conséquence, ils sont éliminés par incinération, ce qui entraine des rejets d'arsenic et d'autres déchets dangereux comme le cadmium et le zinc [32, 33]. L'élimination directe dans les décharges sans incinération n'évite pas le problème puisque l'arsenic est dissipatif et finit par se libérer vers l'environnement [34, 35].

Pour réussir à contrôler les émissions d'arsenic, une compréhension exhaustive des phénomènes cinétiques et thermodynamiques ayant lieu durant le procédé est nécessaire. L'approche traditionnelle pour effectuer une étude thermodynamique consiste à réaliser des mesures expérimentales pour analyser tous les équilibres de phases qui peuvent intervenir durant le procédé de production. Cependant, considérant les compositions très complexes des minerais à teneur élevée d'arsenic, cette approche serait longue, coûteuse et très difficile. Une alternative plus intéressante serait l'utilisation de la thermodynamique computationnelle afin de prédire le comportement d'arsenic et ses différentes interactions. À l'aide de l'optimisation des paramètres de modèles théoriques basés sur des données expérimentales antérieures, l'état d'équilibre peut être décrit en fonction de la composition, de la température et de la pression. Il est ainsi possible de simuler le procédé afin de développer des solutions dans un temps réduit, avec un coût plus faible, sans utilisation de ressource ou génération de produits toxiques [36]. L'approche détaillée utilisée dans le cadre de ce travail est présentée dans le chapitre 2.

Quelques travaux se sont intéressés à la modélisation thermodynamique de systèmes contenant l'arsenic, comme l'évaluation du système As-Cu-Ni par Uhland et al. [37]. Cependant, le nombre de systèmes optimisés n'est toujours pas suffisant pour réaliser une modélisation multiéchelle impliquant tous les éléments importants pour la problématique d'émission d'arsenic. L'objectif de ce travail consiste à adresser ce manque en modélisant des systèmes binaires et ternaires importants contenant l'arsenic et à intégrer ces systèmes dans une base de données. Cela constituera le fondement pour les travaux ultérieurs qui poursuivront le développement de la base de données [36, 38]. L'utilisation de la base de données contribuera également aux travaux à venir qui

s'intéresseront à la simulation de procédés pour trouver une solution pour la problématique d'émission d'arsenic. Les systèmes contenant l'arsenic sélectionnés pour ce projet de recherche ont une grande importance, surtout dans le domaine de la pyrométallurgie des minerais sulfurés de cuivre, de nickel, de cobalt, de plomb et de zinc. Des études expérimentales sont également disponibles dans la littérature pour les systèmes choisis et permettront donc la modélisation. Les paramètres des systèmes optimisés seront ajoutés aux bases de données FScopp et FSlead de FactSage^{TM} qui contiennent déjà des optimisations de plusieurs systèmes d'intérêt pour l'industrie, tels que Cu-S, Fe-S, Ni-S, Pb-S, Zn-S. Dans le cadre de ce travail, les systèmes binaires As-Cd et As-Zn et le système ternaire As-Cd-Zn ont été optimisés et ont fait l'objet d'un article soumis pour publication dans *Metallurgical and Materials Transactions B*. Cet article est présenté dans le chapitre 3. Les systèmes binaires Ag-As, Ag-S, As-S et le système ternaire Ag-As-S ont également été optimisés et ont fait l'objet d'un article soumis pour publication dans *Journal of Phase Equilibria and Diffusion*. Cet article est présenté dans le chapitre 4. Finalement, les systèmes binaires As-Co et As-Fe et le système ternaire As-Fe-S ont été optimisés et ont fait l'objet d'un article soumis pour publication dans *CALPHAD*. Cet article est présenté dans le chapitre 5.

CHAPITRE 2 REVUE DE LA LITTÉRATURE

Le présent chapitre comprend tout d'abord une revue de la méthode CALPHAD utilisée dans le cadre de ce projet de recherche ainsi que les techniques expérimentales principales utilisées pour mesurer les diagrammes de phases et les données thermodynamiques. La méthode DFT qui permet le calcul de certaines propriétés des solides est aussi présentée. Ce chapitre introduit également le modèle Quasichimique Modifié par l'approximation des pairs utilisé dans ce travail pour décrire le comportement des phases liquides binaires ainsi que les techniques d'extrapolations pour les systèmes ternaires. Finalement, la dernière partie de ce chapitre présente le formalisme mathématique généralement utilisé pour décrire les modèles de solutions solides impliquant des sous-réseaux ainsi que les termes à ajouter à l'énergie de Gibbs dans le cas d'un système magnétique. La revue de la littérature des données expérimentales spécifique à chaque système étudié est incluse dans les articles scientifiques présentés dans les chapitres qui suivent ; les systèmes binaires As-Cd et As-Zn et le système ternaire As-Cd-Zn dans le chapitre 3, Les systèmes binaires Ag-As, Ag-S, As-S et le système ternaire Ag-As-S dans le chapitre 4 et les systèmes binaires As-Co et As-Fe et le système ternaire As-Fe-S dans le chapitre 5

2.1 Méthode CALPHAD

CALPHAD, un acronyme de *CALculation of PHAse Diagrams*, est une méthode computationnelle employée pour le calcul de diagrammes de phase basée sur la thermodynamique [39]. La première description générale de cette méthode a été introduite en 1970 par Kaufman et Berntein dans le livre intitulé *Computer Calculation of Phase Diagrams* [40]. La méthode a été raffinée au cours des années qui suivent grâce au progrès de l'informatique et aux nombreuses contributions scientifiques. Le développement d'une approche CALPHAD standard s'est imposé aujourd'hui [36, 41]. Après l'identification du système binaire à évaluer, la première étape de la méthode CALPHAD consiste à effectuer une revue de littérature complète pour recueillir toutes les données thermodynamiques du système. Ces données peuvent provenir de mesures expérimentales, généralement un diagramme de phase, des mesures de tensions de vapeur, d'activité, d'enthalpie de formation standard, etc. Dans le cas d'absence de mesures primaires, les données peuvent provenir des calculs atomistiques basés sur la théorie fonctionnelle de la densité (DFT) ou des estimations basées sur des analogies avec des systèmes chimiquement similaires. Les données recueillies sont ensuite évaluées de manière critique selon la méthode d'acquisition afin d'identifier

les données les plus fiables. Une fois la revue de littérature est complétée et les données évaluées, l'étape suivante est la sélection de modèles thermodynamiques convenables. Les modèles permettent d'obtenir un ensemble de fonctions d'énergies de Gibbs dérivant chaque phase φ du système à l'aide de paramètres optimisables. La méthode CALPHAD calcule l'état d'équilibre chimique du système en minimisant l'énergie de Gibbs totale. Cette énergie correspond la somme de l'énergie de Gibbs molaire G_m^{φ} de chaque phase définie par l'équation suivante :

$$\mathrm{G^{totale}} = \sum_{\varphi} \mathrm{n^{\varphi} G_m^{\varphi}}, \qquad \text{avec } \mathrm{n^{\varphi}} \geq 0 \tag{2.1}$$

où $\mathrm{n^{\varphi}}$ correspond au nombre de moles de la phase φ. La méthode CALPHAD consiste à utiliser un algorithme pour calculer cet état d'énergie minimum pour des valeurs constantes de température, de pression et de composition x d'un élément i dans la phase φ :

$$\min\left(\mathrm{G^{totale}}\right) = \min\left(\sum_{\varphi} \mathrm{n^{\varphi} G_m^{\varphi}}\left(\mathrm{T, P, x_i^{\varphi}}\right)\right) \tag{2.2}$$

L'approche doit être exécutée plusieurs fois de manière itérative pour ajuster les paramètres jusqu'à trouver ceux qui permettent de reproduire adéquatement toutes les données expérimentales disponibles pour le système binaire à l'étude [36, 41-43]. En se basant sur l'optimisation des systèmes binaires et avec une technique d'interpolation appropriée, les systèmes ternaires sont évalués. Des paramètres ternaires peuvent aussi être ajoutés afin d'assurer une meilleure reproduction des données expérimentales ternaires. La méthode CALPHAD permet aussi de prédire les équilibres thermodynamiques des phases binaires et ternaires existantes dans des systèmes multicomposants [44].

À partir de la combinaison des différentes évaluations thermodynamiques, des bases de données informatiques multicomposantes sont construites et permettent le stockage et la mise à jour continus des paramètres thermodynamiques optimisés. Plusieurs logiciels thermodynamiques commerciaux avec leurs bases de données thermodynamiques ont été développés depuis les années 1970. FactSage™ est l'un des logiciels de type CALPHAD les plus puissants et établis [45-47]. Il est équipé de l'algorithme de minimisation d'énergie de Gibbs SOLGAS + SOLGASMIX développé par Erikson [48, 49] intégré dans les modules EQUILIB, PHASE DIAGRAM et ChemApp de FactSage™. Le logiciel permet donc d'effectuer des optimisations, et avec sa base

de données associée, il peut exécuter une variété de calculs thermochimiques et des simulations de procédés [50]. Toutes les optimisations et tous les calculs dans ce travail ont été effectués avec le logiciel FactSage^{TM}.

2.2 Méthodes expérimentales

Les mesures des données du diagramme de phase et des propriétés thermodynamiques constituent le fondement de la modélisation avec la méthode CALPHAD. Des résultats expérimentaux fiables assurent la précision de l'optimisation et donc une description juste du système à l'étude. Pour évaluer la validité des données recueillies, il est essentiel de connaitre les techniques expérimentales utilisées pour discerner les limites de chacune. Cette section présente une brève description des méthodes expérimentales fréquemment utilisées.

2.2.1 Mesures des propriétés thermodynamiques

Méthodes calorimétriques : Le principe consiste à mesurer l'échange de chaleur entre l'échantillon étudié et l'environnement. Il existe une très grande variété de calorimètres, classifiés selon le mode de génération ou de consommation de chaleur, les conditions d'opération (isotherme, adiabatique, isopéribole) et le type de fonctionnement (statique ou dynamique). Les calorimètres adiabatiques, à balayage différentiel (DSC) et à flux de chaleur sont généralement utilisés pour effectuer des mesures directes des capacités calorifiques et des enthalpies de transformation. Les calorimètres isothermes et de chute sont employés pour mesurer le contenu de chaleur, à partir desquels les capacités calorifiques peuvent aussi être dérivées. Des calorimètres de mélanges qui mesurent le l'échange de chaleur lié à l'interaction entre deux ou plusieurs substances sont adaptés pour déterminer l'enthalpie de mélange. À partir de la réaction des éléments purs, les calorimètres à réaction directe sont employés pour déterminer l'enthalpie de formation d'un composé. Les calorimètres de la bombe à combustion sont aussi utilisés pour déterminer cette propriété thermodynamique à partir de mesure de la chaleur produite par une réaction de combustion en présence d'oxygène ou de fluor. Il est nécessaire d'assurer la complétion des réactions ainsi que le transfert efficace de la chaleur afin d'obtenir des résultats adéquats [36, 39, 41, 51].

Techniques d'équilibre en phases gazeuses : Des mesures de données de pression de vapeur peuvent s'effectuer par la méthode du point de rosée, la méthode isopiestique ou une méthode directe comme l'utilisation d'un monomètre. Les méthodes d'effusion de *Knudsen* et d'évaporation libre de *Langmuir* sont aussi des méthodes très souvent utilisées pour mesurer le taux de

vaporisation pour déterminer la pression de vapeur. Les mesures obtenues par les méthodes d'équilibre en phases gazeuses peuvent aussi être utilisées pour dériver des données d'activité en considérant la relation suivante :

$$a_i \approx \frac{P_i}{P_i^\circ} \tag{2.3}$$

Lors de l'emploi d'une de ces techniques, il faut connaitre la composition du gaz, vérifier la pureté de l'échantillon, et assurer l'uniformité de la température durant l'expérience [41, 52].

Méthode de la force électromotrice (EMF) : Le principe est de mesurer la force électromotrice générée par les cellules électrochimiques, ce qui permet la détermination des données d'activités. À partir des mesures, les propriétés molaires partielles peuvent également être calculées [41].

2.2.2 Mesures des données de diagrammes de phases

Les méthodes employées pour mesurer les données de diagramme de phase peuvent être divisées en deux catégories : les méthodes non isothermes qui sont de nature hors d'équilibre et les méthodes isothermes qui sont plus proches de l'état d'équilibre, car l'échantillon est laissé pour de longues périodes.

Méthodes non isothermes : Le principe de l'analyse thermique (TA) consiste à chauffer ou à refroidir un échantillon pour mesurer le changement dans certaines propriétés suite à une transformation de phase imposée par la variation de température [53]. Des techniques plus avancées sont aussi souvent utilisées telle que l'analyse thermique différentielle (DTA), qui permet d'analyser la différence entre la température d'un échantillon et la température d'une référence lorsqu'ils sont soumis à la variation de température. La calorimétrie à balayage différentiel (DSC) peut aussi être utilisée pour mesurer les données de diagramme de phases en analysant la différence entre le débit de chaleur vers un échantillon et vers une référence lorsqu'ils sont soumis à la variation de température. La méthode de la force électromotrice (EMF) permet également de déterminer les limites de phases en enregistrant les ruptures dans certaines propriétés. La méthode dilatométrique est aussi souvent employée et se base sur la contraction ou l'expansion durant une transformation de phase. Dans les systèmes magnétiques, les mesures de susceptibilité magnétique sont utilisées pour déterminer les limites de phase en mesurant les changements dans les propriétés magnétiques durant une transition de phase [41].

Méthodes isothermes : La métallographie est une technique basée sur la caractérisation de la microstructure d'alliage à une température fixe pour déterminer s'il s'agit d'un échantillon monophasique ou biphasique. La diffraction aux rayons X (XRD) est une technique qui permet la détermination des limites de phase à l'aide de la mesure des paramètres de réseau [36, 41].

2.3 Calculs de premiers principes et la théorie de la fonctionnelle de la densité (DFT)

La méthode CALPHAD se base principalement sur la disponibilité des données expérimentales dans la littérature. Dans le cas où les mesures ne sont pas disponibles pour un ou plusieurs composés d'un système, des calculs peuvent être effectués pour combler ce manque. Les calculs de premiers principes (du latin *ab initio*) permettent la prédiction de quelques propriétés des solides en se basent directement sur des lois de la physique quantique, avec très peu ou pas d'apport expérimental [36, 54, 55]. Le développement de la méthode des calculs par DFT durant les années 1960 a marqué le début de l'utilisation des prédictions des propriétés des matériaux cristallins dans plusieurs applications [55, 56]. La théorie des calculs par DFT est basée sur le travail de Kohn et Sham [57] et grâce à cette contribution, Kohn a été corécipiendaire avec Pople du prix Nobel de la chimie en 1998 [36, 54]. Les calculs par DFT consistent à résoudre des équations décrivant le comportement quantique au niveau atomique et moléculaire [56]. Les calculs DFT sont souvent utilisés dans les modélisations thermodynamiques pour prédire l'enthalpie de formation à 0 K et la chaleur spécifique [58]. Dans le cadre de ce travail, deux sources publiques ont été consultés, The Open Quantum Materials Database (OQMD) [59] et The Materials Project [60], afin de calculer les enthalpies de formation à 0 K de quelques composés intermédiaires dans les systèmes étudiés.

2.4 Modélisation des solutions liquides

Une solution idéale est définie comme un mélange énergétiquement favorable à toutes les températures sans énergie additive. Cela signifie qui l'énergie de liaison atomique entre les atomes qui constituent le mélange est identique à l'énergie de liaison des atomes de même nature [61]. Un modèle idéal décrit donc le comportement d'une solution liquide dont les composés qui n'interagissent pas entre eux et qui sont distribués aléatoirement [36]. Pour un système idéal, l'énergie de Gibbs d'un mélange A-B est définie par l'équation suivant :

$$\Delta G_m^{idéal} = \Delta H^{idéal} - T\Delta S^{idéal} = RT(x_A \ln x_A + x_B \ln x_B) \qquad (2.4)$$

Dans le cas d'un système réel, le comportement est plus complexe puisque les nouvelles liaisons atomiques formées à la suite du mélange ont des énergies additives par rapport à l'énergie de liaison des atomes de même nature de chaque constituant [61]. Dans un tel système, ce sont les propriétés en excès qui définissent la différence entre les propriétés du mélange réel et ceux d'un mélange idéal. Ainsi, l'énergie de Gibbs en excès est définie comme étant :

$$G^{excès} = \Delta G_m - \Delta G_m^{idéal} \tag{2.5}$$

En utilisant la méthode CALPHAD, le choix d'un bon modèle thermodynamique pour décrire l'énergie de Gibbs en excès du système est très important [39]. Dans le livre *Phase Diagrams and Thermodynamic Modeling of Solutions*, *Part II,* Pelton [62] décrit de façon détaillée les modèles actuellement utilisés pour représenter les propriétés thermodynamiques d'une solution en fonction de la température, de la pression et de la composition.

Kaufman et Berntein [40] ont utilisés des modèles de type solution régulière où les constituants du liquide sont supposés être distribués de manière aléatoire sur les sous-réseaux et l'énergie de Gibbs en excès est exprimée par un polynôme [36]. Ce type de modèle simple ne permet pas une description satisfaisante des comportements complexes comme le permet l'ordonnancement à courte distance [43]. En effet, les modèles de type solution régulière nécessitent un grand nombre de paramètres d'interaction pour essayer de représenter de manière adéquate les propriétés thermodynamiques de la solution lorsqu'il y a un ordre à courte distance. Pour décrire de manière plus satisfaisante les systèmes non aléatoires ayant un fort ordonnancement, l'introduction d'autres modèles a été requise.

Fowler and Guggenheim [63] ont proposé la théorie Quasichimique qui suppose des interactions entre des paires d'atomes ou de molécules de premiers voisins proches. Ainsi, dans le processus de formation d'un mélange binaire A-B, z paires AA et z paires BB sont détruites pour créer 2z paires AB. En se basant sur cette théorie, quelques modèles ont été proposés [64]. Un des plus importants est le modèle Quasichimique Modifié (MQM) par approximation des pairs développé par Pelton et al. [65, 66] dont le terme d'entropie configurationnelle du modèle tient en compte de l'ordonnancement à courte distance. Ce modèle a été utilisé dans plusieurs travaux qui ont démontré une description des solutions liquides plus fiable que ceux avec des modèles considérant un mélange aléatoire [67].

Pour un système binaire A-B liquide, les pairs de premiers voisins proches (FNN) sont $(\mathrm{A}-\mathrm{A})_{\mathrm{paire}}$, $(\mathrm{B}-\mathrm{B})_{\mathrm{paire}}$ et $(\mathrm{A}-\mathrm{B})_{\mathrm{paire}}$. La réaction d'échange des paires suivante est considérée entre les éléments A et B :

$$(\mathrm{A}-\mathrm{A})_{paire} + (\mathrm{B}-\mathrm{B})_{paire} = 2(\mathrm{A}-\mathrm{B})_{paire}\ ;\ \Delta \mathrm{g}_{\mathrm{AB}} \tag{2.6}$$

avec $\Delta \mathrm{g}_{\mathrm{AB}}$ qui représente le changement d'énergie de Gibbs non configurationnel pour la formation de 2 moles de paires $(\mathrm{A}-\mathrm{B})$. Une description plus détaillée du modèle Quasichimique Modifié par approximation des pairs pour les solutions binaires est présentée dans chacun des pas dans les chapitres 3, 4 et 5.

En considérant que m et n représentent les éléments 1, 2 et 3 d'une solution ternaire, les pairs de premiers voisins proches (FNN) sont $(\mathrm{m}-\mathrm{m})_{\mathrm{paire}}$, $(\mathrm{n}-\mathrm{n})_{\mathrm{paire}}$ et $(\mathrm{m}-\mathrm{n})_{\mathrm{paire}}$. La réaction d'échange des pairs suivante est considérée entre les éléments :

$$(m-m)_{paire} + (n-n)_{paire} = 2(m-n)_{paire}\ ;\ \Delta \mathrm{g}_{\mathrm{mn}} \tag{2.7}$$

avec $\Delta \mathrm{g}_{\mathrm{mn}}$ qui représente le changement d'énergie de Gibbs non configurationnel pour la formation de 2 moles de paires $(m-n)$. Ce terme est développé pour le système ternaire selon un des modèles d'extrapolation géométriques, symétrique ou asymétrique. Les modèles d'extrapolation géométriques importants sont présentés par Pelton [68], détaillant les modèles symétriques Kohler et Muggianu ainsi que les modèles asymétriques de type Kohler/Toop ou Muggianu. Ces modèles permettant d'estimer les propriétés thermodynamiques de la solution ternaire à partir de données optimisées pour ses sous-systèmes binaires. Pour un modèle géométrique donné, l'énergie de Gibbs en excès du système ternaire à toute composition p est calculée à partir des paramètres binaires aux points a, b et c. La différence entre les modèles est le placement de ces trois points et le choix du modèle à utiliser est important, surtout si l'énergie de Gibbs en excès est grande. Les modèles géométriques sélectionnés pour tous les systèmes ternaires à l'étude dans le cadre de ce travail sont présentés dans chacun des articles dans les chapitres 3, 4 et 5.

2.5 Modélisation des solutions solides

Le *Compound Energy Formalism* (CEF) développé par Hillert [69] est un formalisme très utilisé pour modéliser les solutions solides impliquant des sous-réseaux, notamment les composés non stœchiométriques, les solutions interstitielles et les solutions céramiques [62]. Selon le CEF, les espèces d'une solution solide, tel que les atomes, les ions et les lacunes, occupent un ou plusieurs

des sous-réseaux et chaque sous réseau contient une distribution aléatoire des espèces [70]. Pour chaque solution solide, un modèle spécifique peut être développé et ce même modèle peut être directement appliqué à d'autres solutions solides correspondantes au même formalisme [69]. Les paramètres du formalisme correspondent aux énergies de Gibbs des *end-membres*, qui sont définie comme étant les composés stœchiométriques formés quand chaque sous-réseau est entièrement occupé par une seule espèce. Certains de ces composés peuvent être métastables, instables ou même hypothétiques [62]. L'énergie de Gibbs de la solution solide dépend du choix de modèle effectué et son expression est déterminée en fonction des énergies de Gibbs des *end-membres*, des fractions de site relatives à chaque sous-réseau et des paramètres d'interactions. Les paramètres d'interaction du modèle sont estimés de façon à décrire adéquatement la solution solide [62, 69, 71]. Dans ce travail, les propriétés thermodynamiques des solutions solides sont exprimées selon le CEF.

2.6 Modélisation des transitions ferromagnétiques

Certains éléments et composés présentent un ordre magnétique et subissent donc des transitions de second ordre [36]. Pour tenir en compte de cette contribution magnétique, un terme supplémentaire peut être ajouté à l'énergie de Gibbs. Inden [72] a proposé l'équation suivante:

$$G^{magnetic} = RT\ln(\beta + 1)f(\tau) \tag{2.8}$$

β correspond au moment magnétique moyen par mole d'atomes en magnétons de Bohr et τ correspond au ratio entre la température et la température critique d'ordre magnétique. Pour les éléments ferromagnétiques comme le cobalt et le fer, la température critique correspond à la température de Curie T_C. L'expression $f(\tau)$ de l'équation 2.7 a été simplifiée par Hillert et Jarl [73] en l'étendant à une série de puissance. Pour une phase ferromagnétique dans le système A-B, les termes T_C et β peuvent être exprimés en fonction de la composition par les expressions suivantes :

$$T_C(x) = x_A T_C(A) + x_B T_C(B) + T_C^{Excess} \text{ with } T_C^{Excess} = x_A x_B \sum_{i=0\ldots n} T_C(x_A - x_B)^i \tag{2.9}$$

$$\beta(x) = x_A \beta(A) + x_B \beta(B) + \beta^{Excess} \text{ with } \beta^{Excess} = x_A x_B \sum_{i=0\ldots n} \beta(x_A - x_B)^i \tag{2.10}$$

Les paramètres T_C et β sont évalués à partir des données expérimentales [74].

2.7 Revue des systèmes étudiés

Plusieurs systèmes contenant l'arsenic sont sélectionnés et modélisés dans le cadre de ce mémoire, construit sous la forme d'un mémoire par article. Chaque article constitue un chapitre et contient une revue de la littérature très détaillée des données expérimentales de tous les systèmes à l'étude. Dans tous les chapitres, la méthode CALPHAD est employée, avec le modèle Quasichimique Modifié par l'approximation des pairs pour décrire les phases liquides et le *Compound Energy Formalism* (CEF) pour décrire les modèles de solutions solides impliquant des sous-réseaux. Le chapitre 3 présente l'évaluation thermodynamique et l'optimisation des systèmes As-Cd, As-Zn et As-Cd-Zn. Le chapitre 4 présente l'évaluation thermodynamique et l'optimisation des systèmes Ag-As, Ag-S, As-S et Ag-As-S. Le chapitre 5 présente l'évaluation thermodynamique et l'optimisation des systèmes As-Co, As-Fe et As-Fe-S.

CHAPITRE 3 ARTICLE 1: THERMODYNAMIC EVALUATION AND OPTIMIZATION OF THE AS-CD, AS-ZN AND AS-CD-ZN SYSTEMS

Oumaima Kidari[1] and Patrice Chartrand

Center for Research in Computational Thermochemistry (CRCT) - Polytechnique Montréal, Chemical Engineering, Box 6079, Station Downtown, Montréal, Québec, Canada, H3C 3A7.

Article submitted for publication in "Metallurgical and Materials Transactions B" on February 10, 2023

Abstract: In this work, a critical evaluation of all available phase diagrams and thermodynamic data for the As-Cd, As-Zn and As-Cd-Zn systems has been performed and thermodynamic assessments over the whole composition ranges are presented using the CALPHAD method. To predict thermodynamic properties and phase equilibria for these systems, the Modified Quasichemical Model (MQM) for short range ordering was used for the liquid phase and the Compound Energy Formalism (CEF) was used for the solid solutions. The optimized binary systems are in good agreement with existing experimental data. For the ternary system, the predictions of $ZnAs_2$-$CdAs_2$ and Zn_3As_2-Cd_3As_2 are satisfactory. Also, the eutectic temperature is accurately optimized for $ZnAs_2$-Cd_3As_2 and Zn_3As_2-$CdAs_2$. However, the calculated liquidus of these two joins are less satisfactory compared to the experimental data. This is most likely due to the polymerization behavior of arsenic and its multivalence, which is not considered by the model used in this work.

Keywords: Thermodynamic modeling, Modified Quasichemical Model, CALPHAD, Arsenic, Speiss.

3.1 Introduction

As ore concentrates available in the market contain increasing amounts of arsenic, their use will be unavoidable to ensure the viability of the smelting industry. The industry wishes to reduce the atmospheric emissions of this harmful impurity and thus comply with environmental standards. Just like arsenic, cadmium has toxic properties and its presence, particularly in copper smelters, has led to growing concerns of contamination in the surrounding areas due to its high mobility in

[1] Corresponding author
E-mail address: oumaima.kidari@polymtl.ca

the environment and its long body retention time [75]. Cadmium is usually associated with zinc sulfide present in complex ores [76]. To help find a solution to reduce toxic emissions caused by the treatment of copper concentrates in smelters, the development of thermodynamic models of compounds and mixtures, and their associated databases, for systems involving arsenic and other impurities is of much interest for the copper industry. In the present article, the available experimental data of the two binary systems As-Cd and As-Zn and the ternary system As-Cd-Zn is presented and critically evaluated. A set of model parameters is optimized for each phase to predict thermodynamic properties and phase equilibria for these systems. The Modified Quasichemical Model in the Pair Approximation suggested by Pelton et al. [65, 66] was used for the liquid phases, and the Compound Energy Formalism (CEF) suggested by Sundman and Ågren [77] was used for solid solutions. All calculations and optimizations in this work were performed with the FactSage™ thermochemical software [45-47]. The previous assessments of the As-Zn system by Dessureault [78] as well as the one by Ghasemi and Johansson [79] are presented and discussed briefly, similarly to the previous assessments of the Cd-Zn system by Zabdyr [80] and Min et al. [81]. The parameters suggested by Zabdyr [80] are incorporated into the database and are used in this work to evaluate the ternary As-Cd-Zn.

3.2 Literature review

3.2.1 As-Cd and As-Zn binary phase diagrams

There are many similarities between the As-Cd and As-Zn systems. Each system includes two stable compounds at ambient pressure, Cd_3As_2 and Zn_3As_2 that undergo polymorphic transformations as well as $CdAs_2$ and $ZnAs_2$. The crystal structures of the solid phases are presented in Table 3.1.

Table 3.1 Crystallographic description of the phases in As-Cd and As-Zn systems

Phase	Person symbol	Space group	Strukturbericht designation	Reference
Cd_3As_2	$cF12$	$Fm\bar{3}m$	C1	[82]
Zn_3As_2				[83]
Cd_3As_2	$tP40$	$P4_2/nmc$	$D5_9$	[84]
Zn_3As_2				[82]
Cd_3As_2	$tP160$	$P4_2/nbc$	-	[82]

Phase	Person symbol	Space group	Strukturbericht designation	Reference
$\mathbf{Cd_3As_2}$	$tI160$	$I4_1cd$	-	[85]
$\mathbf{Zn_3As_2}$				[82]
$\mathbf{CdAs_2}$	$tI12$	$I4_122$	-	[86]
$\mathbf{ZnAs_2}$	$mP24$	$P2_1/c$	-	[87]

At high cooling rates, the formation of solid $CdAs_2$ is difficult because of the viscosity of the liquid, making possible to measure a metastable liquidus in the range of composition from 55 to 75 at. % As. The experimental studies measuring phase diagram data of As-Cd and As-Zn binary systems are presented in Table 3.2. Details of these studies are also discussed and reviewed in this section.

Table 3.2 As-Cd and As-Zn phase diagram data reported in the literature

References	Experimental methods and results
As-Cd	
[88]	**Raoult's method:** Determination of the melting temperature of cadmium after arsenic addition.
[89]	**TA:** Determination of the phase diagram up to a composition of 52.7 at. % As.
[90]	**TA and metallography:** Determination of the stable and the metastable phase diagrams, up to a composition of 52.7 at. % As.
[91]	**TA, microstructure analysis, XRD and micro-hardness measurements:** Determination of the phase diagram between compositions of 66 and 100 at. % As.
[92]	**DTA, X-ray phase, microstructural analysis, measurements of the microhardness, electrical conductivity and thermo-emf:** Determination of the region of homogeneity of $CdAs_2$.
[93]	**DTA, X-ray phase, microstructural analysis, measurements of the microhardness, electrical conductivity and thermo-emf:** Determination of the region of homogeneity of Cd_3As_2.
[94]	**Emf measurements:** Determination of the liquidus temperatures up to a composition of 45 at. % As, obtained from the breaks in the emf-temperature curves.

References	Experimental methods and results
[95]	**TA, microscopic, XRD and microhardness measurements:** Determination of the phase diagram between compositions of 20 to 100 at. % As.
[96]	**Drop calorimetry measurements:** Determination of the liquidus temperatures up to a composition of 32 at. % As, obtained from deflection points of heat content vs temperature curves.
As-Zn	
[97]	**TA and metallography:** Determination of the phase diagram up to a composition of 12.4 at. % As.
[98]	**TA:** Determination of the phase diagram for all composition range.
[99]	**DTA, X-ray phase, microstructural analysis, measurements of the microhardness, electrical conductivity and thermo-emf:** Determination of the region of homogeneity of $ZnAs_2$.
[100]	**DTA:** Determination of the phase diagram between compositions of 40 to 88 at. % As.
[96]	**Drop calorimetry measurements:** Determination of the liquidus temperatures up to a composition of 48 at. % As, obtained from deflection points of heat content vs temperature curves.

3.2.1.2 As-Cd binary system

Cd-Cd_3As_2 subsystem

Solid solubility: No information has been reported regarding the solubility of arsenic in solid cadmium. Eutectic: The experiments carried out by Heycock and Neville [88] show that the melting temperature of cadmium drops by 1 degree after the addition of 0.45 at. % As. At this composition, a eutectic reaction takes place at a temperature of 592 K to form solid cadmium and Cd_3As_2. This agrees with the eutectic temperatures of 593 K and 592 K measured by Cesaris [89] and Zemczuzny [90] respectively. Liquidus: The liquidus curve of the Cd-Cd_3As subsystem was measured by Cesaris [89], Zemczuzny [90] and Pruchnik [95]. Calculations of the liquidus curve were also made by Komerek et al. [94] and Yamaguchi et al. [96]. The values proposed by these references are all in agreement.

Stable and metastable Cd_3As_2- As subsystem

A stable or a metastable Cd_3As_2-As subsystem can take place, depending on the solidification of $CdAs_2$ that tends to undergo supercooling. There is a tendency for metastable solidification according to Hrubý [101], and it corresponds to the region of existence of a glassy phase. The relation between stable and metastable state can be described by the following reaction:

$$Cd_3As_2 + As_4 \rightleftharpoons 3\,CdAs_2 \tag{3.1}$$

Zemczuzny [90] inoculated the liquid with separately prepared crystallites of $CdAs_2$ before cooling to form a stable crystalline $CdAs_2$. Pruchnik [95] also succeeded in making measurements for the stable subsystem. The results of their measurements are presented below.

Cd_3As_2- $CdAs_2$ subsystem (stable solidification)

Eutectic: Upon stable cooling, a eutectic reaction takes place at a composition around 56 at. % As and a temperature of 883 K to form Cd_3As_2 and $CdAs_2$, according to Zemczuzny [90]. This agrees with the results obtained by Pruchnik [95]. Liquidus: The liquidus curve of the Cd_3As_2-$CdAs_2$ subsystem was measured by Cesaris [89], Zemczuzny [90] and Pruchnik [95]. Calculation of the liquidus curve were also made by Komarek et al. [94]. The values proposed by these references are all in agreement.

$CdAs_2$- As subsystem (stable crystallization)

Solid solubility: No solubility of cadmium in arsenic was reported. Eutectic: During stable cooling, the eutectic reaction to form $CdAs_2$ and solid arsenic takes place at a temperature of 893 K and a composition around 68 at. % As, according to Gukov et al. [91]. This does not correspond to the measurements of Pruchnik [95], according to which the eutectic reaction takes place at a lower temperature of 889 K, at a composition of approximately 72 at. % As. Liquidus: The liquidus curve of the $CdAs_2$- As subsystem was measured by Gukov et al. [91] and it is higher than the one measured by Pruchnik [95].

Cd_3As_2- As subsystem (unstable solidification)

Eutectic: During rapid cooling, a eutectic reaction takes place at a temperature of 799 K and a composition around 62 at. % As to form Cd_3As_2 and solid arsenic, according to Zemczuzny [90]. This agrees quite well with the values measured by Gukov et al. [91]: a eutectic temperature of 803

K and a composition of 63 at. % As obtained at a cooling rate of 5 deg./min. However, Pruchnik [95] measured a lower eutectic temperature of 781 K with a eutectic composition of approximately 68 at. % As at a cooling rate of 10-15 deg./min. The measurements by Pruchnik [95] also suggested the formation of a second unstable system, with the formation of an incongruent compound $CdAs_4$ at cooling rate of 5 deg./min. For this system, the eutectic reaction takes place at a temperature of 853 K at a composition around 63 at. % As to form Cd_3As_2 and $CdAs_4$. Liquidus: The liquidus curve of the $CdAs_2$-As subsystem was measured by Gukov et al. [91] and it is higher than the one measured by Pruchnik [95].

Cd_3As_2 compound

Cd_3As_2 was first reported by Spring [102] who formed the compound using hydraulic pressure and by Granger [103] by heating cadmium in arsenic vapor. Polymorphic transformations: At compositions between 15 and 40 at. % As, thermal effects were observed by Cesaris [89] around 763 K to 863 K. No conclusions were made regarding these effects. According to Zemczuzny [90], Cd_3As_2 is dimorphic and its transformation temperature is 851 K. However, according to the experiments of Trzebiatowski et al. [104], Weglowski and Lukaszewicz [82] and Pietraszko and Lukaszewicz [105], the compound Cd_3As_2 is polymorphic undergoing three phase transitions at the temperatures presented in Table 3.3. No corresponding enthalpy of transformation was found. Melting temperatures: Measured melting temperatures of Cd_3As_2 are also presented in Table 3.3 Solid solution: According to Bokii et al. [106], the compound Cd_3As_2 exists within a small composition interval. This was confirmed by the measurements of Lazarev et al. [93] that showed that the phase is unilateral and can dissolve a small amount of cadmium. The boundaries of the region of homogeneity in at. % of As are 39.5 % at 773 K, 39.7 % at 573 K and less than 39.9 % at 298 K (at. % As). Polymorphic transformations were not considered in these boundary measurements.

$CdAs_2$ compound

As reported by Hrubý [101], $CdAs_2$ exists in three states that can be easily prepared: a stable crystal, a metastable solidified mixture containing Cd_3As_2, $CdAs_2$ and arsenic in a metastable equilibrium state, or a glass in a metastable non-equilibrium state. Polymorphic transformations: According to Ugai and Zyubina [107] and Ugai et al [108], $CdAs_2$ undergoes polymorphic transformations, two crystalline and one amorphous. However, the stability range was not reported. No polymorphic

transformation was considered in the phase diagram compiled by Okamoto [109] since there is only one crystalline structure of $CdAs_2$ known at atmospheric pressure. Vol and Kagan [110] also did not include any $CdAs_2$ transformation in their compiled phase diagram due to a lack of specific information. Melting temperature: Measured melting temperatures of $CdAs_2$ are presented in Table 3.4. The crystalline stable phase is the only congruent according to Hrubý & Štourač [111]. The experiments of Ugai et al. [108] have shown that glassy $CdAs_2$ decomposes into Cd_3As_2 + As upon heating. Therefore, it undergoes an incongruent melting. Hrubý and Štourač [111] measured an incongruent melting temperature of 891 K and a liquidus temperature of 918 K which, according to [111], corresponds approximately to the measurements by Zemczuzny [90]. Solid solution: Marenkin et al. [92] investigated the region of homogeneity of $CdAs_2$ and found that the phase is bilateral. The boundaries of the region of homogeneity in at. % of As are 65.8 % and 67.5 % at 773 K, 66.3 % and 67.2 % at 573 K and 66.4 % and 67.0 % at 473 K.

Table 3.3 Measured and calculated temperatures and heats of transformation of Cd_3As_2

References	Experimental methods	Temperature, in K (in °C)	$\Delta H_{transformation}$ kJ/mol
	$Cd_3As_{2(tI160)} \rightleftharpoons Cd_3As_{2(tP160)}$		
[104]	Dilatometric method	503.15 (230) $\pm$ 3	-
[82]	XRD	503.15 (230) $\pm$ 10	-
[93]	DTA	503.15 (230)	-
[105]	XRD	493.15 (220) $\pm$ 0.5	-
This work	-	498.15 (225)	0.1
	$Cd_3As_{2(tP160)} \rightleftharpoons Cd_3As_{2(tP40)}$		
[104]	Dilatometric method	738.15 (465) $\pm$ 3	-
[82]	XRD	738.15 (465) $\pm$ 10	-
This work	-	738.15 (465)	1
	$Cd_3As_{2(tP40)} \rightleftharpoons Cd_3As_{2(cF12)}$		
[90]	**TA**	851.15 (578)	-
[112]	DTA	868.15 (595)	-
[113]	DTA	867.15 (594)	-
[114]	DTA	868.15 (595)	-
[104]	Dilatometric method	868.15 (595) $\pm$ 3	-
[115]	Dilatometric method	851.15 (578)	-
[116]	TA	888.15(615)	-
[106]	XRD	868.15 (595)	-
[93]	DTA	868.15 (595)	-
[105]	XRD	868.15 (595) $\pm$ 1	-
[83]	TA	858.15 (585) $\pm$ 1	-
This work	-	868.15 (595)	38

References	Experimental methods	Temperature, in K (in °C)	$\Delta H_{transformation}$ kJ/mol
$Cd_3As_{2(cF12)} \rightleftharpoons Cd_3As_{2(liquid)}$			
[89]	TA	986.15 (713)	-
[90]	TA	994.15 (721)	-
[112]	DTA	994.15 (721)	-
[113]	DTA	977.15 (704)	-
[114]	DTA	992.15 (719)	-
[104]	DTA	994.15 (721) $\pm$ 3	-
[115]	Dilatometric method	-	74.1*
[116]	TA	989.35 (716.2)	-
[83]	DTA	971.15 (698) $\pm$ 2	-
[95]	TA	990.15 (717)	-
[117]	Static tensiometric tests	988.15 (715)	-
[118]	Clausius-Clapeyron	-	119.7
This work	-	992.5 (719.35)	63.6

*Uncertain value, ressource no longer available.

Table 3.4 Measured and calculated temperatures and heats of fusion of $CdAs_2$

References	Experimental methods	Temperature, in K (in °C)	ΔH_{fusion} kJ/mol
$CdAs_{2(tI12)} \rightleftharpoons CdAs_{2(liquid)}$			
[90]	TA	894.15 (621)	-
[115]	Dilatometric method	-	35.2*
[111]	DTA	891.15 (618)	-
[119]	DTA	894.15 (621)	-
[95]	TA	894.15 (621)	-
[117]	Static tensiometric tests	897.15 (624)	-
[120]	DTA	900 (626.85)	-
[121]	DTA	898 (624.85)	-
This work	-	902.5 (629.35)	68.5

*Uncertain value, ressource no longer available.

3.2.1.2 As-Zn binary system

Zn-Zn_3As_2 subsystem

Solid solubility: No solubility of arsenic in solid zinc was reported. Eutectic: The eutectic temperature to form solid zinc and Zn_3As_2 is the same as the melting temperature of zinc. It corresponds to 692 K according to the measurements by Friedrich and Leroux [97] and Heike [98]. This temperature agrees with the two values measured by Lazarev et al. [100]. Liquidus: The liquidus curve of the Zn-Zn_3As_2 subsystem was measured by Friedrich and Leroux [97] and Heike

[98]. Calculations of the liquidus curve were also made by Yamaguchi et al. [96]. The values proposed by these references are all in agreement.

Zn_3As_2-$ZnAs_2$ subsystem

Eutectic**:** The eutectic reaction to form $Zn_3As_2$and $ZnAs_2$ occurs at a temperature of 1023 K and a composition of 59 at. % As according to Heike [98].

$ZnAs_2$-As subsystem

Solid solubility: No solid solubility of zinc in arsenic was reported. Eutectic: The eutectic reaction to form $ZnAs_2$ and solid arsenic occurs at a temperature of 996 K and a composition around 79 at. % As according to Heike [98]. Liquidus: The liquidus curve of the $ZnAs_2$-As subsystem was also measured by Heike [98]. The measurements by Lazarev et al. [100] show a liquidus curve about 30 degrees higher than that measured by Heike [98]. Okamoto [122] explains that this disagreement may be due to the difference in the pressure conditions.

Zn_3As_2 compound

Descamps [123] and Spring [102] first reported the formation of Zn_3As_2 by chemical reactions. Polymorphic transformations: Contrary to Cd_3As_2, Zn_3As_2 undergoes only two polymorphic transitions at the temperatures presented in Table 3.5. Melting temperature: The melting temperatures reported for Zn_3As_2 are also presented in Table 3.5. Solid solution: Zn_3As_2 has a very narrow homogeneity range according to Heike [98]. The vapor pressure measurements by Lazarev et al. [100] using the static method confirm that the solubility of arsenic in the α-Zn_3As_2 does not exceed 5×10^{-4} at. %.

$ZnAs_2$ compound

Melting temperature: Congruent melting temperatures of $ZnAs_2$ are presented in Table 3.6. Solid solution: Lazarev et al. [99] investigated the region of homogeneity of $ZnAs_2$ and found that the phase is bilateral. The boundaries of the region of homogeneity in at. % of As are 66.5 % and 67.0 % at 823 K, 66.5 % and 67.0 % at 673 K and 66.66 % and 66.8 % at 573 K.

Table 3.5 Measured and calculated temperatures and heats of transformation of Zn_3As_2

References	Experimental methods	Temperature, in K (in °C)	$\Delta H_{transformation}$ kJ/mol
	$Zn_3As_{2(tI160)} \rightleftharpoons Zn_3As_{2(tP40)}$		
[104]	Dilatometric method	463.15 (190) $\pm$ 3	-
[124]	Dilatometric method	463.15 (190) (heating) 433.15 (160) (cooling)	-
[105]	XRD	435.15 (162) $\pm$ 0.5	-
This work	-	463.15 (190)	1
	$Zn_3As_{2(tP40)} \rightleftharpoons Zn_3As_{2(cF12)}$		
[98]	TA	945.15 (672)	-
[112]	DTA	943.15 (670)	-
[104]	Dilatometric method	945.15 (672) $\pm$ 3	-
[82]	XRD	945.15 (672) $\pm$ 10	-
[124]	Dilatometric method	945.15 (672)	-
[105]	XRD	945.15 (672) $\pm$1	-
[125]	XRD	932.15 (659) $\pm$ 3	-
[113]	DTA	933.15 (660)	-
[126]	DTA extrapolation	929.15 (656)	-
[114]	DTA	943 (670)	-
[83]	TA	924.15 (651) $\pm$1	-
[100]	DTA and XRD	945.15 (672)	-
[127]	Calculated from [128]	947 (673.85)	37.6
This work	-	944.15 (671)	39.2
	$Zn_3As_{2(cF12)} \rightleftharpoons Zn_3As_{2(liquid)}$		
[98]	TA	1288 (1015)	-
[112]	DTA	1295.15 (1022)	-
[113]	DTA	1288 (1015)	-
[126]	DTA	1288 (1015)	-
[114]	DTA	1295.15 (1022)	-
[115]	Dilatometric method	-	92.5*
[118]	Clausius-Clapeyron	-	154.4
[100]	DTA	1288 (1015)	-
This work	-	1292.5 (1019.35)	72.74

*Uncertain value, ressource no longer available.

Table 3.6 Measured and calculated temperatures and heats of fusion of $ZnAs_2$

References	Experimental methods	Temperature, in K (in °C)	$\Delta H_{transformation}$ kJ/mol
	$ZnAs_{2(mP24)} \rightleftharpoons ZnAs_{2(liquid)}$		
[98]	TA	1044.15 (771)	-
[115]	Dilatometric method	-	40.6*
[118]	Calculated by method in [129]	-	85.4
[99]	DTA	1041.5 (768.35)	-
[120]	DTA	1046 (772.85)	-
This work	-	1045 (771.85)	85.9

*Uncertain value, ressource no longer available.

3.2.2 Thermodynamic properties of As-Cd and As-Zn binary systems

As- Cd liquid

Scheil and Kalkuhl [130] used liquid As-Cd alloys to determine the emf for the cell $Cd_{(l)}|Cd^{2+} + (KCl + LiCl)_{(l)}|$ liquid As-Cd alloys, between 673 K and 1073 K. Points were measured with a heating and cooling rate of 30 degrees per hour. Komarek et al. [94] also used liquid As-Cd alloys to determine the emf of the same cell between the liquidus temperature and 1023 K. The measurements were made every 1 to 1.5 K, with a heating and cooling rate of 5 to 8 degrees per hour. Because of the high vapor pressure of arsenic and cadmium, no measurements could be performed at compositions higher than 67 at. % As. Extrapolations to pure arsenic were made for the rest of the compositions. The experimental results and the partial molar properties of Cd referred to liquid Cd as the standard state were given. Also, integral molar quantities were derived by Gibbs-Duhem and given for a temperature of 994 K by Scheil and Kalkuhl [130] and for a temperature of 983 K by Komarek et al. [94]. In the concentration range of 10 to 40 at. % As, the heat content of the binary As-Cd system was determined by Yamaguchi et al. [96] using drop calorimetry from 750 K to 1250 K, and the thermodynamic quantities were derived using the thermodynamic analysis method. The results of Scheil and Kalkuhl [130] and Komarek et al. [94] are in agreement as shown in Figure 3.5. The obtained activities exhibit negative deviation from Raoult's law. Also, the calculated integral enthalpy of mixing is negative over most compositions. It has a minimum around 45 at. % As. The curve calculated by Komarek et al. [94] and Yamaguchi

et al. [96] show slightly positive values for Cd rich alloys compared to the curve calculated by Scheil and Kalkuhl [130].

Mass spectroscopy study by Ivanov and Kaller [131] analyzed the composition of vapor in equilibrium with a liquid alloy of composition of 7.4 at. % As. The measurements were made at temperatures between 726 K and 792 K and revealed the presence of the following ions in the vapor: $Cd^+, As^+, As_2^+, As_4^+$. The heavier Cd_3As_2 and $CdAs_2$ molecules were not detected.

As- Zn liquid

Due to the high melting point of Zn_3As_2 and the high vapor pressure of As and Zn, no direct thermodynamic measurements of the As-Zn liquid have been performed. Mikula and Komarek [132] extrapolated the measured emf data of the ternary As-Cd-Zn system to the binary As-Zn to get values of the Gibbs free energy and Zn activities in the undercooled liquid state for 1023 K and 1123 K. In the concentration range of 4 to 48 at. % As, the heat content of the binary As-Zn system was determined by Yamaguchi et al. [96] using drop calorimetry from 800 K to 1450 K, and the thermodynamic quantities were derived using the thermodynamic analysis method. Zn activities of Mikula and Komarek [132] and Yamaguchi et al.[96] both exhibit negative deviation from the Raoult's law, just like Cd activities in As-Cd system.

Cd_3As_2 compound

Figure 3.1 a) shows the available standard enthalpies of formation of Cd_3As_2. Shchukarev et al. [133] reacted Cd_3As_2 with a solution of KBr saturated with bromine, and under the same conditions, also reacted elemental As and Cd with the same solution. A standard enthalpy of formation of -42 $\pm$ 8 kJ/mol was then calculated from the difference between the measured heat of the reactions. Sirota and Sklyarenko [134] measured the emf of the cell $Cd \mid Cd^{2+} + (KCl + LiCl)_{(l)} \mid Cd_3As_2 + CdAs_2$ and the calculated $\Delta H^{\circ}_{formation}$ is -56 $\pm$ 3 kJ/mol. The heat capacity of Cd_3As_2 was measured for low temperatures by Demidenko et al. [135] using vacuum adiabatic calorimetry between 55 K and 300 K. The measured data is presented in Figure 3.2 a). The standard entropy calculated from these data is also presented in Figure 3.2 b). Several studies determined the vapor pressure of Cd_3As_2 and Figure 3.6 a) shows the data from each study. Using the effusion method in Knudsen cells, Nesmeyanov et al. [136] measured the vapor pressure at temperatures between 511 K and 648 K and it was proposed that the vapor contains mainly Cd_3As_2 molecules. However, subsequent studies have proposed another dissociation mechanism.

Lyons and Silvestri [137] measured vapor pressure between 707 K and 968 K with a dew-point technique, assuming the compound exists as a monomer in the vapor phase. Lyons and Silvestri [137] also measured vapor pressure between 790 K and 865 K with the direct pressure method with a quartz Bourdon gauge. From the ratio of the vapor pressure determined by the two methods, it has been deduced that the dissociation takes place incongruently according to the following reaction:

$$Cd_3As_{2(s)} \rightleftharpoons 3Cd_{(g)} + \frac{1}{2}As_{4(g)} \tag{3.2}$$

This dissociation reaction was confirmed by Westmore et al. [138] using mass spectroscopy technique. Kalevich et al. [139] also measured vapor pressure of Cd_3As_2 using the isoteniscope technique for temperatures between 853 K and 1000 K and using a Bourdon gauge for temperatures between 833 K and 1111 K.

$CdAs_2$ compound

Figure 3.1 a) presents the available standard enthalpies of formation of $CdAs_2$. Sirota and Sklyarenko [134] measured the emf of the cell $Cd \mid Cd^{2+} + (KCl + LiCl)_{(l)} \mid CdAs_2$+As and the calculated standard enthalpy of formation is -23.4 $\pm$ 0.8 kJ/mol. The heat capacity of $CdAs_2$ was measured for low temperatures by Danilenko et al. [140] between 55 K and 300 K. The measured data is presented in Figure 3.2 a). The standard entropy calculated from these data is also presented in Figure 3.2 b). Figure 3.6 b) shows the measured vapor pressure of $CdAs_2$. Using a dew-point technique, Lyons and Silvestri [137] measured the vapor pressure at temperatures between 608 K and 888 K. They also used a direct pressure method employing a quartz Bourdon gauge at temperatures in the range of 717 K and 879 K. $CdAs_2$ is shown to thermally dissociate according to the following reaction:

$$CdAs_{2(s)} \rightleftharpoons \frac{1}{3}Cd_3As_{2(s)} + \frac{1}{3}As_{4(g)} \tag{3.3}$$

Marenkin et al. [141] also measured the vapor pressure using the static method with a Bourdon quartz manometer.

Zn_3As_2 compound

The available standard enthalpies of formation of Zn_3As_2 are presented in Figure 3.1 b). Natta and Passerini [142] measured the heat of formation of the compound indirectly in a Dewar flask. The heat of dissolution of this compound in dilute hydrochloric acid was measured and Hess's law was used to calculate a value of -126.8 kJ/mol. Ariya et al. [143] repeated the same experiment and calculated a value of -127.6 kJ/mol. Sirota and Sklyarenko [134] measured the emf of the cell $Zn \mid Zn^{2+} + (KCl + LiCl)_{(l)} \mid Zn_3As_2 + ZnAs_2$ and the calculated standard enthalpy of formation is -136.4 $\pm$ 5 kJ/mol. As shown in Figure 3.2 a), the heat capacities of Zn_3As_2 were measured at low temperatures by Demidenko et al. [135] between 55 K and 300 K and by Gorbunov et al. [144] between 10 K and 300 K using vacuum adiabatic calorimetry. The standard entropies calculated from these data are presented in Figure 3.2 b). Several studies determined the vapor pressure of Zn_3As_2 Figure 3.7 a) shows data from each study. Using the effusion method in Knudsen cells, Nesmeyanov et al. [136] measured the vapor pressure at temperatures between 601 K and 751 K and it was proposed that the vapor contains mainly Zn_3As_2 molecules. However, subsequent studies rejected the proposed sublimation mechanism. The vapor pressure of the compound was also measured by Schoonmaker and Lemmerman [145] using torsion-effusion method over a range of temperature from 613 K to 853 K. The proposed congruent decomposition reaction is the following:

$$Zn_3As_{2(s)} \rightarrow 3\,Zn_{(g)} + \frac{1}{2}As_{4(g)} \tag{3.4}$$

This dissociation reaction was confirmed by Munir [128] using torsion-effusion technique between 782 K and 905 K. Lazarev et al. [100] also measured the vapor pressure of Zn_3As_2 with the static method by use of a quartz Bourdon gauge, for temperatures between 932 K et 954 K. Greenberg et al. [127] also performed the same measurements for temperatures between 947 K to 1181 K.

$ZnAs_2$ compound

The available standard enthalpies of formation of $ZnAs_2$ are presented in Figure 3.1 b). Sirota and Sklyarenko [134] measured the emf of the cell $Zn \mid Zn^{2+} + (KCl + LiCl)_{(l)} \mid ZnAs_2 + As$ and the calculated standard enthalpy of formation is -73.6 $\pm$ 2 kJ/mol. As shown in Figure 3.2 a), the heat capacities of $ZnAs_2$ were measured at low temperatures by Demidenko et al. [135] between 55 K and 300 K and by Gorbunov et al. [144] between 10 K and 300 K using vacuum adiabatic

calorimetry. The standard entropy calculated from these data is also presented in Figure 3.2 b). Figure 3.7 b) shows the measured vapor pressure of $ZnAs_2$. Using a dew-point technique, Lyons and Silvestri [137] measured the vapor pressure at temperatures between 885 K and 1032 K. Lyons and Silvestri [137] also used the triple point technique at temperatures in the range of 1029 K and 1043 K. $ZnAs_2$ is shown to thermally dissociate according to the following reaction:

$$ZnAs_{2(s)} \rightleftharpoons \frac{1}{3}Zn_3As_{2(s)} + \frac{1}{3}As_{4(g)} \tag{3.5}$$

This dissociation reaction was confirmed by Munir [128] using torsion-effusion technique between 726 K and 786 K.

3.2.3 Assessments of As-Cd and As-Zn binary systems in the literature

No previous assessment was found for the binary As-Cd system. The binary As-Zn system was previously assessed by Dessureault [78] as well as Ghasemi and Johansson [79], considering stoichiometric compounds. Dessureault [78] modeled the liquid phase using the Quasichemical Model and supposed stoichiometric compounds, using the F*A*I*T system *(*Formation Analytique Interactive en Thermodynamique*),* a predecessor of FactSage™ [45-47]. Ghasemi and Johansson [79] used the associate-solution model for the liquid phase with three associate species (As, As_2Zn_3, Zn), using the Thermo-Calc software [146]. Using the same software, the Cd-Zn liquid phase was assessed by Zabdyr [80] employing the Redlich-Kister-Muggianu model. The Cd-Zn liquid was also assessed by Min et al. [81] using the substitutional solution model. The parameters suggested by Zabdyr [80] for the Cd-Zn are incorporated to the FactSage database and are used in this work to evaluate the ternary As-Cd-Zn, for which we have not found a published thermodynamic assessment.

3.2.4 As-Cd-Zn ternary phase diagram

The presence of two quasi-binary sections was established in the As-Cd-Zn system: Zn_3As_2-Cd_3As_2 and $ZnAs_2$-$CdAs_2$. A continuous series of $Cd_{3-x}Zn_xAs_2$ solid solutions is formed at high temperatures in the quasi-binary Zn_3As_2 and Cd_3As_2. A limited solid solubility exists in the quasi-binary $ZnAs_2$ and $CdAs_2$, with two types of solid solutions: $Cd_{1-x}Zn_xAs_2$ and $Cd_xZn_{1-x}As_2$. The studies measuring ternary phase diagram data of As-Cd-Zn system are presented in Table 3.7. Details of these studies are also discussed and reviewed in this section.

Table 3.7 As-Cd-Zn phase diagram data reported in the literature

References	Experimental methods and results
Zn_3As_2-Cd_3As_2	
[147]	**XRD at room temperature:** Suggestion of a phase diagram from room temperature up to 1288 K.
[148]	**Measurements of the Hall coefficient and resistivity:** Suggestion of a phase diagram from room temperature up to 1288 K.
[112]	**DTA and XRD:** Determination of the phase diagram in the temperature range of 867 K and 1288 K.
[113]	**DTA and XRD:** Determination of the phase diagram in the temperature range of 867 K and 1288 K.
[114]	**DTA and XRD:** Determination of the phase diagram in the temperature range of 867 K and 1288 K.
[104]	**Dilatometric method:** Determination of the phase diagram in the temperature range of 463 K and 1288 K.
$ZnAs_2$-$CdAs_2$	
[149]	**DTA and microhardness measurements:** Determination of the phase diagram for all composition range.
As-Cd-Zn	
[132]	**DTA:** Determination of several liquid temperatures and their compositions.
Zn_3As_2-$CdAs_2$	
[120]	**DTA, XRD and microstructural analysis:** Determination of the phase diagram for all composition range.
Zn_3As_2-$CdAs_2$	
[120]	**DTA, XRD and microstructural analysis:** Determination of the phase diagram for all composition range.
Zn_3As_2-$ZnAs_2$-$CdAs_2$-Cd_3As_2	
[120]	Prediction of the phase diagram of the liquidus surface

Zn_3As_2-Cd_3As_2 quasi-binary system

Solid solubility: A slight decrease of the Cd_3As_2 lattice constants measured by Zdanowicz et al. [147] shows that it can dissolve about 1% of Zn_3As_2 below 773 K. Similarly, Zn_3As_2 can also dissolve a small amount of Cd_3As_2. Continuous series of solid solutions: This quasi-binary system forms a continuous series of solid solutions above 738 K. Liquidus and solidus curves measured by Naake and Belcher [112] and Masumoto et al. [114] are in good agreement. 25 to 30 degrees above the solidus transition, a smaller transition was observed by Castellion and Beegle [113] for $Cd_{3-x}Zn_xAs_2$ specimens for $1.2 < x < 2$, but it was not possible to determine the exact temperature of the transition. The polymorphic transition by Naake and Belcher [112], Castellion and Beegle [113], Masumoto et al. [114] and Trzebiatowski et al. [104] is also in good agreement. Below 738 K, the continuous solid solutions is broken for a certain composition interval because of the formation of a superstructure, identified by Żdanowicz [147] [148]. The lattice constant c of the tetragonal cell of the superstructure is equal to twice that of the continuous solid solution The continuous solid solution exists in the ranges of $0.15 \leq x \leq 1.35$ and $2.7 \leq x \leq 3$. It has been found that the superstructure is stable only at low temperatures in the range of $1.35 \leq x \leq 2.7$. Trzebiatowski et al. [104] confirmed a reversible phase transition for $Cd_{3-x}Zn_xAs_2$ specimens in the range of $1.35 < x < 1.95$.

$ZnAs_2$-$CdAs_2$ quasi-binary system

Solid solubility: Ugai et al. [150] reported the formation of solid solutions at all concentrations in this quasi-binary system. However, the measurements by Marenkin et al. [149] showed that the $ZnAs_2$-$CdAs_2$ quasi-binary system has a simple eutectic with restricted ranges of $Cd_xZn_{1-x}As_2$ and $Cd_{1-x}Zn_xAs_2$ solid solutions. Eutectic: According to Marenkin et al. [149], a eutectic reaction forms $Cd_xZn_{1-x}As_2$ and $Cd_{1-x}Zn_xAs_2$ solid solutions at a temperature of 870 K and a composition of 62 % at. $CdAs_2$. From the liquidus surface constructed by Marenkin et al. [120], the eutectic reaction takes place at a slightly higher temperature of 879 K.

$ZnAs_2$-Cd_3As_2 and Zn_3As_2-$CdAs_2$ joins

According to Marenkin et al. [120], both $ZnAs_2$-Cd_3As_2 and Zn_3As_2-$CdAs_2$ joins are not pseudo-binary, and their liquidus consist of two primary crystallization branches. In the $ZnAs_2$-Cd_3As_2 join, the primary crystallisation phase is $ZnAs_2$ based solid solution in the composition range 0 to

15 at. % Cd_3As_2, and $Cd_{3-x}Zn_xAs_2$ in the composition range 15 to 100 at. % Cd_3As_2. In the Zn_3As_2-$CdAs_2$ join, the primary crystallization phase is $Cd_{3-x}Zn_xAs_2$ based solid solution in the composition range 0 to 90 at. % $CdAs_2$, and $CdAs_2$ based solid solution in the composition range 90 to 100 at. % $CdAs_2$. Both joins contain a ternary eutectic, which melts at 863 K.

Liquidus surface of the ternary As-Cd-Zn system

Based on the measurements presented above, Marenkin et al. [120] constructed the phase diagram of the liquidus surface in the composition region Zn_3As_2-$ZnAs_2$-$CdAs_2$-Cd_3As_2. The ternary eutectic in this region has an approximate composition of 26 at. % Cd + 65 at. % As + 9 at. % Zn at a temperature of 863 K. Also, DTA measurements were performed by Mikula and Komarek [132] to determine liquidus temperatures of several ternary alloys.

3.2.5 Thermodynamic properties of As-Cd-Zn ternary system

As-Cd-Zn Liquid

Mikula and Komarek [132] used 45 liquid As-Cd-Zn alloys to determine the emf of the cell $Zn_{(l)}|Zn^{2+} + (KCl + LiCl)_{(l)}|$ liquid As-Cd-Zn alloys. The measurements were made with heating and cooling rates of 8 to 10 degrees per hour. From the results, the iso-activity curves of zinc in the ternary As-Cd-Zn were determined at 1123 K. Thermodynamic functions of formation of solid solutions in the $ZnAs_2$-$CdAs_2$ and Zn_3As_2-Cd_3As_2 quasi-binary systems were also measured using the emf method by Sirota and Smolyarenko [151]. The emf of the following cells were determined, $Zn_xCd_{1-x}|KCl + LiCl + ZnCl_2 + CdCl_2|$ $(Zn_xCd_{1-x})As$ and $Zn_xCd_{1-x}|KCl + LiCl + ZnCl_2 + CdCl_2|$ $(Zn_xCd_{1-x})_3As_2$ + $(Zn_uCd_{1-u})As_2$. Both $ZnAs_2$-$CdAs_2$ and Zn_3As_2-Cd_3As_2 systems exhibit negative deviation from the Raoult law. Also, the heats of formation determined for the Zn_3As_2-Cd_3As_2 system are considerably higher than those for the $ZnAs_2$-$CdAs_2$ system.

3.3 Thermodynamic modeling

All calculations and optimizations in this work were performed with the FactSage™ thermochemical software [45-47]. The properties of pure solid and liquid As, Cd and Zn are from SGTE [152]. The properties of gaseous Zn are from JANAF Thermochemical Tables [153]. The properties of the gaseous species As, As_2, As_3, As_4 and Cd are from Degterov et al. [154] and other of their unpublished optimizations and evaluations.

3.3.1 Thermodynamic model for the liquid phase

The Modified Quasichemical Model in the Pair Approximation suggested by Pelton et al. [65] [66] was used to model the liquid phases to take into account the short-range ordering (SRO). For a liquid binary A-B system, the following pair exchange reaction is considered between the A and B atoms on neighboring lattice sites:

$$(A-A)+(B-B)=2(A-B)\ ;\ \Delta g_{AB} \tag{3.6}$$

$(i-j)$ is the first nearest neighbor (FNN) atom pairs, and Δg_{AB} is the non-configurational Gibbs energy change for the formation of 2 moles of $(A-B)$ pairs. The pair and the overall mole (site) fractions are defined respectively as:

$$X_{ij}=\frac{n_{ij}}{(n_{AA}+n_{BB}+n_{AB})} \tag{3.7}$$

$$X_A=\frac{n_A}{(n_A+n_B)}=1-X_B \tag{3.8}$$

n_A, n_B represent the number of moles of A and B, n_{AB} represents the number of moles of pairs (A-B). If the coordination number of A is Z_A, the "coordination equivalent" fraction of A is defined as:

$$Y_A=\frac{Z_A n_A}{Z_A n_A+Z_B n_B}=\frac{Z_A X_A}{Z_A X_A+Z_B X_B}=1-Y_B=X_{AA}+\frac{X_{AB}}{2} \tag{3.9}$$

The "coordination equivalent" fraction of B is defined similarly. The Gibbs energy of the binary liquid is given by the following equation:

$$G=\left(n_A g_A^{\circ}+n_B g_B^{\circ}\right)-T\Delta S^{\text{configuration}}+\left(\frac{n_{AB}}{2}\right)\Delta g_{AB} \tag{3.10}$$

g_A° and g_B° are the molar Gibbs energies of the pure liquid components, and $\Delta S^{\text{configuration}}$ is the configurational entropy of mixing given by randomly distributing the (A-A), (B-B) and (A-B) pairs. The non-configurational Gibbs energy change for the formation of 2 moles of $(A-B)$ pairs is expended in terms of the pair fractions and their expressions for As-Cd and As-Zn systems are as follows:

$$\Delta g_{AsCd}=\Delta g_{AsCd}^{\circ}+\sum_{i\geq 1} g_{AsCd}^{i0}\,(X_{AsAs})^i+\sum_{j\geq 1} g_{AsCd}^{0j}\,(X_{CdCd})^j \tag{3.11}$$

$$\Delta g_{AsZn} = \Delta g^{\circ}_{AsZn} + \sum_{i\geq 1} g^{i0}_{AsZn} (X_{AsAs})^{i} + \sum_{j\geq 1} g^{0j}_{AsZn} (X_{ZnZn})^{j} \quad (3.12)$$

Δg°_{AsCd}, Δg°_{AsZn}, g'^{i0}_{AsCd}, g^{0j}_{AsCd}, g^{i0}_{AsZn} and g^{0j}_{AsZn} are the temperature dependent model parameters that are optimized in this work.

For a liquid binary A-B system, the coordination numbers can be varied with composition to reproduce the SRO, as given by equations 3.14 and 3.15. The composition of maximum SRO is determined by the ratio Z_B / Z_A:

$$\frac{1}{Z_A} = \frac{1}{Z^A_{AA}}\left(\frac{2n_{AA}}{2n_{AA}+n_{AB}}\right) + \frac{1}{Z^A_{AB}}\left(\frac{2n_{AB}}{2n_{AA}+n_{AB}}\right) \quad (3.13)$$

$$\frac{1}{Z_B} = \frac{1}{Z^B_{BB}}\left(\frac{2n_{BB}}{2n_{BB}+n_{AB}}\right) + \frac{1}{Z^B_{BA}}\left(\frac{2n_{AB}}{2n_{BB}+n_{AB}}\right) \quad (3.14)$$

Z^{A}_{AA} and Z^{A}_{AB} are the coordination numbers when the nearest neighbours of an A atom are A atoms and B atoms respectively. Z^{B}_{BB} and Z^{B}_{BA} are defined similarly. In this work, Z^{As}_{AsAs}, Z^{Cd}_{CdCd} and Z^{Zn}_{ZnZn} are set to be 6 for consistency with previous work. Since maximum SRO occurs at approximately a composition of 40 at. % As, Z^{As}_{AsCd} and Z^{As}_{AsZn} are set to be 3, and Z^{Cd}_{AsCd} and Z^{Zn}_{AsZn} are set to be 2.

The Cd-Zn binary system was previously assessed by Zabdyr [80]. The liquid phase was modeled using the Bragg-Williams random mixing model in the form of Redlish-Kister polynomial [155], with ${}^{i}L_{CdZn}$ as the interaction parameter. The excess contribution to the total Gibbs energy is given by the following equation:

$$g^{excess} = X_{Cd}X_{Zn}\sum_{i\geq 0} {}^{i}L_{CdZn}(X_{Cd} - X_{Zn})^{i} \quad (3.15)$$

Geometric models can be used to estimate the excess Gibbs energy of a ternary system from the parameters of the three binary subsystems [68]. For a given geometric model, the excess Gibbs energy of the ternary system at any composition *p* is calculated from the binary parameters at points *a*, *b* and *c*. The difference between the models is the placement of these three points. Since the binary excess Gibbs energy in As-Cd and As-Zn systems are large and the parameters depend strongly upon composition, the different models will give very different results. Thus, the choice of points *a*, *b* and *c* is very important to correctly interpolate the ternary system. Since As is

chemically different from Cd and Zn, the use an asymmetric model is more reasonable. In this work, the Toop type of extrapolation technique was used to optimize the ternary As-Cd-Zn liquid phase, with arsenic as the asymmetric component.

3.3.2 Thermodynamic model for the solid solutions

The Compound Energy Formalism (CEF) suggested by Sundman and Ågren [77] is used to model solid phases. The sub-lattice model for each solid solution in this work is presented in Table 3.8 and justified below.

Solid solutions of $Cd_{3-x}Zn_xAs_2$ phases

The Cd_3As_2 polymorphic forms have related crystal structures, which are based on the anti-fluorite structure (CaF_2). In the ideal Cd_4As_2 anti-fluorite formula, the cations Cd^{2+} occupy the F^- sites and the anions As^{3-} occupy the Ca^{2+} sites. The Cd_3As_2 is cadmium deficient compared to the ideal anti-fluorite formula, missing one-fourth of the Cd atoms and has 25 % Cd site vacancy, according to Ali et al. [156] and Koumoulis et al. [157]. The ordering and the disordering of the vacancies affects the space group to which the crystal belongs. At temperatures higher than 873 K. the Cd ions are disordered and the Cd_3As_2 adopts the ideal anti-fluorite structure, with the $Fm\bar{3}m$ space group. At lower temperatures, the Cd atoms order and shift from the ideal anti-fluorite positions towards the vacancies, resulting in the other structures [105]. According to Lazarev et al. [93], it can be assumed that the formation of the Cd_3As_2 solid solutions occur due to the filling of the vacant sites, which explains their one-sided nature. Since Cd_3As_2 is an n-type and Zn_3As_2 is a p-type semiconducting material, an n to p transition is expected in $Cd_{3-x}Zn_xAs_2$ solid solutions [158] [159]. Based on Hall coefficient and resistivity measurements by Żdanowicz [148], $Cd_{3-x}Zn_xAs_2$ solid solutions are n-type for $0 \leq x \leq 1.35$ as well as $2.7 \leq x \leq 3$. In the range of existence of the superstructure, that is $1.35 \leq x \leq 2.5$, the solid solutions change to p-type. Two distinct solid solutions are therefore necessary to model this transition. Using X-ray diffraction analysis, Volodina et al. [160] established that Cd and Zn occupy the same site in $Cd_{3-x}Zn_xAs_2$ solid solutions. Based on this information, the sub-lattice models used for $Cd_{3-x}Zn_xAs_2$ solid solutions are presented in Table 3.8.

Solid solutions of $Cd_{1-x}Zn_xAs_2$ and $Cd_xZn_{1-x}As_2$ phases

Marenkin et al. [92] suggest that $CdAs_2$ solid solution is formed as a result of both Frenkel and Schottky point defects. Marenkin et al. [161] also determined the structural defects in $CdAs_2$ by investigating the spectra of optical absorption and photoconductivity. Their results that $CdAs_2$ is always enriched in Cd with respect to the stoichiometric composition. The excess Cd occupies an interstitial lattice and vacancies are formed on the As site. Also, it is unlikely that the $CdAs_2$ solid solution has anti-site defects because of the difference in radius between Cd and As. Since the thermal dissociation of $CdAs_2$ releases As atoms, Morozova et al. [162] proposed that As atoms may pass from lattice sites to interstitial positions. Based on impurity photoconductivity spectra measurements, and since Zn and As have similar covalent radius, Morozova et al. [162] suggested that $CdAs_2$-based solid solutions are likely to have anti-site defects, where Zn atoms fill vacancies on As site. However, according to Sanygin et al. [121], Zn substitution on the As site is very unlikely. Zn is deficient in valence electrons compared to As, and since Zn and Cd are isoelectronic, the Zn in $CdAs_2$-based solid solutions substitutes on the Cd site. Moreover, based on the laser ionisation mass spectrometry and electron probe X-ray microanalysis data for $Cd_{0.95}Zn_{0.05}As_2$ solid solution, Zn substitution for Cd is confirmed.

Marenkin et al. [163] explain that for $ZnAs_2$, As atoms may pass from lattice sites to interstitial positions. Also, Zn atoms are likely to form anti-site defects since its covalent radius is closer to that of As, contrary to Cd atoms. Zn vacancies are also possible, but their concentration must be substantially lower than those of other defects. Unlike $CdAs_2$-based solid solutions, $ZnAs_2$-based solid solutions are interstitial and not substitutional. As explained by Sanygin et al. [121], Zn substitution by Cd atoms is unfavorable since Zn-As bonds are stronger than Cd-As bonds. This is based on the empirical relationship relating the change in molecular weight to the stability of II-V_2 semiconductors. For $Cd_{0.03}Zn_{0.97}As_2$ solid solution, the X-ray diffraction done by Sanygin et al. [121] confirms the presence of interstitial Cd atoms. Investigation of photoconductivity spectra by Morozova et al. [164] also validates that Cd atoms occupy interstices upon the introduction of $ZnAs_2$ into $CdAs_2$. The sub-lattice models used for $Cd_{1-x}Zn_xAs_2$ and $Cd_xZn_{1-x}As_2$ solid solutions are presented Table 3.8.

Table 3.8 Crystallographic description and sublattice model of the phases in the As-Cd-Zn system

Phase	Person symbol	Space group	Reference	Sub-lattice modeling
$\mathbf{Cd_{3-x}Zn_xAs_2}$(**C1**	$cF12$	$Fm\bar{3}m$	[82] [83]	$(\mathbf{Cd}, \mathrm{Zn})_3(\mathbf{Va}, \mathrm{Cd})_1(\mathbf{As})$
$\mathbf{Cd_{3-x}Zn_xAs_2}$ ($\mathbf{D5_9}$)	$tP40$	$P4_2/nmc$	[84] [82]	$(\mathbf{Cd}, \mathrm{Zn})_3(\mathbf{Va}, \mathrm{Cd})_1(\mathbf{As})$
$\mathbf{Cd_{3-x}Zn_xAs_2}$	$tP160$	$P4_2/nbc$	[82]	$(\mathbf{Cd}, \mathrm{Zn})_3(\mathbf{Va}, \mathrm{Cd})_1(\mathbf{As})$
$\mathbf{Cd_{3-x}Zn_xAs_2}$	$tI160$	$I4_1cd$	[85] [82]	$(\mathbf{Cd}, \mathrm{Zn})_3(\mathbf{Va}, \mathrm{Cd})_1(\mathbf{As})$
Super-structure $\mathbf{Cd_{3-x}Zn_xAs_2}$	-	-	-	$(\mathbf{Cd}, \mathrm{Zn})_2(\mathrm{Cd}, \mathbf{Zn})_1(\mathbf{Va})_1$
$\mathbf{Cd_{1-x}Zn_xAs_2}$	$tI12$	$I4_122$	[86]	$(\mathbf{Cd}, \mathrm{Zn})_1(\mathbf{Va}, \mathrm{Cd}, \mathrm{As})_1(A$
$\mathbf{Cd_xZn_{1-x}As_2}$	$mP24$	$P2_1/c$	[87]	$(\mathbf{Zn}, \mathrm{Cd})_1(\mathbf{Va}, \mathrm{As})_1(\mathbf{As}, $

3.4 Results and discussion

The optimization of the thermodynamic parameters was conducted using the FactSage™ thermochemical software. The As-Cd and As-Zn systems are assessed based on the literature data presented in the previous sections, and the optimized thermodynamic model parameters are presented in Table 3.9. The enthalpies of formation (measurements and DFT) of the different compounds of the binary systems are shown in Figure 3.1, along with the optimized values from this work. There is a large discrepancy in the values suggested by various authors, but the enthalpies of formation of the compounds in the As-Zn system are generally about two times more negative than the values of the compounds in the As-Cd system. Also, the enthalpy of formation per atom selected for $\mathrm{Cd_3As_2}$ and $\mathrm{Zn_3As_2}$ are higher than those of the compounds $\mathrm{CdAs_2}$ and $\mathrm{ZnAs_2}$ respectively. The estimated heat capacity ($\mathrm{C_p}$) curves of the intermediate phases are presented in Figure 3.2 a). Since there are no data measured at higher temperatures, the estimation of the curves was done in two steps. A first estimation was made using the Neumann-Kopp rule which gave slightly higher values than the measured experimental data at 298.15 K. The curves were then shifted down to reproduce the measurements at room temperature. The standard entropies of compounds selected in this work are presented in Figure 3.2 b). The calculated binary phase diagrams are shown in Figure 3.3 and Figure 3.4 below, along with the experimental data. For both

As-Cd and As-Zn systems, there is a disagreement in the data reported for arsenic rich alloys, probably due to the high vapor pressure of these alloys. For As-Cd system, arsenic liquidus data in the stable and the metastable systems by the same authors do not match due to the rate of heating and cooling used in each experiment are shown in Figure 3.3 b).

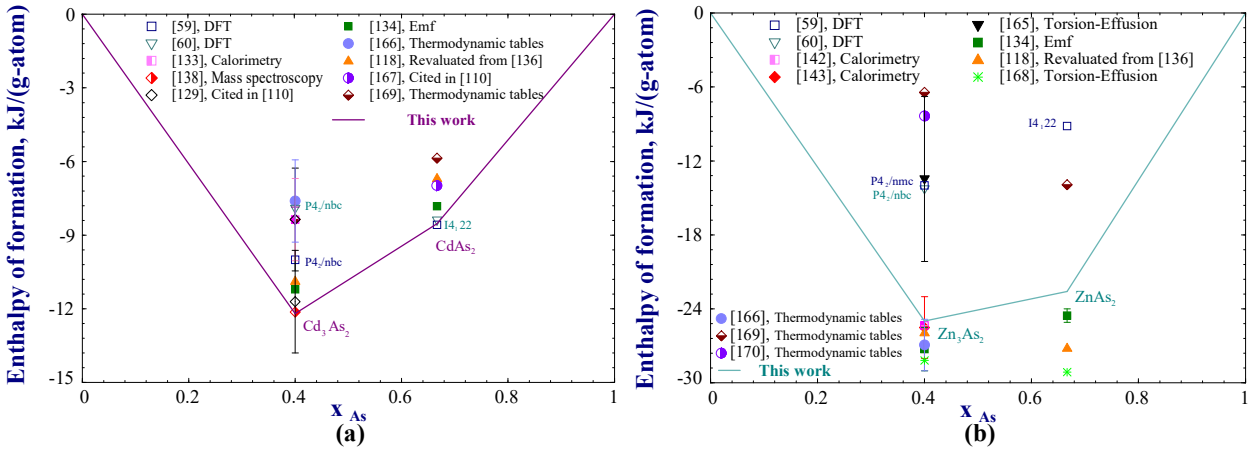

Figure 3.1 Enthalpies of formation of intermediate compounds in a) As-Cd system and b) As-Zn system

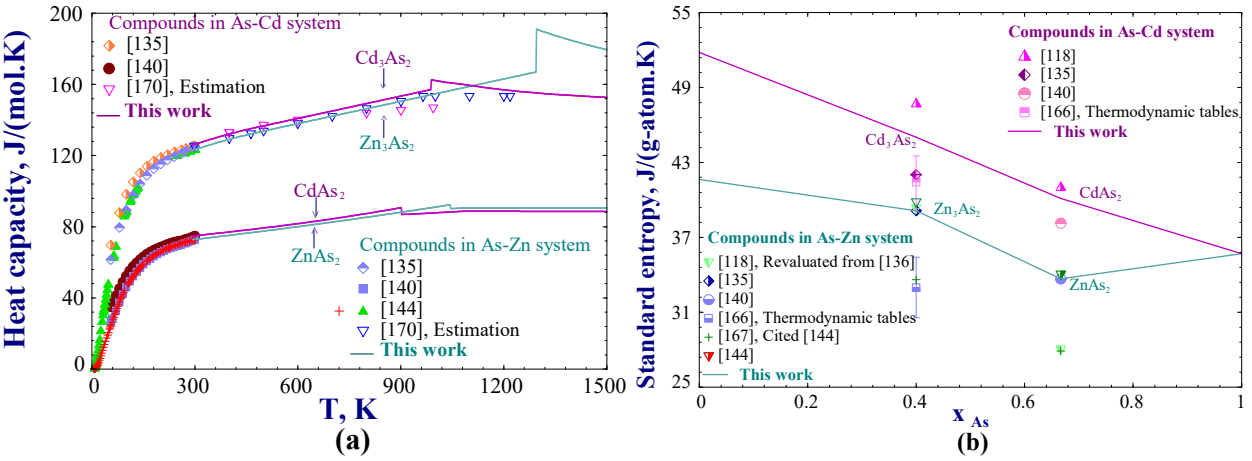

Figure 3.2 a) Heat capacities and b) standard entropies of the intermediate compounds in As-Cd and As-Zn systems

To measure data for the stable As-Cd phase diagram, slower rates were used by Pruchnik [95] and Gukov [91], and higher rates were used to measure data for the metastable phase diagram. To optimize the liquid parameters in the As-Cd system, the stable phase diagram data as well as the activity data were considered. The Cd activity in liquid As-Cd melt by Komarek et al. [94] as well as Scheil and Kalkuhl [130] are directly obtained from emf measurements. However, only the data

from Komarek et al. [94] was used to optimize the liquid phase since it was obtained using a slower heating rate and thus considered more reliable. The calculated As-Cd phase diagram reproduces most experimental data but does not completely fit the measured data at high arsenic content. Because of the disagreement between the different authors and since no activity data is available for arsenic rich alloys, the optimized parameters for the liquid phase at high arsenic compositions has a significant uncertainty. To best reproduce phase diagram data at high arsenic content, a peritectic temperature of 900 K had to be selected for $CdAs_2$-As subsystem instead of the slightly lower eutectic temperature of 893 K reported by Gukov et al. [91] or 889 K by Pruchnik [95]. $CdAs_2$ is then incongruent in this work with a melting point slightly higher than the reported measurements for the crystalline form shown in Table 3.4. Also, the calculated homogeneity range is narrower than what was measured by Marenkin et al. [92] in order to best reproduce the rest of the phase diagram data. The Cd_3As_2 compound is congruent, with an optimized melting point of 992.5 K. The non-stoichiometry of Cd_3As_2 is unilateral and the existence of the different polymorphic forms causes a slight deviation of the stoichiometric composition of 40 at. % As, thus giving a "banana shape" that tends towards cadmium at higher temperatures. The stoichiometric deviation starts from a temperature of 572 K, reaching the largest deviation of 0.3 at. % As towards Cd at the melting point. The calculated As-Zn phase diagram reproduce most experimental data as shown in Figure 3.4. Both $ZnAs_2$ and Zn_3As_2 have congruent melting temperatures of 1046 K and 1293 K respectively. The compound Zn_3As_2 is considered stoichiometric in this work because no homogeneity range data is reported in the literature. The emf measurements performed by Mikula and Komarek [132] were scattered, and the extrapolation of these measurements to predict Zn activity was not considered reliable enough to use in the optimization of the liquid phase. Since there are no other reliable thermodynamic measurements for the liquid phase, only phase diagram data was used for the optimization of this system.

For both As-Cd and As-Zn systems, Yamaguchi et al. [96] did not report the measured heat content in their paper, but only the thermodynamic quantities derived. Moreover, because of the significant dependence of the results on the chosen heat of formation of the compounds and the uncertainty of the method employed in the calculations, the proposed thermodynamic data by Yamaguchi et al. [96] were not directly considered in optimizing the parameters. However, the reported data was used as a reference to compare As-Cd and As-Zn systems. Figure 3.5 a) compares the calculated enthalpy of mixing of the liquids in each binary system. The shape of the calculated curves in both

systems is very similar, positive for high metal composition and very negative around the SRO compositions. The negative deviations from ideality in the liquid As-Zn solution are more pronounced than for the liquid As-Cd solution. Komarek et al. [94] suggested a curve minimum at 48 at. % As for the enthalpy of mixing of the liquid in the As-Cd system, which is consistent with the minimum suggested by Scheil and Kalkuhl [130]. It can also be seen from the same Figure that the enthalpy of mixing of the liquid in the As-Zn system has a minimum of 40 at. % As according to Yamaguchi et al. [96]. In this work, the same coordination numbers were selected in both systems to fix the composition of maximum SRO in As-Cd and As-Zn liquid phases. By setting Z^{As}_{AsCd} and Z^{As}_{AsZn} to 3, and Z^{Cd}_{AsCd} and Z^{Zn}_{AsZn} to 2, the calculated integral enthalpy of mixing of Cd-As system has a minimum around what was measured. Small coordination numbers were selected since the reported enthalpy of mixing curves of the two systems seems to be very sharp. As shown in Figure 3.5, the integral enthalpy of mixing curves have a "V" shape and the integral entropy of mixing curves have an "m" shape. This is due to the highly ordered liquid phases, which can be explained by the large differences of electronegativity between As (2.18) and the metals Cd (1.69) and Zn (1.65). To optimize the liquid phases of As-Cd and As-Zn systems, parameters using the same indices are necessary in both systems as shown in Table 3.9. Also, because the liquid phase of As-Zn system is more stable compared to that of As-Cd system, the optimized parameters of liquid As-Zn are about 2.4 times higher. The high stability of the As-Zn liquid phase implies large parameter values to describe the excess Gibbs energy. Because of the large parameter values used for the T-dependent term for g^{10}_{AsZn} shown in Table 3.9 the model predicts a miscibility gap above 5500 K. To correct the excess Gibbs energy of the liquid phases at high temperatures, the addition of a $C\mathrm{Tln}(T)$ term for the said term is necessary to avoid the formation of an inverted miscibility gap. The correction term $0.35\mathrm{Tln}(T)$ was added as presented in Table 3.9.

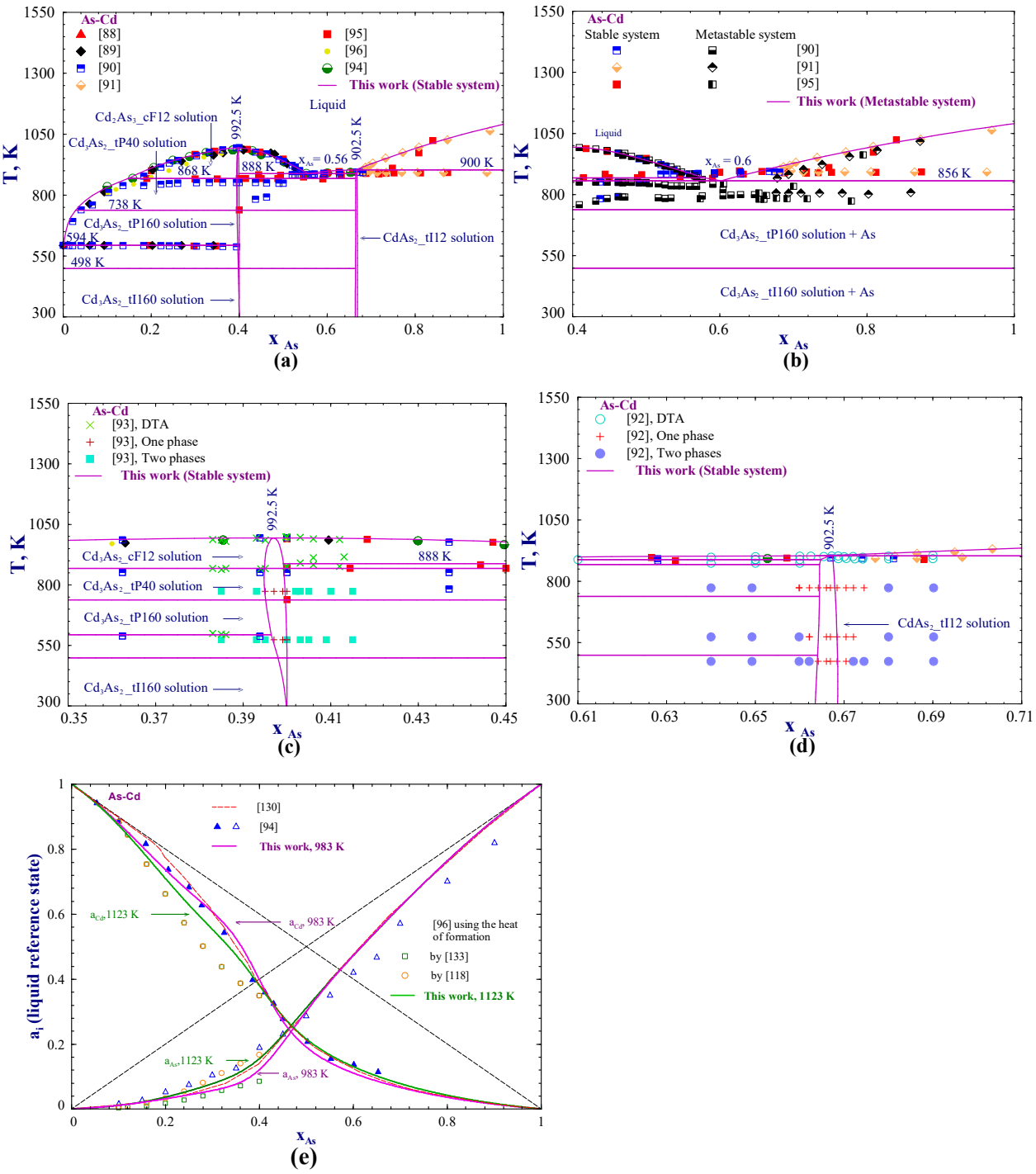

Figure 3.3 a) Calculated As-Cd stable phase diagram, b) calculated As-Cd metastable phase diagram, c) calculated homogeneity region of Cd_3As_2, d) calculated homogeneity region of $CdAs_2$ and e) calculated activities of As and Cd in liquid As-Cd melt, with liquid standard states

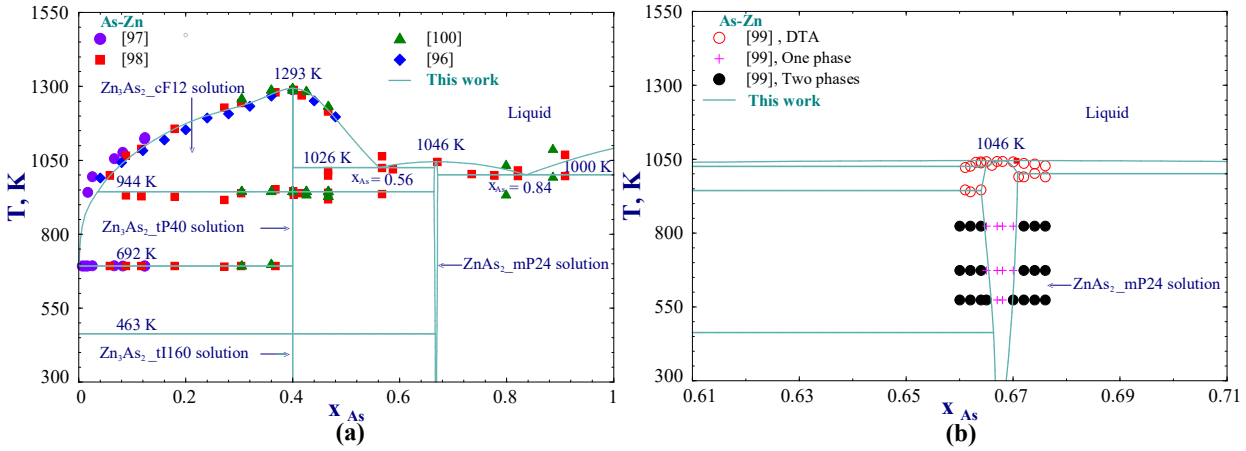

Figure 3.4 a) Calculated As-Zn phase diagram and b) calculated homogeneity region of $ZnAs_2$

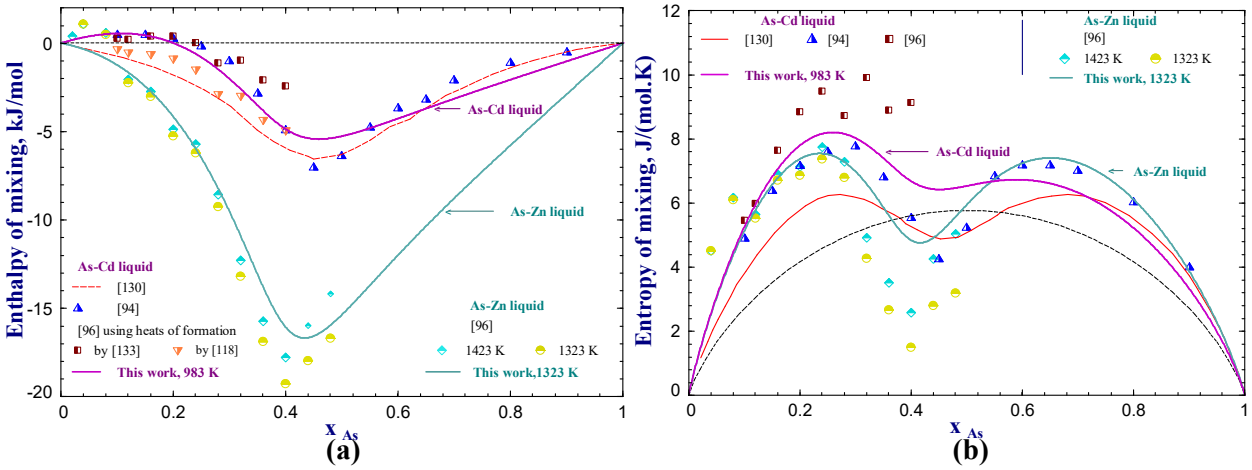

Figure 3.5 a) Calculated integral enthalpy of mixing of liquid in As-Cd and As-Zn systems and b) calculated integral entropy of mixing of liquid in As-Cd and As-Zn system

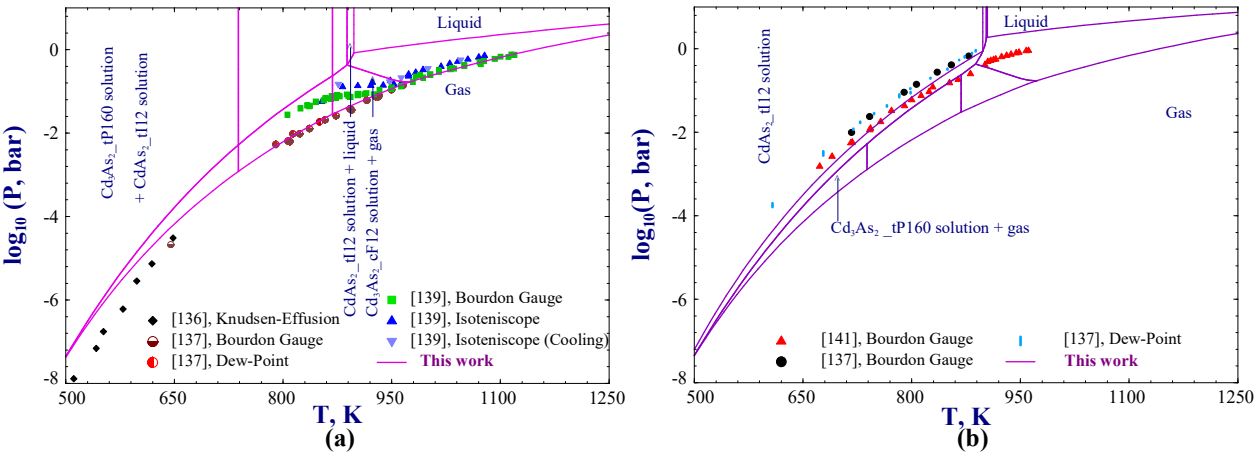

Figure 3.6 Calculated vapor pressures of a) Cd_3As_2 and b) $CdAs_2$ phases

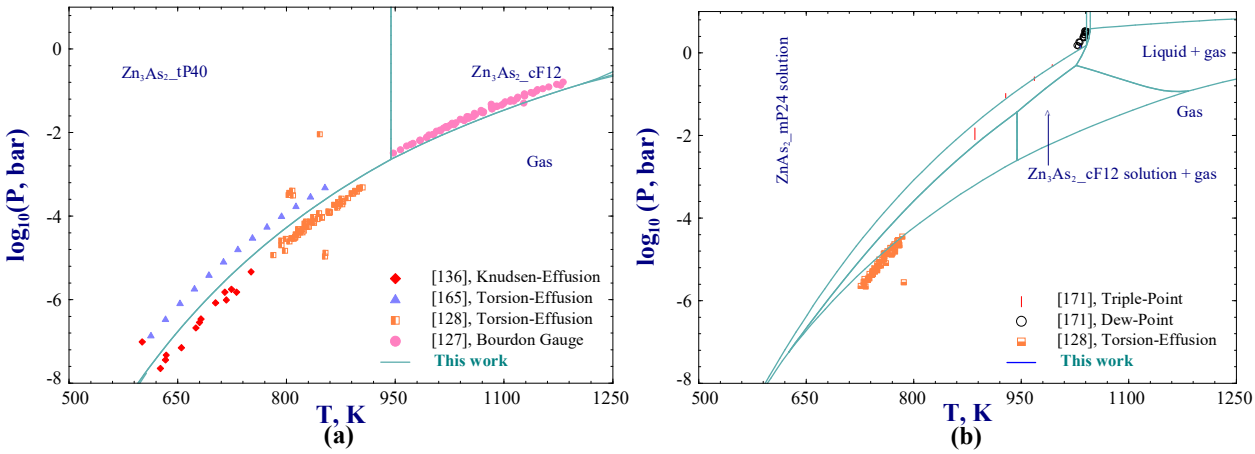

Figure 3.7 Calculated vapor pressures of a) Zn_3As_2 and b) $ZnAs_2$ phase

The predicted vapor pressures of the intermediate compounds are compared to the experimental data in Figure 3.6 and Figure 3.7. For the calculated vapor pressure of Cd_3As_2, the equilibrium includes $CdAs_2$ phase (*tI12*) because of the deviation from stoichiometry at high temperatures discussed previously. Also, there is a disagreement in the data for Zn_3As_2. According to Greenberg et al. [127], the difference is probably due to a non-stoichiometric sublimation.

The As-Cd-Zn system is assessed based on the literature data presented in the previous sections using the Toop interpolation for the liquid solution. The optimized thermodynamic model parameters are presented in Table 3.9. Calculated isopleths of the ternary system are shown in Figure 3.8 and compared with the experimental data. The different phases are identified with their Pearson symbols. Some phases are present at equilibrium in minor quantities and are identified in the Figures with "(minor)". The calculated $ZnAs_2$-$CdAs_2$ and Zn_3As_2-Cd_3As_2 quasi-binary systems are in good agreement with the experimental data. The calculated eutectic temperature is 867 K with a eutectic composition 63 at. % $CdAs_2$. For the pseudo-binary Zn_3As_2-Cd_3As_2, *tI12* and *mP24* solid solutions were found in the phase equilibrium in minor quantities. The superstructure (SS *tP40*) that breaks the continuous $Cd_{3-x}Zn_xAs_2$ solid solutions at low temperatures is also represented.

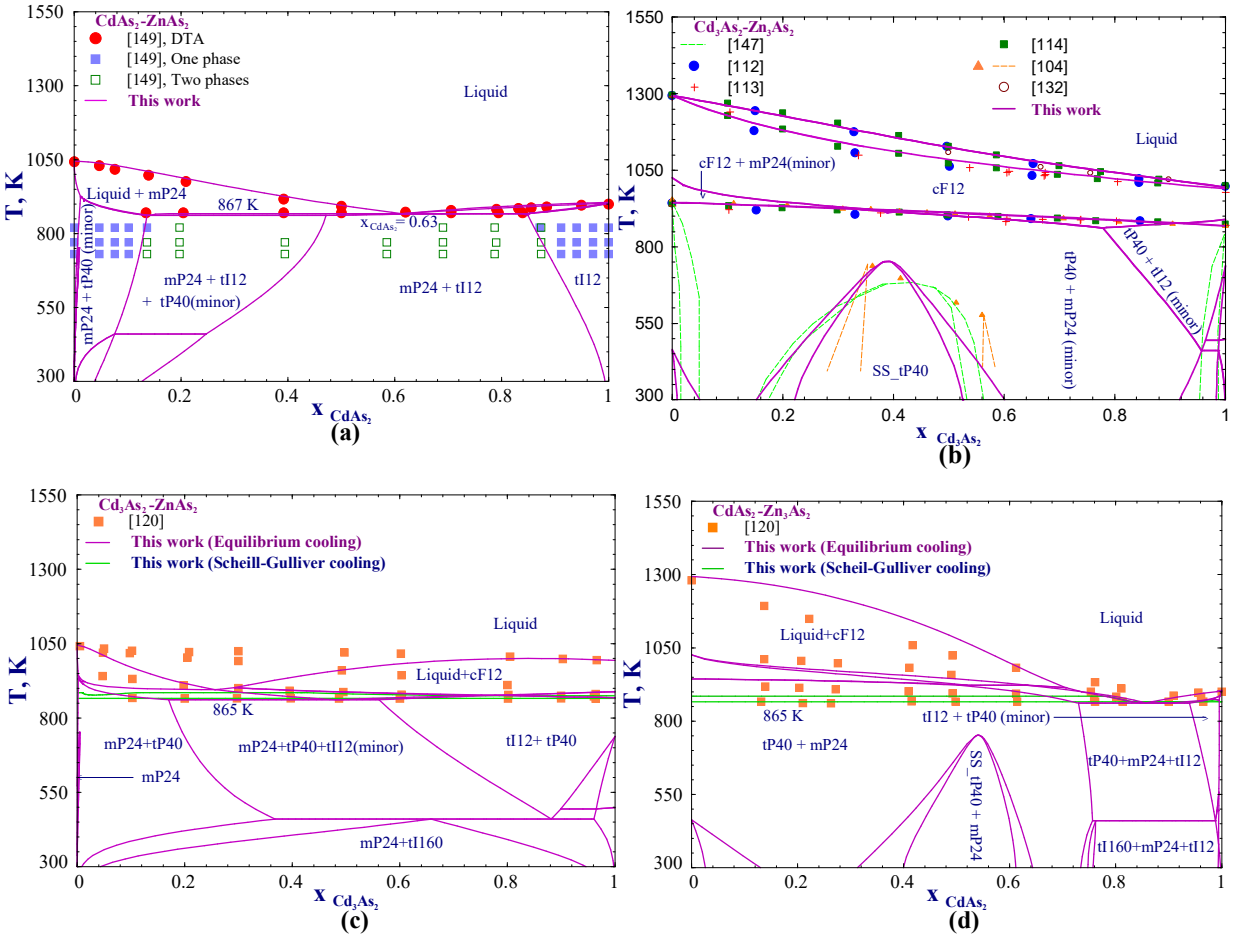

Figure 3.8 Calculated Isopleths of the As-Cd-Zn system: a) $ZnAs_2$- $CdAs_2$ join, b) Zn_3As_2- Cd_3As_2 join, c) $ZnAs_2$- Cd_3As_2 join and d) Zn_3As_2- $CdAs_2$ join

As evident from Figure 3.8, the liquidus in $ZnAs_2$-Cd_3As_2 and Zn_3As_2-$CdAs_2$ joins are not well predicted by the model. Even if the optimized eutectic temperature corresponds to the value measured by Marenkin et al. [120], the crystallization branches calculated for the $ZnAs_2$-Cd_3As_2 are lower than the experimental data, and the $Cd_{3-x}Zn_xAs_2$ crystallization branch in $CdAs_2$-Zn_3As_2 is higher than the experimental data. Since Marenkin et al. [120] used double-walled graphited silica sealed tubes, the data obtained for both these systems appear to be correctly measured. It is likely that the chosen model incorrectly predicts these two joins. The erroneous prediction of these two joins can be explained by the ability of arsenic to be multivalent. In M_3As_2 and MAs_2 ($M = Cd, Zn$), arsenic forms distinct chemical bonds because of its different valence states. When arsenic is monovalent (As^-), each atom forms two single bonds that results in one-dimensional chains. Thus, in MAs_2, arsenic forms an anionic substructure following the Zintl-Klemm concept, resulting

in infinite helical arsenic chains, with tetrahedrally coordinated Cd, Zn and As [172-174]. As_4^{4-} helices were found by Cervinka & Hrubý [86] in crystalline $CdAs_2$, and As_8^{8-} helices were found by Fleet [87] in $ZnAs_2$. The structure of glassy $CdAs_2$ has not been investigated yet but it should be similar to crystalline $CdAs_2$ with a lack of symmetry and periodicity [175]. When arsenic is trivalent arsenic (As^{3-}), as found in M_3As_2, no direct chemical bonds are formed between arsenic atoms [172]. Additionally, the volatilization of elemental arsenic under saturated vapor conditions corresponds to $4As_{(s)} \rightleftharpoons As_{4(g)}$. Other arsenic molecular forms are present under unsaturated vapor conditions ($As_{3(g)}$, $As_{2(g)}$, $As_{(g)}$), with $As_{4(g)}$ remaining as the predominant phase. As the temperature increases, $As_{4(g)}$ decomposes to form mainly $As_{2(g)}$ [176-178]. Since the model used in this work does not consider the complex bonding networks of arsenic, the liquidus in $ZnAs_2$-Cd_3As_2 and Zn_3As_2-$CdAs_2$ joins are not well predicted. The presence of arsenic other than the monomeric form may have to be considered by the model for a more satisfactory prediction of the ternary liquidus surface, even if the binary subsystems are well reproduced by the proposed model. Also, DTA measurements were recorded over the entire composition range at the eutectic temperature in both $ZnAs_2$- Cd_3As_2 and Zn_3As_2-$CdAs_2$ systems. However, the two joins calculated at equilibrium conditions show that the eutectic at 865 K does not extend to all compositions. It is likely that the conditions for measuring the data points approached those of Scheil-Gulliver cooling, represented by the blue curves in the Figures. This type of cooling implies that the solid phases no longer react with the liquid phase and remain unchanged once precipitated. The Gibbs energy change of the following pair-exchange reaction $Cd_3As_2 + ZnAs_2 \rightleftharpoons Zn_3As_2 + CdAs_2$ is positive but quite low (a little less than 50 kJ). This explains the absence of a miscibility gap in the Cd_3As_2-$ZnAs_2$-Zn_3As_2-$CdAs_2$ system. The isotherm at 1123 K is shown in Figure 3.9 along with the Zn iso-activity curves in the liquid state. The calculated curves are in agreement with the experimental curves by Mikula et al. [132]. A summary of the invariant reactions involving four-phase intersection points with liquid in the ternary As-Cd-Zn system is presented in Table 3.10.

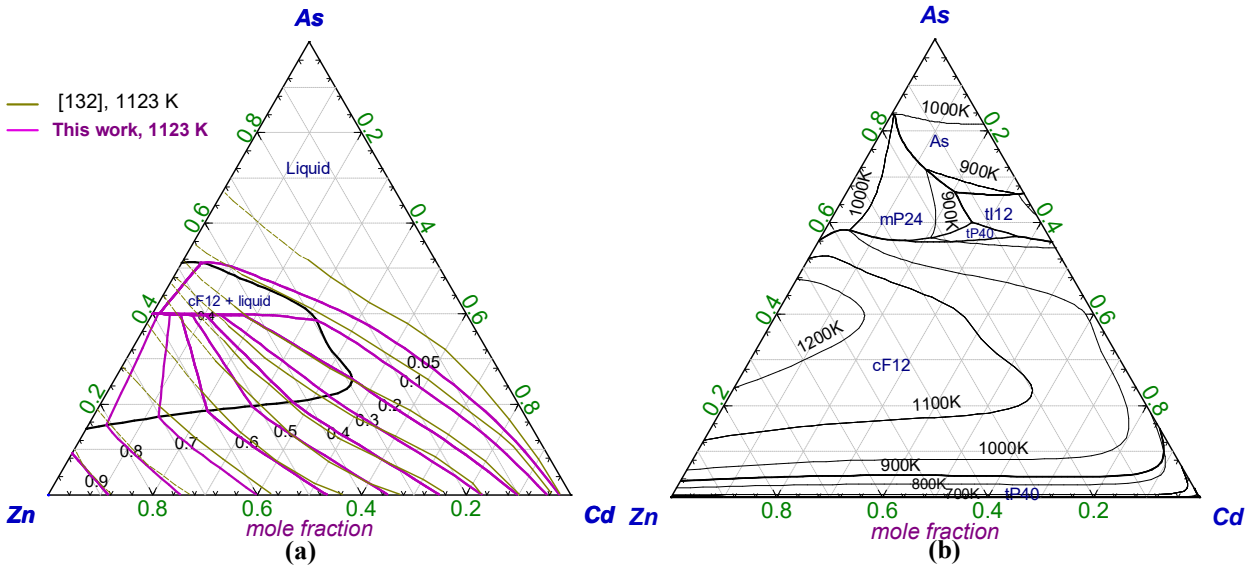

Figure 3.9 a) Calculated isothermal section of the As-Cd-Zn system at 1123 K along with the calculated and the experimental liquid Zn iso-activity curves and b) predicted liquidus projection

Table 3.9 Optimized thermodynamic parameters for the As-Cd, As-Zn and As-Cd-Zn (J mol^{-1})

Phases (model)	**Thermodynamic parameters**	**References**
Liquid (MQM) $(\mathbf{As, Cd, Zn})(\mathbf{Va})$	$Z^{As}_{AsCd} = Z^{As}_{AsZn} = 3$; $Z^{Cd}_{AsCd} = Z^{Zn}_{AsZn} = 2$; $Z^{As}_{AsAs} = Z^{Cd}_{CdCd} = Z^{Zn}_{ZnZn} = 6$	This work
	$\Delta g_{As-Cd} = -16\,623.6037 + 2.6086T + (23\,000 - 18.8400T)X_{CdCd} + (9\,347.8261 - 9.6396T)X_{AsAs} + (-4.8739T)X^3_{CdCd} + (-3\,043.4783)X^3_{AsAs}$	
	$\Delta g_{As-Z} = (-40\,534.2885 + 6T) + (36\,500 - 21.578T)X_{ZnZn}$ (18 900 - 22.1711T+0.35Tln(T))$X_{AsAs} + (-5T)X^3_{ZnZn} + (-7\,000)X^3_{AsAs}$	
	$g^{011}_{ZnAs(Cd)} = -87\,000$	
	$g^{101}_{AsCd(Zn)} = 82\,000$	
	$g^{001}_{ZnAs(Cd)} = -5.5T$	

Phases (model)	Thermodynamic parameters	References
Liquid (B-W) $(\mathbf{Cd, Zn})(\mathbf{Va})$	$L_{Cd-Zn} = (2792.1666 - 0.1597T)Y_{Cd}Y_{Zn} + (-19.4 - 0.1373T)Y_{Cd}Y_{Zn}(Y_{Cd} - Y_{Zn}) + 189.1667Y_{Cd}Y_{Zn}(Y_{Cd} - Y_{Zn})^2$	[80] *
cF12 (CEF) $(\mathbf{Cd, Zn})_3(\mathbf{Va}, \mathbf{Cd})_1(\mathbf{As})_2$	${}^0G_{Cd:Va:As}$=-21900+ 43.618T $+3GHSER_{Cd} +2GHSER_{As}$ ${}^0G_{Zn:Va:As}$=-84800+43.037T$+3GHSER_{Zn} + 2GHSER_{As}$ ${}^0G_{Cd:Cd:As}$==6900+43.6184$+4GHSER_{Cd} + 2GHSER_{As}$ ${}^0G_{Zn:Cd:As}$=-69800+43.037T$+3GHSER_{Cd} + GHSER_{Cd} + 2GHSER_{As}$ ${}^0L_{Cd,Zn:Va:As} = -14000X_{Cd}X_{Zn}$	This work
tP40 (CEF) $(\mathbf{Cd, Zn})_3(\mathbf{Va}, \mathbf{Cd})_1(\mathbf{As})_2$	${}^0G_{Cd:Va:As}$=-21900+43.618T$+3GHSER_{Cd} +2GHSER_{As}$ ${}^0G_{Zn:Va:As}$=-84800+43.037T$+3GHSER_{Zn} + 2GHSER_{As}$ ${}^0G_{Cd:Cd:As}$=-6900+43.6184T$+4GHSER_{Cd} + 2GHSER_{As}$ ${}^0G_{Zn:Cd:As}$=69800+43.037T$+3GHSER_{Zn} + GHSER_{Cd} + 2GHSER_{As}$ ${}^0L_{Cd,Zn:Va:As} = -15000X_{Cd}X_{Zn}$	This work
SS_ tP40 (CEF) $(\mathbf{Cd, Zn})_2(\mathbf{Cd, Zn})_1(\mathbf{Va})_1(\mathbf{As})_2$	${}^0G_{Cd:Cd:Va:As}$=-21900+43.618T$+3GHSER_{Cd} +2GHSER_{As}$ ${}^0G_{Cd:Zn:Va:As}$=-26900-226.779T$+2GHSER_{Cd} +GHSER_{Zn} + 2GHSER_{As}$ ${}^0G_{Zn:Cd:Va:As}$=-69600-188.869T $+2GHSER_{Zn} + GHSER_{Cd} - GHSER_{Zn}$ ${}^0G_{Zn:Zn:Va:As}$=-84800+43.037T$+3GHSER_{Zn} +2GHSER_{As}$ ${}^0L_{Zn:Cd,Zn:Va:As} = 2505X_{Cd}X_{Zn}$	This work

Phases (model)	Thermodynamic parameters	References
tP160 (CEF) $(\mathbf{Cd, Zn})_3(\mathbf{Va}, \mathbf{Cd})_1(\mathbf{As})_2$	${}^0G_{Cd:Va:As}$=-21900+43.618T+3GHSER$_{Cd}$ +2GHSER$_{As}$ ${}^0G_{Zn:Va:As}$=-84800+43.037T+3GHSER$_{Zn}$ +2GHSER$_{As}$ ${}^0G_{Cd:Cd:As}$=-6900+43.6184T+4GHSER$_{Cd}$ + 2GHSER$_{As}$ ${}^0G_{Zn:Cd:As}$=-69800+43.037T+3GHSER$_{Zn}$ + GHSER$_{Cd}$ + 2GHSER$_{As}$	This work
tI160 (CEF) $(\mathbf{Cd, Zn})_3(\mathbf{Va}, \mathbf{Cd})_1(\mathbf{As})_2$	${}^0G_{Cd:Va:As}$=-21900+43.618T+3GHSER$_{Cd}$ +2GHSER$_{As}$ ${}^0G_{Zn:Va:As}$=-84800+43.037T+3GHSER$_{Zn}$ +2GHSER$_{As}$ ${}^0G_{Cd:Cd:As}$=-6900+43.6184T+4GHSER$_{Cd}$ + 2GHSER$_{As}$ ${}^0G_{Zn:Cd:As}$=-69800+43.037T+3GHSER$_{Zn}$ + GHSER$_{Cd}$ + 2GHSER$_{As}$	This work
tI12 (CEF) $(\mathbf{Cd, Zn})_1(\mathbf{Va, Cd, As})_1(\mathbf{As, Va})_2$	${}^0G_{Cd:Va:As}$ =-25600 − 2.833T + GHSER$_{Cd}$ +2GHSER$_{As}$ ${}^0G_{Cd:Va:Va}$ = 70000 + GHSER$_{Cd}$ ${}^0G_{Cd:Cd:As}$ =-15600 − 2.833T + 2GHSER$_{Cd}$ + 2GHSER$_{As}$ ${}^0G_{Cd:Cd:Va}$ = 90000 − 51.8T + 2GHSER$_{Cd}$ ${}^0G_{Cd:As:As}$ = 5400 − 116.319T + GHSER$_{Cd}$ + 3GHSER$_{As}$ ${}^0G_{Cd:As:Va}$ = 64400 − 44.940T + GHSER$_{Cd}$ + GHSER$_{As}$ ${}^0G_{Zn:Va:As}$ =-55300 − 12.009T + GHSER$_{Zn}$ + 2GHSER$_{As}$ ${}^0G_{Zn:Va:Va}$ = 100000 + 41.63T + GHSER$_{Zn}$ ${}^0G_{Zn:Cd:As}$ =-22600 − 51.8T + GHSER$_{Zn}$ + GHSER$_{Cd}$	This work

Phases (model)	Thermodynamic parameters	References
	${}^{0}G_{Zn:Cd:Va} = 60000 + GHSER_{Cd} + GHSER_{Zn}$ ${}^{0}G_{Zn:As:As} = 7200 + 12.009T + GHSER_{Zn} + 3GHSER_{As}$ ${}^{0}G_{Zn:As:Va} = 22200 + 59.37T + GHSER_{Zn} + GHSER_{As}$ ${}^{0}L_{Cd:Va,As:As} = (-30000 + 20.89T)X_{Va}X_{As}$ ${}^{0}L_{Cd:Va,Cd:As} = (-28000 + 17.89T)X_{Va}X_{Cd}$ ${}^{0}L_{Cd,Zn:Va:As} = -1500X_{Cd}X_{Zn}$	
mP24 (CEF) $(\mathbf{Zn, Cd})_1(\mathbf{Va, As})_1(\mathbf{As, Zn})_2$	${}^{0}G_{Zn:Va:As} = -67800 + 12.009T + GHSER_{Zn} + 2GHSER_{As}$ ${}^{0}G_{Zn:Va:Zn} = 25000 + 3GHSER_{Zn}$ ${}^{0}G_{Zn:As:As} = -47800 - 113.009T + GHSER_{Zn} + 3GHSER_{As}$ ${}^{0}G_{Zn:As:Zn} = 90000 + 3GHSER_{Zn} + GHSER_{As}$ ${}^{0}G_{Cd:Va:As} = -15600 + 2.833T + GHSER_{Cd} + 2GHSER_{As}$ ${}^{0}G_{Cd:Va:Zn} = 70000 + 2GHSER_{Zn} + GHSER_{Cd}$ ${}^{0}G_{Cd:As:As} = 24400 - 38.523T + GHSER_{Cd} + 3GHSER_{As}$ ${}^{0}G_{Cd:As:Zn} = 70000 + GHSER_{Cd} + GHSER_{As} + 2GHSER_{Zn}$ ${}^{0}L_{Zn:Va,As:Zn} = (-75000 + 27.9855T)X_{As}X_{Zn}$ ${}^{0}L_{Zn:Va,As:As,} = (-18000 + 25.2002T)X_{Va}X_{As}$ ${}^{0}L_{Zn,Cd:Va:As} = (-5000 + 9.8619T)X_{Zn}X_{Cd}$	This work
FCC_A1 (B-W)	${}^{0}L_{Cd,Zn:Va} = 15000X_{Cd}X_{Zn}$	[80]

Phases (model)	Thermodynamic parameters	References
$(\mathbf{Cd,Zn})_1(\mathbf{Va})_1$		
BCC-A2 (B-W)	${}^0L_{Cd,Zn:Va} = 100000X_{Cd}X_{Zn}$	[80]
$(\mathbf{Cd,Zn})_1(\mathbf{Va})_3$		
HCP-A3 (B-W)	${}^0L_{Cd,Zn:Va} = (17845.8 - 0.639T)X_{Cd}X_{Zn}$	[80]
$(\mathbf{Cd,Zn})_1(\mathbf{Va})_{0.5}$	${}^1L_{Cd,Zn:Va} = (-7167.4 + 7.955T)X_{Cd}X_{Zn}(X_{Cd} - X_{Zn})$	

*Parameters converted according to the MQM.

Table 3.10 Summary of calculated invariant reactions involving the liquid phase in the ternary As-Cd-Zn system

Reactions			Temperatures
at. % As	**at. % Cd**	**at. % Zn**	**K (°C)**
Liquid +As ⇌ tI12+mP24			
0.666	0.205	0.1290	867.16 (594.01)
Liquid ⇌ mP24 + tP40 + tI12			
0.600	0.270	0.129	860.88 (587.73)
Liquid + mP24 + cF12 ⇌ tP40			
0561	0.162	0.277	922.31 (649.16)
Liquid + cF12 ⇌ tP40+ tI12			
0.570	0.373	0.057	875.97 (602.82)

3.5 Conclusion

To ensure the viability of smelters in the future, the use of arsenic-rich concentrates should be considered. The challenge with using this type of concentrate is the reduction of arsenic and cadmium emissions caused by the smelting process. The development of thermodynamic models and their associated databases presented in this work is essential to understand the interaction of arsenic with other metals. To obtain thermodynamic model parameters for As-Cd and As-Zn binary systems, the thermodynamic information available in the literature was critically evaluated and optimized in this work. Both binary systems are highly ordered. To describe the SRO, the Modified Quasichemical Model in the Pair Approximation was used to model the liquid phase, and the

Compound Energy formalism was used to model the solid solutions. The calculated phase diagrams and thermodynamic properties are accurate in describing all the reliable experimental data in both binary systems. Using the Toop interpolation, the As-Cd-Zn ternary system was also assessed. It was not possible to reproduce the ternary As-Cd-Zn liquidus surface over the entire composition and temperature ranges with a relatively small number of parameters. $ZnAs_2$-$CdAs_2$ and Zn_3As_2-Cd_3As_2 joins are correctly reproduced. However, the liquidus of the $ZnAs_2$-Cd_3As_2 and Zn_3As_2-$CdAs_2$ joins are less satisfactory even if the eutectic temperature was optimized. Since the aim is to generate a database which describes the thermodynamic interaction of arsenic with transition metals found in complex concentrates, it is essential to consider the complexity of the behavior of arsenic. To comply with the standard CALPHAD approach, the model used in this work considers liquid arsenic only in its monomeric form. In order to improve the model, it may be necessary to consider more closely the various polymeric forms of liquid arsenic.

Acknowledgments

The authors would like to thank the financial support from NSERC and CRC programs.

Conflict of Interest: The authors declare that they have no conflict of interest.

CHAPITRE 4 ARTICLE 2: THERMODYNAMIC EVALUATION AND OPTIMIZATION OF THE AG-AS-S SYSTEM

Oumaima Kidari[2] and Patrice Chartrand

Center for Research in Computational Thermochemistry (CRCT) - Polytechnique Montréal, Chemical Engineering, Box 6079, Station Downtown, Montréal, Québec, Canada, H3C 3A7.

Article submitted for publication in "Journal of Phase Equilibria and Diffusion" on February 25, 2023

Abstract: A critical evaluation of all available phase diagram and thermodynamic data has been performed for Ag-As, Ag-S, As-S and Ag-As-S systems, including a detailed review of the gaseous species involved in the As-S system. Thermodynamic assessments over the whole composition range for these four systems are presented using the CALPHAD method. To predict thermodynamic properties and phase equilibria, the Modified Quasichemical Model (MQM) for short range ordering (SRO) was used for the liquid phases, and the Compound Energy Formalism (CEF) was used for the solid solutions. For the As-S binary system, natural logarithm terms for the temperature dependence of the excess Gibbs energy of the liquid solution have been used. This led to a significant improvement compared with the previous assessment of this system. The optimization of Ag-As-S systems is in good agreement with the existing experimental data.

Keywords: Thermodynamic modeling, Modified Quasichemical Model, CALPHAD, Arsenic, Speiss.

4.1 Introduction

Over the last decades, the demand for various metals has increased rapidly leading to a growth in their production. The high demand is accompanied by a gradual decline in high-grade ores treated

[2] Corresponding author
E-mail address: oumaima.kidari@polymtl.ca

in smelters and an evident rise in complex ores containing high arsenic contents [13, 179, 180]. This is concerning since arsenic is a toxic impurity that contaminates the surrounding environment and increases the risk of developing health problems [24]. To help the industry develop solutions to overcome the arsenic emission problem, the thermodynamic interaction between arsenic and other elements contained in ores entering the smelting process must be understood. Many transition metal sulfides are found in complex ores, particularly Ag_2S. which is most often associated with lead ores and can also be found in small amounts in copper ores [181]. Ag_2S is important for many operations like the manufacturing of photovoltaic cells and it can also be utilized as an electrode material for various applications [182, 183]. To study complex systems contained in sulfide ores, it is necessary to develop thermodynamic models of compounds and mixtures for Ag-As-S systems and their associated databases. In this work, the available experimental data of Ag-As, Ag-S, As-S and Ag-As-S systems are critically evaluated, and a set of model parameters is optimized for each system to predict thermodynamic properties and phase equilibria. The Modified Quasichemical Model in the Pair Approximation suggested by Pelton et al. [65, 66] was used for the liquid phases, and the Compound Energy Formalism (CEF) suggested by Sundman and Ågren [77] was used for solid solutions. All calculations and optimizations in this work were performed with the FactSage thermochemical software [45, 46]. The obtained results are compared with previous evaluations of Ag-As and Ag-S systems by Shi et al. [184] and As-S system by Prostakova et al. [185].

4.2 Literature review

4.2.1 Experimental determination of Ag-As binary phase diagram

The Ag-As binary system has a single intermediate hcp phase. The experimental studies measuring phase diagram data of this binary system are presented in Table 4.1. Details of these studies are

also discussed and reviewed in this section. Two other studies, by Descamps in 1878 [186] and by Friedrich and Leroux in 1906 [187] were considered obsolete by Hansen & Anderko [188] and were not considered in his compiled phase diagram. These two studies were also not examined in this work.

Table 4.1 Ag-As phase diagram data reported in the literature

References	Experimental methods and results
[189]	**TA and microstructural analysis:** Determination of the phase diagram for the entire composition range.
[190]	**X-ray diffraction:** Determination of the solid solubility of As in Ag and the stability compositions of the hcp solid solution (ξ).
[191]	**X-ray diffraction:** Determination of the solid solubility of As in Ag.
[192]	**X-ray diffraction:** Determination of the solid solubility of As in Ag.
[193]	**TA, microstructure analysis and X-ray diffraction:** Determination of the phase diagram up to a composition of 20 at. % As.
[194]	**X-ray diffraction:** Determination of the stability compositions of the hcp solid solution (ξ).
[195]	**X-ray diffraction and microscopic method:** Determination of the stability compositions of the hcp solid solution (ξ).

Ag-As system

Solid solubility: According to the phase diagram proposed by Heike and Leroux [189], the maximum solubility of arsenic in silver is constant at 7 at. % As at all temperatures below 868 K. Measurements made by Owen and Rowlands [191] and Owen and Morris [192] show that there is a variation in the maximum solubility of As in Ag as a function of temperature, between approximately 4.5 at. % As at 573 K to 8.8 at. % As at 868 K. The results of Eade and Hume-Rothery [193] confirm the variation in maximum solubility as a function of temperature. However, the proposed maximum solubility is about 0.3 at. % As lower than the values of Owen and

Rowlands [191] at 573 K and about 1 at. % As lower at higher temperatures. For the solid solubility of Ag in As, it has been concluded by Heike and Leroux [189] and Broderick and Ehret [190] that the solubility of silver in arsenic is negligeable. Eutectic: According to Heike and Leroux [189], the eutectic reaction takes place at a temperature of 813 K and a composition of 25.3 at. % As to form solid As and an hcp phase (ξ). Liquidus: Liquidus curves on the silver-rich side have been determined by Heike and Leroux [189] and Eade and Hume-Rothery [193] and they are in good agreement. The liquidus curve on the arsenic-rich side has also been measured by Heike and Leroux [189] under pressure.

Hcp phase (ξ)

The Ag-As system contains a single hcp phase (ξ). The phase is stable from 647 K (Ag + As ⇌ ξ) to 868 K (Liquid + Ag⇌ ξ) according to Heike and Leroux [189], with a likely composition of 10.5 at. % As. However, Broderick and Ehret [190] reported a eutectoid temperature greater than 663 K, which does not agree with the temperature measured by Heike and Leroux [189]. The eutectoid temperature according to Eade and Hume-Rothery [193] takes place between 716 K and 723 K and the peritectic temperature between 852 K and 858 K, in contrast with the results of Heike and Leroux [189]. At 813 K, King and Massalski [194] measured the compositions of 10.5 and 12.5 at. % As as the limits of the ξ phase. Hall [195] could not accurately measure the limits of the ξ phase but proposed that it corresponds to a formula of Ag_9As. Hall [195] was also able to find that the phase is not stable below 729 K, contrary to the temperature reported by Heike & Leroux [189]. No thermodynamic information has been reported for this phase.

4.2.2 Experimental determination of thermodynamic properties of Ag-As binary system

For temperatures between 791.8 K and 932.1 K, Ludecke et al. [196] used the pseudo-isopiestic method to measure the vapor pressure above Ag-As alloys for compositions up to 8 at. % As. The data was then used to determine the activity of As in solid Ag-As alloys, with respect to solid As as the standard state. It was concluded that As and As_3 molecules are not present in the vapor. Additionally, it was observed that the vapor above the very low-concentrated alloys consists mainly of As_2 molecules, and as the alloy composition in As increases, As_4 molecules become increasingly dominant in the vapor.

4.2.3 Experimental determination of Ag-S binary phase diagram

The Ag-S binary system forms two fields of liquid immiscibility, as well as an intermediate compound, Ag_2S, stable at ambient pressure. Jeannot et al. [197] also reported the existence of another compound, Ag_4S, at temperatures below 700 K. Kracek [198] is the only one to have measured the Ag_2S-S subsystem, and his work is accurate according to Hansen [188]. The experimental studies measuring phase diagram data are summarized in Table 4.2 and discussed in detail in this section.

Ag-Ag_2S subsystem

Solid solubility: The experiments by Friedrich and Leroux [199] show that the solid solubility of sulfur in silver is very small, probably less than 0.17 at. % S. The solid solubility has been measured subsequently by Barbouth and Oudar [200], Raub and Roschel [201] and Fueki et al. [202]. As shown in Figure 4.2, the data obtained by Raub and Roschel [201] are in very good agreement with those of Fueki et al. [202]. However, the measurements performed by Barbouth and Oudar [200] show a lower solubility. Monotectic: The Ag-Ag_2S subsystem forms a miscibility gap and the

meaured monotectic temperatures are in excellent agreement: 1177 K by Bisset [203], 1178 K by Friedrich and Leroux [199] and Jaeger and Klooster [204], and 1179 $\pm$ 1 K by Kracek [198]. The boundary of the miscibility gap was determined by Rosenqvist [205] and Fukatu and Kozula [206]. The boundary proposed by Fukatu and Kozula [206] is slightly wider on the silver rich side. The critical temperature is 1398 $\pm$ 25 K according to Rosenqvist [205]. Eutectic : The eutectic reaction that forms Ag and Ag_2S lies at approximately 32 at.% S at a temperature of 1080 K by Friedrich and Leroux [199], 1079 K by Jaeger and Klooster [204], 1077 K by Bissett [203] and 1077 $\pm$ 2 K by Kracek [198]. Liquidus: The liquidus curves measured by by Friedrich and Leroux [199], Jaeger and Klooster [204], Bisset [203], Kracek [198], Rosenqvist [205] and Fukatu and Kozula [206] are in very good agreement. Contrary to what was stated by Jeannot et al. [197], no indication of Ag_4S was found [203].

Table 4.2 Ag-S phase diagram data reported in the literature

References	Experimental methods and results
[199]	**TA and metallography:** Determination of the phase diagram up to a composition of 33 at. % S.
[204]	**TA:** Determination of the phase diagram up to a composition of 33 at. % S.
[203]	**TA and microphotography:** Determination of the phase diagram up to a composition of 33 at. % S.
[198]	**TA and DTA:** Determination of the phase diagram for the entire composition range.
[205]	**Gaz-metal equilibria:** Determination of the liquidus and the phase boundary of the miscibility gap between compositions of 5 and 31 at. % S.
[207]	**Emf:** Determination of the solubility of Ag in Ag_2S between 433 K and 573 K.
[200]	**Tracer method with the radio isotope ^{35}S:** Determination of the solid solubility of S in Ag.

References	Experimental methods and results
[201]	**Microscopic investigations, conductivity measurements and sulfide formation temperature measurements:** Determination of the solid solubility of S in Ag.
[208]	**H_2S/H_2 method and dew point method:** Determination of the homogeneity range of Ag_2S.
[209]	**Emf:** Determination of the homogeneity range of Ag_2S between 296 K and 449 K.
[210]	**Emf:** Determination of the homogeneity range of Ag_2S between 466 K and 823 K.
[202]	**Coulometric method:** Determination of the solid solubility of S in Ag**.**
[211]	**Dew point method:** Determination of the solubility of S in Ag_2S between 503 K and 742 K.
[212]	**Electrochemical investigation:** Determination of the solubility limit of Ag_2S at 723 K.
[206]	**Emf:** Determination of the eutectic temperature, the monotectic temperature and the phase boundary of the miscibility gap up to a composition of 32 at. %.

Ag_2S- S subsystem

Solid solubility: No information has been reported regarding the solid solubility of silver in sulfur. It is most likely to be negligeable according to [213]. Monotectic: The Ag_2S-S subsystem forms a miscibility gap and the monotectic temperature is 1013 K according to Kracek [198] and 1017 K according to Rau [208]. There has been no experimental determination of the phase boundary of the miscibility gap. Eutectic: The eutectic reaction that forms S and Ag_2S occurs at a temperature of 392 K according to Kracek [198].

Ag_2S compound

The natural form of Ag_2S is acanthite with a monoclinic structure. A reversible polymorphic transformation takes place to form argentite which has a body centered cubic structure (bcc) [214]. In mineralogy, argentite refers to a pseudomorph of acanthite after argentite [215]. A third polymorphic transformation takes place to form a face-centered cubic phase (fcc) [216]. The transformation temperatures reported in the literature for are shown in Table 4.3. The transformation temperatures of Ag_2S vary with composition, especially at higher temperatures, which indicates its non-stoichiometry. According to the experiments performed by Kracek [198], the Ag_2S compound undergoes the first polymorphic transformation at a temperature of 450.8 ± 0.7 K with excess sulfur and 449.3 ± 0.5 K with excess silver. The second polymorphic transformation varies largely with composition: 895 ± 3 K with excess sulfur and 859 ± 3 K with excess silver [198]. Ag_2S melts congruently and the reported melting temperatures are also presented in Table 4.3. According to Hansen and Anderko [188], the lower values of the melting point reported can be explained by the insufficient protection against oxidation or a small excess of silver or sulfur. A narrow Ag_2S homogeneity range is suggested, and the different results are in very good agreement. Wagner [207] determined the solubility of Ag in Ag_2S by meausring the emf of the cell $Ag/AgI/Ag_2S/Pt$ for temperatures from 433 K to 573 K. Using the H_2S/H_2 and the dew point methods, Rau [208] constructed a defect model from S_2 fugacity measurements and calculated the complete homogeneity range of Ag_2S. Bonnecaze et al. [209, 210] also determined the homogeneity range from 296 K to 449 K and 466 K to 823 K, and the non stoichiometry was controled by coulometry using the battery $Ag/RbAg_4I_5/Ag_{2+e}S/Pt$. Ditman and Kulikova [211] determined the excess sulfur that Ag_2S can solubilize by dew point method at temperatures of 503 ± 10 K and 743 ± 25 K. Finally, Mitteilung [212] determined by an electrochemical

investigation the solubility limit of Ag_2S at a temperature of 723 K. The various results agree that the low temperature form has nearly an ideal stoichiometric composition.

Table 4.3 Measured temperatures and heats of transformation of Ag_2S

References	**Experimental methods**	**Temperatures, in K (in °C)**	**$\Delta H_{transformation}$, in kJ/mol**
		$\mathbf{Ag_2S_{(mP12)} \rightarrow Ag_2S_{(I20)}}$	
[217]	Calorimetry	448 (175)	3.98 ± 0.04
[199]	TA	448 (175)	-
[204]	TA	448 (175)	-
[218]	TA	448 (175)	-
[219]	XRD	453 (180)	-
[220]	P-T studies, Clausius-Clapeyron	449 (176)	6.38 ± 2
[221]	Adiabatic calorimetry	450 (177)	$3.98 \pm 0.4^{\text{Stoichiometric}}$ $6.48 \pm 0.4^{\text{Non-stoichiometric}}$
[222]	DTA and thermographic analysis	441 (168) - 453 (180)	4.37
[223]	Drop calorimetry	449 (176)	3.93 ± 0.20
[224]	Adiabatic calorimetry	449.3 (176.3)-451.3 (178.3)	4.045
[225]	DTA	448 (175)	-
[226]	DTA	458 (185)	-
[227]	DTA	449 (176)-450 (177)	3.7-3.9
[228]	DSC and dilatometry	$452 (179) \pm 1$	4.2 ± 0.4
[229]	XRD	440 (167)-442 (169)	-
This work	-	450 (177)	3.987
		$\mathbf{Ag_2S_{(cI20)} \rightarrow Ag_2S_{(cF44)}}$	
[223]	Drop calorimetry	859 (586)	0.50 ± 0.54
[224]	Adiabatic calorimetry	865 (592)	0.784 ± 0.005

References	Experimental methods	Temperatures, in K (in °C)	$\Delta H_{transformation}$, in kJ/mol
[226]	DTA	867 (594)	-
[228]	DSC and dilatometry	863 (590)±1	1.2±0.3
[229]	XRD	850 (577)-860 (587)	-
[230]	Adiabatic scanning calorimetry	859 (586)	0.774
This work	-	860 (587)-895 (622)	0.749
	$\mathbf{Ag_2S_{(cF44)} \rightarrow Ag_2S_{(liquid)}}$		
[231]	TA	1098 (825)	-
[218]	TA	1107 (834)	-
[232]	Freezing-point-depression	1111 (838)	14.23
[223]	Drop calorimetry	1103 (830)	7.87 ± 0.6
[233]	Adiabatic calorimetry	1113 (840) ± 2	7.66 ± 0.23
[224]	Adiabatic calorimetry	1109 (836)	-
This work	-	1117 (898)	15.7

The heat of formation of Ag_2S determined using a variety of techniques are listed in Table 4.4 and are in good agreement. Certain values were obtained by evaluation of the third law of galvanic cell data and equilibrium data for the following reactions:

$$2Ag_{(s)} + H_2S_{(g)} \rightleftharpoons Ag_2S_{(s)} + H_{2(g)} \quad (4.1)$$

$$2Ag_{(s)} + S_{(l)} \rightleftharpoons Ag_2S_{(s)} \quad (4.2)$$

Several studies have been conducted to measure the heat capacity of Ag_2S phases, and some results do not agree. Over the range 323 K to 673 K, Perrott and Fletcher [221] measured the heat capacity of the stoichiometric Ag_2S using adiabatic calorimetry. They also measured the heat capacity of non-stoichiometric Ag_2S containing 1 mole % excess silver or 1 mole % excess sulfur. The absolute

accuracy of their measurements was estimated as ± 10%. As can be seen from Figure 4.4, the data measured for the stoichiometric compound differ greatly from the other measurements. The main difference comes from an additional transition reported at 623 K. This was explained by the partial disordering of the stoichiometric compound, analogous to that observed for AgI. Grønvold and Westrum [224] rejected this explanation and suggested that this non reproducible transition might be associated with the presence of another phase in their sample. The heat capacity of Ag_2S was also measured using calorimetry by Bellati and Lussana [217] for temperatures from 320 K to 490 K, by Gultyaev and Petrov [234] from 80 K to 300 K, by Walsh et al. [235] from 13 K to 296 K, and by Jost and Kubaschewski [236] from 200 K to 300 K. Okazaki and Takano [230] also measured the heat capacity using adiabatic scanning calorimetry from 350 K à 1200 K. Thompson and Flengas [223] also determined the heat capacity from 448 K to 997 K using drop calorimetry. Grønvold and Westrum [224] performed the measurements from 5 K to 1000 K using adiabatic-shield calorimetry with a sample with a stoichiometric composition and a sample with $Ag_2S_{1.0526}$ composition. The results of both samples agree and only the values obtained for the stoichiometric composition are shown in Figure 4.4. Gusev and Sadovniko [228] measured the heat capacity for a coarse-crystalline sample and for nanoparticles. The difference in particle size showed different heat capacity values. A good agreement was obtained between the results of Thompson and Flengas 1971 [223], Grønvold and Westrum [224], and Gusev and Sadovnikov [228], showing a slight decrease over the range of 460 K to 620 K. The experimental data of Grønvold and Westrum [224] are the most reliable according to Sadonikov and Gusev [237]. The standard entropy obtained from low temperature heat capacity measurements and second law evaluation of galvanic cell measurements are presented in Table 4.4.

Table 4.4 Standard thermodynamic properties of Ag_2S reported in the literature

References	**Methods**	$\Delta H^{\circ}_{formation}$ **kJ mol^{-1}**	S° **J mol^{-1}K^{-1}**	C_p **J mol^{-1}K^{-1}**
[238]	Equilibrium	-29.29	-	-
[239]	Equilibrium	-28.90	-	-
[240]	Emf	-33.05	-	-
[241]	Calorimetry	-27.61	-	-
[205]	Equilibrium	-30.54	-	-
[242]	Emf	-32.13	138.07	-
[243]	Equilibrium	-29.29	-	-
[244]	Emf	-31.59	142.67	-
[234]	Calorimetry	-	141	92
[235]	Calorimetry	-	143.51	81.46
[245]	Equilibrium	28.45	-	-
[197]	Equilibrium	31.38	--	-
[224]	Adiabatic calorimetry	-	142.89$\pm$0.44	75.31
[246]	High temperature calorimetry	- 31.21$\pm$0.7	-	-
This work	-	-32.59	144.01	75.24

According to the mass spectroscopic studies of Glazov and Korenchuk [247] and Dutchak et al. [248], Ag_2S thermally decomposes according to the following reaction:

$$Ag_2S_{(s,l)} \rightleftharpoons 2\,Ag_{(s,l)} + \frac{1}{2}S_{2(g)} \tag{4.3}$$

Vapor pressure measurements were also performed using the Knudsen effusion method. Piacente et al [249] also measured the vapor pressure using torsion and Knudsen effusion methods and found no significant difference using cells of different materials (graphite, pyrophyllite and quartz). Smith and Smeltzer [250] carried sulfidation tests of iron using Ag_2S and reported a P_{S_2} value for a temperature of 1023 K. The vapor pressure data is presented in Figure 4.2.

4.2.4 Experimental determination of thermodynamic properties of Ag-S binary system

Rosenqvist [205] determined the partial pressure of S_2 by measuring the ratio H_2S/H_2 of the gas in equilibrium with Ag-S alloys. The measurements were performed for alloys with compositions up to 33.3 at. % S, between 773 K and 1573 K, according to the following equilibrium:

$$2H_2S \rightleftharpoons 2H_2 + S_2 \tag{4.4}$$

The composition of the gas mixture was determined from its density obtained by magnetic balancing. Fukatsu and Kozuka [206] determined the emf for the following cell: $Pt, Air|ZrO_2(+CaO)|$Ag-S, $SO_2, Ir, Kanthal$, and from the measured oxygen partial pressures, the partial pressure of S_2 was calculated between 867 K and 1538 K, for compositions up to 32 at. % S. Yazawa, et al. [251] also measured the partial pressure of sulfur over Ag-S liquid alloys up to 33 at. % S. The measurements were performed between 1273 K and 1473 K by bubbling nitrogen through the melt, and the sulphur content was determined by chemical analysis. The different measurements of the partial pressure of S_2 are in good agreement.

4.2.5 Experimental determination of As-S binary phase diagram

The As-S binary system contains three stoichiometric intermediate compounds stable at ambient pressure: As_2S_3, As_4S_4 et As_4S_3. Phase diagram data for this binary system are challenging to measure. For compositions lower than 45 at. % As, the measurements are hard to record due to the

glass formation tendency of the alloys. And for compositions higher than 45 at. % As, the thermodynamically stable As_4S_3 tends to not crystallize from synthetic melts, creating a metastable system. The experimental studies measuring phase diagram data are summarized Table 4.5 and discussed in detail in this section.

Table 4.5 As-S phase diagram data reported in the literature

References	Experimental methods and results
[252]	**TA, analytical and quantitative analysis:** Determination of the phase diagram for the entire composition range at atmospheric pressure**.**
[253]	**TA:** Determination of the liquidus temperature of an alloy of the sub-system As_2S_2-As at unspecified pressures above atmospheric pressure.
[254]	**DTA:** Determination of the phase diagram between compositions of 80 to 100 at. % As.
[255]	**DTA, XRF and electron microscopy:** Determination of the phase diagram up to a composition of 50 at. % As, with crystallized alloys from a pressure of 70 kbar and a temperature of 673 K.
[256]	**DTA:** Determination of the phase diagram between compositions of 50 to 100 at. % As.
[257]	**TA:** Determination of the phase diagram up to a composition of 40 at. % As**.**
[258]	**DSC:** Determination of the metastable phase diagram up to a composition of 40 at. % As. **High temperature XRD:** Proposition of a stable phase diagram for the entire composition range.

S-As_2S_3 subsystem

As-S alloys with compositions lower than 45 at. % As are highly viscous according to the experiments of Jonker [252]. Since the liquid-solid equilibrium is reached very slowly, it was not possible to measure the liquidus curve of the S-As_2S_3 subsystem using thermal analysis. Therefore, Jonker [252] estimated the liquidus curve by comparing the viscosities of several alloys with that of As_2S_3 at its melting temperature. Thus, at temperatures between 473 K and 673 K, the viscosities of pure sulfur and alloys at the compositions of 5, 10, 20 and 28.6 at. % As were evaluated quantitatively. It was possible to estimate two points of the liquidus curve. Jonker [252] also

analytically determined the vapor curve in equilibrium with boiling liquid of known compositions and identified an azeotropic point at the composition of S_3As_2. It was concluded that the vapor coexisting with the liquid is rich in sulfur. Blachnik et al. [258] also failed to measure the liquidus curve due to the high alloy viscosities in this subsystem.

As_2S_3-As_4S_4 subsystem

According to measurements by Jonker [252], a eutectic reaction takes place at a temperature of 565 K to form As_2S_3 and As_4S_4 at a composition around 43 at. % As. It was also concluded that the vapor coexisting with the liquid is rich in arsenic. However, according to Fedorova and Epova [259], As_4S_4 is incongruent and decomposes at temperatures above 569 ± 2 K. A monotectic reaction occurs at a temperature of 576 ± 2 K. According to the suggested phase diagram of Blachnik et al. [258], As_2S_3 et As_4S_4 form by a eutectic reaction at a temperature of 573 K for a composition around of 43 at. % As.

As_4S_4-As subsystem

According to the work of Jonker [252], an invariant equilibrium between the gaseous phase, the liquid phase and solid arsenic exists at an estimated temperature of 807 K at 52.2 at. % As. Since the experiments were performed at atmospheric pressure, no liquid phase was formed for alloys very rich in arsenic due to the sublimation. For this subsystem, the vapor is richer in arsenic relative to the liquid in equilibrium. Clark [253] estimated that at a temperature of 873 K, the saturated liquid contains 60 ± 0.2 at. % As. He also confirms that the vapor phase is richer in arsenic compared to the liquid in equilibrium. According to the results obtained by Barton [254], a monotectic reaction takes place at a temperature of 1070 ± 5 K. The miscibility gap of two liquids forms between the compositions of 83 ± 3 and 97 ± 3 at. % As. According to Ceolin et al. [256], the monotectic reaction involves a vapor phase in addition to solid arsenic and the two liquids. The

reaction takes place at a temperature of 1056 ± 1 K, with an upper critical temperature of 1210 K. The metallographic examination confirms the presence of the miscibility gap. The monotectic reaction takes place at a temperature of 1048 ± 3 K according to the experiments of Fedorova & Epova [257]. Also, the formation of $As_4S_3$was reported for the first time by Fedorova & Epova [257]. The compound is incongruent and stable only at temperatures below 404 ± 3 K. The eutectic reaction between As_4S_4 and As takes place at a temperature of 452 ± 4 K and at a composition around 56 at. % As. The limits of the miscibility gap could not be determined by Blachnik et al. [258] due to technical difficulties encountered. The liquidus curves of Blachnik et al. [258] and Ceolin et al [256] are in agreement, unlike the curve measured by Barton [254] found at lower arsenic compositions. The phase diagram measured by Blachnik et al. [258] does not show the formation of the thermodynamically stable As_4S_3. The metastable eutectic temperature forming As_4S_4 and As is 515 K, while the eutectic temperature forming As_4S_3 and As_4S_4 in the suggested stable phase diagram is 473 ± 4 K.

As_2S_3 compound

The natural crystalline form of As_2S_3 is orpiment. At high pressures, the crystalline form undergoes two polymorphic transformations according to the experiments of Timofeeva et al. [255], at 463 K and 483 K. At an atmospheric pressure, As_2S_3 occurs only in one form [260]. The synthesized As_2S_3 is usually amorphous and almost impossible to crystallize. Also, As_2S_3 melt is a strong glass-forming liquid at an ambient pressure, with a viscosity of 8000 $Pa.s$ near the melting temperature [261]. Pure As_2S_3 crystals cannot be prepared from As_2S_3 melts. However, the amorphization of As_2S_3 crystals is relatively easy. The optically induced transition of crystalline As_2S_3 to the amorphous state studied by Frumar et al. [262] results in a glass transition temperature T_g of 453 K. Slightly higher T_g values have been reported for synthetic samples [260, 263-265].

The temperatures and heats of fusion for crystalline As_2S_3 are presented in Table 4.6. Espeau et al. [260] measured and compared the melting temperatures obtained from synthetic and natural samples. According to the DSC results, with a heating rate of 5 K. min^{-1}, the average melting temperature obtained for the synthetic samples is 601 K, while the average for the natural samples of two different sources is 596 K and 591 K. Even though elemental analyzes showed that the synthetic sample and the natural samples have the same composition, Espeau et al. [260] suggests that the difference may be due to the higher purity of the synthetic sample. The average heat of fusion (ΔH_{fusion}) for the synthetic samples is 26.7 kJ/mol, and for natural samples from the different sources are 29.8 kJ/mol and 27.4 kJ/mol.

Table 4.6 Measured melting temperatures and heats of fusion of As_2S_3

References	**Experimental methods**	**Temperatures, in K (in °C)**	$\mathbf{\Delta H_{Fusion}}$**kJ/mol**
		$\mathbf{As_2S_{3(mP20)} \rightarrow As_2S_{3(liquid)}}$	
[252]	TA	583 (310)	-
[195]	TA	590 (317)	
[266]	DTA	583 (310)$\pm$5	-
[255]	DTA	583 (310) $\pm$10	-
[267]	DSC	588 (315)$\pm$5	28.7$\pm$1,3
[257]	DTA	591 (318)	-
[258]	DSC	581 (308)	30.05
[268]	DTA	591 (318)	-
[269]	DSC	580 (307)	19.19
[260]	DSC	591 (318) synthetic samples	26.7
		596 (323) natural samples 1	29.8
		601 (328) natural samples 2	27.4
This work	-	585 (312)	24.7

Since the synthesized As_2S_3 is usually glassy and difficult to crystallize, several studies have used natural orpiment to determine its thermodynamic properties. Černošek et al. [269] successfully synthesized high purity As_2S_3 crystals for the first time in 1999 and questioned the purity of the natural samples used in the previous studies. As can be seen from Table 4.7, there is a large discrepancy between the suggested heat of formation values by the different sources, ranging from -83 kJ/mol to -169 kJ/mol. Britzke et al. [270] obtained the first enthalpy of formation value of -145 kJ/mol by combustion calorimetry in oxygen. From the data of [270], Wagman et al. [169] recalculated a value of -169 kJ/mol, and Mills [271] a value of 159 ± 42 kJ/mol. Neverov et al. [272] calculated two enthalpy of formation values from the reactions of arsenic sulfide with an alkaline solution of NaOH saturated with bromine as well as with an alkaline solution of NaOH saturated with chlorine. The values obtained are -138 ± 12 kJ/mol and -126 ± 10 kJ/mol respectively. Barton [254] does not agree with such negative values of $\Delta H^{\circ}_{formation}$ of orpiment and estimated a value of -96.23 kJ/mol from his equilibrium study on As-Fe-S alloys. From the combustion energy of the glassy As_2S_3 measured in fluorine by Johnson et al. [273], a value of $\Delta H^{\circ}_{formation}$ of the crystalline compound of -91.6 ± 4, 8 kJ/mol was derived, agreeing with the value of Barton [254]. This is also close to the recalculated value of -88.7 ± 3.8 kJ/mol, recalculated by O'Hare [274]. Using high temperature calorimetry, a value of -83 ± 3.8 kJ/mol was obtained by Bryndzia & Kleppa [275]. Babanly et al. [276] calculated a value of -94.09 ± 2.11 kJ/mol from emf measurements, with a liquid electrolyte d KBr in glycol with 0.01% mass of Br_3As and solid arsenic as reference electrode. Nordstrom et Archer [277] evaluated and fitted the different enthalpy of formation values reported in the literature with a weighted least-squares regression and suggested a value of 85.8 kJ/mol. Enthalpy of formation values for amorphous As_2S_3 are also shown in Table 4.7. The heat capacity of crystalline As_2S_3 was first measured at low temperatures by Romanovsky

& Tarasov [278] using adiabatic calorimetry between 65 K and 300 K. The heat capacity was also measured at higher temperatures by Blachnik et al. [258] using DSC between 300 K and 650 K. For vitreous As_2S_3, heat capacities were also measured at low temperatures by Hattori et al. [279], Kageyama et al. [280], Tarasov & Zhdanov [281], Haggerty et al. [282] and Schnaus et al. [283] and are in reasonable agreement. Only the heat capacity data for the crystallin As_2S_3 is presented in Figure 4.4. The standard entropy calculated from these data is presented in Table 4.7.

Table 4.7 Standard thermodynamic properties of As_2S_3 reported in the literature

References	**Methods**	$\Delta H^{\circ}_{formation}$ **kJ mol^{-1}**	S° **J mol^{-1}K^{-1}**	C_p **J mol^{-1}K^{-1}**
[270]	Oxygen bomb calorimetry	-145.6	-	-
[278]	Adiabatic calorimetry	-	163.18	116.2
[254]	High-temperature equilibria	-96.2	163.2	-
[273]	Fluorine combustion calorimetry	-91.6±4.8	-	-
[258]	DSC	-	-	114.9
[284]	Solubility measurements	-86.5	-	-
[169]	Recalculated from [270]	-169	-	-
[275]	High-temperature calorimetry	-83 ± 3.8	-	-
[272]	Calorimetry	-138±12	-	-
[272]	Calorimetry	-126 ± 10	-	-
[285] cited in **[272]**	-	-146	-	-
[286] cited in **[272]**	-	-126	-	-
[274]	Recalculated from [270]	-88.7±3.8	-	-
[166]	-	-91.6±5		-
[276]	Emf measurements	-94.1±2.1	162±5.7	-
[277]	Weighted least-squares regression	-85.8	163.78	-
This work	-	-81.8	162	115.4

References	Methods	$\Delta H^{\circ}_{formation}$ kJ mol^{-1}	S° J $mol^{-1}K^{-1}$	C_p J $mol^{-1}K^{-1}$
	Amorphous compound			
[273]	Fluorine combustion calorimetry	-69.6±4.2	-	-
[287]	Solubility measurements	-88.1±5	-	-
[277]	Weighted least-squares regression	-66.9	200	76.8

The compound As_2S_3 sublimates congruently, and the experiments determining the composition of its vapor are not in agreement. The electron diffraction study results suggested by Lu and Donohue [288] shows that As_4S_6 molecules are probably the only species present in the vapor state. The interpretation of the results of this study is very doubtful according to Rogstad [289]. Based on their mass spectrometric analyses, Janai and Rudman [290] also suggest that the compound evaporates as As_4S_6 based on the appearance of all its possible fragments in the spectra. The composition of the vapor in equilibrium with As_2S_3 was also studied by Ban and Knox [291] using mass spectrometry with laser-induced vaporization. It was concluded that vaporization of As_2S_3 forms S_2 and As_3S_n species (n = 1, 2, 3, 4), with abundance of As_3S and As_3S_4 species. According to the mass spectrometry by Faure et al. [292], the vaporization of As_2S_3 forms gaseous AsS and S_2 The mass spectrum was obtained by scanning the ion accelerating voltage at a constant magnetic field, instead of the usual practice of varying the magnetic field at a constant ion accelerating voltage. This method used to obtain the spectrum does not allow the identification of species with higher masses according to Brittain et al. [293]. Moreover, according to Chakraborti and Lynch [294], the presence of AsS species in their results can be associated with the destruction of larger molecules due to the high ionization potentials used. The high temperature mass spectrometry by Pashinkin et al. [295] reveals the following gaseous specie: As_2S_2, As_3S_3 et As_4S_4. Since the measurements were made with ionizing electron energies of the order of 50 eV, the results

also reflect the presence of products associated with the destruction of larger molecules according to Brittain et al. [293] and Chakraborti and Lynch [294]. High temperature mass spectrometry performed by Brittain et al. [293] was obtained with an ionizing potential of 15 eV. The results show that the vaporization of the compound As_2S_3 mainly produces the following gaseous species: As_4S_4, As_4S_3, S_2 and a minor amount of As_4S_5. It was also concluded that the vapor does not contain AsS, As_2S_2 et As_3S_3. Thus, the process of vaporization is mainly done according to the following reactions:

$$As_2S_{3(s)} \rightleftharpoons \frac{1}{2}As_4S_{4(g)} + \frac{1}{2}S_{2(g)} \tag{4.5}$$

$$As_2S_{3(s)} \rightleftharpoons As_2S_{3(g)} \tag{4.6}$$

The ion intensity data indicates that reaction 4.5 predominates over reaction 4.6 Also, the following reaction contributes slightly to the process:

$$As_2S_{3(s)} \rightleftharpoons \frac{1}{2}As_4S_{5(g)} + \frac{1}{4}S_{2(g)} \tag{4.7}$$

According to the results obtained by Brunetti et al. [296], reactions 4.5 and 4.6 take place independently of temperature. Several experiments determined the vapor pressures of As_2S_3. Figure 4.5 shows data from each experiment. Using the Knudsen-Langmuir technique, Hsiao and Schlechten [297] determined the vapor pressures for temperatures between 453 K and 603 K. The vapor pressure values were labeled by Hsiao and Schlechten [297] as “apparent” because of the uncertainty as to how much is due to evaporation and how much to dissociation. Chakraborti and Lynch [294] rejects the values measured by Hsiao and Schlechten [297]. Isakova and Nesterov [298] determined the vapor pressures for temperatures between 623 K and 723 K using an indirect statistical method based on the amount of condensate formed during cooling in a closed container. When processing experimental data, it was assumed that only high dosage As_2S_3 molecules are in

the vapor phase. Since the obtained vapor pressures measured are very close to those obtained for As_4S_4, Chakraborti and Lynch [294] suggest the presence of a small amount of As_4S_4 in the solid sample used by Isakova and Nesterov [298]. Isakova [299] determined the vapor pressures using flux and boiling point methods between 623 K and 773 K. Ustyugov et al. [300] determined the vapor pressures with the static method between 729 K and 966 K using a quartz membrane manometer. Faure et al. [292] determined the vapor pressures with the Knudsen method between 497 K and 569 K, and Novoselova and Pashinkin [301] expressed the vapor pressure as a function of temperature. Gospodinov and Pashinki [302] determined the vapor pressures with the Knudsen method between 476 K and 536 K, and the Langmuir method between 470 K and 546 K. Brunetti et al. [296] determined the total vapor pressures with the torsion-effusion method between 501 K and 583 K. The boiling temperature of the compound As_2S_3 is around 980 K according to Jonker [252] and it corresponds to an azeotropic point.

As_4S_4 compound

As_4S_4 is found in nature in a crystalline form called realgar and it can easily change to orpiment with light exposure [289]. The formula of realgar is also given by AsS or As_2S_2 in some references. Since the mineral consists of As_4S_4 rings [303], the formula considered in this work is As_4S_4. Realgar undergoes a polymorphic transformation to form pararealgar. Since both forms are monoclinic [304], the transformation enthalpy is very small. The experiments performed by Rolland [305] show that the transformation temperature for the stoichiometric compound occurs at 525 K and it varies between 512 K and 536 K in the presence of elemental As and As_2S_3 respectively. The compound has a very narrow homogeneity range [305], and it is still not experimentally investigated. The measured transformation temperatures are shown in Table 4.8. Hall [195] defined three distinguishable optical properties of As_4S_4, and more recently, a third form

was reported by Bindi et al. [306], analogous to the new mineral bonazziite found in Khaidarkan deposit in Kyrgystan. The As_4S_4 compound is reported as congruent, except for the measurements of Fedorova et al. [307] that show an incongruent compound. The measured melting temperatures are shown in Table 4.8.

Table 4.8 Measured transformation temperatures and heats of fusion of As_4S_4

References	**Experimental methods**	**Temperatures, in K (in °C)**	**$\Delta H_{transformation}$, kJ/mol**
	$As_4S_{4(mP32)} \rightarrow As_4S_{4(mP32)}$		
[308] cited in [305]	-	525 (252)±2	-
[309] cited in [195]	-	529 (256)±5	-
[310]	DTA	553 (280)	3.47±0.2
[311] cited in [255]	-	540 (267)	-
[258]	DSC	539 (266)	3.37
[312]	DTA	540 (267)±2	3.42±0.04
[305]	Quenching technique	525 (252) ± 3	-
This work	-	539 (266)	3.42
	$As_4S_{4(mP32)} \rightarrow As_4S_{4(liquid)}$		
[308] cited in [305]	-	597 (306)±2	-
[195]	TA	580 (307)	-
P.C.* cited in [195]	DTA	580 (307)	-
[310]	DTA	580 (307)	-
[312]	DSC	582 (309)±1	31.56±0.2
[255]	DTA	588 (315)	-
[258]	DCS	591 (318)	31.68
[273]	Calorimetry	580 (307)	25.1±1.25
[257]	DTA	580 (296)±2	-

References	Experimental methods	Temperatures, in K (in °C)	$\Delta H_{transformation}$, kJ/mol
[313]	DSC	569 (296)±2 (incongruent)	31.68
[273]	Calorimetry	580 (307)	26.67±0.20
This work	-	585 (312)	30.19

P.C.*: Personal communication by Yund

The heat of formation values of As_4S_4 reported in the literature are presented in Table 4.9. Britzke et al. [270] obtained a first value of -242 kJ/mol by combustion calorimetry in oxygen. From the data of [270], Wagman et al. [169] recalculated a value of -285.4 kJ/mol, and Mills [271] a value of -284.5 ± 42 kJ/mol. Neverov et al. [272] calculated a $\Delta H^{\circ}_{formation}$ value of -236 ± 12 kJ/mol from the reactions of arsenic sulfide with an alkaline solution of NaOH saturated with bromine. These values are erroneous according to Barton [254], who estimated a value of -145.6 ± 6 kJ/mol based on the equilibrium studies in As-Fe-S alloys. Data from vapor phase analyses seem to indicate a value closer to what was suggested by Barton [254] according to Mah [314]. A value of -138.1 ± 6.7 kJ/mol was obtained from Fluorine bomb calorimetry measurements by Johnson et al. [273], which is close to the value suggested by Barton. The $\Delta H^{\circ}_{formation}$ value obtained by mass spectroscopy by Steblevskii et al. [315] is -127.6 ± 5.2 kJ/mol. This value agrees with that calculated by O'Hare [274] of -127.5 ± 5.3 kJ/mol. Using high temperature calorimetry, the $\Delta H^{\circ}_{formation}$ obtained by Bryndzia et al. [275] is -108.8 ± 1.6 kJ/mol, which is less negative than other reported values. This may be due to an incomplete chemical reaction in the synthesis calorimeter according to O'Hare [274]. In the most recent study performed by Babanly et al. [276], the $\Delta H^{\circ}_{formation}$ calculated from the emf measurements is -158.4 ± 4.4 kJ/mol. The heat capacity of synthetic AsS was determined for low temperatures by Weller and Kelley [316]. Heat capacities of synthetic As_4S_4 was also measured by DSC at higher temperatures by Blachnik et al. [258] and

Chattopadhyay et al. [312], but the obtained results do not fully agree. According to Chattopadhyay et al. [312], this is due to the partial evaporation of the sample during the measurements by Blachnik et al. [258]. Also, according to Emelina et al. [317], Chattopadhyay et al. [312] obtained the most reliable data. The standard entropy derived from the heat capacity data is presented in Table 4.9.

Table 4.9 Standard thermodynamic properties of As_4S_4 reported in the literature

References	**Methods**	$\Delta H^{\circ}_{formation}$ **kJ mol^{-1}**	S° **J mol^{-1}K^{-1}**	C_p **J mol^{-1}K^{-1}**
[316]	Calorimetry	-	254±3	187.8
[254]	High-temperature equilibria	-145.6 ± 6	254.4	-
[273]	Fluorine combustion calorimetry	-138.1± 0.8	247.6	-
[275]	High-temperature calorimetry	-108.8	-	-
[272]	Calorimetry	-236	-	-
[274]	Recalculated from [270]	-127.5±5.3	-	-
[166]	-	-138.0±6.8	-	-
[258]	DSC	-	-	190
[312]	DSC	-	-	189
[277]	Weighted least-squares regression	-125.2	251.6	-
[276]	Emf	-158.4 ± 4.4	250±13.2	-
This work	-	-135.3	257	189.8

Several experiments studied the composition of the vapor in equilibrium with As_4S_4. By determining the vapor density at several temperatures, Szarvasy and Messinger [318] concluded that the vapor contains mainly As_4S_4 molecules at temperatures below 823 K, and at higher temperatures, the molecules dissociate into As_2S_2. At temperatures above 1473 K, Szarvasy and Messinger [318] suggested that another dissociation might occur. Castro et al. [319] confirm that the gaseous As_4S_4 dissociates in two stages at high temperatures to As_2S_2 and AsS. According to the results of the mass spectrometry performed by Munir et al. [320], the vaporization of synthetic and natural realgar produces a vapor that mainly contains As_4S_4 species at high temperatures. The following species were also found in minor quantities: As_4S_3, As_4 et As_2, and their presence decreases with increasing temperature. Therefore, it was concluded that the process of vaporization takes place according to the following reaction:

$$As_4S_{4(s)} \rightleftharpoons As_4S_{4(g)} \tag{4.8}$$

This agrees with the results of Brittain et al. [293] who used mass spectrometry and mass-torsion effusion. It was concluded that at least 90% of the vapor produced following the sublimation of realgar comprises the gaseous As_4S_4 species. Also, it was determined that the vapor pressure of the two forms, α-S_4As_4 and β-S_4As_4, are similar. Various experiments determined the vapor pressures of As_4S_4. The measured data is shown in Figure 4.5. Using spoon gauge, Strathdee and Pidgeon [321] performed vapor pressure measurements for temperatures between 573 K and 773 K. Ustyugov et al. [300] also determined the vapor pressures for temperatures between 663 K and 838 K using the same technique. The data obtained by Ustyugov et al. [300] have a systematic error caused by the non-uniformity of the thermal field according to Novoselova and Pashinkin [301]. This is due the large sizes of the membrane chambers. Munir et al. [320] performed vapor pressure measurements using Torsion-effusion for temperatures between 452 K and 534 K and using

Torsion-Langmuir between 411 K and 465 K. Godovikov et al. [313] also performed vapor pressure measurements using a quartz membrane manometer for temperatures between 614 K and 814 K. Their pressures are lower than the one measured by Strathdee and Pidgeon [321] and Ustyugov et al. [300]. Finally, measurements were performed by Pashinkin et al. [322] between 470 K and 580 K using the Knudsen method, and the results are in good agreement with those by Munir et al. [320].

As_4S_3 compound

The natural form of As_4S_3 is dimorphite. There is few thermodynamic information in the literature for this compound and the data available is inconsistent across the sources. As_4S_3 undergoes a polymorphic transformation and the measured transformation temperatures are shown in Table 4.10. The orthorombic structure of the synthetic forms has been determined by Whitfield [323, 324], and has been confirmed for the natural forms by Gavezzoti et al. [325]. Since both forms are orthorombic, the transformation enthalpy is very small [258]. Another modification from crystalline to plastic crystalline has been found by Blachnik et al. [258] and Chattopadhyay et al. [326]. It is probably of tetragonal symmetry similar to the one found in P_4S_3 and it possibly only occurs under non-equilibrium conditions according to Blachnik et al. [258]. The compound is reported as congruent and the measured melting temperatures are shown in Table 4.11. Fedorova and Epova [257] measured a much lower melting point of 404 ± 3 K which is incongruent with no polymorphic transformation.

Table 4.10 Measured temperatures and heats of transformation of As_4S_3

References	Experimental methods	Temperatures, in K (in °C)	$\Delta H_{transformation}$ kJ/mol
		$\mathbf{As_4S_{3(oP28)} \rightarrow As_4S_{3(o**)}}$	
[323]	XRD	415 (142)	-
[258]	DSC	404 (131)	1.0
[312]	DSC	422 (149)±0.5	1.44±0.02
This work	-	422 (149)	2.34
		$\mathbf{As_4S_{3(o**)} \rightarrow As_4S_{3(plastic)}}$	
[258]	DSC	425 (152)	13.07
[312]	DSC	432 (159)±0.5	13.04±0.15
		$\mathbf{As_4S_{3(plastic)} \rightarrow As_4S_{3(liquid)}}$	
[258]	DSC	474 (201)	3.77
[312]	DSC	484 (211)±5	3.86±0.04
		$\mathbf{As_4S_{3(o**)} \rightarrow As_4S_{3(liquid)}}$	
[257]	TA	404±3 (incongruent)	-
This work	-	485 (212)	21.28

Based on emf measurements, Babanly et al. [276] calculated a $\Delta H^{\circ}_{formation}$ value of -125.5 kJ/mol for As_4S_3. Using the second law of thermodynamics, Pashinkin et al. [327] calculated a value of -111.1 kJ/mol. A lower value of -82.4 kJ/mol from Isabaev et al. [328] was cited by Prostakova et al. [185] without reporting the measurement method. The heat capacity of As_4S_3 was first measured by Blachnik et al. [258] using DSC for temperatures between 130 K and 600 K. These measurements are uncertain because the sample has undergone partial evaporation according to Chattopadhyay et al. [312]. Measurements were also performed using DSC by Chattopadhyay et al. [312] between 100 K and 400 K. Pashinkin et al. [327] approximated the heat capacity of As_4S_3 by structural analogy to P_4S_3. As shown in Figure 4.4, the heat capacity values from each source

agree only for a limited temperature range. The standard thermodynamic properties of As_4S_3 are presented in Table 4.11.

Table 4.11 Standard thermodynamic properties of As_4S_3 reported in the literature

References	Experimental methods	$\Delta H^{\circ}_{formation}$ kJ mol^{-1}	S° J $mol^{-1}K^{-1}$	C_p J $mol^{-1}K^{-1}$
[258]	DSC	-	-	166.67
[312]	DSC	-	-	165.4
[328] cited in **[185]**	-	-82.4±13.8	240.6	-
[327]	Knudsen and Langmuir	-111.1±8	240.6±13	167.4
[276]	Emf	-125.5±4.5	229.9±13.7	-
This work	-	-110	209.6	164.88

The vaporization behavior of solid As_4S_3 is still not well established in the literature. As reported by Pashinkin et al. [327], the process of vaporization of As_4S_3 may occur according to the following reaction:

$$As_3S_{4(s)} \rightleftharpoons As_3S_{4(g)} \tag{4.9}$$

Godovikov et al. [307] measured the saturation vapor pressure of As_4S_3 at temperatures above its melting temperature, between 600 K and 780 K. Using the Knudsen method, Pashinkin et al. [327] measured the vapor pressure of the metastable As_4S_3 plastic phase between 400 K and 430 K and the stable plastic phase between 434 K and 481 K. Pashinkin et al. [327] also measured the vapor pressure of $As_4S_{3(oP28)} + As_4S_{3(o**)}$ for temperatures between 402 K and 429 K, and of $As_4S_{3(oP28)}$ between 394 K and 418 K using the Langmuir method. All measured data is presented in Figure 4.5.

4.2.6 Thermodynamic properties of the gas in As-S binary system

In addition to the complexity of the vaporization mechanism of As-S system, there is still a gap in the thermodynamic information available for the gaseous species. In fact, the thermodynamic properties for $As_4S_{5(g)}$ and $As_2S_{3(g)}$ are still unavailable in the literature. Mah [314] calculated the standard enthalpy of formation for the predominant species $As_4S_{4(g)}$ and $AsS_{(g)}$ but the values have significant uncertainties A standard enthalpy of formation of 0.189 $\pm$ 0.038 kJ/mol for $AsS_{(g)}$ was obtained based on the dissociation energy of 0.385 ± 0.038 kJ /mol from Sullivan [329]. For gaseous $As_4S_{4(g)}$, a standard enthalpy of formation of -2.092 $\pm$ 10.5 kJ /mol was obtained based on the sublimation studies of Munir et al. [320] and Gospodinov & Pashinkin [302].

4.2.7 Experimental determination of Ag-As-S ternary phase diagram

Several minerals have compositions within the Ag-As-S ternary system, including proustite and xanthoconite (Ag_3AsS_3) which are very abundant, smithite and trechmannite ($AgAsS_2$) as well as a rare sulfosalt bearing called billingsleyite (Ag_7AsS_6). Just like the system As-S, the Ag-As-S system tend to form as a glass under certain conditions. Measurements of phase diagram data of this system are presented in Table 4.12.

Table 4.12 Ag-As-S phase diagram data reported in the literature

References	Experimental methods and results
	Ag_2S-As_2S_3
[204]	**TA:** Determination of the quasi-binary diagram up to a composition of 75 at. % As_2S_3.
[330]	**DTA and XRD:** Determination of the quasi-binary diagram up to a composition of 58 at. % As_2S_3.
[331]	**DTA and XRD:** Determination of the liquidus curves between compositions of 23 at. % and 67 at. % As_2S_3 for annealed and annealed samples.
[332]	**DTA, XRD and microhardness:** Determination of the quasi-binary diagram up to a composition of 70 at. % As_2S_3.

References	Experimental methods and results
	Ag_7AsS_6-Ag_3AsS_3
[333]	**DTA, XRD and DSC:** Prediction of the quasi-binary diagram for the entire composition range.
	Ag_7AsS_6-Ag_2S
[333]	**DTA, XRD and DSC:** Prediction of the quasi-binary diagram for the entire composition range.
	$AgAsS_2$-As_4S_4
[334]	**Quenching experiments and XRD:** Prediction of the quasi-binary diagram for the entire composition range in the presence of vapor.
	Ag_3AsS_3-S
[335]	**Quenching experiments and XRD:** Determination of the cross section for the entire composition range in the presence of vapor.
	Ag_3AsS_3-As
[308] reproduced by [336]	**XRD:** Determination of the eutectic temperature and the liquidus from 30 % to 60 % As.
	$Ag_{0.5}As_{0.5}$-S
[332]	**DTA, XRD and microhardness:** Determination of the cross section for compositions from 30 % to 58 % S.
	$Ag_{0.75}As_{0.25}$-S
[332]	**DTA, XRD and microhardness:** Determination of the cross section up to a composition of to 55 % S.
	$Ag_{0.5}As_{0.5}$-As
[332]	**DTA, XRD and microhardness:** Determination of the cross section up to a composition of to 45 % As.
	$Ag_{0.33}As_{0.67}$-As
[332]	**DTA, XRD and microhardness:** Determination of the cross section for compositions from 10 % to 40 % As.
	Ag_2S-As
[308] reported by [337]	**Quenching experiments and XRD:** Determination of the liquidus from 13 % to 56 % As.
[337]	**DTA and XRD:** Determination of the cross section for compositions for the entire composition range.

References	Experimental methods and results
	Ag_3AsS_3-Ag
[338]	**DTA and microhardness:** Suggestion of the quasi-binary diagram up to a composition of 50 % Ag.

Ag_2S-As_2S_3 system

In the ternary Ag-As-S system, the quasi-binary Ag_2S-As_2S_3 is the most important experimentally and mineralogically [334]. Jaeger and Klooster [204], Elli and Giudici [330] and Kovaleva et al. [332] evaluated the Ag_2S-As_2S_3 phase diagram and reported two congruently melting compounds along this system: Ag_3AsS_3 and $AgAsS_2$. The measurements could not be performed for the entire composition range due to glass formation at high As_2S_3 compositions. Solid solubility: No solid solubility has been reported in the Ag_2S-As_2S_3 system. Eutectic: According to Jaeger & Klooster [204], the eutectic reaction that forms Ag_2S and Ag_3AsS_3 takes place at a temperature of 742 K and a composition of 29 at. % As_2S_3. The eutectic reaction that forms Ag_3AsS_3 and $AgAsS_2$ takes place at a temperature of 672 K and a composition around 58 at. % As_2S_3. This agrees with the eutectic measurements of Elli and Giudici [330] and Kovaleva et al. [332]. Liquidus: The liquidus of Ag_2S-Ag_3AsS_3 measured by Kovaleva et al. [332] is slightly higher than the one measured by Jaeger and Klooster [204]. The liquidus measurements of Ag_3AsS_3-$AgAsS_2$ determined by Jaeger and Klooster [204] and Kovaleva et al. [332] are in good agreement and are higher than the liquidus measured by Wehmeier et al. [331]. Gaudin and McGlashan [339] proposed a tentative Ag_2S-As_2S_3 phase diagram under non equilibrium conditions based on selective iridescent filming and reported an additional incongruent phase "A". Sommerlad [340] reported the synthesis of Ag_5AsS_4, and Hall [195] also reported an additional intermediate phase along this quasi-binary system. The phase has possibly a composition of Ag_5AsS_4 by analogy with stephanite (Ag_5SbS_4) [195]. Roland [334] was not able to detect the formation of this phase.

Ag_3AsS_3 compound

Ag_3AsS_3 corresponds the mineral xanthoconite that undergoes a polymorphic transformation to form proustite as seen from Table 4.13. For this compound, Bryndzia and Kleppa [246] determined a standard heat of formation of 111.3 ± 3.4 kJ/mol using high-temperature calorimetry. This value is slightly lower than the one calculated by Gasanova et al. [341] from emf measurements of the following cell: $(-)\mathrm{Pt}|\mathrm{Ag\ (reference\ electrode)}|\mathrm{Ag_4RbI_5}_{(s)}|(\mathrm{Ag_2S\text{-}As_2S_3\text{-}S})|\mathrm{Pt}(+)$. The measurements were made at temperatures from 300 to 380 K and the calculated enthalpy is 121.4 ± 2.8 kJ/mol. Using adiabatic calorimetry, Gorbunov et al. [342] and Gurevich et al. [343] measured the heat capacity of the compound in the 10 K to 350 K range and they are in very good agreement. The standard thermodynamic properties of Ag_3AsS_3 are presented in Table 4.14. Godovikov et al. [344] and Fedorova et al. [345] suggested that Ag_3AsS_3 vaporizes incongruently according to the following reaction:

$$\mathrm{Ag_3AsS_3}_{(g)} \rightleftharpoons \frac{3}{2}\mathrm{Ag_2S}_{(s)} + \frac{1}{4}\mathrm{As_4S_4}_{(g)} + \frac{1}{4}\mathrm{S_2}_{(g)} \tag{4.10}$$

Godovikov et al. [344] also calculated the vapor pressure as a function of temperature based on quartz manometer measurements for 846 K to 1013 K. Using the Knudsen method, Fedorova et al. [345] measured the vapor pressure for temperatures between 673 K et 723 K. Godovikov et al. [307] also measured the vapor pressure for temperatures between 769 K et 901 K using the isoteniscope method.

Table 4.13 Measured temperatures and heats of transformation of Ag_3AsS_3

References	Experimental methods	Temperatures, in K (in °C)	$\Delta H_{transformation}$ kJ/mol
	$Ag_3AsS_{3(LT)} \rightleftharpoons Ag_3AsS_{3(HT)}$		
[346]	Abrasive stripping voltammetry	465 (192)	35±14
This work	-	465 (192)	21.66
	$Ag_3AsS_{3(HT)} \rightleftharpoons Ag_3AsS_{3(liquid)}$		
[204]	TA	763 (490)	-
[347]	TA and XRD	753 (480)	-
[348]	TA and metallographic analysis	753 (480) ±10	-
[349]	DDC and dilatometry	753 (480) ±5	36.82±1.68
[331]	DTA and XRD	756 (483)	-
[332]	DTA and XRD	763 (490)	-
[350]	DTA and XRD	-	38.07±1.67
[351]	Calvet micro-calorimetry	757 (484) ±0.5	41.23±0.84
This work	-	760 (487)	28.53

Table 4.14 Standard thermodynamic properties of Ag-As-S ternary compounds reported in the literature.

References	Experimental methods	$\Delta H^{\circ}_{formation}$ kJ mol^{-1}	S° J mol^{-1}K^{-1}	C_p J mol^{-1}K^{-1}
		Ag_3AsS_3		
[342]	Adiabatic calorimetry	-	302.6	164.7
[343]	Adiabatic calorimetry	-	303.68 ± 0.52	164.02 ± 0.14
[246]	High temperature calorimetry	-111.3 ± 3.4	303	-
[341]	Emf	-121.4 ± 2.8	283 ± 10	-
This work	-	-120.4	277	164.7

References	Experimental methods	$\Delta H^{\circ}_{formation}$ kJ mol^{-1}	S° J $mol^{-1}K^{-1}$	C_p J $mol^{-1}K^{-1}$
		$AgAsS_2$		
[343]	Adiabatic calorimetry	-	150.51 $\pm$ 0.14	96.01 $\pm$ 0.06
[246]	High temperature calorimetry	-74.8 $\pm$ 2.9	-	-
[341]	Emf	-75.69 $\pm$ 1.6	151 $\pm$ 5	-
This work	-	-73.89	146	96.03
		Ag_7AsS_6		
[341]	Emf	-201.9 $\pm$ 6.0	594 $\pm$ 19	-
This work	-	-201.9	596	338.59
		Ag_2AsS_2		
This work	-	-95.89	188.55	121.42
		AgAsS		
This work	-	-57.39	113.93	73.34

$AgAsS_2$ compound

$AgAsS_2$ is present in nature as the mineral trechmannite and it undergoes a polymorphic transformation to form smithite. The standard heat of formation of $AgAsS_2$ by Bryndzia and Kleppa [246] and Gasanova et al. [341] are in very good agreement. Using adiabatic calorimetry, Gurevich et al. [343] measured the heat capacity of the compound in the 10 K to 350 K range. The measured standard thermodynamic properties and transformation temperatures are presented in Table 4.14 and Table 4.15 respectively. Godovikov et al. [344] and Fedorova et al. [345] suggested that $AgAsS_2$ vaporizes incongruently according to the following reaction:

$$AgAsS_{2(s)} \rightleftharpoons \frac{1}{3}Ag_3AsS_{3(s)} + \frac{1}{6}As_4S_{4(g)} + \frac{1}{6}S_{2(g)} \quad (4.11)$$

Using the Knudsen method, Fedorova et al. [345] measured the vapor pressure for temperatures between 575 K et 623 K. Godovikov et al. [307] calculated the vapor pressure as a function of temperature based on quartz manometer measurements from 709 K to 980 K. Using the same technique, Fedorova et al. [352] also calculated the vapor pressure for temperatures from 724 K to 1013 K. The measurements of Godovikov et al. [307] and Fedorova et al. [352] are in good agreement.

Table 4.15 Measured temperatures and heats of transformation of $AgAsS_2$

References	**Experimental methods**	**Temperatures, in K (in °C)**	**$\Delta H_{transformation}$ kJ/mol**
		$AgAsS_{2(LT)} \rightleftharpoons AgAsS_{2(HT)}$	
[246]	High temperature calorimetry	593 (320)±5	15.6±1.7
This work	-	593 (320)	13.55
		$AgAsS_{2(HT)} \rightleftharpoons AgAsS_{2(liquid)}$	
[204]	TA	690 (417)	-

References	Experimental methods	Temperatures, in K (in °C)	$\Delta H_{transformation}$ kJ/mol
[331]	DTA and XRD	686 (413)	-
[332]	DTA and XRD	702 (429)	-
[353]	Drop calorimetry	643 (370)	9.87±0.84
This work	-	696 (423)	7.32

Ag_7AsS_6, Ag_2AsS_2 and AgAsS compounds

The only standard entropy and heat of formation values available in the literature for Ag_7AsS_6 are from Gasanova et al. [341]. The values are presented in Table 4.14. The compound undergoes a polymorphic transformation around 523 K, but no enthalpy of transformation is available. There are still no studies done to investigate the properties and the melting temperatures of Ag_2AsS_2 and AgAsS. Values of heat of formation of these compounds predicted by DFT are given in Table 4.16 as a reference.

Table 4.16. Enthalpies of formation of Ag-As-S ternary compounds predicted by DFT from the Open Quantum Materials Database [59] and the Materials Project [60]

References	Space group	$\Delta H_{formation}$ kJ mol^{-1}
Ag_3AsS_3		
OQMD	*C2/c*	-156.69
OQMD	*R3c*	-153.99
The Materials Project	*R3c*	-198.57
$AgAsS_2$		
The Materials Project	$R\bar{3}$	-139.71
Ag_7AsS_6		
OQMD	$P2_13$	-267.46
The Materials Project	$P2_1\bar{3}$	-379.57
AgAsS		
OQMD	$Pna2_1$	-52.68

4.2.8 Previous thermodynamic assessment of Ag-As-S systems

The binary Ag-As system was previously assessed by Shi et al. [184]. The liquid phase was described by the substitutional solution model $(Ag, As)_1$, using the PARROT program of the Thermo-Calc software [146]. Shi et al. [184] also performed a thermodynamic assessment of the binary Ag-S system using the same program of the Thermo-Calc software. The liquid was modeled by the associate model $(Ag, Ag_2S, S)_1$ and Ag_2S was considered as a stoichiometric compound. The sub-solidus phase equilibria in the As-S system were calculated by Emelina et al. [317] by constructing convex envelopes of primary thermodynamic surfaces using PhDi software [354]. The As-S system was also assessed by Prostakova et al. [185] with FactSage thermochemical software using the Modified Quasichemical Model (MQM) for the liquid phase similarly to the present work. However, different choices were made that distinguish the two optimizations. First, As_2S_5 is obtained only at high pressures and Prostakova et al. [185] included it in their optimization. This compound is not considered in the present assessment. Also, different coordination numbers are set in this work. This choice is made because Liu et al. [355] investigated the structural stability of various As-S clusters based on DFT calculations and demonstrated that $(As_2S_3)_n$ has the highest stability. The stability is due to the 4p-orbital in As atom binding with 3p-orbital of S atom, which decreases the energy level of the highest occupied molecular orbital. Additionally, Tsuchihashi et al. [356] studied the glasses in the As-S system, and the results show that the hardness, T_g and the thermal expansion are maximum at 40 at. % As, which corresponds to the composition of As_2S_3. Hattori et al. [279] also reported that thermal conductivity of As-S glasses shows a maximum near the composition of As_2S_3. Since Tsuchihashi et al. [356] confirms that the SRO arrangement of glassy As_2S_3 is similar to the crystalline structure, the maximum SRO is set in this work to occur at a composition of 40 at. % As. This selected SRO composition was also confirmed to be the most

appropriate by studying the measurements made for the ternary Ag-As-S system as well as the favored oxidation state of arsenic. Thus, the values of the coordination numbers set in this work are Z_{AsS}^{As}=3 and Z_{AsS}^{S}=2, contrary to the values of Z_{AsS}^{As}=Z_{AsS}^{S}=3 used in the work of Prostakova et al. [185]. Finally, the most significant distinction between the two optimizations comes from the parameters of the excess Gibbs energy of the liquid solution. Linear terms to describe the liquid as used by Prostakova et al. [185] predicts that the liquid is internally unstable at high temperatures and form inverted miscibility gaps, even if the real As-S liquid is not prone to separation. To correct the excess Gibbs energy of the liquid at high temperatures, CTln(T) terms were added in this work to avoid the formation of inverted liquid miscibility gaps in this system. This led to an improvement compared with the previous assessment of this system.

4.3 Thermodynamic modeling

All calculations and optimizations in this work were performed with the FactSage thermochemical software [45] [46]. The properties of pure solid and liquid Ag, As and S are from SGTE [152]. The properties of the gaseous species S, S_2, S_3, S_4, S_5, S_6, S_7 and S_8 are from JANAF Thermochemical Tables [153]. The properties of the gaseous species As, As_2, As_3 and As_4 are from Degterov et al. [154] and other of their unpublished optimisations and evaluations. The properties of the gaseous species AsS and As_4S_4 are from Barin [170] based on the calculations of Mah [314]. The gaseous AgS is from Mills [271], Ag is from Barin et al. [357] and Ag_2 is from Wagman et al. [358].

4.3.1 Thermodynamic model for the liquid phase in the binary systems

The Modified Quasichemical Model in the Pair Approximation suggested by Pelton et al. [65] [66] was used to model the liquid phases to take into account the short-range ordering (SRO). For a liquid binary A-B system, the following pair exchange reaction is considered between the A and B atoms on neighbouring lattice sites:

$$(A-A)+(B-B)=2(A-B)\ ;\ \Delta g_{AB} \tag{4.12}$$

$(i-j)$ is the first nearest neighbor (FNN) atom pairs, and Δg_{AB} is the non-configurational Gibbs energy change for the formation of 2 moles of $(A-B)$ pairs. The pair and the overall mole (site) fractions are defined respectively as:

$$X_{ij}=\frac{n_{ij}}{(n_{AA}+n_{BB}+n_{AB})} \tag{4.13}$$

$$X_A=\frac{n_A}{(n_A+n_B)}=1-X_B \tag{4.14}$$

n_A, n_B represent the number of moles of A and B, n_{AB} represents the number of moles of pairs (A-B). If the coordination number of A is Z_A, the "coordination equivalent" fraction of A is defined as:

$$Y_A=\frac{Z_A n_A}{Z_A n_A+Z_B n_B}=\frac{Z_A X_A}{Z_A X_A+Z_B X_B}=1-Y_B=X_{AA}+\frac{X_{AB}}{2} \tag{4.15}$$

The "coordination equivalent" fraction of B is defined similarly. The Gibbs energy of the binary liquid is given by the following equation:

$$G=\left(n_A g_A^{\circ}+n_B g_B^{\circ}\right)-T\Delta S^{\text{configuration}}+\left(\frac{n_{AB}}{2}\right)\Delta g_{AB} \tag{4.16}$$

g_A° and g_B° are the molar Gibbs energies of the pure liquid components, and $\Delta S^{\text{configuration}}$ is the configurational entropy of mixing given by randomly distributing the (A-A), (B-B) and (A-B) pairs. The non-configurational Gibbs energy change for the formation of 2 moles of $(A-B)$ pairs is expended in terms of the pair fractions:

$$\Delta g_{AB}=\Delta g_{AB}^{\circ}+\sum_{i\geq 1} g_{AB}^{i0}\,(X_{AA})^i+\sum_{j\geq 1} g_{AB}^{0j}\,(X_{BB})^j \tag{4.17}$$

Δg°_{AB}, g^{i0}_{AB} and g^{0j}_{AB} are the temperature dependant model parameters that are optimized in this work for the Ag-As, Ag-S and As-S systems. The coordination numbers can be varied with composition to reproduce the SRO, as given by equations 4.18 and 4.19. The composition of maximum SRO is determined by the ratio Z_B / Z_A:

$$\frac{1}{Z_A} = \frac{1}{Z^A_{AA}}\left(\frac{2n_{AA}}{2n_{AA}+n_{AB}}\right) + \frac{1}{Z^A_{AB}}\left(\frac{2n_{AB}}{2n_{AA}+n_{AB}}\right) \tag{4.18}$$

$$\frac{1}{Z_B} = \frac{1}{Z^B_{BB}}\left(\frac{2n_{BB}}{2n_{BB}+n_{AB}}\right) + \frac{1}{Z^B_{BA}}\left(\frac{2n_{AB}}{2n_{BB}+n_{AB}}\right) \tag{4.19}$$

$\mathrm{Z^A_{AA}}$ and $\mathrm{Z^A_{AB}}$ are the coordination numbers when the nearest neighbours of an A atom are A atoms and B atoms respectively. $\mathrm{Z^B_{BB}}$ and $\mathrm{Z^B_{BA}}$ are defined similarly. In this work, $\mathrm{Z^{Ag}_{AgAg}}$, $\mathrm{Z^{As}_{AsAs}}$ and $\mathrm{Z^S_{SS}}$ are set to be 6 for consistency with previous work.

4.3.2 Thermodynamic model for the liquid phase in the ternary system

Geometric models can be used to estimate the excess Gibbs energy of a ternary system from the parameters of the three binary subsystems [68]. For a given geometric model, the excess Gibbs energy of the ternary system at any composition p is calculated from the binary parameters at points a, b and c. The difference between the models is the placement of these three points which is very important to correctly interpolate the ternary system. After trying several extrapolation methods, the Kohler-Toop type extrapolation technique, with Ag as the asymmetric component, provided the most satisfactory description of the ternary system. It is then the selected technique in this work to optimize the ternary Ag-As-S liquid phase.

4.3.3 Thermodynamic model for Ag_2S solid solutions

The low temperature monoclinic form is a semiconductor and has nearly an ideal stoichiometric composition [214, 359]. The second bcc form has a high conductivity due to the increase of number

of vacancies in the silver sublattice and the transfer of silver atoms to adjacent vacancy sites. Silver is distributed among the tetrahedrally and octahedrally coordinated positions [360]. At higher temperatures, the tetrahedral occupancy increases at the expense of the octahedral occupancy, and above 533 K the occupied sites are entirely tetrahedral [360]. The sulfur atoms arrangement stays unchanged [360, 361]. Based on this information and by analogy to the model established by Waldner [362] for the Cu_2S, a simplified sub-lattice model is used for Ag_2S solid solutions and is presented in Table 4.17.

Table 4.17. Crystallographic description of the phases in Ag-As-S system as reported by Schmid-Fetzer et al. [363] and Shi et al. [184] as well as the sublattice model of Ag_2S selected in this work

Phase	Person symbol	Space group	Sub-lattice modeling
Ag-S system			
$\mathbf{Ag_2S_{(HT)}}$	$cF44$	$Fm\bar{3}m$	$(\mathbf{Ag_2}, \mathrm{Va})_1(\mathbf{Va}, \mathrm{Ag})_1(\mathbf{S})_1$
$\mathbf{Ag_2S_{(MT)}}$	$cI20$	$Im\bar{3}m$	$(\mathbf{Ag_2}, \mathrm{Va})_1(\mathbf{Va}, \mathrm{Ag})_1(\mathbf{S})_1$
$\mathbf{Ag_2S_{(LT)}}$	$mP12$	$P2_1/n$	stoichiometric
As-S system			
$\mathbf{As_4S_{3\,(HT)}}$	o^{**}	-	stoichiometric
$\mathbf{As_4S_{3\,(LT)}}$	$oP28$	$Pnma$	stoichiometric
$\mathbf{As_4S_{4\,(HT)}}$	$mP32$	$P2_1/n$	stoichiometric
$\mathbf{As_4S_{4\,(LT)}}$	$mP32$	$P2_1/c$	stoichiometric
$\mathbf{As_2S_3}$	$mP20$	$P2_1/c$	stoichiometric
Ag-As-S system			
$\mathbf{Ag_3AsS_{3\,(HT)}}$	$hR42$	$R3c$	stoichiometric

Phase	Person symbol	Space group	Sub-lattice modeling
$\mathbf{Ag_3AsS_{3\,(LT)}}$	$mc56$	$C2/c$	stoichiometric
$\mathbf{AgAsS_{2\,(HT)}}$	$mP24$	$A2/a$	stoichiometric
$\mathbf{AgAsS_{2\,(LT)}}$	$hR72$	$R\bar{3}$	stoichiometric
$\mathbf{Ag_7AsS_{6\,(HT)}}$	$cF56$	$F4\bar{3}m$	stoichiometric
$\mathbf{Ag_7AsS_{6\,(LT)}}$	$cP56$	$P2_13$	stoichiometric
$\mathbf{Ag_2AsS_2}$	mP^*	$P2/a$	stoichiometric
AgAsS	$oP12$	$Pna2_1$	stoichiometric

4.4 Results and discussion

The optimization of the thermodynamic parameters was conducted using the FactSage thermochemical software. The Ag-As-S systems are assessed based on the literature data presented in the previous sections, and the optimized thermodynamic model parameters are presented in Table 4.18. The calculated Ag-As binary phase diagram is shown in Figure 4.1 along with the experimental data. No information on the composition of maximum short-range ordering (SRO) of this system is reported. Nevertheless, analyzing the measured phase diagram data shows an increase of the slope of the tangent line of the liquidus curves around 20 at. % As. Thus, the coordination numbers Z_{AgAs}^{Ag} and Z_{AgAs}^{As} are set in this work to 1.5 and 6 respectively to reproduce SRO at 20 at. % As. As seen from Figure 4.1, the calculated eutectic and liquidus curves reproduce very well the measured data. However, silver solubilizes slightly less arsenic compared to the measured values below 625 K and above 900 K. The hcp phase (ξ) may not occur as a mineral according to Hall [195], but it is still modeled in this work. The optimized Gibbs free energy of the

phase is shown in Table 4.18. As explained in the previous section, there is a disagreement regarding the formation and the decomposition temperatures of the hcp phase. Elliot [364], Baren [365] and Shi et al. [184] selected peritectic and eutectoid temperatures in accordance with the measurements of Eade and Hume-Rothery [193]. The same choice is made in this work since the measurements of Eade and Hume-Rothery [193] are considered more reliable than those of Heike and Leroux [189]. The activity data suggested by Ludecke et al. [196] is very scattered and could not be reproduced in the work by Shi et al. [184]. After examining the experimental method and the inconsistency with phase diagram data, the activity data suggested by Ludecke et al. [196] is considered doubtful and is not used in the present optimization.

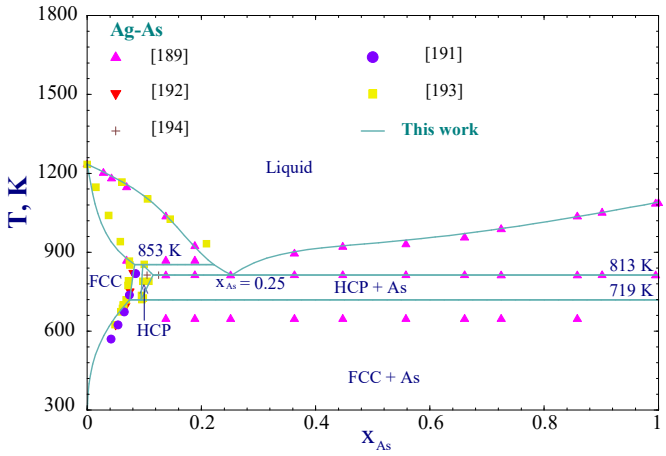

Figure 4.1 Calculated Ag-As phase diagram

The calculated Ag-S binary phase diagram is shown in Figure 4.2, and the different phases are identified with Pearson symbols. According to the integral molar quantities of the liquid phase determined by Fukatsu and Kozuka [206], the SRO is maximum at a composition of Ag_2S, which is expected. Considering the sharpness of the curves, the coordination numbers Z_{AgS}^{Ag} and Z_{AgS}^{S} are set in this work to 1.5 and 3 respectively to reproduce SRO at 33.33 at. % As. The solubility of sulfur in silver is very small as shown in Figure 4.2 a). The most reliable solubility data obtained

by Raub and Roschel [201] and Fueki et al. [202] are in very good agreement with the solubility calculated in this work. As reported in the literature, the low temperature form of Ag_2S is considered stoichiometric, and the high temperature forms are considered non-stoichiometric. The homogeneity range, the non-symmetrical polymorphic temperatures, and the partial pressure of S_2 over the solid solutions are well reproduced. The optimized Gibbs free energy of the Ag_2S phases are presented in Table 4.18.

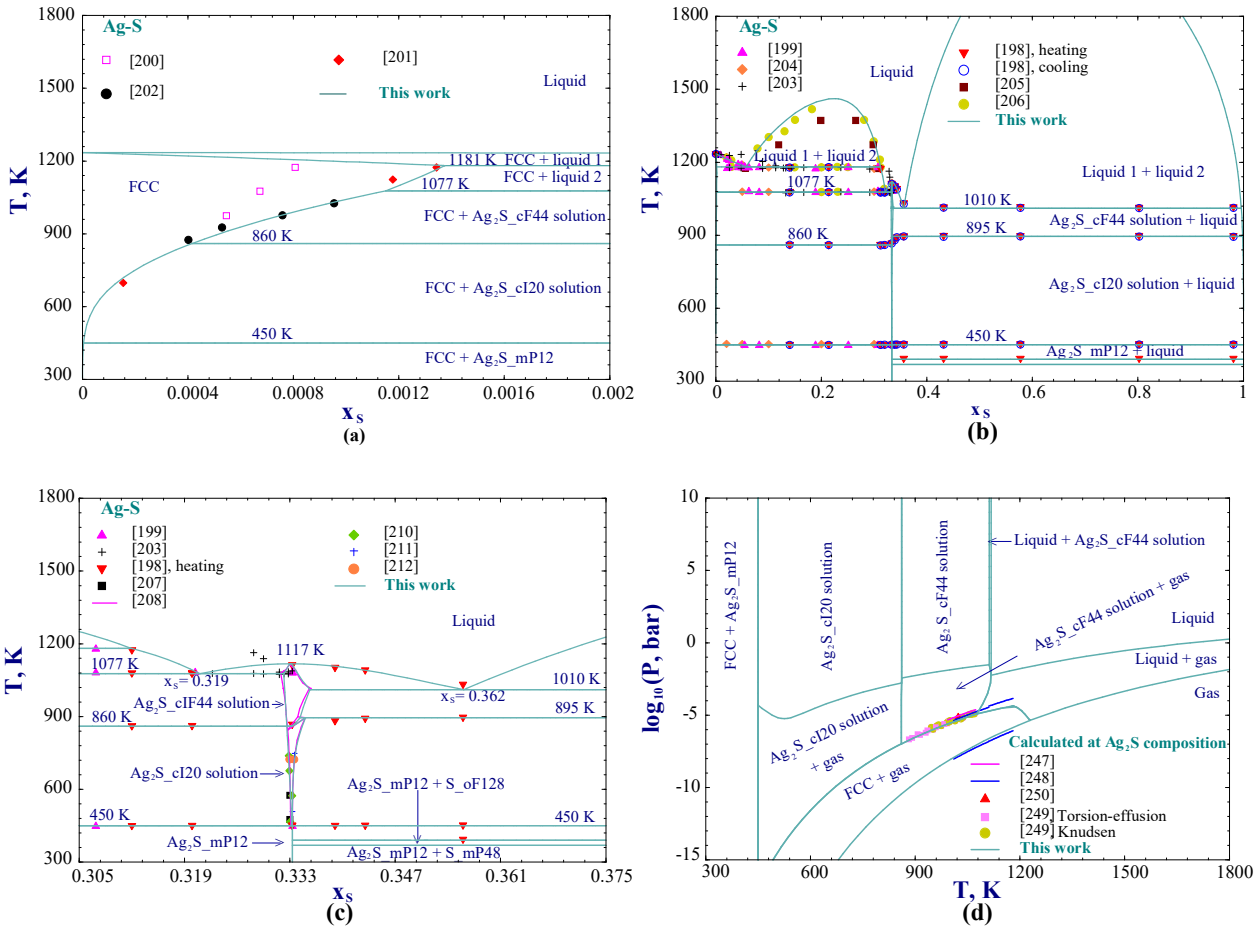

Figure 4.2 Calculated a) solid solubility of S in Ag, b) Ag-S phase diagram at all compositions, c) homogeneity region of Ag_2S, d) vapor pressures for a composition of Ag_2S

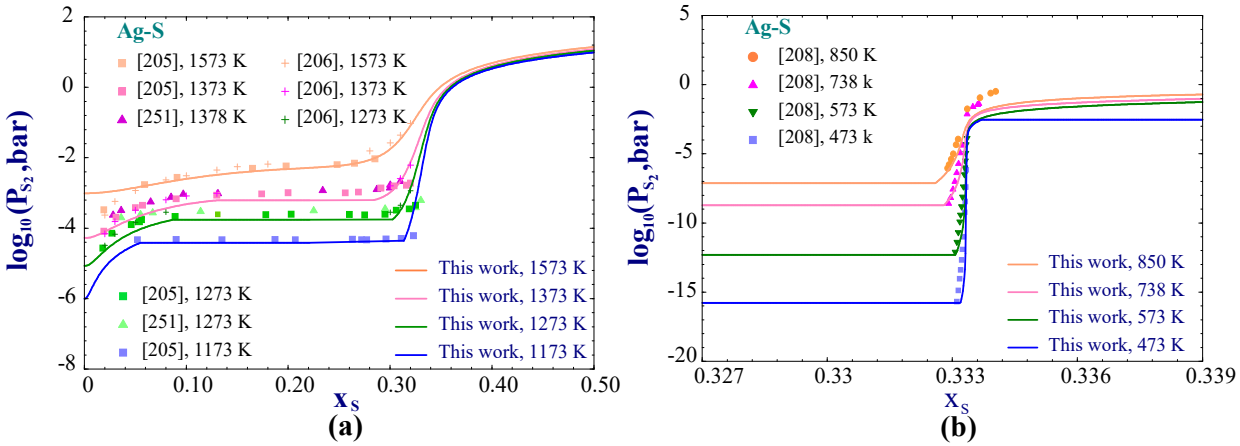

Figure 4.3 Calculated partial pressure of S_2 in a) Ag-S liquid alloys and b) in Ag_2S solid solutions

Table 4.3 shows that the selected heat of fusion of Ag_2S is slightly higher than what was measured experimentally by Kelly [366] and nearly double of what was measured by Thompson and Flengas [223] and Koh and Itagaki [233]. This choice was necessary to adequately reproduce not only the binary Ag-S phase diagram, but also the Ag_2S liquidus in the quasi-binary Ag_2S-As_2S_3. As shown in Figure 4.2 d), the sulphur contained in Ag_2S completely vaporizes like observed by Piacente et al [249], and the compound becomes constituted of pure silver before completely vaporizing too.

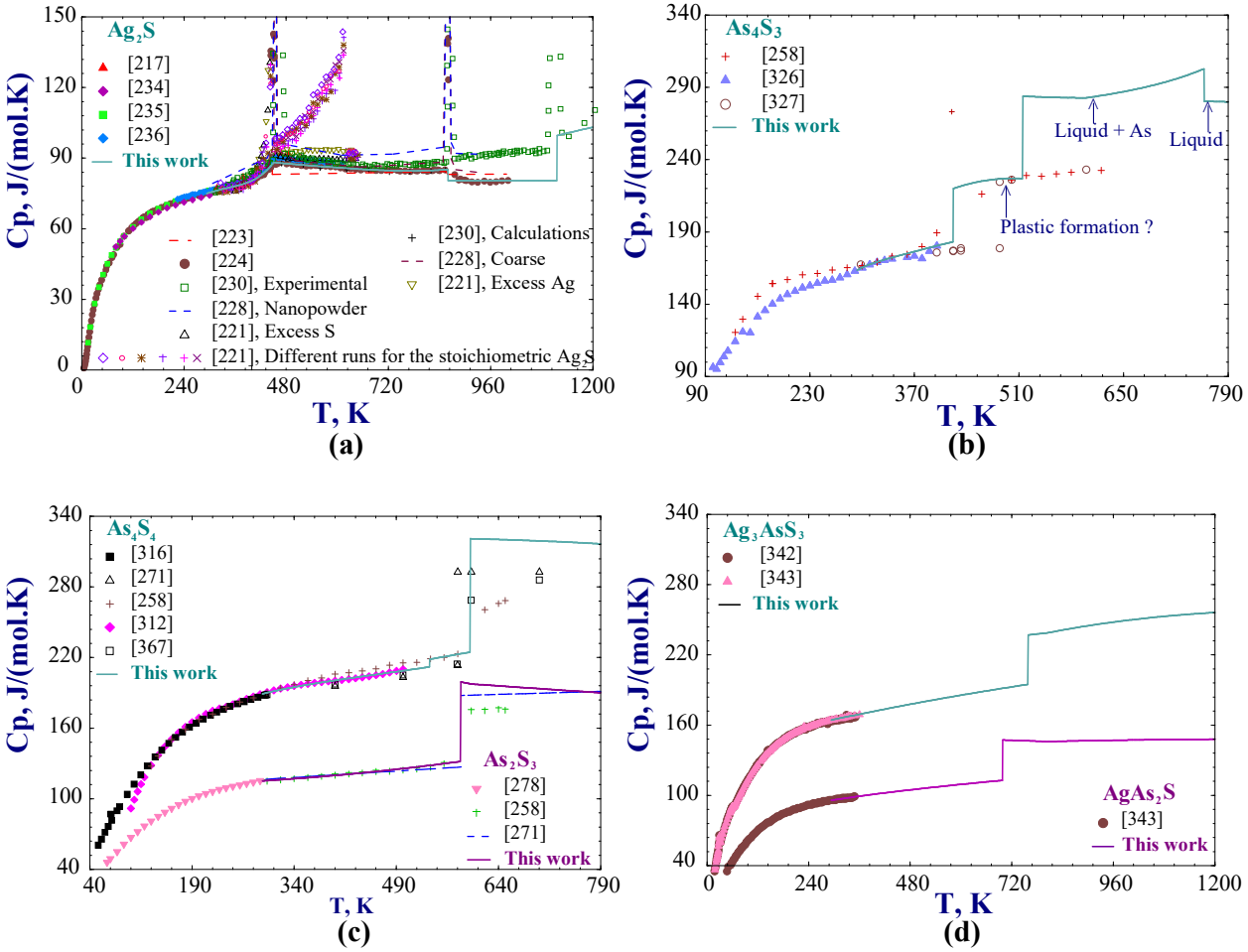

Figure 4.4 Calculated heat capacity of a) Ag_2S, b) As_4S_3, c) As_4S_4 and As_2S_3, d) Ag_3AsS_3 and $AgAsS_2$

The calculated heat capacity of Ag_2S as function of temperature is presented in Figure 4.4 a). As was concluded by Sadonikov and Gusev [237], the experimental data of Grønvold and Westrum [224] is considered the most reliable in the context of this work.

The optimization of the binary As-S system presents a great challenge. First, there are many contradictions and uncertainties in the measurements of this system as explained in the literature review. This is mainly due to the complexity of performing experiments of polymer structured samples. Above its melting temperature, sulfur is organised as ring shaped S_8 molecules, and at higher temperatures, it can form long polymer chains S_n with high molecular weight [368, 369]. The addition of arsenic to sulfur causes a significant increase in polymer chains and a reduction of S_8 molecules. This leads to glass formation and metastable tendencies for a wide range of

composition in the As-S system [176, 370]. Also, the high vapor pressure in the region rich in arsenic and its toxicity add to the difficulty of performing experiments to study this binary system.

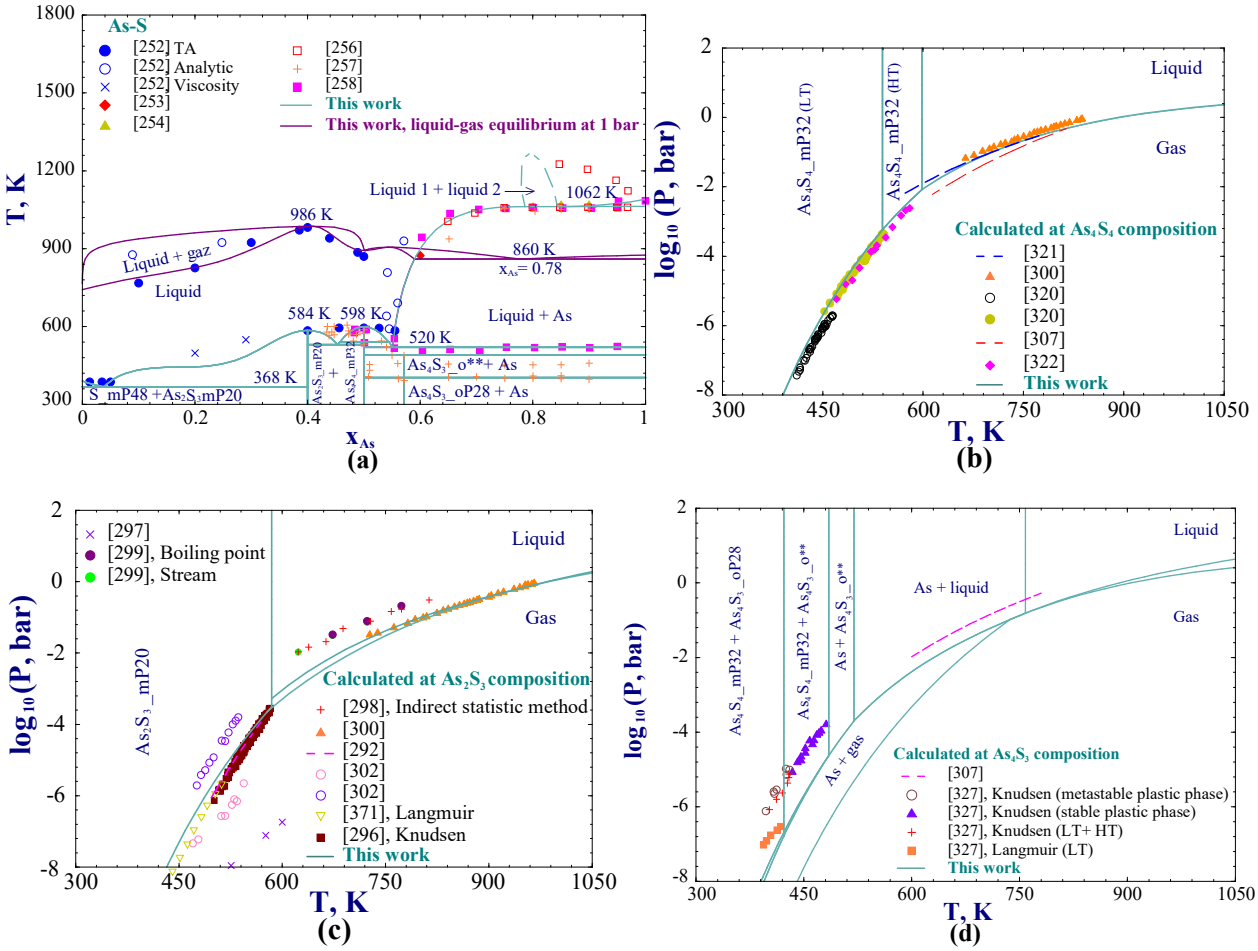

Figure 4.5 Calculated a) As-S phase diagram, b) vapor pressures for a composition of As_4S_4, c) vapor pressures for a composition of As_2S_3, d) vapor pressures for a composition of As_4S_3

The calculated As-S binary phase diagram is shown in Figure 4.5 and the optimized thermodynamic model parameters are presented in Table 4.18. Two calculations are superimposed on the figure, one with only the solids and the liquid phase, and another including the gaseous species. As justified in section 2.8, the coordination numbers set in this work are Z_{AsS}^{As}=3 and Z_{AsS}^{S}=2. By adding CTlnT terms to the model parameters of the liquid, no artifact miscibility gap is generated up to 6000 K. However, this also lead the an unusual shape of the actual miscibility gap excisting in the arsenic rich region, hence why it is represented by a dotted line. The

extrapolation of this gap to the Ag-As-S ternary system is shown in the isothermal section of Figure 4.7. As stated in section 2.6, the thermodynamic information available in the literature for the gaseous species in the As-S system is incomplete. Despite this, the liquid was still optimized using the limited information available to reproduce as best as possible the liquid-vapor equilibrium. The azeotrope at the composition of As_2S_3 measured by Jonker [252] is well reproduced. But this work suggests more than one azeotrope, as shown in Figure 4.5 a), which was also predicted by Emelina [317]. Also, it is important to acknowledge that the MQM model used to optimize the liquid phase describes a monomeric melt and does not consider the complex structure of liquid As-S which tends to form polymer chains.

There is a large discrepancy in the measured standard enthalpies of formation of the three solid compounds in the As-S system, as presented in Table 4.7, Table 4.9 and Table 4.11. In this work, low enthalpy values were selected for each compound. This was necessary to avoid stabilizing the liquid too much and consequently pushing the gas curve towards very high temperatures. With the few contradicting thermodynamic information available in the literature for As_4S_3, it is difficult to predict the behaviour of this compound very accurately. In this work, only the two orthorhombic crystalline phases were modeled, the plastic phase found by Blachnik et al. [258] and Chattopadhyay et al. [326] was not considered. The transformation and melting temperatures measured by Chattopadhyay et al. [326] are the most reliable in the context of this work and their values are the ones selected in this optimization. However, it was not possible to optimize the system to have a congruent compound as found by Chattopadhyay et al. [326], so As_4S_3 is incongruent in this work like what was measured by Fedorova and Epova [257]. The calculated heat capacity of the three compounds in the As-S system is shown in Figure 4.4. Blachnik et al. [258] performed heat capacity measurements, but the evaporation of their samples during the

experiments causes uncertainties. The most reliable measurements are again those by Chattopadhyay et al. [157]. As seen in Figure 4.4, the heat capacity of the liquid is high, and a possible explanation is its tendency to polymerize.

Table 4.18 Optimized thermodynamic model parameters for Ag-As-S systems (J mol^{-1})

Phases (model)	**Thermodynamic parameters**
Liquid (MQM) $(\mathbf{Ag}, \mathbf{As}, \mathbf{S})$	$Z_{AgAs}^{Ag} = 1.5$; Z_{AgAs}^{As}=6 ; $Z_{AgS}^{Ag} = 1.5$; Z_{AgS}^{S}=3 ; $Z_{AsS}^{As} = 3$; Z_{AsS}^{S}= 2 ; Z_{AgAg}^{Ag}=Z_{AsAs}^{As}=Z_{SS}^{S}= 6 $\Delta g_{Ag-As} = -4\,552.16 + 500\,X_{AgAg} + 8\,368\,X_{AsAs}$ $\Delta g_{Ag-S} = -19\,450 - 102.964719T + 11.67703149T\ln T$ $+(40\,000 - 14.30843944T)X_{AgAg} - 3\,928.8\,X_{AgAg}^2$ $+ (48\,000 - 25.6995888T)X_{SS}$ $+ 38\,472\,X_{SS}^2$ $\Delta g_{As-S} = (-48\,000 + 88.06745852T - 9.15509875T\ln T)$ $+(-30\,000 + 92.12448546T - 10.0723164T\ln T)X_{AsAs}$ $+(-74000 + 249.3309779T - 27.09164012T\ln T)X_{AsAs}^2$ $+(52\,500\text{-}23.0525498T)X_{AsAs}^3 + 3\,000X_{SS}$+$2500X_{SS}^3$ $g_{SAg(As)}^{001} = -27T$ $g_{AsS(Ag)}^{001} = 18T$ $g_{SAg(As)}^{101} = -12T$ $g_{AsS(Ag)}^{301} = -30\,000$ $g_{SAg(As)}^{033} = -8\,500$
FCC-A1 (CEF) $(\mathbf{Ag}, \mathbf{As}, \mathbf{S})_1(\mathbf{Va})_1$	${}^0L_{AgAs} = -1\,500 + 4.11350455T$ ${}^0L_{AgS} = -56\,443.6364 - 27T$
HCP-A3 (CEF) $(\mathbf{Ag}, \mathbf{As})_1(\mathbf{Va})_{0.5}$	${}^0L_{AgAs} = 4\,590$ ${}^1L_{AgAs} = -12\,492.22 - 7.8T$

Phases (model)	Thermodynamic parameters
$\mathbf{Ag_2S}$_cI20 (CEF) $(\mathbf{Ag_2, Va})_1(\mathbf{Va, Ag})_1(\mathbf{S})_1$	${}^0G_{Ag_2:Va:S} = -93939.62879 + 46.19560346T + 2\ {}^oG_{Ag}^{fcc} + {}^oG_S^{fcc}$ ${}^0G_{Ag_2:Ag:S} = -78939.62879 + 70.19560346T + 3\ {}^oG_{Ag}^{fcc} + {}^oG_S^{fcc}$ ${}^0G_{Va:Va:S} = {}^oG_S^{fcc}$ ${}^0G_{Va:Ag:S} = +933917.3719 + 25.28230559T + {}^oG_{Ag}^{fcc} + {}^oG_S^{fcc} G^o_{Va:Va:S}$ ${}^0L_{Ag,Va:Va:S} = -28.472T$ ${}^1L_{Ag,Va:Va:S} = -16.736T$
$\mathbf{Ag_2S}$_cF44 (CEF) $(\mathbf{Ag_2, Va})_1(\mathbf{Va, Ag})_1(\mathbf{S})_1$	${}^0G_{Ag_2:Va:S} = -94688.62879 + 45.32460346 + 2\ {}^oG_{Ag}^{fcc} + {}^oG_S^{fcc}$ ${}^0G_{Ag_2:Ag:S} = -79688.62879 + 69.32460346T + 3\ {}^oG_{Ag}^{fcc} + {}^oG_S^{fcc}$ ${}^0G_{Va:Va:S} = {}^oG_S^{fcc}$ ${}^0G_{Va:Ag:S} = +933917.3719 + 25.28230559T + {}^oG_{Ag}^{fcc} + {}^oG_S^{fcc}$ ${}^0L_{Ag,Va:Va:S} = -33.472T$ ${}^1L_{Ag,Va:Va:S} = -16.736T$

For the ternary Ag-As-S system, the thermodynamic properties of Ag_3AsS_3 and $AgAsS_2$ are available in the literature and were optimized first to reproduce the vapor pressure measurements presented in Figure 4.6. For Ag_7AsS_6, the enthalpy of formation and standard entropy were set to the values suggested by Gasanova et al. [341] since they are the only thermodynamic properties based on measurements available for this compound. The present calculations confirm the decomposition reactions 10 and 11 proposed by Godovikov et al. [344] and Fedorova et al. [345].

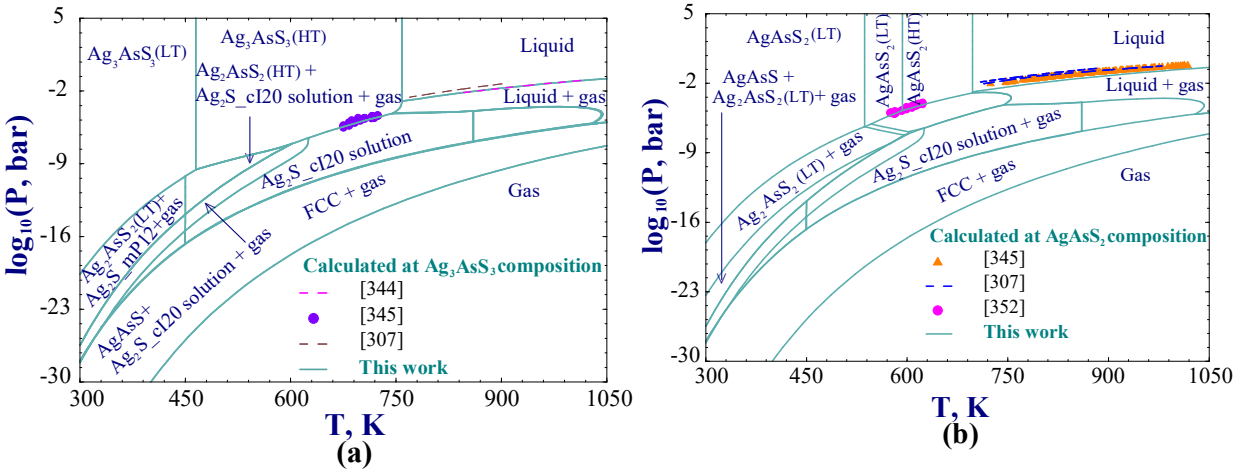

Figure 4.6 Calculated vapor pressures for a) a composition of Ag_3AsS_3 and b) a composition of $AgAsS_2$

The liquid phase was then modeled and five ternary parameters, presented in Table 4.18, were used to reproduce more accurately the experimental data. Since three large positive terms are used to describe the three miscibility gaps in the Ag-S and As-S binary systems, three corrective ternary parameters have been added to balance these positive terms to avoid the formation of large ternary gaps and thus obtain a more precise interpolation. As there are no thermodynamic information available for Ag_2AsS_2 and AgAsS and their decomposition temperatures are still uncertain, the Neumann-Kopp rule was used as a first approximation of these two compounds. Their Gibbs energies were then adjusted to reproduce as best as possible the available phase diagram data. A group of calculated phase diagrams together with the experimental data are shown in Figure 4.7, Figure 4.8, Figure 4.9 and Figure 4.10. Some phases are present at equilibrium in minor quantities and are identified in the figures as such. The quasi-binary Ag_2S-As_2S_3 is the most important in the Ag-As-S ternary system and it is well reproduced as seen from Figure 4.7 b). The two quasi-binaries Ag_7AsS_6-Ag_3AsS_3 and Ag_7AsS_6-Ag_2S are also well reproduced as shown in Figure 4.7 c) and Figure 4.7 d). There is however a negligeable amount of a second liquid calculated, which was not detected by the measurements of Blachnik and Wickel [333]. The four cross sections measured by Kovaleva [332] along with the calculations from this work are presented in Figure 4.8. Also, the predictions of Roland [308, 334-336] along with the calculations are presented in Figure 4.9. There is a good agreement between the predictions and the calculations of Ag_3AsS_3-S and Ag_3AsS_3-As. However, a miscibility gap was predicted for $AgAsS_2$-As_4S_4, but is not present in this

work. Figure 4.10 shows the calculated Ag_2S-As and Ag_3AsS_3-Ag along with the experimental data. Eutectic compositions and temperatures deviate slightly from measured values. Il was expected to have a certain difference to what was measured for Ag_3AsS_3-Ag diagram since Schmid-Fetzer et al. [363] already noted non-considered features in what was suggested by chaus [338]. A summary of some invariant reactions involving four-phase intersection points with liquid in the ternary Ag-As-S system is presented in Table 4.19.

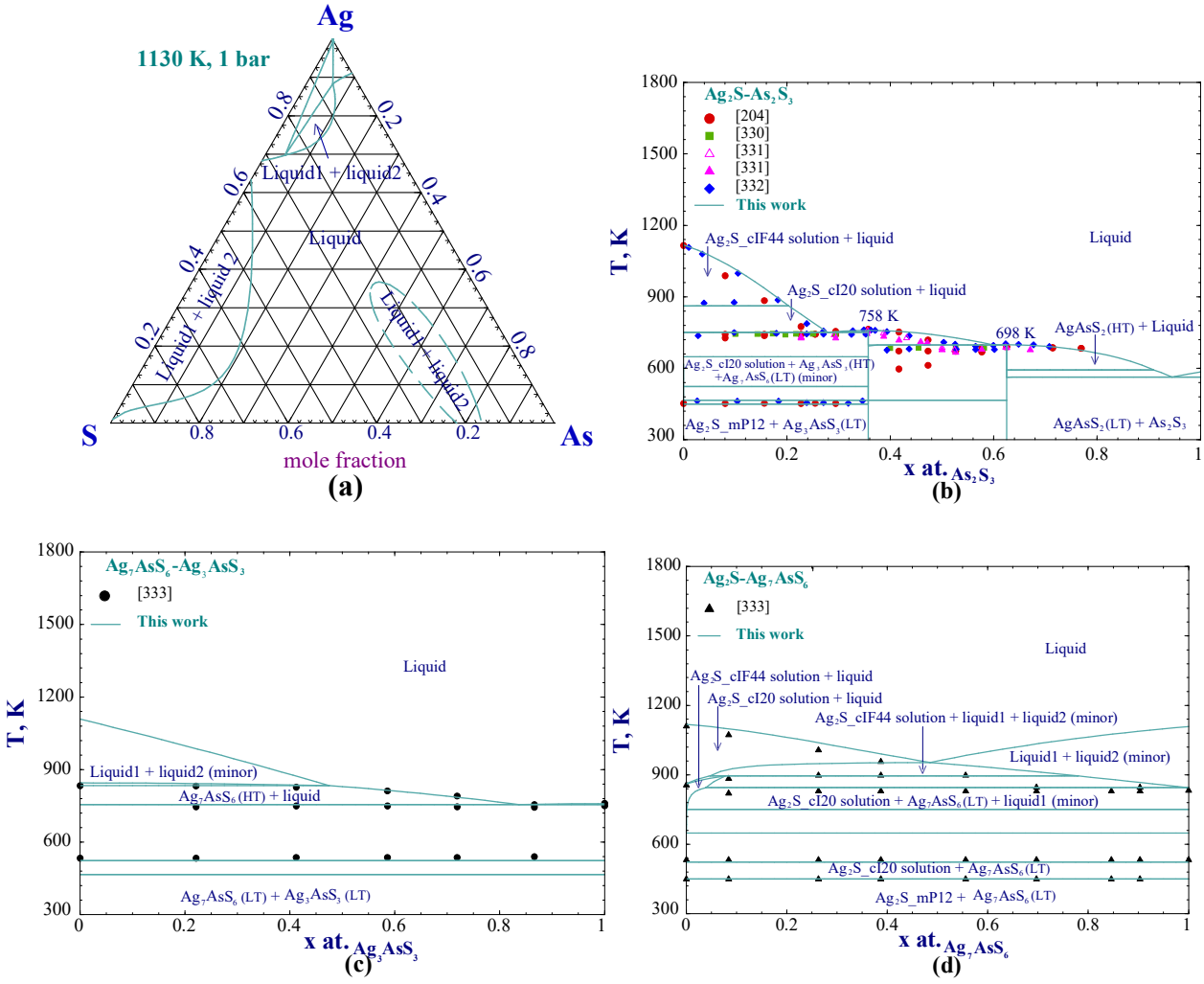

Figure 4.7 a) Predicted Ag-As-S and calculated b) Ag_2S-As_2S_3, c) Ag_7AsS_6-Ag_3AsS_3 and d) Ag_7AsS_6-Ag_2S quasi-binary phase diagrams

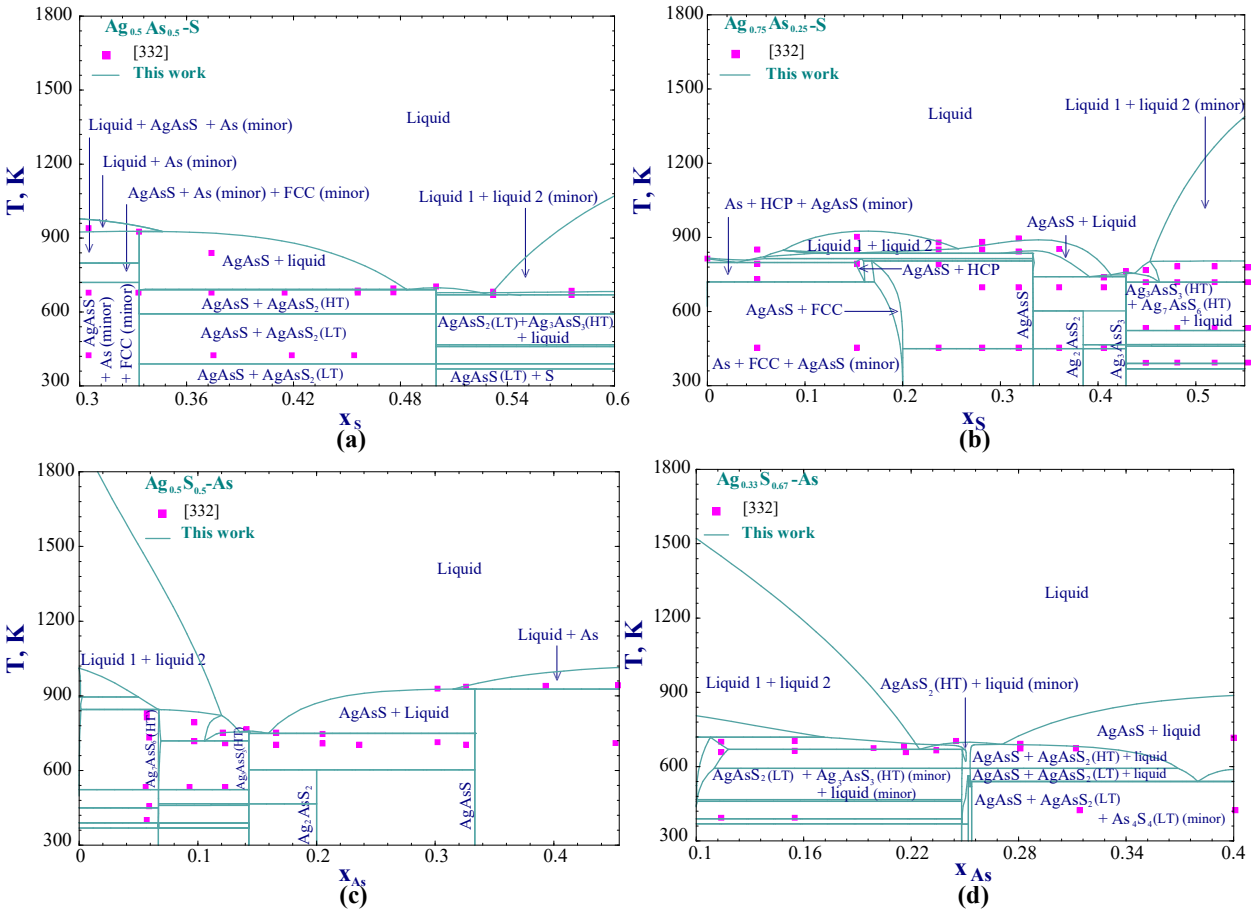

Figure 4.8 Calculated a) $Ag_{0.5}As_{0.5}$-S, b) $Ag_{0.75}As_{0.25}$-S, c) $Ag_{0.5}As_{0.5}$-As and d) $Ag_{0.33}As_{0.67}$-As cross section

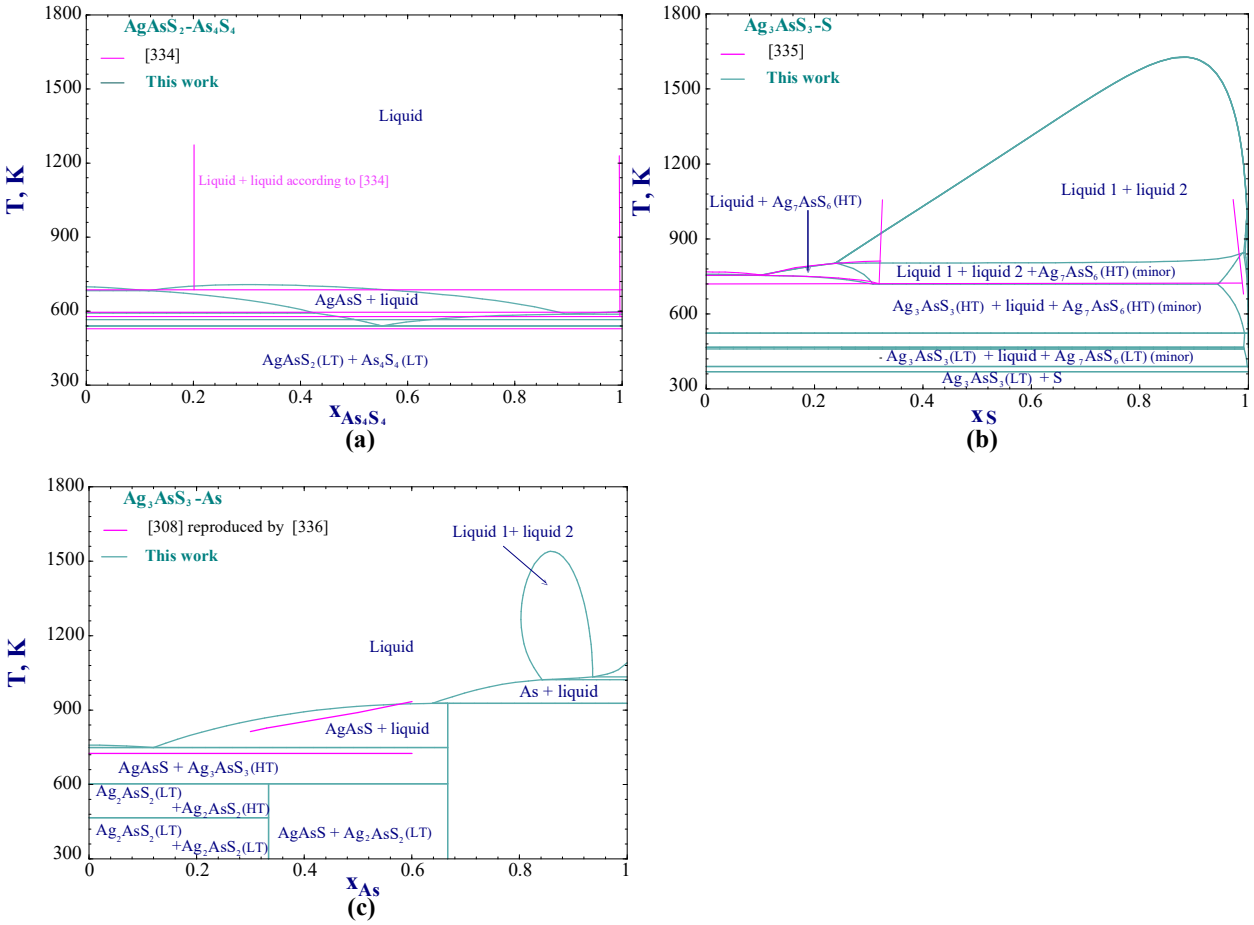

Figure 4.9 Calculated a) $AgAsS_2$-As_4S_4, b) Ag_3AsS_3-S and c) Ag_3AsS_3-As phase diagrams

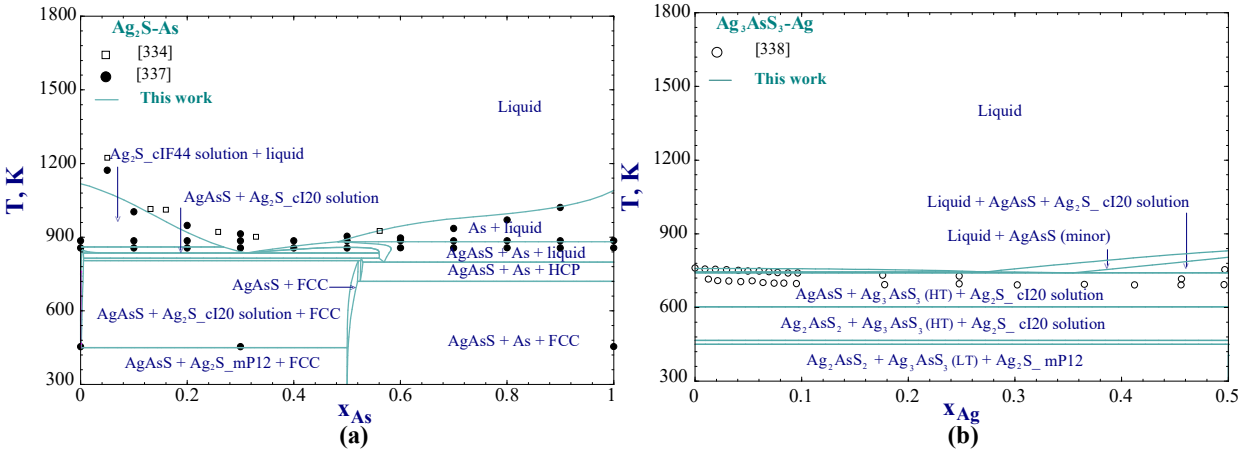

Figure 4.10 Calculated a) Ag_2S-As and b) Ag_3AsS_3-Ag phase diagrams

Table 4.19 Summary of some invariant reactions involving the liquid phase in the ternary Ag-As-S system

Reactions			**Temperatures**	**References**
at. % Ag	**at. % As**	**at. % S**	**K (°C)**	
Liquid 2 + FCC ⇌ Liquid 1 + $Ag_2S_{(cF44)}$				
0.64390	0.07641	0.27970	920.65 (647.5)	This work
-	-	-	923.15-1023.15 (650-750)	[338]
Liquid 1 + $Ag_7AsS_{6(solid\ 2)}$ ⇌ Liquid 2 + $Ag_3AsS_{3(solid\ 2)}$				
0.00317	0.03231	0.96452	718.26 (445)	This work
-	-	-	719.15 (446)	[338]
Liquid 1 ⇌ $Ag_3AsS_{3(solid\ 2)}$ + $Ag_7AsS_{6(solid\ 2)}$ + $Ag_2S_{(cI20)}$				
0.48011	0.10979	0.41010	749.86 (476.71)	This work
-	-	-	723.15-742.15 (450-469)	[338]
Liquid ⇌ FCC + HCP + $Ag_2S_{(cF44)}$				
0.72807	0.22435	0.04758	822.81 (549.06)	This work
-	-	-	-	[338]

4.5 Conclusion

The increasing use of complex ores in smelters causes many problems due to their high arsenic content. To predict the behaviour of arsenic during the smelting process and help elaborate solutions, the development of thermodynamic models and their associated databases is essential.

In this work, the thermodynamic information available in the literature was critically evaluated and was used to optimize the Ag-As, Ag-S and As-S binary systems. The MQM was applied to model the liquid phase while the CEF was utilized for solid solutions. The optimization of the binary As-S system presented a great challenge due the lack of complete thermodynamic information. The calculated phase diagrams for the three binary systems assessed provide an accurate description of all reliable experimental data. Using the Kohler-Toop interpolation, the Ag-As-S ternary system was assessed for the first time, and the calculations also provide a satisfactory description of the ternary data.

Acknowledgments

The authors would like to thank the financial support from NSERC and CRC programs.

CHAPITRE 5 ARTICLE 3 : THERMODYNAMIC EVALUATION AND OPTIMIZATION OF THE AS-CO, AS-FE AND AS-FE-S SYSTEMS

Oumaima Kidari[3] and Patrice Chartrand

Center for Research in Computational Thermochemistry (CRCT) - Polytechnique Montréal, Department of Chemical Engineering, Box 6079, Station Downtown, Montréal, Québec, Canada, H3C 3A7.

Article submitted for publication in "CALPHAD" on March 21, 2023

Abstract: A critical evaluation of all available phase diagram and thermodynamic data for the As-Co and As-Fe binary systems as well as the As-Fe-S ternary system has been performed and thermodynamic assessments over the whole composition ranges are presented using the CALPHAD method. To predict thermodynamic properties and phase equilibria for these systems, the Modified Quasichemical Model (MQM) for short range ordering was used for the liquid phases. The Compound Energy Formalism (CEF) was used for the solid solutions. Since Co and Fe are ferromagnetic, magnetic contributions were added to describe the Gibbs energy of cobalt and iron rich solid solutions. Important uncertainties remain for the liquidus of As-rich regions in the binary subsystems.

Keywords: Thermodynamic modeling, Modified Quasichemical Model, CALPHAD, Arsenic, Speiss.

5.1 Introduction

Cobalt and iron are commonly found together in arsenic containing sulfide minerals. Cobalt is a transition metal with many desirable characteristics; it is a ferromagnetic element with unique valency and corrosion resistance over a wide temperature range. Its many properties make it valuable for various applications such as superalloys and ceramics manufacturing as well as lithium-ion batteries. It is also frequently used as a desulphurization catalyst of petroleum [372-376]. Cobalt is strongly siderophile and therefore often associated with iron minerals. Iron is a widely used transition metal due to its ferromagnetic ability, low cost and conductivity [377]. Both cobalt and iron are chalcophile, and since arsenic is very common in sulphide mineralization, the processing of ores containing cobalt and iron minerals can cause major challenges [378]. In fact, arsenic is a very toxic element and sulfide ore processing can be a major source of arsenic

[3] Corresponding author
E-mail address: oumaima.kidari@polymtl.ca

contamination to the environment. Arsenopyrite (FeAsS) is a ubiquitous arsenic bearing sulfide mineral, primarily associated with sulfide minerals of mostly copper, silver, and gold [379, 380]. Cobalt is found mainly in cobaltite (CoAsS) and it is usually produced as a by-product of processing various metals. The close ionic radius of cobalt and iron and other similarities in their physical properties make iron substitution by cobalt very common. So minerals like glaucodot ((Co, Fe)AsS) and skutterudite ((Co, Ni, Fe)As_3) are widely found in various ores [372, 373, 381]. To find solutions to reduce toxic arsenic emissions caused by the treatment of complex concentrates, the development of thermodynamic models of compounds and mixtures and their associated databases for arsenic, cobalt, iron, and sulfur systems is advantageous for the sulfide smelting industry. In the present article, the available experimental data of the two binary systems As-Co and As-Fe and the ternary systems As-Co-S and As-Co-Fe is presented and critically evaluated. A set of model parameters is optimized for each phase to predict thermodynamic properties and phase equilibria for these systems using the CALPHAD approach. The Modified Quasichemical Model in the Pair Approximation developed by Pelton et al. [65, 66] was used for the liquid phases, and the Compound Energy Formalism (CEF) introduced by Sundman and Ågren [77] was used for solid solutions. All calculations and optimizations in this work were performed with the FactSage^{TM} thermochemical software [45-47]. The previous assessments of As-Fe system by Pei et al. [382] and Ohno and Yoh [383] are presented and discussed briefly. For the As-Fe-S ternary system, the work of Xing et al. [384] presenting thermodynamic models for some ternary solid solutions is also mentioned. The parameters suggested by the previous assessments of Fe-S system by Waldner and Pelton [385] and As-S system by Kidari and Chartrand [386] are added to the present work to evaluate the ternary As-Fe-S systems.

5.2 Literature review

5.2.1 As-Co binary phase diagram

The As-Co system has six intermediate compounds stable at ambient pressure: Co_5As_2, Co_2As, Co_3As_2, CoAs, $CoAs_2$ and $CoAs_3$. The crystal structures of the phases are presented in Table 5.4. The arsenic rich side of the As-Co phase diagram has not been investigated. The experimental studies measuring phase diagram data for the cobalt rich side are presented in

Table 5.1. Details of these studies are discussed and reviewed in this section.

Table 5.1 As-Co phase diagram data reported in the literature.

References	Experimental methods and results
[387]	**TA:** Determination of the phase diagram up to a composition of 48 at. % As.
[388]	**TA, thermal expansion test and magnetic content analysis:** Determination of the phase diagram up to a composition of 28.5 at. % As and determination of the magnetic transition.
[389]	**TA:** Determination of the phase diagram up to a composition of 25 at. % As.
[390]	**Ignition analysis:** Study of the oxidation kinetics and determination of the limits of solid solutions for Co_5As_2, Co_2As, Co_3As_2 and CoAs.
[391]	**Quenching method combined with EPMA:** Determination of the limits of the biphasic liquid + fcc cobalt region between 1273 K and 1473 K.

Co-Co_5As_2 subsystem

Solid solubility: The solubility of arsenic in cobalt is not negligible. A maximum solubility of 3 at. % As in Co at 1180 K was measured by Friedrich [387]. For the same temperature, Koster and Mulfinger [389] measured a higher maximum solubility of 5.6 at. % As in Co and estimated that the solubility decreases to at least to 4 at. % As with decreasing temperature. The measured value by Koster and Mulfinger [389] is in agreement with the measurements of the solidus curve by Hino and Azakami [391]. Eutectic: According to Friedrich [387] , a eutectic reaction takes place at a temperature of 1189 K to form solid cobalt and Co_5As_2 at a composition around 26 at. % As. This is close to the eutectic temperature of 1193 K measured by Koster and Mulfinger (Koster & Mulfinger, 1938) for the same eutectic composition. Haschimoto [388] measured a higher eutectic temperature of 1270 K. Liquidus: The liquidus curve has been measured up to 25 at. % As by Friedrich [387], Koster and Mulfinger [389], Haschimoto [388] as well as Hino and Azakami [391]. The curve measured by Friedrich [387] is higher than that measured by Koster and Mulfinger [389] and slightly lower than the measurements made by Haschimoto [388] and Hino and Azakami [391]. Magnetism: The Curie temperature of pure fcc Co is lowered from 1396 K to a fixed value of 1198 K in the two-phase region according to Koster and Mulfinger [389] and at a temperature of 1336 K according to Haschimoto [388].

Co_5As_2-CoAs subsystem

The only measurements for this subsystem are made by Friedrich [387]. Also, thermal effects between 13 at. % to 37 at. % As were recorded, for temperatures between 521 K and 625 K. Since a considerable increase in volume occurred at the composition of Co_2As, Friedrich [387] suggested that the thermal effects were probably due to a polymorphic transformation of the compound. According to Hansen and Anderko [188], this assumption is doubtful.

Non-stoichiometry of the intermediate phases

The compounds Co_5As_2, Co_2As, Co_3As_2 and $CoAs$ are not stoichiometric according to Kochner [390]. Based on his measurements of ignition temperatures, a curve was determined, and its evolution shows that when the solubility limit for a compound is reached, the curve evolves horizontally at a constant temperature and rises from the composition of the adjacent arsenide, showing a narrow homogeneity range. Kochner [390] therefore concluded the limits of the following solid solutions: from 27.5 at. % to 30.1 at. % As for Co_5As_2, from 32.7 at. % to 35.8 at. % As for Co_2As, from 39 at. % to 43% molar arsenic for Co_3As_2 and up to 47.6 at. % As for CoAs.

Co_5As_2

Much uncertainty still surrounds the temperature range of the stability of Co_5As_2 and if it exists in more than one structural form. At a temperature of 1101 K, the compound undergoes a polymorphic transformation according to Friedrich [387], but he observed no structural change. The compound is not congruent, and it decomposes by a peritectic reaction at 1196 K. According to Haschimoto [388], the polymorphic transformation of the compound occurs at a temperature of 1139 K, which is higher than the temperature measured by Friedrich [387]. According to the XRD experiments performed by Heyding and Calvert [392], if the compound Co_5As_2 exists, it is only stable at high temperatures, and it decomposes into Co_2As and the fcc Co solid solution above 1073 K. The DTA measurements by Ellner et al. [393] confirmed the existence of Co_5As_2 at high temperatures only, in a range of about 50°. It decomposes at a temperature of 1140 K, 70° lower than the decomposition temperature of Ni_5As_2. According to measurements of Espeleta [394] performed by drop calorimetry between 800 K and 1500 K, there is a polymorphic transformation of Co_5As_2 at a temperature of 1176 $\pm$ 3 K. The measured heat of transformation is 27.3 ± 2.5 kJ/mol. Espeleta

[394] measured a peritectic temperature of 1224 ± 3 K, and the calculated heat of fusion is 36.7 ± 0.9 kJ/mol. The existence of the compound Co_5As_2 is doubtful according to Elliott [364].

Co_2As

Nylund et al. [395] reported a rhombohedral structure for Co_2As. Heyding and Calvert [392] showed the existence of Co_2As at room temperature in a pseudo-hexagonal form, and after a slow polymorphic transition, a hexagonal form appears between 763 K and 793 K upon heating, and between 661 K and 675 K upon cooling. The XRD results of Kjekshus and Skaug [396] showed a transformation at 725 $\pm$ 5 K, which does not agree with the ranges suggested by Heyding and Calvert [392]. They also showed that Co_2As is paramagnetic at temperatures above 60 K. According to Friedrich [387], Co_2As decomposes following a peritectic reaction at 1230 K.

Co_3As_2

At a temperature of 1182 K, Co_3As_2 undergoes a polymorphic transformation according to Friedrich [387]. Also, the compound is not congruent and decomposes by a peritectic reaction at a temperature of 1287 K. This does not agree with the results of Heyding and Calvert [392], which show that Co_3As_2 is stable only at high temperatures, above 1213 K.

$CoAs$

According to Friedrich [387], CoAs is congruent with a melting temperature around 1453 K. Heyding and Calvert [392] show that the compound exists at room temperature and undergoes a polymorphic transformation, between 1217 K and 1233 K. The transformation takes place at a higher temperature, of 1248 ± 20 K according to the XRD results obtained by Selte and Kjekshus [397], from an orthorhombic structure to an hexagonal structure.

$CoAs_2$

$CoAs_2$ is found as the minerals smaltine and safflorite with a monoclinic structure [398-400]. High temperature investigations by XRD, DTA and quenching experiments performed by Kjekshus and Rakke [401] showed a polymorphic transformation at a temperature of 870 K. According to the thermal-scanning experiments of Siegrist and Hulliger [402], the transformation occurs at 800 $\pm$

2 K upon heating and 797 ± 2 K upon cooling. The corresponding transformation enthalpy is 800 J/mol. The melting point of this compound is still uncertain.

$CoAs_3$

$CoAs_3$ corresponds to the mineral skutterudite and it appears to exist in only one cubic form [403]. The melting point of this compound is still uncertain.

5.2.2 Thermodynamic properties of As-Co binary system

As- Co liquid

Vaisburd and Remen [404] determined the activity of Co in As-Co melt by measuring the emf on concentration cells without transport. The measurements were performed at 1573 K over a composition range of 35 to 50 at. % As. Hino and Azakami [391] also determined the activity of As in As-Co alloys using the isopiestic method. The measurements were performed at 1273 K and 1423 K over a composition range of 25 to 50 at. % As, with a conversion to liquid arsenic as the standard state. The measured activities show negative deviation from Raoult's law. The activity data is presented in Figure 5.4.

As- Co compounds

There is a lack of direct thermodynamic data measurements for compounds of the As-Co system. Niessen et al. [405] and Hisham and Benson [406] estimated the standard heats of formation of some of the compounds in this binary system but the estimated values seem unreliable given the disagreement between their estimates and measured enthalpy values of other known compounds. Standard heats of formation of some compounds were also listed in the thermodynamic tables by Naumov et al. [407], Wagman et al. [169], Kubaschewski et al. [166] and Smithells and Brandes [408]. The methods used to obtain these values have not been listed, apart from Kubaschewski et al. [166] who cited the work of Kochnev [409]. Kochnev [409] studied the thermal dissociation of Co_5As_2, Co_2As, Co_3As_2, $CoAs$, Co_2As_3 and $CoAs_2$ by determining the pressure of As_4 by the molecular flow method at a certain temperature for each compound. It was assumed that arsenic vapors under these conditions obey the laws of ideal gases, and all thermodynamic equations

derived for ideal gases were used to calculate the heats of formation. Kochnev [409] explains that his work is only approximative since the dissociation products were partially dissolved in the primary arsenide during the experiments and the total weight loss during several experiments was around 0.6 %. The heat content of Co_5As_2 was determined using drop calorimetry by Espeleta et al. [394] over a temperature range of 800 K to 1500 K. Temperature coefficients of the heat content were then determined with a regression analysis method using the Shomate function, from which the heat capacity at high temperatures was derived. The standard enthalpy of formation value suggested for Co_5As_2 is -435.7 ± 54.1 kJ/mol. This value is much more negative than the value of -270.9 kJ/mol estimated by Klingbeil et al. [27] using the Miedema model which tends to overestimate the standard heats of formation. For $CoAs_{2.92}$, Majzlan [410] recently determined a standard enthalpy of formation value of -88.2 $\pm$ 6.1 kJ/mol using high-temperature oxide-melt solution calorimetry. Figure 5.1 presents the standard enthalpies of formation reported in the literature for the compounds in the As-Co system including the DFT values reported in The Materials Project [60] and the Open Quantum Materials Database [59]. Majzlan [410] also measured the heat capacity of $CoAs_{2.92}$ using relaxation calorimetry (PPMS) between 2 K and 303 K and using DSC between 280 K and 366 K. The measurements had to be stopped upon reaching 366 K because the data became unusually scattered. The DSC values were slightly higher than the PPMS values in the overlap region. The calculated heat capacity curves for the compounds in the As-Co system are presented in Figure 5.2 and the standard entropies at 298.15 K are presented in Figure 5.3.

5.2.3 As-Fe binary phase diagram

The As-Fe system has three stoichiometric intermediate compounds stable at ambient pressure: Fe_2As, $FeAs$ and $FeAs_2$. The crystal structures of the phases are presented in Table 5.4. The Experiments of Friedrich and Borchers [411] and Sawamura et al. [412] also indicated the existence of a high temperature solid solution around a composition of Fe_3As_4. Just like for the As-Co system, measurements in the arsenic-rich side of the As-Fe system were difficult to obtain. The experimental studies measuring phase diagram data are presented in Table 5.2. Details of these studies are discussed and reviewed in this section.

Table 5.2 As-Fe phase diagram data reported in the literature.

References	Experimental methods and results
[411]	**TA and metallography:** Determination of the phase diagram between the compositions of 6 at. % and 49 at. % As.
[413]	**TA, metallography, and magnetic content analysis:** Determination of the phase diagram up to a composition of 32 at. % As and determination of the magnetic transition.
[414]	**Diffusion measurement of arsenic in iron:** Determination of the saturation composition of iron (fcc) at 1423 K.
[415]	**Dilatometric, metallography and XRD:** Determination of the limits of the iron (fcc) saturation loop.
[416]	**TA and metallography:** Suggestion of the solubility of arsenic in iron (fcc) based on extrapolations from measurements made on alloys of iron and arsenic containing low concentrations of carbon.
[412]	**DTA:** Determination of the phase diagram between the compositions of 40 at. % and 57 at. % As.
[417]	**Magnetic content analysis: D**etermination of the magnetic transition.
[418]	**TA, metallography and XRD:** Determination of the limits of the iron (fcc) saturation loop.
[419]	**Microhardness, metallography and XRD:** Determination of the solid solubility of arsenic in iron (bcc).
[253]	**TA:** Determination of phase diagram data for two alloys at compositions of 58 at. % and 70 at. % As.
[420]	**DTA:** Determination of the solid solubility of arsenic in iron (bcc).
[421]	**TA:** Determination of the maximum solid solubility of arsenic in iron (bcc) at the eutectic temperature.

Fe-Fe_2As subsystem

Fe loop: The fcc form of iron becomes unstable and the bcc form becomes stable after arsenic additions. The solubility limit of arsenic in fcc iron is therefore limited by a closed loop according

to Wever [422]. At 1423 K, the saturated fcc iron solution contains approximately 2.8 at. % As as measured by Jones [414]. For the same temperature, the extrapolation by Sawamura et al. [416] showed a saturation composition of 1.65 at. % As. The limits of the region Fe (fcc) + Fe (bcc) were measured by Svechnikov and Gridnev [415], between 1.1 and 1.9 at. % As at a temperature of 1273 K and between 1.8 and 2.5 at. % As at 1373 K. Solid solubility: Friedrich and Borchers [411] measured a maximum solid solubility of 6 at. % As in bcc Fe at the eutectic temperature, Oberhoffer and Gallaschik [413] measured a maximum value of 5.1 at. % As and Sawamura et al. [416] measured a maximum value of 8.4 at. % As at the eutectic temperature. These three values were not obtained under equilibrium conditions according to Hansen and Anderko [188]. Svchnikov and Shurin [418], Predel and Fredel [420] and Bovzic and Lucic [423] measured a higher solid solubility around 10 at. % As at the eutectic temperature. Eutectic: Oberhoffer and Gallaschik [413] concluded that a peritectic reaction Liquid + Fe (bcc) $\rightleftarrows$ Fe (fcc) takes place at a temperature of 1713 K. This conclusion is not supported by convincing evidence according to Hansen and Anderko [188]. According to the experiments of Friedrich and Borchers [411], a eutectic reaction takes place between 1106 K and 1041 K to form Fe_2As and the bcc Fe solid solution at a composition around 24.4 at. % As. This agrees with the eutectic temperature of 1100 K and the eutectic composition of 25.2 at. % As measured by Oberhoffer and Gallaschik [413]. A slightly higher eutectic temperature of 1113 K was measured by Sawamura et al. [416] with a eutectic composition of 24 at. % As. The eutectic temperature according to Bozic and Lucic is 1118 $\pm$ 5 K. Liquidus: Friedrich and Borchers [411] and Oberhoffer and Gallaschik [413] both measured the liquidus and they are in good agreement. Magnetism: Oberhoffer and Gallaschik [413] performed measurements to determine the magnetic transformation of iron containing less than 1.7 at. % As. According to their results, the magnetic transition in the Fe (bcc)-Fe_2As region is constant at 1041 K upon heating. However, the temperature of the magnetic transformation decreases upon cooling and the difference is about 60°. The magnetic transformation temperature during heating by Oberhoffer and Gallaschik [413] agrees with the results obtained by Sawamura et al. [417] who measured the same temperature during heating and cooling; constant at 1041 K up to a composition of 3 at. % As. The temperature then gradually decreases until it reaches 1003 K C at 7.65 at. % As.

Fe_2As-FeAs subsystem

Friedrich and Borchers [411] and Sawamura et al. [417] also measured phase diagram data from Fe_2As to FeAs compositions. Based on their measurements, Friedrich and Borchers [411]

suggested the formation of a high temperature solid solution with a composition around Fe_3As_2. The solid solution decomposes at a temperature of 1073 K. However, the XRD and the microscopic investigation by Hagg [424] failed to find the Fe_3As_2 solid solution while Hagg [425] confirms that it does not exist at temperatures lower than 1068 K. According to the experiments of Sawamura et al. [417], a solid solution identified as ε exists, but it could not be confirmed whether it corresponds to Fe_3As_2. The ε phase forms by a peritectic reaction (Liquid+ FeAs ⇌ ε) at a temperature of 1275 K at 42.1 at. % As. The phase decomposes by a eutectoid reaction (ε ⇌ Fe_2As + FeAs) at a temperature of 1097 K at. 40 at. % As. Alloys quenched from temperatures above 1073 K by Heyding and & Calvert [392] did not indicate the presence of the Fe_3As_2 phase. Also, according to the PXRD experiments by Seitkan et al. [426], there is no evidence of the presence of the Fe_3As_2 phase at temperatures between 1068 K to 1122 K.

$FeAs$-$FeAs_2$ subsystem

Clark [253] performed a single measurement for this subsystem at a composition of 58 at. % As, corresponding to the eutectic temperature of 1281 ± 5 K.

$FeAs_2$-As subsystem

According to Clark [253], the eutectic composition is greater than 93.5 at. % As and the eutectic temperature around 1073 ± 10 K. The solubility of Fe in As was estimated at 99.93 at. % As at the eutectic temperature.

Fe_2As

No natural occurrence is known for Fe_2As. This compound has a tetragonal structure [425]. Its melting point is 1192 K according to Friedrich and Borchers [411]. A higher temperature of 1203 K was measured by Sawamura et al. [412].

$FeAs$

No natural occurrence is known for FeAs. This compound has an orthorhombic structure [424]. Its melting point is 1281 $\pm$ 5 K according to Clark [253]. A higher temperature of 1325 K was measured by Gonzalez-Alvarez et al. [427] who also observed a transition where the magnetic helical structure disappears at a temperature of 70.95 ± 0.02 K.

$FeAs_2$

$FeAs_2$ corresponds to the mineral loellingite with an orthorhombic structure [428]. Heyding and Calvert [429] observed the phase with a minor arsenic defficiency but without quantifying it. The melting point of this phase is 1289 $\pm$ 8 K.

5.2.4 Thermodynamic properties of As-Fe binary system

As- Fe liquid

The activity of Fe in As-Fe melt was determined by Vaisburd and Remen [404] by measuring the emf on concentration cells without transport. The measurements were performed at 1573 K over a composition range of 11 to 47 at. % As. Hino and Azakami [430] determined the activity of As in As-Fe alloys using the isopiestic method. The measurements were performed at 1423 K over a composition range of 20 to 50 at. % As, with a conversion to liquid arsenic as the standard state. Arsenic properties used in their calculation are from Hultgren et al. [431]. Botor et al. [432] also determined the activity of As in As-Fe alloys based on vapor pressure measurements using two effusion methods: the Knudsen method and the Knudsen cell-mass spectrometry method. The measurements were performed over the temperature range of 1198 K and 1580 K from 21 to 35 at. % As and over the range of 1624 K and 2013 K from 0.99 to 10 at. % As. Arsenic properties used in their calculation are from Gokcen et al. [177]. Botor et al. [432] also recalculated the arsenic activity from the results of Hino and Azakami [430] using arsenic properties from Gokcen et al. [177]. The recalculated values as well as the original values by Hino and Azakami [430] are higher than those determined based on the vapor pressure measurements of Botor et al. [432]. Dong et al. [433] calculated activity coefficients of As and Fe at 1873 K using the method of free energy of fusion for alloys with compositions up to 24 at. % As. Tsukihashi et al. [434] also determined activity coefficients of As in pure Fe between 1823 K and 1923 K relative to pure liquid using chemical equilibration technioque. Yan et al. [435] calculated the activity of As and Fe in the As-Fe system using a combination of the molecular interaction volume model, Miedema's semi-empirical enthalpy model and the Tanaka equation. Their calculations are in good agreement with the activity values from Hino and Azakami [430] and Dong et al. [433]. Like the activities in the As-Co system, all measured activities in the As-Fe system show strong negative deviation from Raoult's law. The activity data is presented in Figure 5.5. At at a temperature of 1123 K, Wypartowicz et al. [436] performed three experiments measuring the liquid enthalpy of mixing at the eutectic composition of 24 at. % As using high temperature drop calorimetry. The obtained values were -11.7, -12.1 and -14.1 kJ/mol.

As- Fe compounds

No thermodynamic data available for Fe_3As_2. For Fe_2As, FeAs and $FeAs_2$, Barton [254] suggested standard heat of formation values based on extrapolations of phase equilibrium measurements for the ternary system As-Fe-S from 773 K to 1073 K. According to Perfetti et al. [437], the extrapolations of Barton [254] present significant uncertainties. Stolyarova [438, 439] measured the heat of formation of Fe_2As, FeAs and $FeAs_2$ using high-temperature calorimetry and as seen from Figure 5.1, the values are higher than those suggested by Barton [254]. The heat content of $FeAs_2$was determined using drop calorimetry by Espeleta et al. [394] over a temperature range of 800 K to 1500 K. From the measurements Espeleta et al. [394] calculated a standard heat of formation value of 114.3 ± 17.2 kJ/mol. This value is much higher than the value 86 ± 3 kJ/mol by Stolyarova [438]. Niessen et al. [405] and Klingbeil et al. [440] estimated the standard heats of formation of some compounds in the As-Fe binary system using Miedema's model but their values are overestimated compared to the measured values. Figure 5.1 also shows the enthalpy of formation of some compounds at 0 K obtained from DFT calculations reported in The Materials Project [60] and The Open Quantum Material Database (OQMD) [59]. Espeleta et al. [394] determined the temperature coefficients of the heat content by a regression analysis method using the Shomate function, from which the heat capacity of Fe_2As at high temperatures was derived. No heat capacity measurements were found for this compound. Gonzalez-Alvarez et al. [427] measured the heat capacity of FeAs using adiabatic calorimetry over the range 5 K to 1030 K and using drop calorimetry relative to 298.15 K over the range 875 K to 1350 K. Pashinkin et al. [441] measured the heat capacity of $FeAs_2$ for temperatures between 5 K to 300 K using adiabatic calorimetry. For higher temperatures. Perfetti et al. [437] estimated the heat capacity of $FeAs_2$ by analogy with the heat capacity of isostructural FeS_2 (marcasite) and FeAsS (arsenopyrite). The heat capacity data for the compounds in the As-Fe system are presented in Figure 5.2 and the standard entropies are presented in Figure 5.3.

5.2.5 Thermodynamic assessments of As-S, As-Co, As-Fe and Fe-S binary systems in the literature

No previous assessment was found for the binary As-Co system. Using the PARROT program [442], the binary As-Fe system was previously assessed by Pei et al. [382] with an ionic two-

sublattice model for the liquid phase and a substitutional regular solution model for the terminal bcc Fe and fcc Fe solid solutions. Ohno and Yoh [383] developed a thermodynamic model combined with first-principles total energy calculations based on the projector augmented wave (PAW) method [443] within the generalized gradient approximation (GGA) [444]. The liquid phase was described using a substitutional solution model. The assessment of thermodynamic properties of the As-Fe system was also performed by Botor et al. [432] using the NRTL model and by Yan et al. [435] using a combination of the molecular interaction volume model, the Miedema's semi-empirical enthalpy model et the Tanaka equation [445]. Thermodynamic modeling of the As-S binary system was performed by Prostakova et al. [185] using the Modified Quasichemical Model (MQM) for the liquid phase. A subsequent and improved thermodynamic model of the As-S binary system was performed by Kidari and Chartrand [386] including three intermediate stoichiometric compounds stable at atmospheric pressure: As_2S_3, As_4S_4 et As_4S_3. Thermodynamic modeling of the Fe-S binary system was performed by Waldner and Pelton [385], and according to their model, the system includes six intermediate stoichiometric compounds stable at atmospheric pressure: FeS (troilite), $Fe_{11}S_{12}$, $Fe_{10}S_{11}$, Fe_9S_{10}, Fe_7S_8 (monoclinic pyrrhotite) and FeS_2 (pyrite). The system also includes the $Fe_{1-x}S$ (pyrrhotite) solid solution that exhibits a substantial deviation from stoichiometry toward excess S. For both As-S and Fe-S binary systems, the calculations and optimizations were performed with the FactSage^{TM} thermochemical software [45-47]. The Modified Quasichemical Model (MQM) was used for the liquid phase and the compound energy formalism (CEF) was used to model the pyrrhotite solution. The optimized parameters of the As-S system in our previous work [386] and the Fe-S system by Waldner and Pelton [385] are used in this work to evaluate the ternary As-Fe-S system.

5.2.6 As-Fe-S ternary phase diagram

Several investigations examined the As-Fe-S system, contrary to the less studied As-Co-S system. FeAsS is the only known compound in the As-Fe-S ternary system [446], and the studies concerning this ternary system are presented in Table 5.3 and discussed in this section.

Table 5.3 As-Fe-S phase diagram data reported in the literature.

References	Experimental methods and results
	Fe_2As-FeS
[447]	**TA, XRD and microscopic examination:** Determination of the quasi-binary section for the entire composition range.
	Isothermal sections
[253, 448]	**Evacuated, sealed silica tubes experiments, XRD and optical examination:** Determination of equilibrium phase relations at 873 K, and changes in assemblages between 673 K and 1023 K.
[254]	**Quenching experiments, XRD, optical examination and pyrrhotite-indicator method:** Determination of four-phase invariant reactions during solidifications and prediction of isothermal sections between 554 K and 1103K.
[449]	**Based on literature descriptions of natural assemblages:** Proposition of a As-Fe-S phase diagram.
[450]	**Sub-solidus recrystallization experiments, microprobe analysis and XRD:** Determination of the composition and phase relations involving FeAsS.
	Liquidus surface
[446]	**Based on the work of Clark [253] and Barton [254]:** Suggestion of a schematic liquidus surface.

Fe_2As-FeS pseudo-binary system

According to the measurements performed by Nishihara and Izaki [447], a eutectic reaction forming Fe_2As + FeS occurs at a temperature of 1154 K and a composition around 22.5 mol % FeS. Also, a monotectic reaction occurs at a temperature of 1323 K. The mutual solid solubility of Fe_2As and FeS could not be measured.

As-Fe-S isothermal sections

Based on mineral occurrences reported in the literature, McKinstry [449] proposed a As-Fe-S ternary phase diagram without considering the phases FeAs and Fe_2As. According to Clark [448], tie-lines change as function of deposition temperature and pressure, and since the proposed phase

diagrams by McKinstry [449] is based on a series of isolated mineral occurrences, it may include assemblages that are not stable at any given temperature. Clark [253, 448] investigated phase relations in the synthetic As-Fe-S ternary system and the measurements were performed with the presence of vapor. Vapor pressures could not be measured, and Clark [253] assumed that the pressures of all vapors in equilibrium with condensed phases lie between 1.3×10^{-1} and 6.5 bar at 873 K. The determined isothermal diagram at 873 K shows eight univariant four-phase assemblages. Clark [253] also studied the changes in stable phases and produced five isothermal sections in the following temperature ranges: T < 764 $\pm$ 12 K, 764 $\pm$ 12 K < T < 961 $\pm$ 3 K, 961 $\pm$ 3 K < T < 975 $\pm$ 3 K, 975 $\pm$ 3 K < T < 1016 $\pm$ 2 K and T > 1016 $\pm$ 2 K. Barton [254] measured five ternary univariant equilibria in presence of vapor and the proposed isothermal ternary diagrams are in good agreement with the work of Clark [253]. Based on the results of Clark [448] and Barton [254], Raghavan [446] suggested a liquidus surface. In addition to the liquid miscibility gap on the FeS-Fe_2As pseudo-binary system, Raghavan [446] suggests another liquid miscibility gap originating along the Fe-S side and extending to the As corner.

Fe solubility in As-S liquid

Since orpiment (As_2S_3) and realgar (As_4S_4) melt at temperatures slightly above 573 K, Clark [448] reported a very narrow liquid field extending along the As-S binary system. The solubility of iron could not be measured, but according to previous measurements by Drs. Wiik and Paavo Vaananen (cited in [253]), liquid As-S contains around 0.16 at. % Fe.

FeAsS

FeAsS correspond to the naturally occurring mineral arsenopyrite. Like the structure of loellingite ($FeAs_2$), the structure of arsenopyrite also derives from the structure of marcasite (FeS_2), a polymorph of pyrite [451]. Arsenopyrite with the ideal stoichiometry is monoclinic [428], and the deviation from the ideal chemical formula results in a triclinic structure [428, 452]. Twining in arsenopyrite gives rise to a pseudo-orthorhombic structure [428, 453]. Analyses by Klemm [454] and Kretschmar and Scott [450] showed that naturally occurring arsenopyrite may be slightly iron deficient, less than 1 at. %. However, according to Marimoto and Clark [453], the variations of iron content in arsenopyrite represent sampling and analytical errors rather than a deficiency. Clark [253] investigated the composition of synthetic arsenopyrite and found that it exists over a range of As and S. At 873 K, synthetic arsenopyrite has a small solid solubility and it does not encompass

the ideal stoichiometric composition FeAsS. The approximate limits suggested are $FeAs_{1.08}S_{0.92}$ and $FeAs_{1.05}S_{0.95}$. Chemical analysis on natural arsenopyrite performed by Clark [253] showed that it is sulfur rich relative to the ideal stoichiometric formula. The composition is found to be around $FeAs_{0.97}S_{1.06}$. Kretchmar and Scott [450] determined the compositions of arsenopyrite in different assemblages. The measurements are more precise in the assemblage arsenopyrite + pyrrhotite + liquid + vapor and arsenopyrite + pyrrhotite + loellingite + vapeur. For other assemblages, it was more difficult to find arsenopyrite grains suitable for analysis. At 573 K, their results show that the composition range of arsenopyrite extends from less than 30 at. % As in equilibrium with pyrite and arsenic to approximately 33.5 at. % As in equilibrium with pyrrhotite and loellingite. Kretchmar and Scott [450] also showed that arsenopyrite contains around 38.5 at. % As at 973 K. According to Clark [253], arsenopyrite is incongruent and stable up to a temperature of 975 ± 3 K before decomposing to form pyrrhotite, loellingite and liquid. The homogeneity range of AsFeS is shown in Figure 5.6 d).

Solubility of As in FeS_2

Thermodynamic modeling of the Fe-S binary system was performed by Waldner and Pelton [385], and their model includes the intermediate stoichiometric compound FeS_2. Natural pyrite (FeS_2) exists in various geological environments, and depending on the hydrothermal conditions, it can incorporate arsenic in a wide composition range [455, 456]. Pyrite is reported in deposits with and without the presence of arsenopyrite. In assemblages of pyrite and arsenopyrite, arsenic content was found to vary from sample to sample, ranging from below the detection limit to about 5.2 at. % As in pyrite. Stepanov et al. [456] presents a literature survey detailing the results of the various experimental studies of arsenic content in pyrite in assemblages containing pyrite and arsenopyrite. In deposits without arsenopyrite, arsenic content in pyrite was also found to vary largely, reaching much higher arsenic values around 10.5 at. % As [457]. Few experiments synthesised pyrite and studied its arsenic content. At low temperatures, the nucleation of pyrite does not proceed at a significant rate, making it difficult to obtain an equilibrium state experimentally [458-460]. Low temperature experiments at 573 K to 773 K by Fleet and Mumin [461] synthetized metastable pyrite with an arsenic content of up to 5 at. % As. At higher temperatures, lower arsenic contents were reported. According to Clark [253], very little arsenic is soluble in pyrite coexisting with pyrrhotite and the As-S liquid. The value does not exceed 0.28 at. % As at 873 K. Kretchmar and Scott [450] agree with this value. At 773 K, Hem and Makovicky [462] produced nickel and cobalt bearing

pyrite in equilibrium with arsenopyrite. Pyrite contained from 0.1 at. % to 4.5 at. % As. Using first-principles and monte Carlo calculations, Reich and Becker [463] investigated the thermodynamic mixing properties of As into pyrite. According to their predictions, pyrite can incorporate up to 3 at. % As in solid solution before unmixing into pyrite + arsenopyrite.

Solubility of As in $Fe_{1-x}S$

Thermodynamic modeling of the Fe-S binary system was performed by Waldner and Pelton [385], and their model includes the pyrrhotite $Fe_{1-x}S$ solid solution. Clark [253] examined the solid solubility of arsenic in synthetic pyrrhotite with the composition $Fe_{0,92}S$ and found no evidence of As solubility in pyrrhotite at 873 K. XRD measurements performed by Barton [254] on pyrrhotites from arsenic and arsenic-free charges showed an agreement with the results of Clark [253]. The analyses by Foley and Ayuso [464] also show that arsenic substitutes as a minor element in natural pyrrhotite, no more than 0.06 at. % As according to the chemical analysis of Ettler and Johan [465].

Solubility of S in Fe_2As and $FeAs$

Sulfur may be slightly soluble in Fe_2As and FeAs according to Clark [253] but the exact amount was not determined.

Solubility of S in $FeAs_2$

The solubility of sulfur in $FeAs_2$ reaches a maximum of 7 at. % S at 975 K and drops slightly at 923 K according to Clark [253]. The solubility can reach up to 0.21 at. % S in natural samples [466].

5.2.7 Thermodynamic properties of As-Fe-S ternary system

Activity measurements

Using the isopiestic method, the iso-activity of arsenic in Fe-S-As ternary alloys was measured by Hino [467] at a temperature of 1423 K. Arsenic activity has been found to increase with increasing sulfur content. The iso-activity lines of arsenic referred to liquid As as the standard state are shown in Figure 5.7.

FeAsS

Naumov et al. [407] proposed an estimation of the heat capacity of arsenopyrite in the temperature range from 248 K to 975 K and subsequently, Pashinkin et al. [468] determined experimentally the

heat capacity of arsenopyrite at a composition of $FeAs_{1.08}S_{0.92}$ in the temperature range from 5 K to 620 K. The heat capacity was measured using vacuum adiabatic calorimetry from 5 K to 250 K, dynamic calorimetry from 55 K to 530 K and DSC from 350 K to 620 K. The measurements were then stopped because of the noticeable thermal dissociation of arsenopyrite starting from 700 K to 750 K. The data obtained by Pashinkin et al. [468] is in good agreement in the overlapping regions. However, the estimation by Naumov et al. [407] gives higher heat capacities then what was measured by Pashinkin et al. [468]. Based on the phase equilibrium study results, Barton [254] estimated a value of $-92.7\ \mathrm{kJ/mol}$ for the standard heat of formation of arsenopyrite. Pashinkin et al. [468] calculated a higher value of -108.6 kJ/mol at the stoichiometric composition. Barton [254] also estimated a standard entropy value of $103.8\ \mathrm{J/(mol.\,K)}$. This value is overestimated according to Pashinkin et al. [468], who calculated a value of $68.49 \pm 0.9\ \mathrm{J/(mol.\,K)}$ for arsenopyrite at the stoichiometric composition. Pashinkin et al. [468] explains that arsenopyrite is formed by partial substitution of sulfur atoms by arsenic in FeS_2 resulting in a less symmetrical structure. And by comparing the obtained standard entropy to the values of pyrite ($53.89 \pm 0.47\ \mathrm{J/(mol.\,K)}$), the order of magnitude corresponds to the replacement of one sulfur atom by a heavier arsenic atom.

For temperatures between 773 K and 975 K, Barton [254] measured the activity of S_2 using the pyrrhotite-indicator method [469] during the following sulfidation reaction involving arsenopyrite:

$$2FeAs_2 + 2FeS + S_2 \rightarrow 4FeAsS \tag{5.1}$$

The data is presented in Figure 5.6.

Strathdee and Pidgeon [321] measured the vapor pressure over arsenopyrite using quartz spoon gauge. The thermal decomposition of arsenopyrite occurs according to reaction 2, and in the presence of pyrite, reaction 3 also occurs according to Strathdee and Pidgeon [321] :

$$4FeAsS_{(s)} \rightarrow 4FeS_{(s)} + As_{4(g)} \tag{5.2}$$

$$4FeAsS_{(s)} + 4FeS_{2(s)} \rightarrow 8FeS_{(s)} + As_4S_{4(g)} \tag{5.3}$$

Three sets of measurements were performed for temperatures between 473 K and 923 K. The measurements using two different arsenopyrite sample sizes are in good agreement. Another run was also performed using partially distilled arsenopyrite at 873 K to remove some of the volatile sulfur from the sample. The measurements show a “break” which was explained as the point

separating the equilibrium between arsenic vapor and liquid As_4S_4 and the equilibrium between arsenic vapor and gaseous As_4S_4. The interpretation of the present phases seems to be erroneous according to Chakraborti and Lynch [294]. Fushimi and Webster [470] also noted that FeS in reaction 2 should be given as $Fe_{1-x}S$. Using the thermographic method, Zviadadze and Rtskhiladze [471] also measured the vapor pressure between 640 K and 677 K. The measurements of Strathdee and Pidgeon [321] and Zviadadze and Rtskhiladze [471] are difficult to interpret according to Barton [254] because the equilibrium is difficult to obtain at temperatures of the order of 773 K. For temperatures between 868 K and 969 K, Pashinkin et al. [472] measured the dissociation pressure of natural arsenopyrite with a composition of $FeAs_{0.96}S_{1.04}$ using a static method with a membrane zero-manometer. The obtained data is in good agreement with the measurements of Zviadadze and Rtskhiladze [471]. The vapor pressure data is presented in Figure 5.6.

5.2.8 Thermodynamic modeling of As-Fe-S ternary system in the literature

Using the SELEKTOR software [473], Vilor et al. [474] performed thermodynamic analysis and numerical simulation of mineral formation in the system Fe-As-S-Cl-Na-H_2O, where the composition of parageneses including arsenopyrite (FeAsS) and pyrite (FeS_2) was calculated. Xing et al. [384] presented thermodynamic models of solid solutions for arsenic in pyrite and arsenic in arsenopyrite contained in gold ores under hydrothermal conditions using the HCh software [475]. But according to Stepanov [476], some predictions of their thermodynamic model are inconsistent with observations in both natural samples and experimental data.

5.3 Thermodynamic modeling

All calculations and optimizations in this work were performed with the FactSage™ thermochemical software [45-47]. The properties of pure solid and liquid As, Co and Fe are from SGTE [152]. The properties of the gaseous species S, S_2, S_3, S_4, S_5, S_6, S_7 and S_8 are taken from JANAF Thermochemical Tables [153]. The properties of the gaseous species As, As_2, As_3 and As_4 are from Degterov et al. [154] and other of their unpublished optimisations and evaluations. The properties of the gaseous species AsS and As_4S_4 are from Barin [170] based on the calculations of Mah [314]. The properties of gaseous Co and Fe are from Barin et al. [357] and the properties of gaseous FeS are from JANAF Thermochemical Tables [153].

5.3.1 Thermodynamic model for the liquid phase in the As-Co an As-Fe binary systems

The Modified Quasichemical Model in the Pair Approximation [65, 66] was used to model the liquid phases to take into account the short-range ordering (SRO). For a liquid binary A-B system, the following pair exchange reaction is considered between the A and B atoms on neighbouring lattice sites:

$$(A-A)+(B-B)=2(A-B)\ ;\ \Delta g_{AB} \tag{5.4}$$

$(i-j)$ is the first nearest neighbor (FNN) atom pairs, and Δg_{AB} is the non-configurational Gibbs energy change for the formation of 2 moles of $(A-B)$ pairs. The pair and the overall mole (site) fractions are defined respectively as:

$$X_{ij}=\frac{n_{ij}}{(n_{AA}+n_{BB}+n_{AB})} \tag{5.5}$$

$$X_A=\frac{n_A}{(n_A+n_B)}=1-X_B \tag{5.6}$$

n_A, n_B represent the number of moles of A and B, n_{AB} represents the number of moles of pairs (A-B). If the coordination number of A is Z_A, the "coordination equivalent" fraction of A is defined as:

$$Y_A=\frac{Z_A n_A}{Z_A n_A+Z_B n_B}=\frac{Z_B X_B}{Z_A X_A+Z_B X_B}=1-Y_B=X_{AA}+\frac{X_{AB}}{2} \tag{5.7}$$

The "coordination equivalent" fraction of B is defined similarly. The Gibbs energy of the binary liquid is given by the following equation:

$$G=\left(n_A g_A^{\circ}+n_B g_B^{\circ}\right)-T\Delta S^{\text{configuration}}+\left(\frac{n_{AB}}{2}\right)\Delta g_{AB} \tag{5.8}$$

g_A° and g_B° are the molar Gibbs energies of the pure liquid components, and $\Delta S^{\text{configuration}}$ is the configurational entropy of mixing given by randomly distributing the (A-A), (B-B) and (A-B) pairs. The non-configurational Gibbs energy change for the formation of 2 moles of $(A-B)$ pairs is expended in terms of the pair fractions:

$$\Delta g_{AB} = \Delta g^{\circ}_{AB} + \sum_{i\geq 1} g^{i0}_{AB} (X_{AA})^i + \sum_{j\geq 1} g^{0j}_{AB} (X_{BB})^j \quad (5.9)$$

Δg°_{AB}, g^{i0}_{AB} and g^{0j}_{AB} are the temperature dependant model parameters that are optimized in this work for the As-Co and As-Fe systems. The coordination numbers can be varied with composition to reproduce the SRO, as given by equations 5.10 and 5.11. The composition of maximum SRO is determined by the ratio Z_B / Z_A:

$$\frac{1}{Z_A} = \frac{1}{Z^A_{AA}}\left(\frac{2n_{AA}}{2n_{AA} + n_{AB}}\right) + \frac{1}{Z^A_{AB}}\left(\frac{2n_{AB}}{2n_{AA} + n_{AB}}\right) \quad (5.10)$$

$$\frac{1}{Z_B} = \frac{1}{Z^B_{BB}}\left(\frac{2n_{BB}}{2n_{BB} + n_{AB}}\right) + \frac{1}{Z^B_{BA}}\left(\frac{2n_{AB}}{2n_{BB} + n_{AB}}\right) \quad (5.11)$$

Z^A_{AA} and Z^A_{AB} are the coordination numbers when the nearest neighbours of an A atom are A atoms and B atoms respectively. Z^B_{BB} and Z^B_{BA} are defined similarly. In this work, Z^{As}_{AsAs}, Z^{Co}_{CoCo} and Z^{Fe}_{FeFe} are set to be 6 for consistency with previous work. Analyzing the measured activity data in both As-Co and As-Fe binary systems (Figure 5.4 b) and Figure 5.5 b)) shows that the maximum SRO occurs at approximately a composition of 45 at. % As. The coordination numbers Z^{As}_{AsCo} and Z^{As}_{AsFe} are set to be 6, and Z^{Co}_{AsCo} and Z^{Fe}_{AsFe} are set to be 5 in this work.

5.3.2 Thermodynamic model for the liquid phase in the As-Fe-S ternary system

Geometric models can be used to estimate the excess Gibbs energy of a ternary system from the parameters of the three binary subsystems [62, 68]. For a given geometric model, the excess Gibbs energy of the ternary system at any composition p is calculated from the binary parameters at points a, b and c. The difference between the models is the placement of these three points. Since the binary excess Gibbs energy in As-Fe and As-S systems depend strongly upon composition, the different models will give very different results. Thus, the choice of points a, b and c is very important to correctly interpolate the ternary As-Fe-S system. Since Fe is a transition metal and exhibits different properties from As and S, the use an asymmetric model is more reasonable. In this work, the Toop type of extrapolation technique was used to optimize the ternary As-Fe-S liquid phase, with iron as the asymmetric component.

5.3.3 Thermodynamic model for solid solutions

The Compound Energy Formalism (CEF) [77] is used to model the solid solutions. For As-Co and As-Fe binary systems, a magnetic contribution to the Gibbs energy was added to describe the cobalt and iron rich solid solutions. For the ternary solid solutions, the sublattice models considered in this work are presented in Table 5.4 and justified in this section. The solubility of As in $Fe_{1-x}S$ as well as the solubility of S in Fe_2As and FeAs are neglected in the present work.

Co and Fe rich solid solutions

Since cobalt and iron exhibits magnetic ordering, an additional term can be added to the Gibbs energy to include the magnetic contribution. Inden [72] derived the following equation:

$$G^{magnetic} = RT\ln(\beta + 1)f(\tau) \tag{5.12}$$

β corresponds to the average magnetic moment per mole of atoms in Bohr magnetons and τ corresponds to the ratio of the temperature and the critical temperature of magnetic ordering. For ferromagnetic elements, the critical temperature corresponds to the Curie temperature T_C. For antiferromagnetic elements, the critical temperature corresponds to the Neel temperature T_N. The expression $f(\tau)$ was subsequently simplified by Hillert and Jarl [73] by expanding it into a power series. For the ferromagnetic Co and Fe, T_C and β can be expressed as a function of composition. For each disordered phase in the Fe-As system, T_C and β are given by the following expressions:

$$T_{C(x)} = x_{Fe}T_C(Fe) + T_C^{Excess} \text{ with } T_C^{Excess} = x_{Fe}\,x_{As}\sum_{i=0\ldots n} T_C(x_{As} - x_{Fe})^i \tag{5.13}$$

$$\beta(x) = x_{Fe}\beta(Fe) + \beta^{Excess} \text{ with } \beta^{Excess} = x_{Fe}\,x_{As}\sum_{i=0\ldots n} \beta(x_{As} - x_{Fe})^i \tag{5.14}$$

The expansion parameters T_C and β are evaluated based on the experimental data available. The same expressions can be derived for cobalt [74].

FeS_2

Electron microscopy and X-ray absorption spectroscopy studies on natural FeS_2 samples indicate a preferential substitution of arsenic into sulfur atomic positions [457, 461, 477-483]. This substitution mechanism usually occurs at reduced conditions such as in orogenic gold deposits [456, 484, 485]. XANES measurements on gold-bearing pyrite by Simon et al. [480] showed that

arsenic is present in FeS_2 as As^{-1} and it substitutes for sulfur in the S_2^{-2} units as AsS^{-2} pairs. Blanchard et al. [486] investigated the arsenic substitution mechanism in FeS_2 using DFT. Their results also suggest that the formation of AsS dianion groups is energetically the most favorable. Substitution of arsenic into iron atomic positions was also reported. This substitution mechanism is less common and observed mainly at oxidised conditions in hydrothermal deposits [456, 484, 485]. In a hydrothermal gold deposit, Deditius et al. [484] observed arsenic substituting iron as As^{3+}. Qian et al. [487] synthetized FeS_2 for temperatures of 398 K and 493 at the saturation pressure and their analyses suggest that arsenic substitutes for iron in FeS_2. In this work, the FeS_2 solid solution is modeled considering the preferential substitution of arsenic into sulfur atomic positions as presented in Table 5.4.

FeAsS

Möller and Kersten [488] showed that the conductivity of AsFeS depends on the As/S ratio. The substitution of sulfur by arsenic has been shown using X-ray spectroscopies by Savage et al. [481] and Le Pape et al. [482, 489]. This substitution results in a p-type conductivity [488]. In arsenopyrite enriched in sulfur, sulfur substitute for arsenic according to the electron microprobe results obtained by Nesbitt et al. [490]. This substitution results in an n-type conductivity [488]. Like in $FeAs_2$, Tossell et al. [491] and Nesbitt et al. [490] suggest that sulfur and arsenic form pairs of atoms occurring as AsS^{2-} in AsFeS. The measurements of Clark [253] and Kretschmar and Scott [450] on natural samples shown in Figure 5.6 d) indicate a deviation towards the arsenic rich side but below 673 K, Kretschmar and Scott [450] explain that uncertainty still remains in the sulfur rich side of AsFeS. In this work, the AsFeS solid solution is modeled by considering both substitution mechanisms and the sublattice model is presented in Table 5.4.

$FeAs_2$

The structure of $FeAs_2$ derives from the structure of FeS_2 (marcasite), where arsenic is substituted for sulfur [451, 492] as modeled in this work.

Table 5.4 Crystallographic description of the phases in As-Co and As-Fe systems and sublattice models selected for solid solutions in the As-Fe-S system.

Phase	Person symbol	Space group	Prototype	Reference	Sublattice models
$\mathbf{Co_5As_2}$	$hP42$	$P6_3/mmc$		[393]	stoichiometric
$\mathbf{Co_2As}$ (**HT**)	$hP9$	$P\bar{6}2m$		[392]	stoichiometric
$\mathbf{Co_2As}$ (**LT**)	-	-		-	stoichiometric
$\mathbf{Co_3As_2}$	-	-		-	stoichiometric
CoAs (**HT**)	$hP4$	$P6_3/mmc$		[397]	stoichiometric
CoAs (**LT**)	$oP8$	$Pna2_1$		[397]	stoichiometric
$\mathbf{CoAs_2}$ (**HT**)	$oP6$	Pnnm		[401]	stoichiometric
$\mathbf{CoAs_2}$ (**LT**)	$mP12$	$P2_1/c$		[399]	stoichiometric
$\mathbf{CoAs_3}$	$cI32$	$Im\bar{3}$		[403]	stoichiometric
$\mathbf{FeAs_2}$	$oP6$	Pnnm		[428]	$(Fe, Va)_1(As, S)_2$
FeAs	$oP8$	Pnma		[424]	stoichiometric
$\mathbf{Fe_3As_2}$	-	-		-	$(Fe)_3(As, Va)_2$
$\mathbf{Fe_2As}$	$tP6$	$P4/nmm$		[425]	stoichiometric
$\mathbf{FeS_2}$ (pyrite)	$cP12$	Pa3		[493]	$(Fe)_1(S, As)_2$
FeAsS	$mP12$	$P2_1/c$		[402]	$(Fe)_1(As, S)_1(S, As)_1$

5.4 Results and discussions

The optimization was conducted using the FactSage™ thermochemical software. The As-Co, As-Fe and As-Fe-S systems are assessed based on the literature data presented in the previous sections, and the optimized thermodynamic model parameters are presented in Table 5.6. The enthalpies of formation of the compounds of the As-Co system from thermodynamic tables and DFT calculations

are shown in Figure 5.1 a) along with the optimized values from this work. For compounds of the As-Fe system, the enthalpies of formation from measurements and DFT calculations are shown in Figure 5.1 b) along with the optimized values from this work. To best reproduce the phase diagram and the activity data, the selected enthalpy of formation values for Fe_2As and FeAs are slightly higher than the values measured by Stolyarova [438, 439]. The values suggested by Espelata et al. [394] and the ones estimated by the Miedema model [405, 406, 440] are not considered reliable in the context of this work and therefore not included in the Figures. The thermodynamic properties proposed in this work for Fe_3As_2 have a significant uncertainty due to the lack of data et the doubt surrounding its existence.

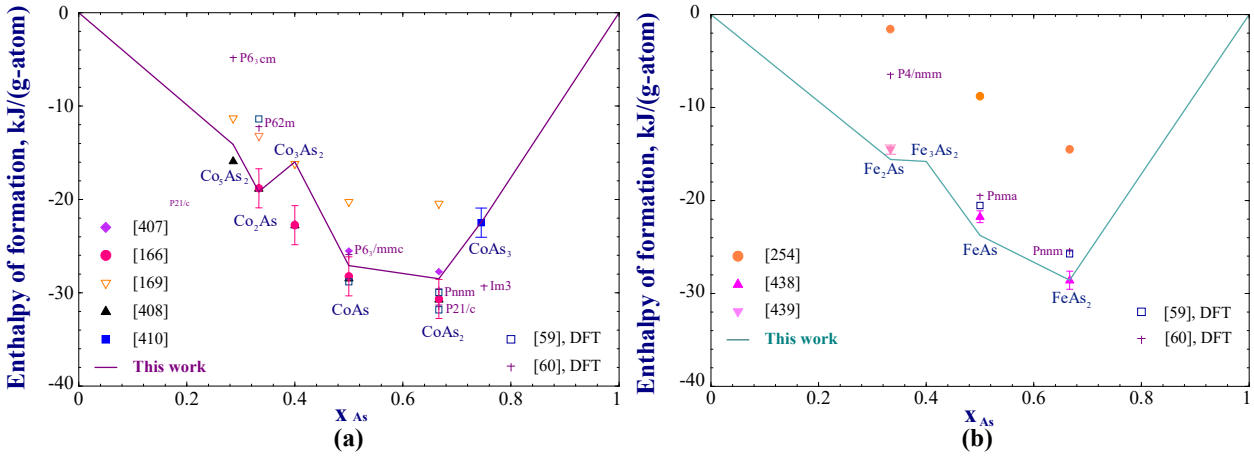

Figure 5.1 Enthalpies of formation of intermediate compounds in a) As-Co system and b) As-Fe system

The heat capacity (C_p) curves of the intermediate compounds of both binary systems are presented in Figure 5.2 and the functions are presented in Table 5.5. The Neumann-Kopp rule was used to estimate the heat capacity of the compounds with no measured data. For $FeAs_2$, the calculated heat capacity curve corresponds to the estimation of Perfetti et al. [437] by analogy with the heat capacity of isostructural FeS_2 (marcasite) and FeAsS (arsenopyrite). Since the heat capacity of FeAs derived by Gonzalez-Alvarez et al. [427] from enthalpy increment have a higher uncertainty, the calculated curve is based on the measurements obtained using adiabatic calorimetry. The standard entropies ($S^o_{298.15\,K}$) of the As-Co compounds from thermodynamic tables and the selected values in this work are presented in Figure 5.3 a). The standard entropies ($S^o_{298.15\,K}$) of the As-Fe compounds based on C_p measurements and the selected values in this work are presented in Figure

5.3 b). Due to the uncertainties surrounding the thermal dissociation experiments performed by Kochnev [409], their results were not used to optimize the properties of the As-Co compounds. The thermodynamic properties of the phases were optimized to-reproduce the phase diagram data and the activity measurements shown in Figure 5.4.

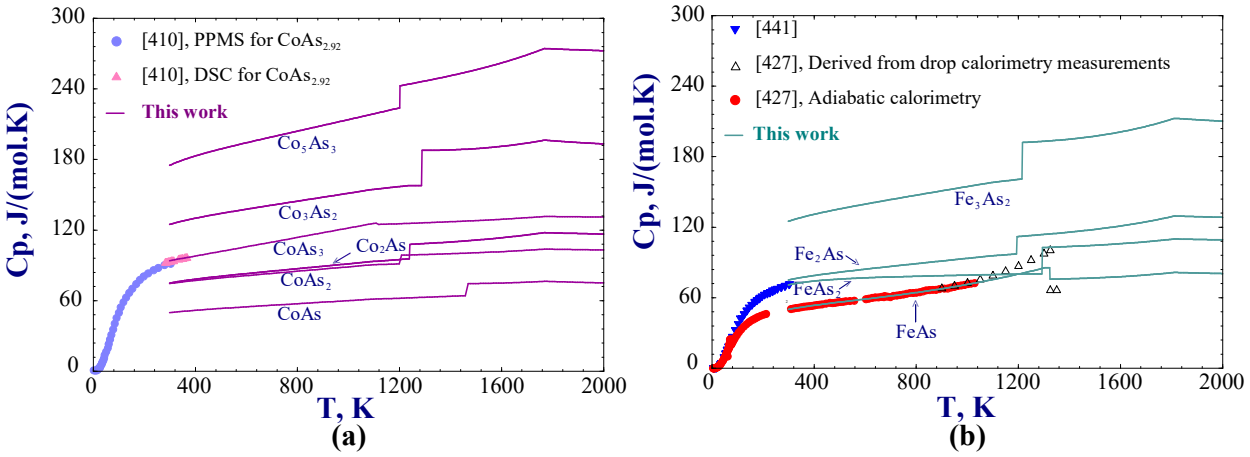

Figure 5.2 Calculated heat capacity of compounds of the a) As-Co system, b) As-Fe system

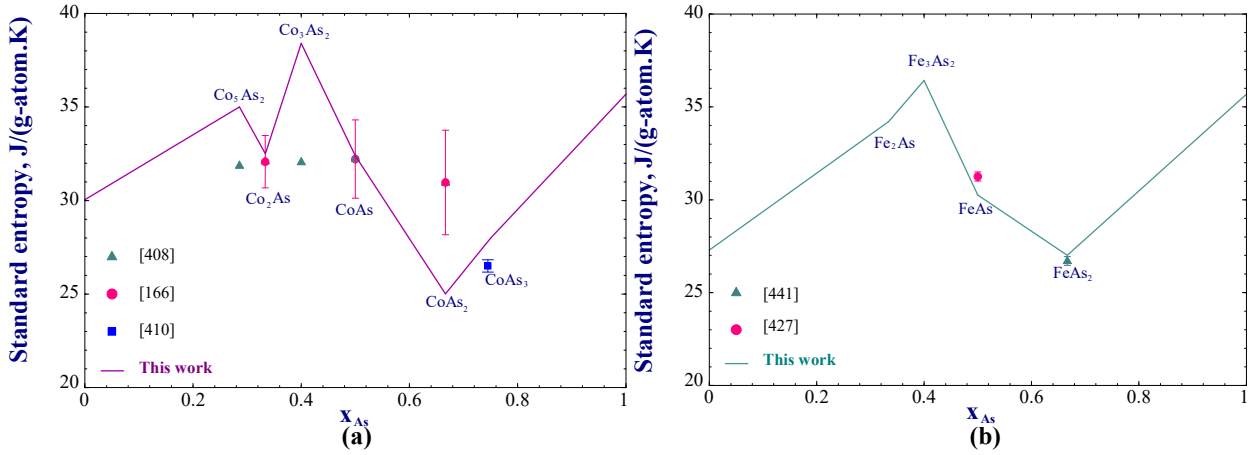

Figure 5.3 Standard entropies of the intermediate compounds in a) As-Co, b) As-Fe systems

The calculated binary phase diagrams are shown in Figure 5.4 a) and Figure 5.5 a). For compounds undergoing polymorphic transformations, the enthalpies of transformations reported in the literature are used in this work and the different phases are identified as LT (low temperature) or HT (high temperature). The calculated phase diagrams are in good agreement with the experimental data. To optimize the cobalt rich side of the As-Co system, the measurements from Friedrich [387]

and Koster [389] are selected since their measured eutectic temperature and composition are in good agreement, contrary to the data by Hashimoto [388] suggesting a much higher eutectic temperature. The selected data to optimize the magnetic parameter for the As-Co system is also from Koster [389]. The calculated magnetic transformations in both As-Co and As-Fe systems are shown in the same Figures. Since there is a lack in information on the excess magnetic moment, the excess contribution to the β term is considered nonsignificant in this work for both systems and only the T_C^{Excess} parameters are optimized. This simplified model gives adequate results as seen from the Figures. In this work, Co_5As_2 is stable only from 1141 K to 1192 K, in a range of about 50° like proposed by Ellner et al. [393]. Since the decomposition temperatures of $CoAs_2$ and $CoAs_3$ have not been measured, the proposed values in this work are uncertain. The calculated activities are presented in Figure 5.4 b) and Figure 5.5 b). To determine the activity of As, the thermodynamic properties used by Hino and Azakami [430] in their calculation are from Hultgren et al. [431]. The data is considered reliable in the context of this work, contrary to what was suggested by Botor [432]. For the As-Fe system, the calculated liquid enthalpy of mixing at 1123 K at the composition of 0.24 at. % As is -19.1 kJ/mol, slightly higher than the measured values of Wypartowicz et al. [436].

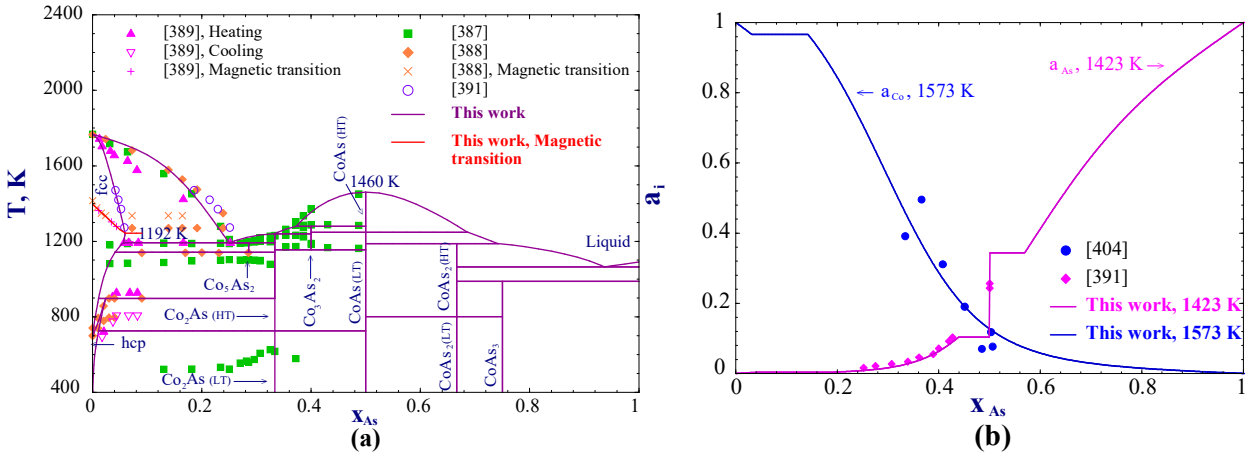

Figure 5.4 Calculated a) As-Co phase diagram, b) activities of As and Co in As-Co system, with solid cobalt and liquid arsenic standard states

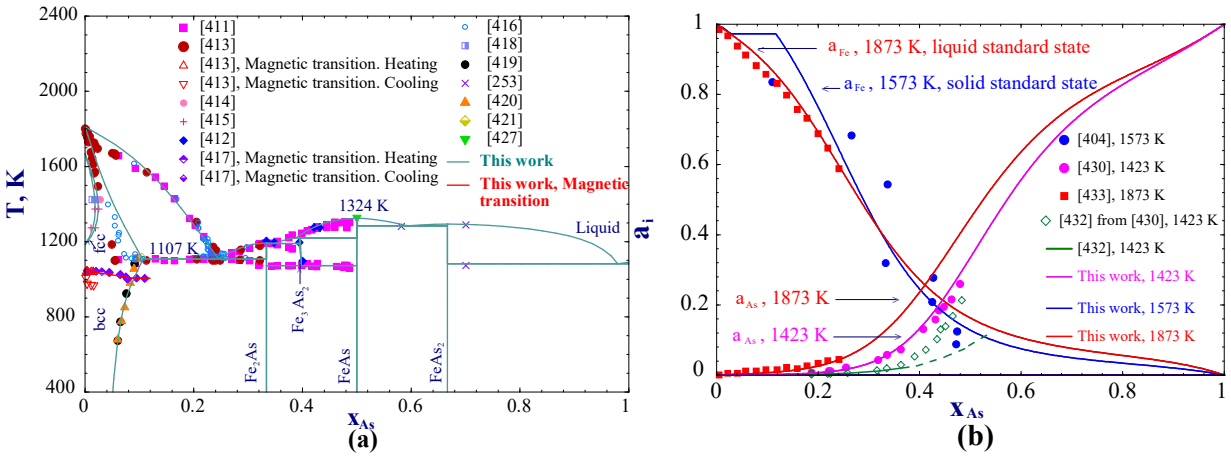

Figure 5.5 Calculated a) As-Fe phase diagram, b) activities of As and Fe in As-Fe system, with solid iron, liquid iron and liquid arsenic standard states

For the ternary FeAsS compound, the calculated heat capacity curve is based on the measurements of Pashinkin et al. [468] as seen from Figure 5.6 a). The standard entropy of 68.5 $J/(mol.\,K)$ by the same authors is selected in this work. The standard enthalpy of formation is -139.9 kJ/mol to reproduce the decomposition temperature of the compound at 975 $\pm$ 3 K as measured by Clark [253]. Figure 5.6 b) and Figure 5.6 c) show that the optimized thermodynamic properties of FeAsS reproduce well the vapor pressure data and the equilibrium of reaction 1. The calculations shown are performed for FeAsS at the stoichiometric composition even if some measurements are from experiments performed with FeAsS samples of a slightly different or a non controlled composition. Even if FeAsS exists in nature in a variable composition range, only the measurements of Clark [253] and Kretschmar and Scott [450] are considered in this work to model the limits of the solid solution. Figure 5.6 d) presents the homogeneity range of FeAsS along the FeS_2-$FeAs_2$ join. Some phases are present at equilibrium in minor quantities in this join and are identified in the Figure with "(minor)". FeAsS decomposes at a temperature of 974 K and a composition of 38 at. % As, which agrees with the experimental measurements. It decomposes to form $Fe_{1-x}S$ solid solution, $FeAs_2$ solid solution and a minor quantity of arsenic, and at a slightly higher temperature, the equilibrium becomes $Fe_{1-x}S$ solid solution, $FeAs_2$ solid solution and liquid. This is in accordance with the measurements performed in the presence of vapor by Clark [253] and Barton [254]. The calculations also show that the AsFeS solid solution is in equilibrium with $FeAs_2$ solid solution and arsenic in the arsenic rich side. In the sulfur rich side, the AsFeS solid solution is in equilibrium with $Fe_{1-x}S$ solid solution and liquid above 772 K. Below this temperature, the equilibrium exists

with FeS_2 solid solution and liquid. This corresponds to the equilibrium suggested by Clark [253] at 764 ± 12 K. The FeAsS + FeS_2 + As equilibrium line suggested at 636 ± 50 K by Barton [254] is not obtained in the present work. The maximum solubility of S in $FeAs_2$ measured by Clark [253] is reproduced as seen from Figure 5.6 d). The maximum solubility of As in FeS_2 is set to 2 at. % As.

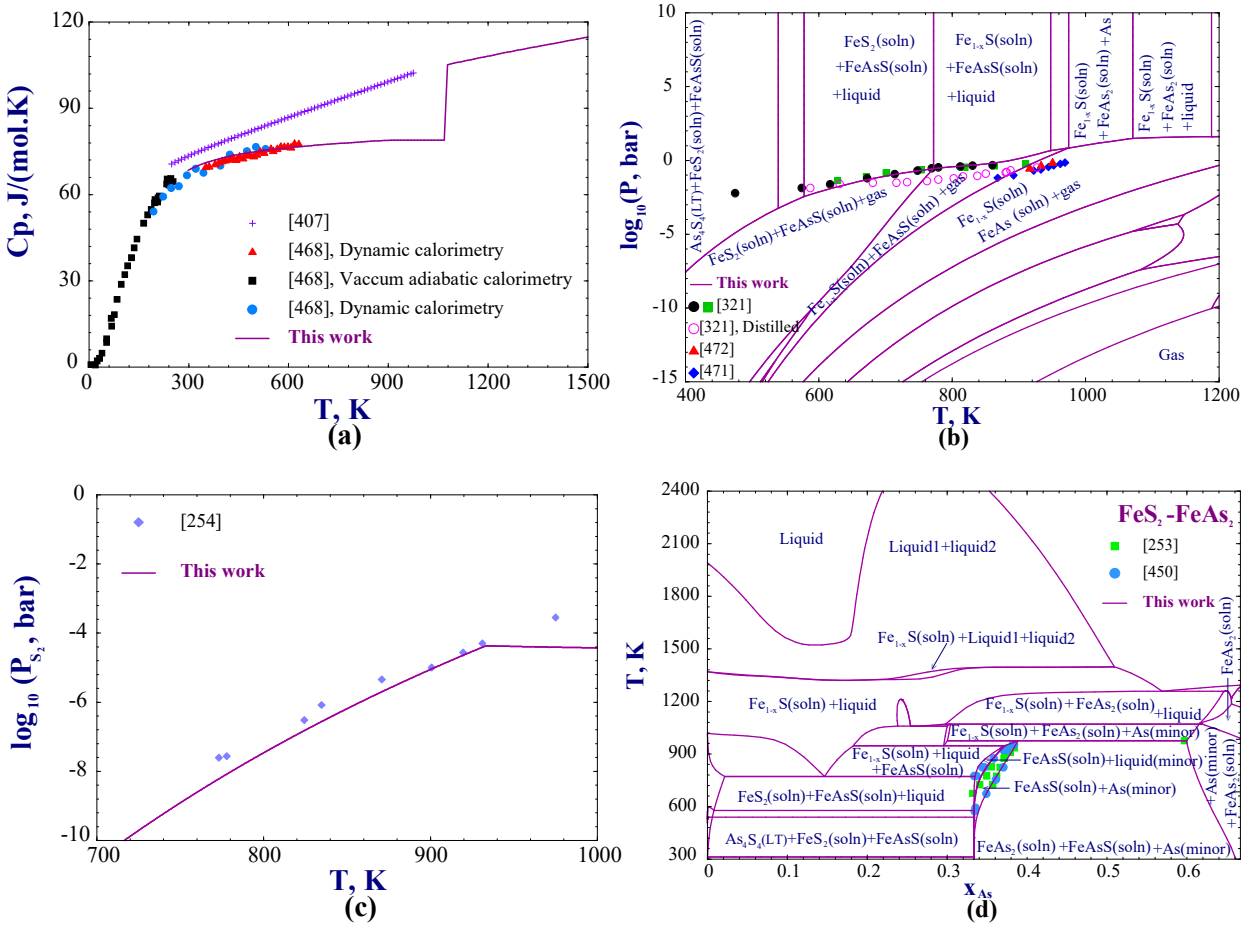

Figure 5.6 Calculated a) heat capacity of AsFeS, b) vapor pressures of AsFeS, c) activity of S_2, d) FeS_2-$FeAs_2$ join

The liquid phase is modeled with four ternary parameters, presented in Table 5.6, to reproduce accurately the experimental data. The pseudo-binary Fe_2As-FeS is presented in Figure 5.7 a). The calculated eutectique temperature is 1147 K and the eutectique composition is 18 mol % FeS, slightly lower than the composition of 22.5 mol % FeS suggested by Nishihara and Izaki [447]. The calculated monotectic reaction occurs at a temperature of 1337 K. The isotherm at 1423 K is also shown in Figure 5.7 b) along with the As iso-activity curves with liquid arsenic as the standard

state. The calculated curves are in good agreement with the measurements of Hino [467]. The calculated isothermal sections at 673 K, 873 K and 1073 K presented in Figure 5.8 are in excellent agreement with the work of Clark [253] and Barton [254]. A summary of the invariant reactions involving four-phase intersection points with liquid in the ternary As-Fe-S system is presented in Table 5.7.

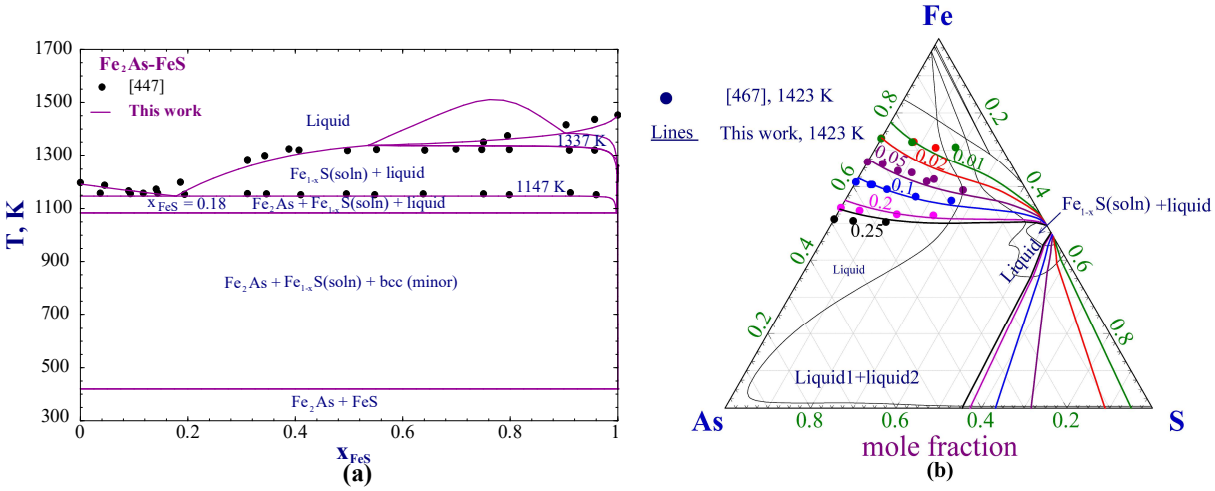

Figure 5.7 Calculated a) pseudo-binary Fe_2As-FeS system b) isothermal section of the As-Fe-S system at 1423 K along with the calculated and the experimental liquid As iso-activity curves

Table 5.5 Heat capacity (C_p) functions of the solid phases in this work

Phases	T range, K	C_p (T), J/(mol. K)
Co_5As_2	298.15-1196.15	$172.0593 + 0.03741191T - 771670T^{-2} + 5.2044 \times 10^{-6}T^2$
Co_2As (LT)	298.15-725.15	$73.4866 + 0.016051216T - 313308T^{-2} + 2.08176 \times 10^{-6}T^2$
Co_2As (HT)	725.15-1090	$73.4866 + 0.016051216T - 313308T^{-2} + 2.08176 \times 10^{-6}T^2$
	1090-1230.15	$79.388237 + 0.01618956T - 290108T^{-2} + 2.08176 \times 10^{-6}T^2$
Co_3As_2	298.15-1090	$121.8871 + 0.026792954T - 481562T^{-2} + 3.12264 \times 10^{-6}T^2$
	1090-1230.15	$133.690374 + 0.015928434T - 435162T^{-2} + 3.12264 \times 10^{-6}T^2$
CoAs (LT)	298.15-1090	$48.4005 + 0.010741738T - 168254T^{-2} + 1.04088 \times 10^{-6}T^2$
	1090-1248.15	$54.3021 + 0.005309478T - 145054T^{-2} + 1.04088 \times 10^{-6}T^2$
CoAs (HT)	1248.15-1453.15	$54.3021 + 0.005309478T - 145054T^{-2} + 1.04088 \times 10^{-6}T^2$

$\mathbf{CoAs_2}$ **(LT)**	298.15-800	$71.7149 + 0.016173998T - 191454T^{-2} + 1.04088 \times 10^{-6}T^2$
$\mathbf{CoAs_2}$ **(HT)**	800-1090	$71.7149 + 0.016173998T - 191454T^{-2} + 1.04088 \times 10^{-6}T^2$
	1900-1193.15	$83.518174 + 0.005309478T - 145054T^{-2} + 1.04088 \times 10^{-6}T^2$
$\mathbf{CoAs_3}$	298.15-1100	$82.39189 + 0.038517T + 8.48 \times 10^{-7}T^2$
$\mathbf{FeAs_2}$	298.15-1300	$76.69 + 0.0031T - 603000T^{-2}$
FeAs	298.15-1300	$102.9396 - 0.0385038T + 287228.09T^{-2} + 3.2524 \times 10^{-5}T^2 - 821.217T^{-0.5}$
$\mathbf{Fe_3As_2}$	298.15-1090	$120.6217 + 0.03340964T - 510554T^{-2} + 1.060686 \times 10^{-6}T^2$
	1090-1811	$132.4249 + 0.02254512T - 464154T^{-2} + 1.060686 \times 10^{-6}T^2$
$\mathbf{Fe_2As}$	298.15-1090	$72.643 + 0.02046234T - 332636T^{-2} + 7.07124 \times 10^{-7}T^2$
	1090-1212	$78.5446 + 0.01503008T - 309436T^{-2} + 7.07124 \times 10^{-7}T^2$
FeAsS	1090-1000	$75.51 + 0.00478T - 754300T^{-2}$

Table 5.6 Optimized thermodynamic parameters for As-Co and As-Fe-S systems (J mol^{-1})

Phases (model)	**Thermodynamic parameters**	**References**
Liquid (MQM) $(\mathbf{As}, \mathbf{Co})(\mathbf{Va})$	Z^{As}_{AsCo}= 6 ; Z^{Co}_{AsCo}= 5 ; Z^{As}_{AsAs}=Z^{Co}_{CoCo}= 6	This work
	$\Delta g_{As-Co} = -25000 + 3.655T + 4000\ X_{AsAs}$+ (-15000+11.60787129)$X^3_{CoCo}$	
Liquid (MQM) $(\mathbf{As}, \mathbf{Fe}, \mathbf{S})(\mathbf{Va})$	$Z^{As}_{AsFe} = 6$; Z^{Fe}_{AsFe}= 5 ; $Z^{As}_{AsS} = 3$; Z^{S}_{AsS}= 2 ; $Z^{As}_{AsAs} = Z^{Fe}_{FeFe} = Z^{S}_{SS}$= 6	[386]
	$\Delta g_{As-S} = (-48\,000 + 88.067T - 9.155T\ln T)+(-30\,000 + 92.124T - 10.072T\ln T)X_{AsAs}$ +$(-74000 + 249.331T - 27.092T\ln T)X^2_{AsAs}$ +(52 500-23.053)X^3_{AsAs} + 3 000X_{SS}+2500X^3_{SS}	This work
	$\Delta g_{As-Fe} = -25090 + 6.1T - 5TX_{AsAs} - 5500\ X_{FeFe}$ -1.936X^3_{CoCo}	[385]
	$\Delta g_{Fe-S} = -104.888 + 0.338T + (35.043 - 9.880T)X_{FeFe}$ + 23.972TX^2_{FeFe}+30.437X^3_{FeFe} + (8.626T)X_{FeFe} + (72.954-26.178T)X^2_{SS}+25.106X^4_{SS}	This work
	$g^{101}_{FeS(As)} = -25000$	

Phases (model)	Thermodynamic parameters	References
	$g^{102}_{FeS(As)} = 40000$	
	$g^{103}_{FeS(As)} = -11000$	
	$g^{001}_{AsFe(S)} = 13200$	
Fcc(A1) (CEF)	${}^0L_{As,Co:Va} = -61000 + 10.072T$;	This work
$(\mathbf{As, Co, Fe, S})_1(\mathbf{Va})_1$	$T_C^E = -1354.057X_{As}X_{Co}$	This work
	${}^0L_{Fe,As:Va} = -75000 + 22.912T$	[385]
	${}^0L_{Fe,S:Va} = -59070.737 - 34.612T$	
Bcc(A2) (B-W)	${}^0L_{Fe,As:Va} = -77000 + 22.986T$;	This work
$(\mathbf{As, Fe, S})_1(\mathbf{Va})_3$	$T_C^E = 549.252X_{As}X_{Fe} - 150X_{As}X_{Fe}(X_{As} - X_{Fe})^1$	
	${}^0L_{Fe,S:Va} = -31.041 - 10.657T$	[385]
Hcp(A3) (CEF)	${}^0L_{As,Co:Va} = -58905$	This work
$(\mathbf{As, Co})_1(\mathbf{Va})_{0.5}$		
hP4-$Fe_{1-x}S$ (CEF)	${}^0G_{Fe:S} = -96291.00 - 21.991T + GHSER_{Fe} + 2GHSER_S$*	[385]
$(\mathbf{Fe, Va})_1(\mathbf{S})_2$	${}^0G_{Va:S} = 140049.39 + 32.086 + 2GHSER_S$*	
	${}^0L_{Fe,Va:S} = -225830.67 - 26.359T$	
$\mathbf{Fe_3As_2}$ **(CEF)**	${}^0G_{Fe:As} = -75300 + 28.867T + 3GHSER_{Fe} + 2GHSER_{As}$	This work
$(\mathbf{Fe})_3(\mathbf{As, Va})_2$	${}^0G_{Fe:Va} = 72448.5 - 44.975T + 3GHSER_{Fe}$	
	${}^0L_{(Fe:As,Va)} = 56000 - 52.190T$	

Phases (model)	Thermodynamic parameters	References
cP12-FeS_2(CEF) $(\mathbf{Fe})_1(\mathbf{S},\mathbf{As})_2$	${}^0G_{Fe:S} = -171048.025 - 38.490T + GHSER_{Fe} + 2GHSER_S$*	[385] This work
	${}^0G_{Fe:As} = -75772 + 17.659T + GHSER_{Fe} + 2GHSER_{As}$	
	${}^0L_{(Fe:S,As)} = -25000$	
oP6-$FeAs_2$(CEF) $(\mathbf{Fe},\mathbf{Va})_1(\mathbf{As},\mathbf{S})_2$	${}^0G_{Fe:As} = -85772 + 17.659T + GHSER_{Fe} + 2GHSER_{As}$	This work
	${}^0G_{Fe:S} = -154500 + 37.51T + GHSER_{Fe} + 2GHSER_S$	
	${}^0G_{Va:As} = 20000 + 2GHSER_{As}$	
	${}^0G_{Va:S} = 860082.627 - 19.251T + 2GHSER_S$	
	${}^0L_{(Fe:As,S)} = -48500$	
mP12-FeAsS (**CEF**) $(\mathbf{Fe})_1(\mathbf{As},\mathbf{S})_1(\mathbf{S},\mathbf{As})_1$	${}^0G_{Fe:As:S}$ =-139900+27.510T+$GHSER_{Fe} + GHSER_{As} + GHSER_S$	This work
	${}^0G_{Fe:As:As} = -51272 - 17.280 + GHSER_{Fe} + 2GHSER_{As}$	
	${}^0G_{Fe:S:S} = -81048 + 38.490T + GHSER_{Fe} + 2GHSER_S$	
	${}^0G_{Fe:S:As} = -89900 + 26.539 + GHSER_{Fe} + GHSER_{As} + GHSER_S$	
	${}^0L_{(Fe:As:S:As)} = 6000 - 38.805T$	

*Heat capacity functions given in Table 5 of the reference [385]

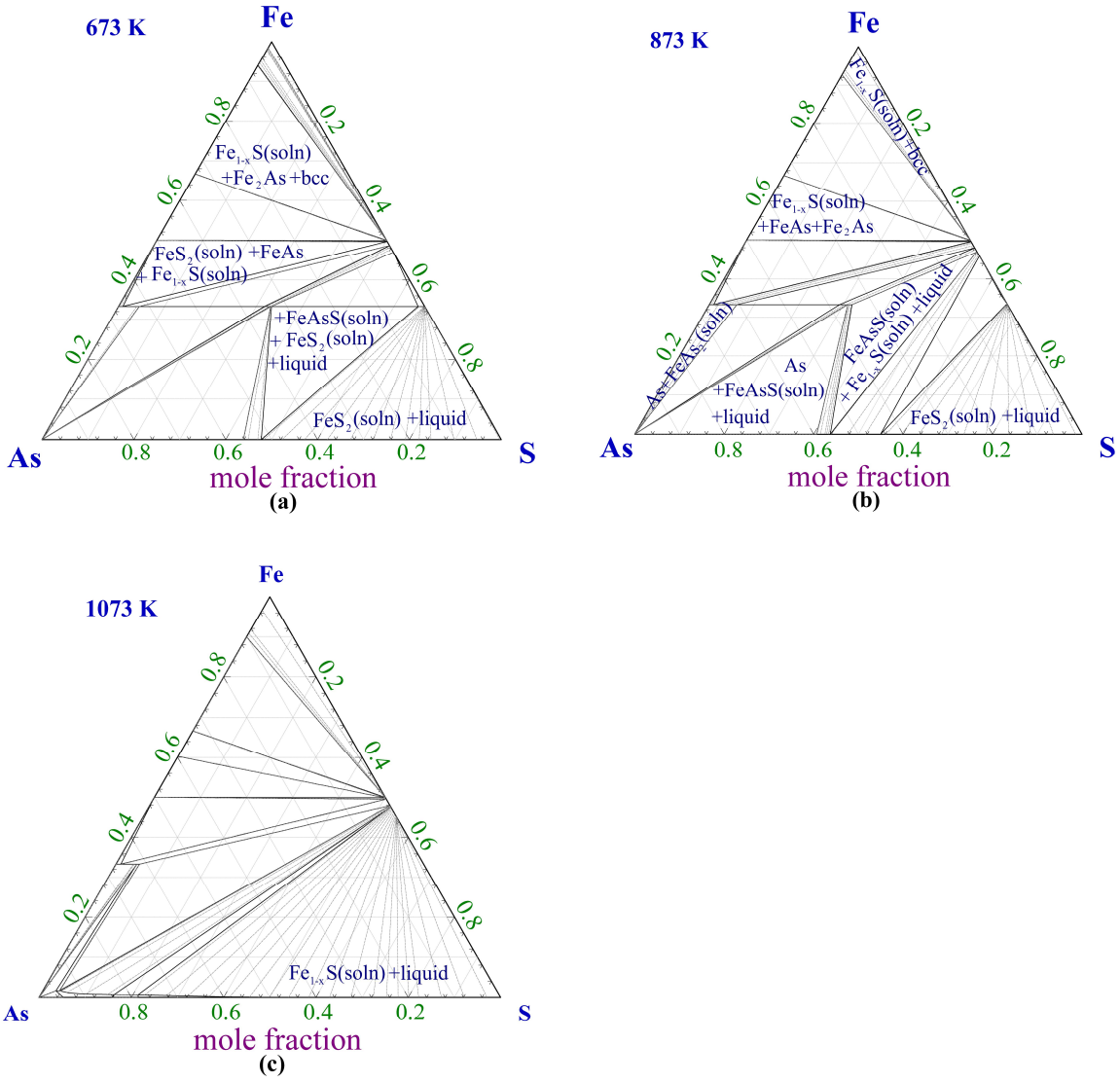

Figure 5.8 Calculated isothermal section at 673 K, b) 873 K, c) 1073 K

Table 5.7 Summary of some invariant reactions involving the liquid phase in the ternary As-Fe-S system

Reactions			**Temperatures**
at. % Fe	**at. % S**	**at. % As**	**K (°C)**
Liquid ⇌ Liquid 2 + $Fe_{1-x}S$ + bcc			
0.629	0.318	0.053	1233.3 (960.15)
0.629	0.085	0.170	
Liquid 1 ⇌ $Fe_{1-x}S$ + bcc + Fe_2As			
0.465	0.131	0.404	1220 (946.85)
Liquid ⇌ $Fe_2As + Fe_{1-x}S + bcc$			
0.735	0.032	0.233	1083.14 (809.99)

5.5 Conclusion

In this work, the thermodynamic information available in the literature is critically evaluated and used to optimize the As-Co and the As-Fe binary systems. Important uncertainties remain due to the lack of experimental data in the arsenic rich regions of both phase diagrams. The binary systems are assessed based on all available literature data to propose a reasonable set of model parameters for the arsenic rich region. The MQM with the pair approximation is applied to model the liquid phase. This model is well adapted to introduce extra parameters in X(As-As) pairs that can be adjusted with minimal impact on the rest of the optimization, contrary to the correlated Redlich-Kister parameters. For the ternary As-Fe-S, the Toop extrapolation technique was used with iron as the asymmetric component. The CEF was used for solid solutions, with added magnetic contributions to describe the Gibbs energy of cobalt and iron rich solid solutions. The calculated phase diagrams and thermodynamic properties provide an accurate description of all reliable experimental data.

Acknowledgments

The authors would like to thank the financial support from NSERC and CRC programs.

Declaration of competing interest

The authors declare that they have no known competing financial interests or personal relationships that could have appeared to influence the work reported in this paper.

Data availability

Data will be made available on request.

CHAPITRE 6 DISCUSSION GÉNÉRALE

Ce projet de recherche vise principalement à développer un outil pour adresser la problématique de l'augmentation des émissions d'arsenic durant les procédés de smeltages ainsi que les procédés de recyclage et de disposition de certains produits électroniques. La présence d'arsenic dans ces procédés peut favoriser la formation de plusieurs équilibres thermodynamiques et phases intermétalliques, et pouvoir prédire leurs formations potentielles seraient grandement bénéfique pour les industries affectées par le problème de contamination par l'arsenic. Plusieurs systèmes d'intérêts pour l'industrie du smeltage des minerais sulfurés et pour l'industrie électronique ont été modélisés dans le cadre de ce projet.

Le mémoire est présenté sous forme de trois articles constituants des chapitres de ce mémoire. La méthodologie employée est l'approche CALPHAD qui repose principalement sur les données disponibles dans la littérature pour effectuer la modélisation. Ainsi, chacun des chapitres 3, 4 et 5 a présenté une revue de la littérature exhaustive des données expérimentales des systèmes à l'étude. Chacun des chapitres a présenté également une revue critique de toutes les données expérimentales extraites de la littérature pour déterminer leurs fiabilités. Le modèle sélectionné pour décrire les phases liquides est le modèle Quasichimique Modifié par l'approximation des pairs. Ce modèle est unique par sa capacité à représenter l'ordonnancement à courte distance. Il est aussi très bien adapté pour les systèmes où il y a un manque de données expérimentales puisque des paramètres peuvent être introduits ou ajustés pour certaines régions, tout en ayant un impact minimal sur le reste de l'optimisation. Le *Compound Energy Formalism* (CEF) a été sélectionné pour décrire les modèles de solutions solides impliquant des sous-réseaux. Des techniques d'interpolation ont été sélectionnées pour évaluer les systèmes ternaires en se basant sur l'optimisation des systèmes binaires. Des paramètres ternaires ont aussi être ajoutés pour assurer la reproduction des données expérimentales ternaires. Le chapitre 3 a présenté l'évaluation thermodynamique et l'optimisation des systèmes As-Cd, As-Zn et As-Cd-Zn. Les optimisations des systèmes binaires As-Cd et As-Zn et des systèmes quasi-binaires $ZnAs_2$-$CdAs_2$ et Cd_3As_2-Zn_3As_2 sont en très bon accord avec les données expérimentales existantes dans la littérature. Cependant les liquidus calculés pour $ZnAs_2$-Cd_3As_2 et $CdAs_2$-Zn_3As_2 sont moins satisfaisants comparé aux données expérimentales. Cela est très probablement dû à polymérisation de l'arsenic liquide et à sa multivalence, ce qui n'est pas pris en compte par le modèle utilisé dans ce travail. Le chapitre 4 a présenté l'évaluation thermodynamique et l'optimisation des systèmes Ag-As, Ag-S, As-S et Ag-As-S. L'optimisation

du système binaire As-S a présenté un très grand défi en raison du manque de données thermodynamiques. De plus, des termes de logarithme naturel ont été employés pour décrire l'énergie de Gibbs en excès de la phase liquide afin de reproduire les données du diagramme de phase sans avoir la formation de lacune de miscibilité inversée à hautes températures. Cela constitue une autre indication de la polymérisation à la phase liquide non considérée dans le modèle utilisé dans le cadre de ce travail. Les optimisations effectuées dans ce chapitre fournissent une très bonne description des données expérimentales fiables. Finalement, le chapitre 5 a présenté l'évaluation thermodynamique et l'optimisation des systèmes As-Co, As-Fe et As-Fe-S. Pour l'optimisation des systèmes binaires As-Co et As-Fe, il y a des incertitudes importantes en raison du manque de données expérimentales dans les régions riches en arsenic. Toutes les données expérimentales fiables des systèmes étudiés dans ce chapitre sont bien reproduites.

La base de données associée au logiciel FactSage^{TM} développée constitue une contribution importante pour comprendre les phénomènes thermodynamiques survenant dans les systèmes étudiés et offrira un outil puissant pour les travaux antérieurs qui simuleront différents procédés pour résoudre le problème d'émission d'arsenic.

CHAPITRE 7 CONCLUSION ET RECOMMANDATIONS

La thermodynamique computationnelle a été utilisées dans ce projet de recherche pour prédire le comportement et les interactions de l'arsenic avec le soufre et certains métaux de transition. L'objectif était de modéliser des systèmes d'intérêts pour l'industrie de smeltage des minerais sulfurés et pour l'industrie électronique et de développer une base de données associée au logiciel FactSage^{TM}. Cette base de données offrira un outil puissant pour simuler différents procédés et contribuera ainsi à résoudre le problème d'émission d'arsenic. Dans le cadre de ce travail, la modélisation des systèmes binaires Ag-As, Ag-S, As-Cd, As-Co et As-Fe, As-S, As-Zn ainsi que des systèmes ternaires Ag-As-S, As-Cd-Zn et As-Fe-S a été effectuée à l'aide de la méthode CALPHAD. Le travail a été présenté sous forme de trois articles distincts. Le premier article présenté dans le chapitre 3 a examiné des systèmes d'arsenic avec le cadmium et le zinc. Le deuxième article présenté dans le chapitre 4 a traité tous les systèmes arsenic-argent-soufre. Finalement, le troisième article présenté dans le chapitre 5 a étudié des systèmes d'arsenic contenant le cobalt et le fer magnétiques. Les systèmes As-Cd, As-Co, Ag-As-S, As-Cd-Zn et As-Fe-S ont été modélisés pour la première fois dans le cadre de ce travail. Une réévaluation des systèmes binaires Ag-As, Ag-S, As-Fe et As-Zn a aussi été réalisée, offrant une amélioration par rapport aux modélisations thermodynamiques antérieurs.

Pour les systèmes étudiés, il y a généralement un manque de mesures expérimentales, surtout dans les régions très riches en arsenic. Cela est due principalement à la sublimation de l'arsenic à pression atmosphérique, à sa haute pression de vapeur et à sa toxicité. Les systèmes ont été optimisés de façon à bien reproduire les propriétés thermodynamiques et les données des diagrammes de phases disponibles à l'intérieur des marges d'incertitudes expérimentales. Dans le cas d'absence de mesures, les propriétés et les diagrammes calculés constituent de bonnes estimations. La modélisation de certaines régions des systèmes étudiés pourrait être toujours être amélioré advenant de nouvelles données, notamment pour les régions dont la complexité à effectuer des mesures expérimentales a limité l'obtention de résultats précis. Le modèle Quasichimique modifié (MQM) par approximation des paires a été utilisé pour prédire les propriétés thermodynamiques et les équilibres de phase liquide. Ce modèle est bien adapté pour introduire des paramètres supplémentaires dans les paires X(As-As) qui peuvent être ajustés avec un impact minimal sur le reste de l'optimisation, contrairement aux paramètres corrélés de *Redlich-Kister*. Le

Compound Energy Formalism (CEF) a été utilisé pour modéliser toute phase non stœchiométrique avec un domaine d'homogénéité mesuré.

Le travail présenté dans ce mémoire constitue une contribution importante pour comprendre les phénomènes thermodynamiques survenant dans les systèmes étudiés. Toutefois, il serait nécessaire de réaliser ultérieurement des modélisations incluant d'autres d'éléments souvent associé à l'arsenic afin de compléter la base de données. Cela permettra de réaliser des calculs et d'effectuer des simulations multiéchelle des procédés dans le but de développer des solutions viables au problème d'émission d'arsenic. Il serait aussi très intéressant de vérifier l'éventualité de développer un modèle thermodynamique amélioré pour la phase liquide afin de tenir compte des phénomènes de polymérisation de l'arsenic. Ainsi, au lieu de traiter l'arsenic comme un monomère, le modèle pourrait considérer aussi ses formes polymérisées, par exemple un mélange de As, As_2 et As_4. Cela permettra d'améliorer la prédiction du liquide, particulièrement le liquide des joints $ZnAs_2$-Cd_3As_2 et $CdAs_2$-Zn_3As_2. De cette façon, le monomère As serait ordonné avec Cd_3As_2 et Zn_3As_2 (équivalent à $3\,Cd^{2+}$, $3\,Zn^{2+}$ et $2\,As^{3-}$) et le dimère As_2 serait ordonné avec $CdAs_2$ et $ZnAs_2$ (équivalent à Cd^{2+}, Zn^{2+}et As_2^{2-}).

RÉFÉRENCES

[1] Gouvernement du Canada, Canadian Mineral Exploration Information Bulletin, 2022.

[2] Gouvernement du Canada, Minerals and the economy, 2022.

[3] Gouvernement du Canada, Canadian Mineral Production Information Bulletin, 2022.

[4] J. Wilkinson, Canada's Critical Minerals Strategy: Discussion Paper. Opportunities from Exploration to Recycling: Powering the Green and Digital Economy for Canada and the World, 2022.

[5] R.C. Selley, L.R.M. Cocks, I.R. Plimer, Encyclopedia of geology, Elsevier Academic2005.

[6] T. Norgate, S. Jahanshahi, Low grade ores–smelt, leach or concentrate?, Minerals Engineering, 23 (2010) 65-73.

[7] T. Tanaka, Distribution of arsenic in the natural environment with emphasis on rocks and soils, Applied Organometallic Chemistry, 2 (1988) 283-295.

[8] B.K. Mandal, K.T. Suzuki, Arsenic round the world: a review, Talanta, 58 (2002) 201-235.

[9] R.W. Boyle, I.R. Jonasson, The geochemistry of arsenic and its use as an indicator element in geochemical prospecting, Journal of Geochemical Exploration, 2 (1973) 251-296.

[10] A. Garcia-Sanchez, E. Alvarez-Ayuso, Arsenic in soils and waters and its relation to geology and mining activities, Journal of Geochemical Exploration, 80 (2003) 69-79.

[11] G.F. Nordberg, B.A. Fowler, M. Nordberg, Handbook on the Toxicology of Metals, Academic press.2014.

[12] D.M. Whitacre, Reviews of environmental contamination and toxicology, Springer, Berlin, 2008.

[13] G.A. Flores, C. Risopatron, J. Pease, Processing of complex materials in the copper industry: challenges and opportunities ahead, Jom, 72 (2020) 3447-3461.

[14] L. Drewniak, A. Sklodowska, Arsenic-transforming microbes and their role in biomining processes, Environmental Science and Pollution Research, 20 (2013) 7728-7739.

[15] N. Madhavan, V. Subramanian, Sulphide mining as a source of arsenic in the environment, Current Science, 78 (2000) 702-709.

[16] A. Keeling, J. Sandlos, Giant Mine: Historical Summary, 2012.

[17] J. Sandlos, A. Keeling, Toxic legacies, slow violence, and environmental injustice at Giant Mine, Northwest Territories, Northern Review, 42 (2016) 7-21.

[18] G. Canada, Que se passe-t-il à la mine Giant? Juillet et août 2022, 2022.

[19] S. Wang, C.N. Mulligan, Occurrence of arsenic contamination in Canada: sources, behavior and distribution, Science of the total Environment, 366 (2006) 701-721.

[20] P. Bradley, Current perspectives in contaminant hydrology and water resources sustainability, InTech, Croatia, 2013.

[21] R. Martin, K. Dowling, D. Pearce, J. Sillitoe, S. Florentine, Health effects associated with inhalation of airborne arsenic arising from mining operations, Geosciences, 4 (2014) 128-175.

[22] H. Garelick, H. Jones, A. Dybowska, E. Valsami-Jones, Arsenic pollution sources. Reviews of Environmental Contamination, 2009.

[23] K. Yakabuski, Glencore's 95-year-old copper smelter in Quebec is a prized asset. It should pay to clean up its act, The Globe and Mail Montreal, Canada, 2022.

[24] M. Valcke, G. Ponce, M.-H. Bourgault, Évaluation du risque cancérigène attribuable aux concentrations d'arsenic et de cadmium dans l'air de la ville de Rouyn-Noranda, Avis scientifique, Santé publique du Québec, Québec, 2022, pp. 37.

[25] T.C. press, Quebec public health wants to cap arsenic emissions in Rouyn-Noranda above limit, CTV News Montreal, 10 août, 2022.

[26] J.K. Saxe, T.S. Bowers, K.R. Reid, Arsenic, Academic Press1964.

[27] J. Graul, A. Glasl, H. Murrmann, High-performance transistors with arsenic-implanted polysil emitters, IEEE Journal of Solid-State Circuits, 11 (1976) 491-495.

[28] E. Grossman, High tech trash: Digital devices, hidden toxics, and human health, Island press2007.

[29] B. Pignataro, Molecules at Work: Selfassembly, Nanomaterials, Molecular Machinery, John Wiley & Sons2012.

[30] H. Yamauchi, A. Takata, Arsenic Contamination Asia, Springer, New York, 2019.

[31] A.V.d. Bossche, W. Vereycken, T.V. Hoogerstraete, W. Dehaen, K. Binnemans, Recovery of gallium, indium, and arsenic from semiconductors using tribromide ionic liquids, ACS Sustainable Chemistry & Engineering, 7 (2019) 14451-14459.

[32] V.A. Bampidis, E. Nistor, D. Nitas, Arsenic, Cadmium, Lead and Mercury as Undesirable Substances in Animal Feeds, Animal Science and Biotechnologies, 46 (2013) 17-22.

[33] T. Uryu, J. Yoshinaga, Y. Yanagisawa, Environmental fate of gallium arsenide semiconductor disposal: a case study of mobile phones, Journal of Industrial Ecology, 7 (2003) 103-112.

[34] R.U. Ayres, Toxic heavy metals: materials cycle optimization, Proceedings of the National Academy of Sciences, 89 (1992) 815-820.

[35] L.J. Ungers, J.H. Jones, A.J. McIntyre, C.R. McHenry, Release of arsenic from semiconductor wafers, American Industrial Hygiene Association Journal, 46 (1985) 416-420.

[36] B. Sundman, H.L. Lukas, S.G. Fries, Computational thermodynamics: the Calphad method Cambridge university press, Cambridge, 2007.

[37] S. Uhland, H. Lechtman, L. Kaufman, Assessment of the As-Cu-Ni system: an example from archaeology, Calphad, 25 (2001) 109-124.

[38] A. Kroupa, Modelling of phase diagrams and thermodynamic properties using Calphad method–Development of thermodynamic databases., Computational Materials Science, 66 (2013) 3-13.

[39] H. Czichos, T. Saito, Springer handbook of materials measurement methods, Springer, Berlin, 2006.

[40] Kaufman, Berntein, Computer Calculations of Phase Diagrams, Academic press, New York, 1970.

[41] N. Saunders, A.P. Miodownik, CALPHAD (calculation of phase diagrams): a comprehensive guide, Elsevier, (1998).

[42] T. Kitashima, Coupling of the phase-field and CALPHAD methods for predicting multicomponent, solid-state phase transformations, Philosophical Magazine, 88 (2008) 1615-1637.

[43] R. Ursula, The Calphad method and its role in material and process development, Tecnologia em metalurgia, materiais e mineracao, 13 (2016) 3-15.

[44] S. Gorsse, O.N. Senkov, About the reliability of CALPHAD predictions in multicomponent systems, Entropy, 20 (2018) 899.

[45] C.W. Bale, P. Chartrand, S.A. Degterov, G. Eriksson, K. Hack, R.B. Mahfoud, J. Melançon, S. Petersen, FactSage thermochemical software and databases, Calphad, 26 (2002) 189-228.

[46] C.W. Bale, E. Bélisle, P. Chartrand, S.A. Decterov, G. Eriksson, K. Hack, L.-H. Jung, Y.-B. Kang, J. Melançon, A.D. Pelton, C. Robelin, S. Petersen, FactSage thermochemical software and databases—recent developments, Calphad, 33 (2009) 295-311.

[47] C.W. Bale, E. Bélisle, P. Chartrand, S.A. Decterov, G. Eriksson, A. Gheribi, K. Hack, I.-H. Jung, Y.-B. Kang, J. Melançon, A.D. Pelton, S. Petersen, C. Robelin, J. Sangster, P. Spencer, M.-A.V. Ende, Reprint of: FactSage thermochemical software and databases, 2010–2016, Calphad, 55 (2016) 1-19.

[48] G. Eriksson, SOLGASMIX, a computer program for calculation of equilibrium compositions in multiphase systems, Chem. Scripta, 8 (1975) 100-103.

[49] G. Eriksson, K. Hack, Calculation of phase equilibria in multicomponent alloy systems using a specially adapted version of the program 'SOLGASMIX', Calphad, 8 (1984) 15-24.

[50] I.H. Jung, M.A.V. Ende, Computational thermodynamic calculations: FactSage from CALPHAD thermodynamic database to virtual process simulation, Metallurgical and Materials Transactions B, 51 (2020) 1851-1874.

[51] M.E. Brown, Handbook of thermal analysis and calorimetry, Elsevier2003.

[52] R.F. Berg, Correcting "static" measurements of vapor pressure for time dependence due to diffusion and decomposition., Journal of Chemical & Engineering Data, 60 (2015) 3496-3505.

[53] F.C. Campbell, Phase diagrams: understanding the basics, ASM international2012.

[54] J. Klarbring, A first-principles study of highly anharmonic and dynamically disordered solids, Linköping University Electronic Press2020.

[55] A. Hermann, D. Kurzydłowski, First-principles prediction of structures and properties in crystals, Crystals2019.

[56] D.S. Sholl, J.A. Steckel, Density functional theory: a practical introduction, John Wiley & Sons2022.

[57] W. Kohn, L.J. Sham, Self-consistent equations including exchange and correlation effects, Physical review, 140 (1965) A1133.

[58] Y.Z. Zhan, Y. Du, Y.H. Zhrang, Methods for phase diagram determination, elsevier2011.

[59] The Open Quantum Materials Database.

[60] The materials Project.

[61] K.G.F. Janssens, D. Raabe, E. Kozeschnik, M.A. Miodownik, B. Nestler, Computational materials engineering: an introduction to microstructure evolution, Academic Press2010.

[62] A.D. Pelton, Phase diagrams and thermodynamic modeling of solutions, Academic Press2018.

[63] S.R. Fowler, E.A. Gugggenheim, Statistical thermodynamics., 2nd edition ed., CUP1956.

[64] S. Hashemi, C. Ghotbi, V.A.H.I.D. Taghikhani, B. Behzadi, Application of quasi-chemical models to liquid–liquid equilibrium calculations for ternary systems containing water, propionic acid and organic solvents, Fluid phase equilibria, 226, (2004) 251-259.

[65] A.D. Pelton, S.A. Degterov, G. Eriksson, C. Robelin, Y. Dessureault, The modified quasichemical model I—Binary solutions, Metallurgical and Materials Transactions B, 31 (2000) 651-659.

[66] A.D. Pelton, P. Chartrand, The modified quasi-chemical model: Part II. Multicomponent solutions, Metallurgical and Materials Transactions A, 32 (2001) 1355-1360.

[67] A.D. Pelton, Y.B. Kang, Modeling short-range ordering in solutions, International Journal of Materials Research, 98 (2007) 907-917.

[68] A.D. Pelton, A general “geometric” thermodynamic model for multicomponent solutions, Calphad, 25 (2001) 319-328.

[69] M. Hillert, The Compound Energy Formalism, Journal of Alloys and Compounds, 320 (2001) 161-176.

[70] G. Cacciamani, An introduction to the calphad method and the compound energy formalism (CEF), Tecnologia em Metalurgia, Materiais e Mineração, 13 (2016) 16-24.

[71] T. Abe, B. Sundman, A description of the effect of short range ordering in the compound energy formalism, Calphad, 27 (2003) 403-408.

[72] G. Inden, The role of magnetism in the calculation of phase diagrams, Physica B, 103 (1981) 82-100.

[73] M. Hillert, M. Jarl, A model for alloying in ferromagnetic metals, Calphad, 2 (1978) 227-238.

[74] I. Ansara, N. Dupin, H.L. Lukas, B. Sundman, Thermodynamic assessment of the Al-Ni system, Journal of Alloys and Compounds, 247 (1997) 20-30.

[75] B.J. Alloway, A.P. Jackson, The behaviour of heavy metals in sewage sludge-amended soils, Science of the Total Environment, 100 (1991) 151-176.

[76] T.O. Llewellyn, Cadmium (materials flow), Department of the Interior. Bureau of Mines, United States, 1994.

[77] B. Sundman, J. Ågren, A regular solution model for phases with several components and sublattices, suitable for computer applications, Journal of physics and chemistry of solids, 42 (1981) 297-301.

[78] Y. Dessureault, Modelisation thermodynamique du smeltage du plomb dans un haut fourneau, Génie métallurgique, Polytechnique, Montréal, 1994.

[79] M. Ghasemi, J. Johansson, Thermodynamic assessment of the As–Zn and As–Ga–Zn systems, Journal of Alloys and Compounds, 638 (2015) 95-102.

[80] L.A. Zabdyr, Phase equilibria in ternary Cd-Sb-Zn system, Calphad, 21 (1997) 349-358.

[81] S. Min, W.G. Jung, J. Lee, Thermodynamic reassessment of the Cd− Zn system, Metals and Materials International, 13 (2007) 421-425.

[82] S. Weglowski, K. Lukaszewicz, Phase Transitions of Cd3As2 and Zn3As2, Bull Acad. Pol. Sci., Set. Sci. Chim., 16 (1968) 177-182.

[83] C.W.F.T. Pistorius, Melting and polymorphism of Cd3As2 and Zn3As2 at high pressures, High Temperatures - High Pressures, 7 (1975) 441-449.

[84] M.V. Stackelberg, R. Paulus, Investigation on Phosphides and Arsenides of Zinc and Cadmium, Z. Phys. Chem., B, 28 (1935) 427-460.

[85] G.A. Steigmann, J. Goodyear, The Crystal Structure of Cd3As, Acta Crystallogr. B, 24 (1968) 1062-1067.

[86] L. Cervinka, A. Hrubý, The crystal structure of CdAs2, Acta Crystallogr. B, B26 (1970) 457-458.

[87] M.E. Fleet, The crystal structure of ZnAs2, Acta Crystallographica Section B: Structural Crystallography and Crystal Chemistry, 30 (1974) 122-126.

[88] C.T. Heycock, F.H. Neville, On the Lowering of the Freezing Points of Cadmium, Bismuth, and Lead When Alloyed with Other Metals, J. Chem. Soc., 61 (1892) 899.

[89] P.D. Cesaris, Alloys of cadmium and arsenic, Rend. Soc. Chim. Ital. (Rome), 4 (1912) 196-199.

[90] S.F. Zemczuzny, Cadmium Arsenides, Intern. Z. Metallog, 4 (1913) 228-247.

[91] O.Y. Gukov, Y.A. Ugai, V.R. Pshestanchik, E.G. Gonchrov, N.V. Pakhomova, Phase Diagram of the System Cd-As, Inorg. Mater., USSR, 6 (1970) 1693-1695.

[92] S.F. Marenkin, S.I. Maksimova, B. Khuseinov, V.Y. Shevchenko, Region of Homogeneity of CdAs2, Inorganic Materials USSR, 14 (1970) 295-298.

[93] V.B. Lazarev, N.P. Luzhnaya, S.F. Marenkin, V.Y. Shevchenko, S.F. Chistov, Interaction of Cadmium with Arsenic in the Domaine of Existence of cadmium arsenide, Zh. Neorg. Khim., 17 (1972) 1620-1622.

[94] K.L. Komarek, A. Mikula, E. Hayer., Thermodynamic Properties and Compound Formation in Liquid Cadmium-Arsenic Alloys, Berichte der Bunsengesellschaft für physikalische Chemie, 80 (1976) 765-770.

[95] Z. Pruchnik, On the Existence of Cadmium Tetraarsenide and Its Phase Relation in the Cadmium-Arsenic System, Mater. Sci., 3 (1977) 121-125.

[96] K. Yamaguchi, A. Mikula, K. Komarek, K. Itagaki, Thermodynamic Investigations of the Liquid As-Zn and As-Cd Systems by Drop Calorimetry, Z. Metallkd., 82 (1991) 591-598.

[97] K. Friedrich, A. Leroux, Zink und Arsen, Metallurgie, 3 (1906) 477-479.

[98] W. Heike, Das Erstarrungsbild der Zink-Arsen-Legierungen, Z. anorg. Chem., 118 (1921) 264-268.

[99] V. Lazarev, S.F. Marenkin, S.I. Maksimova, B. Hkuseinov, V.Y. Shevchenko, The region of homogenity of ZnAs2, Izv. Akad. Nauk SSSR, Neorg. Mater., 15 (1979) 586-587.

[100] V.B. Lazarev, V.N. Guskov, J.H. Greenberg, P-T-X phase equilibria in the system Zn-As, Materials Research Bulletin, 16 (1981) 1113-1120.

[101] A. Hrubý, The nature of glass-forming tendency in Cd-As system, Czechoslovak Journal of Physics B, 26 (1976) 593-598.

[102] W. Spring, Formation of Arsenides Using Pressure, Ber. Deut. Chem. Ges., 16 (1883) 324-326.

[103] A. Granger, Sur un arsénure de cadmium, Compt. rend., 138 (1904) 574-575.

[104] W. Trzebiatowski, F. Krolicld, W. Zdanowicz, Dilatometric Studies in the Semiconductor System, Cd3As2-Zn3As2, Bull Acad. Pol. Sci., Ser. Sci. Chim., 16 (1968) 343-346.

[105] A. Pietraszko, K. Lukaszewicz, Thermal Expansion and Phase Transitions of Cd3As2 and Zn3As2, Phys. Status Solidi (a), 18 (1973) 723-730.

[106] G.B. Bokii, G.I. Goncharenko, G.G. Dvoryankina, V.I. Kovalev, V.Y. Shevchenko, Properties of the β-Phase Cadmium Arsenide, Dokl. Akad. Nauk SSSR, 195 (1970) 603-606.

[107] Y.A. Ugai, T.A. Zyubina, Electrical Properties and Prodyction of Semiconducting Single Crystal and Polycristaline CdAs2 and Cd3As4, Izv. Akad. Nauk SSSR, Neorg. Mater., 1 (1965) 860-867.

[108] Y.A. Ugai, T.A. Zyubina, K.B. Aleinikova, Preparation and electrical properties of CdAs2, Izv. Akad. Nauk SSSR, Neorg. Mater., 4 (1968) 17-21.

[109] H. Okamoto, The As-Cd (arsenic-cadmium) system, JPE, 13 (1992) 147-154.

[110] A.E. Vol, I.K. Kagan, Cadmium Arsenic (Cd-As), National Bureau of Standards and National Science Foundation, Washington, DC, (1986) 136-157.

[111] A. Hrubý, L. Štourač, Glassy semiconducting CdAs2, Materials Research Bulletin 6(1971) 247-250.

[112] H.J. Naake, C.S. Belcher, Solid Solutions in the System Zn3As2-Cd3As2, J. Appl. Phys., 35 (1964) 3064-3065.

[113] G.A. Castellion, L.C. Beegle, The Preparation and Properties of CdaAs2-ZnaAs2 Alloys, J. Phys. Chem. Solids, 26 (1965) 766-773.

[114] K. Masumoto, S. Isomura, W. Gotô, The Physical and Electronic Properties of Semiconducting Solid Solutions of the Cd3As2-Zn3As2 System, Journal of the Japan Institute of Metals, 31 (1967) 594-600.

[115] V.M. Glazov, M. Kasymova, Density of Zinc and Cadmium Arsenides in Solid And Liquid States, and Volume Change on Melting, Dokl. Akad. Nauk SSSR, 183 (1968) 141-143.

[116] S.E.R. Hiscocks, The Cd3As2-NiAs Pseudobinary Eutectic, J. Mater. Sci., 4 (1969) 773-778.

[117] G.D. Nipan, V.B. Lazarev, Y.K. Grinberg, P-T-X Diagram of the As-Cd System, Russ. J. Inorg. Chem, 27 (1982) 1008-1010.

[118] A.S. Jordan, Some Thermodynamic Properties of Zn3As2. Cd3As2 , and ZnP2, J. Electrochem. Soc.: Solid State Science, 118 (1971) 1362-1365.

[119] J.B. Clark, C.W.F.T. Pistorius, Stable and Metastable Equilibria Near the Melting Curves of CdAs2 and ZnAs2 to High Pressures, High Temp.-High Press., 5 (1973) 319-326.

[120] S.F. Marenkin, A.Y. Vol'fkovich, S.G. Mikhailov, V.V. Astakhov, Phase Relations in the Zn3As2–ZnAs2–CdAs2–Cd3As2 System, Inorganic materials, 39 (2003) 911-915.

[121] V.P. Sanygin, S.G. Mikhailov, K.K. Palkina, A.V. Steblevskii, A.M. Kvardakov, S.F. Marenkin, Crystal-chemical aspect of formation of CdAs2-ZnAs2 solid solutions, Inorganic materials, 41 (2005) 3-6.

[122] H. Okamoto, The As-Zn (arsenic-zinc) system, Journal of phase equilibria, 13 (1992) 155-161.

[123] A. Descamps, Sur la formation des arséniures métalliques Compt. rend., (1878) 1065-1066.

[124] W. Zdanowicz, F. Krolicki, P. Plenkiewicz, Acta physica polonica. A, 1973.

[125] G.A. Silvey, Zn3As2, A Semiconducting Intermetallic Compound, J. Appl. Phys., 29 (1958) 226-227.

[126] A. Jayaraman, T.R. Anantharaman, J. W. Klement, Melting and Polymorphism of Zn3As2 and Cd3As2 at High Pressures, J. Phys. Chem. Solids, 27 (1966) 1605-1609.

[127] J.H. Greenberg, V.N. Guskov, V.B. Lazarev, Vapour-pressure investigation of thermodynamics of non-stoichiometric crystals. Sublimation of β-Zn3As2, The Journal of Chemical Thermodynamics, 17 (1985) 739-746.

[128] Z. Munir, Thermodynamic Stabilities of the Arsenides of Zinc High Temperature Science 6(1974) 73-79.

[129] O. Kubaschewski, E.L. Evans, C.B. Alcock, Metallurgical Thermochemistry 4th edition ed., Pergamon Press Ltd1967.

[130] E. Scheil, A. Kalkuhl, Measurement of the Electromotive Forces on Liquid Cadmium-Arsenic and Cadmium-Atimony Alloys, Z. Metallkunde, 52 (1961) 557.

[131] Y.M. Ivanov, Y.A. Kaller, Chalcogenides of Zinc, Cadmium and Mercury, Metallurgiya, Moscow, 1973.

[132] A. Mikula, K. Komarek, The Gibbs Free Energy in the Liquid As-Cd-Zn and As-Zn System International Journal of Materials Research, 81 (1990) 209-213.

[133] S.A. Shchukarev, M.P. Morozova, M.M. Bortnikova, Enthalpy of Formation of Cadmium Compounds with Phosphorus, Arsenic, and Antimony Zhurnal Obshchel Khimii, 28 (1958) 3289-3292.

[134] N.N. Sirota, E.M. Sklyarenko, Thermodynamic Properties of Compounds in the Zn-As and Cd-As Systems, Russian Metallurgy (Metally), 6 (1968).

[135] A.F. Demidenko, G.N. Danilenko, V.E. Danilenko, V.B. Lazarev, V Ya Shevchenko, S.F. Marenkin, S.E. Koslov, Heat Capacity and Thermodynamic Propreties of A3IIB2V Compounds, Izvestiya Akademii Nauk SSSR, Neorganicheskie Materialy, 13 (1977) 214-216.

[136] A.N. Nesmeyanov, B.Z. Iofa, A.A. Strelnikov, V.G. Fursov, Measuring the Saturated Vapor Pressure of Hard Alloys by the Method of Radioactive Indicators Zhurnal Fizichesko. Khimii, 30 (1956) 1250-1257.

[137] V.J. Lyons, V.J. Silvestri, Solid-Vapor Equilibria for the Compounds Cd3As2 and CdAs2, J. Phys. Chem., 64 (1960) 266-269.

[138] J.B. Westmore, K.H. Mann, A.W. Tickher, Mass Spectrometric Study of the Nonstoichiometric Vaporization of Cadmium Arsenide, J. AppL Chem., 68 (1964) 606-612.

[139] E.S. Kalevich, S.P. Marenkin, V.F. Ponomarev, V.Y. Shevchenko, Thermal Dissociation of Cadmium Arsenide (Cd3As2), Izv. Akad. Nauk SSSR, Neorg. Mater., 14 (1978).

[140] G.N. Danilenko, V.E. Danilenko, M.K. Karapet'yants, V.B. Lazarev, S.F. Marenkin, V. Shevchenko, Termodinamicheskie funktsii ZnAs2 i CdAs2, Izvestiya Akademii Nauk SSSR Neorganicheskie Materialy 13 (1977) 1736-1738.

[141] S.F. Marenkin, V.B. Lazarev, V.Y. Shievchenko, K.A. Sokolovsky, The growth of CdAs2 and ZnAs2 single crystals by directed zone melting recrystallization, Journal of Crystal Growth, 50 (1980) 761-763.

[142] G. Natta, L. Passerini, Arsenides of magnesium and zinc, 58 (1928) 541-550.

[143] S.M. Ariya, M.P. Morozova, T. Huan, E. Volf, Enthalpy of Formation of the Arsenides of Lithium, Magnesium and Zinc, Zhurnal Obshchei Khimii, 27 (1957) 293-295.

[144] V.E. Gorbunov, K.S. Gavrichev, G.A. Totrova, V.N. Guskov, J.H. Greenberg, V.B. Lazarev, Low-temperature heat capacity of zinc diarsenide and zinc arsenide (Zn3As2), Zhurnal Fizicheskoi Khimii, 61 (1987) 328-329.

[145] R.C. Schoonmaker, K.J. Lemmerman, Vaporization of Zn3As2, J. Chem. Eng. Data, 17 (1972) 139-143.

[146] J.O. Andersson, T. Helander, L. Höglund, P. Shi, B. Sundman, Thermo-Calc & DICTRA, computational tools for materials science, Calphad, 26 (2002) 273-312.

[147] W. Zdanowicz, W. Trzebiatowski, K. Lukaszewicz, Crystal structure of semiconducting system Cd3As2-Zn3As2, Bulletin de l'académie Polonaise des sciences-Série des sciences chimiques, 12 (1964) 169-177.

[148] L. Żdanowicz, W. Żdanowicz, Semiconducting Properties of Cd3− xZnxAs2-Type Solid Solutions, Physica status solidi (b), 6 (1964) 227-234.

[149] S.F. Marenkin, I.S. Kovaleva, M. Saidullaeva, V.P. Sanygin, System ZnAs2–CdAs2, Izv. Akad. Nauk SSSR, Neorg. Mater., 19 (1983) 837–838.

[150] J.A. Ugai, T.A. Zubina, E.A. Malygin, Continuous solid solutions in the ZnAs2-CdAs2 and the electrical properties of ZnxCd1-xAs2 single crystals Neorg. Mater., 17 (1966) 876-880.

[151] N.N. Sirota, É.M. Smolyarenko, Thermodynamic Properties of Alloys of the ZnAs2-CdAs2 and Zn3As2-Cd3As2 Quasibinary Systems. In Chemical Bonds in Solids, Springer, Boston, MA, 1972.

[152] A.T. Dinsdale, SGTE data for pure elements, Calphad, 15 (1991) 317-425.

[153] D.R. Stull, H. Prophet, JANAF Thermochemical Tables, U.S. Department of Commerce, Washington, DC, 1985.

[154] S.A. Degterov, A.D. Pelton, J.D. L'Ecuyer, Thermodynamic optimization of the selenium-arsenic (Se-As) system, Journal of phase equilibria, 18 (1997) 357-368.

[155] O. Redlich, A.T. Kister, Algebraic representation of thermodynamic properties and the classification of solutions, Industrial & Engineering Chemistry, 40 (1948) 345-348.

[156] M.N. Ali, Q. Gibson, S. Jeon, B.B. Zhou, A. Yazdani, R.J. R J Cava, The crystal and electronic structures of Cd3As2, the three-dimensional electronic analogue of graphene, Inorganic chemistry, 53 (2014) 4062-4067.

[157] D. Koumoulis, R.E. Taylor, J. McCormick, Y.N. Ertas, L. Pan, X. Che, K.L. Wang, L.S. Bouchard, Effects of Cd vacancies and unconventional spin dynamics in the Dirac semimetal Cd3As2, The Journal of chemical physics, 147 (2017).

[158] L.M. Rogers, R.M. Jenkins, A.J. Crocker, Transport and optical properties of the Cd3-xZnxAs2 alloy system, Journal of Physics D: Applied Physics, 4 (1971) 793-809.

[159] H. Lu, X. Zhang, S. Jia, Topological phase transition in single crystals of (Cd1− xZnx)3As2, Scientific reports, 7 (2017) 1-10.

[160] G.F. Volodina, V.S. Zakhvalinskii, V.K. Kravtsov, Crystal structure of α‴-(Zn1− x Cd x) 3As2 (x= 0.26), Crystallography Reports, 58 (2013) 563-567.

[161] S.F. Marenkin, V.A. Morozova, O.G. Koshelev, G. Biskupski, Lattice defects in undoped CdAs2 monocrystals, Physica status solidi (b), 210 (1998) 569-573.

[162] V.A. Morozova, S.F. Marenkin, S.G. Mikhailov, O.G. KosheleV, Structural Defects in Cd1− x Zn x As2 Solid Solutions, Solid Solutions. Inorganic materials, 41 (2005) 1039-1042.

[163] S.F. Marenkin, V.A. Morozova, O.G. Koshelev, Structural defects and band-structure parameters of CdAs2, ZnAs2, Cd1− x Zn x As2, and Zn1− x Cd x As2 single crystals, Inorganic Materials, 46 (2010) 1001-1006.

[164] V.A. Morozova, S.F. Marenkin, O.G. Koshelev, D.V. Chernoguzov, S.G. Mikhailov, A.V. Molchanov, Optical and photoelectric properties of monoclinic Zn1− x Cd x As2 crystals, Inorganic Materials, 43 (2007) 215-220.

[165] R. Schoonmaker, K. Lemmerman, Vaporization of Zn3As2, Journal of Chemical and Engineering Data, 17 (1972) 139-143.

[166] A. Kubaschewski, C.B. Alcock, Tables of metallurgical thermochemistry, Elsevier Science & Technology Books1979.

[167] Thermal Constants of Materials (in Russian), Institute of High Temperature, Moscow, 1972.

[168] Z.A. Munir, G.B. Street, N.F. Winters, Mass-Spectrometric and Vapor Pressure Studies on the Sublimation of Realgar (AS4S4), The Journal of Chemical Physics 55 (1971) 4520-4527.

[169] D.D. Wagman, W.H. Evans, V.B. Parker, R.H. Schumm, L. Halow, S.M. Bailey, L. Kenneth, R. Nuttal, Selected Values for Inorganic and C1 and C2 Organic Substances in SI Units, J. Phys. Chem. Ref. Data, 11 (1982) 37-38.

[170] I. Barin, Thermochemical Data of pure Substances 3rd edition ed., VCH Verlag GmbH, Weinheim, Germany, 1995.

[171] V.J. Lyons, The dissociation pressure of ZnAs2, J. Phys. Chem., 63 (1959) 1142–1144.

[172] H. Hosono, K. Tanabe, E. Takayama-Muromachi, H. Kageyama, S. Yamanaka, H. Kumakura, M. Nahara, H. Hiramatsu, S. Fujitsu, Science and Technology of Advanced Materials, 2015.

[173] R. Pöttgen, D. Johrendt, Intermetallics. Synthesis, Structure, Function. Second edition. , De Gruyter2019.

[174] N. Katayama, K. Kudo, S. Onari, T. Mizukami, K. Sugawara, Y. Sugiyama, Y. Kitahama, K. Iba, K. Fujimura, N. Nishimoto, M. Nohara, H. Sawa, Superconductivity in Ca1-x La x FeAs2: a novel 112-type iron pnictide with arsenic zigzag bonds, Journal of the Physical Society of Japan, 82 (2013).

[175] W. Freyland, Physics of Non-Tetrahedrally Bonded Elements and Binary Compounds I/Physik Der Nicht-tetraedrisch Gebundenen Elemente und Binären Verbindungen I, Springer Science & Business Media1983.

[176] N.I. Kopylov, Y.D. Kaminsky, G.A. Tolstikov, Arsenic (in Russian), Siberia, 2004.

[177] N.A. Gokcen, The As (Arsenic) system, Bulletin of Alloy Phase Diagrams, 10 (1989) 11-22.

[178] C.C. Herrick, R.C. Feber, Vaporization studies on arsenic, The Journal of Physical Chemistry, 72 (1968) 1102-1110.

[179] S. Northey, S. Mohr, G.M. Mudd, Z. Weng, D. Giurco, Modelling future copper ore grade decline based on a detailed assessment of copper resources and mining, Resources, Conservation and Recycling, 83 (2014) 190-201.

[180] A. Elshkaki, T.E. Graedel, L. Ciacci, B.K. Reck, Copper demand, supply, and associated energy use to 2050, Global environmental change, 39 (2016) 305-315.

[181] C.C. Patterson, Native copper, silver, and gold accessible to early metallurgists, American Antiquity, 36 (1971) 286-321.

[182] J.M. Mazurków, A. Kusior, A. Mikuła, M. Radecka, Transition metal sulfides for electrochemical applications: Controlled chemical conversion of CuS to Ag2S, Applied Surface Science, 606 (2022) 154984.

[183] S.C. Sharath, D. Gayathri, S.R. Mannopantar, M.N. Kalasad, Growth and characterization of Ag2S semiconductor nanoparticles, Materials Today: Proceedings, 67 (2022) 276-279.

[184] C. Shi, Y. Du, H. Biao, B. Yang, Y. Pan, F. Guo, S. Liu, Q. Du, Thermodynamic descriptions of the Ag-X (X= S, As, Lu) systems, Calphad,, 62 (2018) 207-214.

[185] V. Prostakova, D. Shishin, E. Jak, Thermodynamic Optimization of the As–S System, Calphad, 72 (2021).

[186] A. Descamps, De la formation des arséniures métalliques, Compt. rend., 86 (1878) 1022-1023.

[187] K. Friedrich, A. Leroux, Silber und Arsen, Metallurgie, 3 (1906) 192-195.

[188] M. Hansen, K. Anderko, Constitution of Binary Alloys, McGraw-Hill New York, 1958.

[189] V.W. Heike, A. Leroux, Das Erstarrungsbild der Silber-Arsen-Legierungen, Z. Anorg. Chem., 92 (1915) 119-126.

[190] S.J. Broderick, W.F. Ehret, An X-Ray Study of the Alloys of Silver with Bismuth, Antimony and Arsenic. Part II, Phys. Chem., 35 (1931) 3322-3329.

[191] E.A. Owen, V.W. Rowlands, Solubility of Certain Elements in Copper and in Silver, J. Inst. Metals, 66 (1940) 361-378.

[192] E.A. Owen, D.P. Morris, The Application of X-Ray Methods to the Determination of Phase Boundaries in Metallurgical Equilibrium Diagram, J. Inst. Metals, 76 (1949) 145-168.

[193] G.A. Eade, W. Hume-Rothery, The Constitution of Silver-Rich Silver-Arsenic Alloys, Z. Metallkd., 50 (1959) 123-126.

[194] H.W. King, T.B. Massalski, Lattice spacing relationships and the electronic structure of H.C.P. ζ phases based on silver, Philosophical Magazine, 6 (1961) 669-682.

[195] H.T. Hall, The systems Ag-Sb-S, Ag-As-S, and Ag-Bi-S: Phase relations and mineralogical significance, Brown University, 1966, pp. 185.

[196] D. Ludecke, C. Ludecke, T. Hehenkamp, Thermodynamic Activity from Quasi-isopiestic Measurements in α-Ag-As and α-Cu-As, Acta Metall., 31 (1983) 95-100.

[197] C. Jeannot, P. Perrot, G. Tridot, Sur les équilibres argent-soufre, c. R. Acad. Sc. Paris. Ser. C, 268 (1969) 2177-2180.

[198] F.C. Kracek, Phase relations in the system sulfur—Silver and the transitions in silver sulfide, Transactions American Geophysical Union, 27 (1946) 364-374.

[199] V.K. Friedrich, A. Leroux, Silber und Schwefelsilber, Metallurgie, 3 (1906) 361-367.

[200] N. Barbouth, J. Oudar, Étude de la solubilité du soufre dans l'argent Comptes rendus hebdomadaires des séances de l'Académie des sciences. Série C, Sciences chimiques, 264 (1967) 2120-2122.

[201] E. Raub, E. Roshel, Die Loslichkeit von Schwefel, Selen und Tellur in Festem Silber (in German), Metall. , 25 (1971) 7-10.

[202] K. Fueki, K. Ota, K. Kishio, Solubility and Diffusion Coefficient of Sulfur in Silver, Bulletin of the Chemical Society of Japan, 51 (1978) 3067-3068.

[203] C.C. Bissett, The Systen Silver-Silver Sulfide, J. Chem. Soc., 105 (1914) 1223-1228.

[204] F.M. Jaeger, H.S.V. Klooster, Studien über natürliche und künstliche Sulfoantimonite und Sulfoarsenite, Zeitschrift für anorganische Chemie, 78 (1912) 245-268.

[205] T. Rosenqvist, A thermodynamic investigation of the system silver-silver sulphide, JOM, 1 (1949) 451-460.

[206] N. Fukatsu, Z. Kozuka, Measurement of the Thermodynamic Quantities for the Ag-S System by the EMF Method (in Japanese), J. Jpn. Inst. Met., 45 (1981) 1263-1270.

[207] C. Wagner, Investigations on silver sulfide, The Journal of chemical physics, 21 (1953) 1819-1827.

[208] H. Rau, Defect equilibria in silver sulphide, Journal of Physics and Chemistry of Solids, 35 (1974) 1553-1559.

[209] G. Bonnecaze, A. Lichanot, S. Gromb, Proprietes electroniques et electrogalvaniques du sulfure d'argent α domaine d'existence, Journal of Physics and Chemistry of Solids, 39 (1978) 813-821.

[210] G. Bonnecaze, A. Lichanot, S. Gromb, Proprietes electrogalvaniques et electroniques du sulfure d'argent β: Domaine d'existence, Journal of Physics and Chemistry of Solids, 39 (1978) 299-310.

[211] A.V. Ditman, I.N. Kulikova, Investigation of the Dissociation of Solid and Fused Silver Sulphide by the Dew Point Method Zhurnal Fizixheskoi Khimii, 53 (1979) 260-261.

[212] K. Mitteilung, State Diagram of Ag-S in the Region of the Compound Ag 2±δS (in German), Z. Phys. Chem. Neue Folge (Wiesbaden), 119 (1980) 251-255.

[213] R.C. Sharma, Y.A. Chang, The Ag-S (Silver-Sulfur) system, Bulletin of Alloy Phase Diagrams, 7 (1986) 263-269.

[214] A.J. Frueh, The crystallography of silver sulfide, Ag2S, Zeitschrift für Kristallographie-Crystalline Materials, 110 (1958) 136-144.

[215] L.A. Taylor, The significance of twinning in Ag2S, American Mineralogist: Journal of Earth and Planetary Materials, 54 (1969) 961-963.

[216] B.J. Skinner, The system Cu-Ag-S, Economic Geology, 61 (1966) 1-26.

[217] M. Bellati, S. Lussana, Sui Calori Specifici E Di Transformazione Dei Solfuri E Seleniuri Di Argento E Di Rame (in Italian), Atti. Classe di scienze fisiche, matematiche e naturali, 6 (1889) 1051-1059.

[218] W. Truthe, Über das Verhalten der Sulfide von Ph, Cu., Ag und des Cu2 in den Schmelzen der zugehörigen Chloride, Zeitschrift für anorganische Chemie, 76 (1912) 161-173.

[219] R.C. Emmons, C.H. Stockwell, R.H.B. Jones, Argentite and Acanthite, American Mineralogist, 11 (1926) 326-328.

[220] R. Roy, A.J. Majumdar, C.W.H. Hulbe, The Ag2S and Ag2Se transitions as geologic thermometers, Economic Geology, 54 (1959) 1278-1280.

[221] C.M. Perrott, N.H. Fletcher, Heat capacity of silver sulfide, The Journal of Chemical Physics, 50 (1969) 2344-2350.

[222] K.P. Mamedov, M.F. Gadzhiev, Z.J. Suleimanov, Z.D. Nurieva, X-ray and thermographic study of phase transition α→ β in Ag2S, Russ J Inorg Mater., 16 (1980) 241-243.

[223] W.T. Thompson, S.N. Flengas, Drop calorimetric measurements on some chlorides, sulfides, and binary melts, Canadian Journal of Chemistry, 49 (1971) 1550-1563.

[224] F. Grønvold, E.F. Westrum, Silver (I) sulfide: Ag2S Heat capacity from 5 to 1000 K, thermodynamic properties, and transitions, The Journal of Chemical Thermodynamics, 18 (1986) 381-401.

[225] J. Jang, K. Cho, S H Lee, S. Kim, Synthesis and electrical characteristics of Ag2S nanocrystals, Materials Letters, 62 (2008) 1438-1440.

[226] D. Živković, V. Ćosović, Ž. Živković, N. Štrbac, M. Sokić, N. Talijan, B. Boyanov, A. Mitovski, Kinetic investigation of silver sulfide phase transformations, Materials science in semiconductor processing, 16 (2013) 217-220.

[227] S.I. Sadovnikov, A.I. Gusev, A.A. Rempel, An in situ high-temperature scanning electron microscopy study of acanthite–argentite phase transformation in nanocrystalline silver sulfide powder, Physical Chemistry Chemical Physics, 17 (2015) 20495-20501.

[228] A.I. Gusev, S.I. Sadovnikov, Effect of small size of particles on thermal expansion and heat capacity of Ag2S silver sulfide, Thermochimica Acta, 660 (2018) 1-10.

[229] A.A. Valeeva, S.I. Sadovnikov, A.I. Gusev, Polymorphic Phase Transformations in Nanocrystalline Ag2S Silver Sulfide in a Wide Temperature Interval and Influence of Nanostructured Ag2S on the Interface Formation in Ag2S/ZnS Heteronanostructure, Nanomaterials, 12 (2022) 1668.

[230] H. Okazaki, A. Takano, The Specific Heat of Ag2S in α-phase, Zeitschrift für Naturforschung A, 40 (1985) 986-988.

[231] H. Pélabon, Sur le sulfure, le séléniure et le tellure d'argent, Comptes rendus, 143 (1906) 294-296.

[232] K.K. Kelley, Heats of fusion of inorganic substances, US Government Printing Office1936.

[233] J. Koh, K. Itagaki, Measurements of Thermodynamic Quantities for Molten Ag2S–Sb2S3 and Cu2S–Ni3S2 Systems by Quantitative Thermodynamic Analysis, Transactions of the Japan institute of metals, 25 (1984) 367-373.

[234] P.V. Gultyaev, A.V.P. Petrov, The specific heats of a number of semiconductors Soviet Physics, solid state, 1 (1959) 330-.

[235] P.N. Walsh, A. E W, D. White, The Heat Capacity of the Silver Chalcogenides, Ag1. 99S, Ag1. 99Se, and Ag1. 88Te from 16 to 300° K, The Journal of Physical Chemistry, 66 (1962) 1546-1549.

[236] W. Jost, P. Kubaschewski, Spezifische Wärmen von Silber-und Kupfer (I)-Chalkogeniden von− 70° C bis zu 550° C, Zeitschrift für Physikalische Chemie, 60 (1968) 69-78.

[237] S.L. Sadovnikov, A.I. Gusev, Thermal expansion and the heat capacity of nanocrystalline and coarse-crystalline silver sulfide Ag2S, Physics of the Solid State, 59 (2017) 1887-1894.

[238] F.G. Keyes, W.A. Felsing, The Equilibrium Conditions of the Reaction Between Silver Sulfide and Hydrogen, Journal of the American Chemical Society, 42 (1920) 246-251.

[239] K. Jellinek, J. Zakowski, Ueber die Affinitat der Metalle zum Schwefe, Zeitschrift fur Anorganische und allgemeine Chemie, 142 (1925) 1-53.

[240] H. Reinhold, Über die Bestimmung der Bildungsaffinität des Silbersulfids (-Selenids-Tellurids) durch elektrometrische Messungen an festen Ketten (in German), Zeitschrift für Elektrochemie und angewandte physikalische Chemie, 40 (1934) 361-364.

[241] H.A. Zeumer, W.A. Roth, Die Bildungswarme einiger sulfide (in German), Z. physik. chem (A), 173 (1935) 365.

[242] J.R. Goates, A.G. Cole, E.L. Gray, N.D. Faux, Thermodynamic Properties of Silver Sulfide, Journal of the American Chemical Society, 73 (1951) 707-708.

[243] E. Kordes, B. Rackow, Bestimmung der Schwefeltensionen von Schwermetall-sulfiden durch Beobachtung des Anlaufens von Metallen im H2/H2S-Gasgemisch (in German), Z. Phys. Chem., 200 (1952) 129-157.

[244] K. Kiukkola, C. Wagner, Measurements on galvanic cells involving solid electrolytes, Journal of the Electrochemical Society, 104 (1957) 379.

[245] H. Bielen, Bestimmungen von Dissoziationsdampfdrucken fester Verbindungen nach der Anlaufmethode. IV. Schwefeltensionen einiger Schwermetallsulfide (in German), Zeitschrift für anorganische und allgemeine Chemie, 338 (1965) 185-194.

[246] L.T. Bryndzia, O.J. Kleppa, Standard molar enthalpies of formation of sulfosalts in the Ag-As-S system and thermochemistry of the sulfosalts of Ag with As, Sb, and Bi, American Mineralogist, 74 (1989) 243-249.

[247] V.M. Glazov, N.M. Korenchuk, Vapour Pressure and Thermodynamic Properties of Copper and Silver Chalcogenides Russ. J. Phys. Chem., 45 (1971) 1520-1521.

[248] Y.I. Dutchak, I.A. Tishchenko, N.M. Korenchuk, Mass Spectrometric Study Vapor Pressures over Solid and Liquid Silver Halides Izv. Akad. Nauk SSSR, Neorg. Mater., 13 (1977) 1980-1983.

[249] V. Piacente, P. Scardala, D. Ferro, Study on the thermal decomposition of Ag2S, Journal of materials science letters, 9 (1990) 365-367.

[250] P.J. Smith, W.W. Smeltzer, A method for long-term sulfidation of metal at low sulfur pressures and its application to sulfidation of an Fe-20 at.% Al alloy at 1023 K, Oxidation of metals, 28 (1987) 291-308.

[251] A. Yazawa, F. Sehnale'k, K. Koike, Thermodynamic Studies on the Liquid Silver-Sulphur System, Journal of the Mining and Metallurgical Institute of Japan, 81 (1965) 395-398.

[252] W. Jonker, Untersuchungen über das System: Schwefel und Arsen, Z. anorg. Chem., 62 (1909) 89- 107.

[253] L. Clark, The Fe-As-S System: Phase Relations and Applications, Economic Geology 55 (1960) 1345-1381.

[254] P.B. Barton, Themochemical study of the system Fe-As-S, Geochimica et Cosmochimica Acta, 33 (1969) 841-857.

[255] N.V. Timofeeva, G.Z. Feklichev, E.M. Apollonov, V.N. Kalashniko, Arsenic-Sulfur and Arsenice-Selenium Glass Forming Systems at High Pressures and Temperatures Sovremennye Problemy Fizicheskoi Khimii, 6 (1971) 234-259.

[256] R. Ceolin, B. Legendre, P. Khodadad, Sur le système arsenic-soufre: étude, entre 500 et 950 °C, des équilibres de phases dans le secteur limité par l'arsenic et le sulfure As2S, Comptes rendus hebdomadaires des séances de l'Académie des sciences. Série C, Sciences chimiques, 284 (1977) 495-498.

[257] Z. Fedorova, E. Epova, Thermal Study of an Arsenic-Sulfur System, Issled po Eksperim Mineral, Novosibirsk, (1979) 12-18.

[258] R. Blachnik, A. Hoppe, U. Wickel, Die Systeme Arsen-Schwefel und Arsen-Selen und die thermodynamischen Daten ihrer Verbindungen, Zeitschrift für anorganische und allgemeine Chemie, 463 (1980) 78-90.

[259] Z.N. Fedorova, I.V. Osipova, V.V. Gurov, Behaviour of Proustite at the Annealing in the As2S3 Vapours (in Russian), Izv. Akad. Nauk SSSR, Neorg. Mater., 21 (1985) 14-16.

[260] P. Espeau, J. Tamarit, M. Barrio, D. López, M. Perrin, H. Allouchi, R. Céolin, Solid State Studies on Synthetic and Natural Crystalline Arsenic(III) Sulfide, As2S3(Orpiment): New Data for an Old Compound, Chemistry of Materials, 18 (2006) 3821–3826.

[261] P. Debenedetti, S.A. Rice, A.R. Dinner, V.V.J.W.S. R. (2013). Liquid Polymorphism, Liquid Polymorphism. Advances in Chemical Physics, John Wiley & Sons2013.

[262] M. Frumar, A.P. Firth, A.E. Owen, Optically induced crystal-to-amorphous-state transition in As2S3, Journal of non-crystalline solids, 192 (1995) 447-450.

[263] J. Doupovec, I. Thurzo, B. D, V.P. Shilo, Anisotropy of some physical parameters in As-prepared As2S3 bulk glass, Materials Research Bulletin, 12 (1977) 119-125.

[264] J. Málek, Dilatometric study of structural relaxation in arsenic sulfide glass, Thermochimica acta, 311 (1998) 183-198.

[265] F. Zhang, Y. Chen, R. Wang, X. Shen, J. Wang, T. Xu, Study of glass transition kinetics of As2S3 and As2Se3 by ultrafast differential scanning calorimetry, Chinese Physics B, 28 (2019) 047802.

[266] S.A. Dembovskii, Y.A. Polyakov, A.A. Vaipolin, Prepation and Some Properties of Arsenic Trisulfide Single Crystals Izv. Akad. Nauk SSSR, Neorganicheskiye. Mater., 4/5 (1968) 767-768.

[267] M. Myers, E. Felty, Heats of Fusion of the A2V B3VI Compounds As2 S3, As2 Se3, As2 Te3, and Sb2 S3. , Journal of The Electrochemical Society, 117 (1970) 818-820.

[268] B. Voigt, B. Jacob, Zum Kristallisations- und Schmelzverhalten von Auripigment und den strukturanalogen Verbindungen Claudetit und Arsenselenid. Monatshefte Für Chemie, Chemical Monthly, 113 (1982) 895–906.

[269] Z. Černošek, E. Černošková, L. Beneš, Crystalline arsenic trisulfide: preparation, differential scanning calorimetry and Raman scattering measurements, Materials Letters, 38 (1999) 336-340.

[270] E.V. Britzke, A.F. Kapustinskii, L.G. Chentzova, A study of the thermal dissociation of the disulfide and trisulfide of arsenic, Zhurnal Khimicheskoi Promyshlennosti 8(1931) 1-7.

[271] K.C. Mills, Thermodynamic Data for Inorganic Sulphides, Selenides and tellurides, 1974.

[272] V.G. Neverov, G.A. Rybakova, V.R. Panus, , Thermochemical study of compounds in the arsenic-sulfur system, Izv. Akad. Nauk. SSSR - Neorganicheskiye Mater., 25 (1989) 713–716.

[273] G. Johnson, G. Papatheodorou, C. Johnson, The enthalpies of formation and high-temperature thermodynamic functions of As4S4 and As2S3, The Journal of Chemical Thermodynamics, 12 (1980).

[274] P.A.G. O'Hare, Calorimetric measurements of the specific energies of reaction of arsenic and of selenium with fluorine. Standard molar enthalpies of formation ΔfHom at the temperature 298.15 K of AsF5, SeF6, As2Se3, As4S4, and As2S3. Thermodynamic properties of AsF5 and SeF6 in the ideal-gas state. Critical assessment of ΔfHom (AsF3, l), and the dissociation enthalpies of As-F bonds, The Journal of Chemical Thermodynamics, 25 (1993) 391-402.

[275] L. Bryndzia, O. Kleppa, Standard molar enthalpies of formation of realgar (α-AsS) and orpiment (As2S3) by high-temperature direct-synthesis calorimetry, The Journal of Chemical Thermodynamics, 20 (1988) 755–764.

[276] M. Babanly, G. Muradova, T. Il'yasly, D. Babanly, Thermodynamic properties of arsenic sulfides studied by EMF measurements, Inorganic Materials, 47 (2011) 227-230.

[277] D.K. Nordstrom, D.G. Archer, Arsenic Thermodynamic Data and Environmental Geochemistry, Springer Science & Business Media2003.

[278] V.A. Romanovsky, V.V. Tarasov, Low-Temperature Specific Heat and Entropy of Sulfides ofv thr Group V Elements at 298.15 K, Solid State Physics (USSR)

11 (1960) 1294-1299.

[279] M. Hattori, K Nagaya, S. Umebachi, M. Tanaka, Heat capacities of As-S glasses, Journal of Non-Crystalline Solids, 3 (1970) 195-204.

[280] K. Kageyama, M. Imaoka, H. Suga, S. Seki, Fourth Japan Calorimetry Meeting, quoted by Hattori et al., 1970, 1968.

[281] V.V. Tarasov, V.M. Zhdanov, Zhurnal Fizichesko. Khimii, 44 (1970) 2384, quoted in Hattori et al., 1970.

[282] J.S. Haggerty, A.R. Cooper, J.H. Heasley, Heat Capacity of Three Inorganic Glasses and Liquids and Supercooled Liquids, Phy. Chem. Glass, 9 (1968) 47-51, quoted in Hattori et al., 1970.

[283] U.E. Schnaus, C.T. Moynihan, R.W. Gammon, P.B. Macedo, Heat Capacities of glassy and liquid As2S3 and As2Se3, Catholic Univ. of America Washington D C, 1969.

[284] G.D. Mironova, A.V. Zotov, N.I. Gul'ko, Determination of the solubility of orpiment in acid solutions at 25–150° C, Geochemistry InternationaL, 21 (1984) 53-59.

[285] G.W.C. Kaye, T.H. Laby, Tables of Physical and Chemical Constants (in Russian), Fizmatgiz1962.

[286] M.K. Karapet'yants, M.L. Karapet'yants, Fundamental Thermodynamic Constants of Inorganic Matter (in Russian), Khimiya1962.

[287] L.E. Eary, The solubility of amorphous As2S3 from 25 to 90 C, Geochimica et Cosmochimica Acta, 56 (1992) 2267-2280.

[288] C.-S. Lu, J. Donohue, An Electron Diffraction Investigation of Sulfur Nitride, Arsenic Disulfide (Realgar), Arsenic Trisulfide (Orpiment) and Sulfur, Journal of the American Chemical Society, 66 (1944) 818-827.

[289] A. Rogstad, High-Temperature Laser Raman Spectroscopic Study on Mixtures of Arsenic and Sulphur Vapours, Journal of Molecular Structure, 14 (1972) 421-426.

[290] M. Janai, P.S. Rudman, A. Mandelbaum, Mass spectrometric analysis of arsenic trisulfide, Journal of Non-Crystalline Solids, 27 (1978) 67-73.

[291] V.S. Ban, B.E. Knox, Mass-Spectrometric Study of the Laser-Induced Vaporization of Compounds of Arsenic and Antimony with the Elements of Group VIa, The Journal of Chemical Physics, 52 (1970) 248-253.

[292] F.M. Faure, M.J. Mitchell, R.W. Bartlett, Thermodynamics of Vaporization of Sulfides of Antomony and Arsenic, High Temp. Sci., 5 (1973) 128.

[293] R.D. Brittain, K.H. Lau, R.H. Lamoreaux, D.L. Hildenbrand, Studies of the Vaporisation Chemistry of Arsenic in Sulfide Smelting Phase Advances in Sulfide Smelting1983, pp. 197-215.

[294] N. Chakraborti, D.C. Lynch, Thermodynamics of roasting arsenopyrite., Metallurgical Transactions B, 14 (1983) 239-251.

[295] S.A. Pashinkin, A.D. Molodyk, V.I. Belousov, S.S. Strel'chenko, V.A. Fedorov, Composition of Arsenic(III) Sulfide Vapor, Izv. Akad. Nauk SSSR, Neorg. Mater., 10 (1974) 1600.

[296] B. Brunetti, V. Piacente, P. Scardala, Torsion measurement of orpiment vapor pressure, Journal of Chemical & Engineering Data, 52 (2007) 1343-1346.

[297] C. Hsiao, A. Schlechten, Volatility and Stability of Metallic Sulphides, The Journal of The Minerals, Metals & Materials Society 4(1952) 65–69.

[298] R.A. Isakova, V.N. Nesterov, Vapor Pressure of Arsenic and Thallium Sulfides, Trudy Institua Metallurgii i Obogashcheniya, Akademiya Nauk Kazakhskoi SSR, 5 (1962) 29-33.

[299] R.A. Isakova, Vapor Pressure and Dissociation of Metal Sulfides,, Nauka, Almaty1968.

[300] G.P. Ustyugov, A.A. Kudryavtsev, B.M. Kuadzhe, Saturated Vapor Pressure of Arsenic Sulfides, Izv. Akad. Nauk. SSSR - Neorganicheskiye Mater., 4 (1968) 1338–1339.

[301] A.V. Novoselova, A.S. Pashinkin, Vapor Pressure of Volatile Metal Chalcogenides, Nauka, Moscow, 1978.

[302] G.G. Gospodinov, A.S. Pashinkin, Saturated Vapor Pressure of Solid Arsenous Sulfide, Inorg. Mater., USSR, 10 (1974) 1777–1778.

[303] K. Henke, A. Hutchison, Arsenic: environmental chemistry, health threats and waste treatment, John Wiley & Sons.2009.

[304] E.J. Porter, G.M. Sheldrick, Crystal structure of a new crystalline modification of tetra-arsenic tetrasulphide (2, 4, 6, 8-tetrathia-1, 3, 5, 7-tetra-arsatricyclo [3, 3, 0, 0 3, 7]-octane). Journal of the Chemical Society, Dalton Transactions, 13 (1972) 1347-1349.

[305] G.W. Roland, Concerning the alpha-AsS<--> realgar inversion, The Canadian Mineralogist, 11 (1972) 520-525.

[306] L. Bindi, G. Pratesi, M. Muniz-Miranda, M. Zoppi, L. Chelazzi, G.O. Lepore, S. Menchetti, From ancient pigments to modern optoelectronic applications of arsenic sulfides: bonazziite, the natural analogue of β-As4S4 from Khaidarkan deposit, Kyrgyzstan, Mineralogical Magazine, 79 (2015) 121-131.

[307] A.A. Godovikov, Z.N. Fedorova, V.V. Gurov, Study of Volatile Components in Systems Containing Sulfur and Arsenic, Akad. Nauk SSSR, Sib. Otd., Inst. Geol. Geofiz, (1981) 26-32.

[308] G.W. Roland, Phase Relations and Geological Application of the System Ag-As-S. Unpubl., Lehigh University, 1966, pp. 191.

[309] L.G. Berry, R.M. Thompson, X-ray powder data for ore minerals: The Peacok atlas Geological Society of America1962.

[310] G. Street, Z. Munir, The structure and thermal properties of synthetic realgar (As4S4), Journal of Inorganic and Nuclear Chemistry, 32 (1970) 3769–3774.

[311] Y.I. Gerasimov, A.N. Krestovnikov, Chemical Thermodynamics in Non-ferrous Metallurgy, Dep. Sci. Tech. Inf.1934.

[312] T.K. Chattopadhyay, E. Gmelin, H.G.v. Schnering, Heat capacity study of the phase transitions in As4S3 and As4S4, physica status solidi (a), 76 (1983) 543-551.

[313] A.A. Godovikov, Z.N. Fedorova, V.V. Gurov, Study of Volatile Components in Systems Containing Sulfur and Arsenic, Akad. Nauk SSSR, Sib. Otd., Inst. Geol. Geofiz., (1981) 26–32.

[314] A.D. Mah, Thermodynamic Data for Arsenic Sulfide Reactions Albany Research Center, Bureau of Mines, Albany, Oreg. , (1982).

[315] A.V. Steblevskii, A.S. Alikhanyan, V.I. Gorgoraki, A.S. Pashinkin, Vapor formation in the arsenic-selenium system, Zh. Neorg. Khim., 31 (1986) 834–837.

[316] W. Weller, K. Kelley, Low Temperature Heat Capacities and Entropies at 298.15 K of Sulfides of Arsenic, Germanium and Nickel, in: B.o.M. U.S. Department of the Interieur (Ed.), 1964.

[317] A. Emelina, A. Alikhanian, A. Steblevskii, E. Kolosov, Phase Diagram of the As-S System., Inorganic materials, 43 (2007) 95-104.

[318] E. Szarvasy, C. Messinger, Ueber die Molekulargrösse der Arsenamphid-Verbindungen, Chem. Ber., 30 (1897) 1343-1347.

[319] K. Castro, E. Balladares, O. Jerez, M. Pérez-Tello, Á Aracena , 457., Behavior of As/AsxSy in Neutral and Oxidizing Atmospheres at High Temperatures—An Overview, Metals, 12 (2022) 457.

[320] Z.A. Munir, G.B. Street, H.F. Winters, Mass-Spectrometric and Vapor Pressure Studies on the Sublimation of Realgar (As4S4), The Journal of Chemical Physics, 55 (1971) 4520-4527.

[321] B.A. Strathdee, L.M. Pidgeon, Thermal Decomposition and Vpour Pressure Measurements on Arsenopyrite and an Arsenical Ore, The Canadian Mining and Metallurgical Bulletin, 64 (1961) 883-887.

[322] A.S. Pashinkin, A.A. Izergin, R.A. Amirov, A.S. Alikhanyab, A.V. Steblevskii, Saturarted Vapor Pressure and Heat of Formation in Arsenic Sulfide (As4S4), Izvestiya Akademii Nauk SSSR Neorganicheskie Materialy, 18 (1982) 1253-1256.

[323] H.J. Whitfield, Crystal structure of tetraarsenic trisulfide, J. Chem. Soc. A, (1970) 1800–1803.

[324] H.J. Whitfield, Crystal structure of the b-form of tetraarsenic trisulfide, J. Chem. Soc., Dalton Trans. , (1973) 1737–1738.

[325] A. Gavezzotti, F. Demartin, C. Castellano, I. Campostrini, Polymorphism of As4S3 (tris-(μ2-sulfido)-tetra-arsenic): accurate structure refinement on natural α-and β-dimorphites and inferred room temperature thermodynamic properties, Physics and Chemistry of Minerals, 40 (2013) 175-182.

[326] T. Chattopadhyay, C. Carlone, A. Jayaraman, H. Schnering, Effect of temperature and pressure on the raman spectrum of As4S3, Journal of Physics and Chemistry of Solids, 43 (1982) 277-284.

[327] A. Pashinkin, V. Zharov, M. Sotnikova, E. Zhukov, Pressure of Arsenic-Sulfide As4S3 Vapor, Zhurnal Neorganicheskoi Khimii, 32 (1987) 1701-1704.

[328] S.M. Isabaev, A.S. Pashinkin, E.G. Milke, M.I. Zhambekov, Physical and chemical principles of sulfidation of arsenic-containing compounds, Alma-Alta, USSR1986.

[329] C.L. Sullivan, Dissociation Energies of New Group Va Chalcogenide Molecules, Case Western Reserve University Cleveland Ohio, 1971, pp. 144.

[330] M. Elli, E. E Giudici, Hydrothermal Processes VII: Synthesis of Silver-Sulfur-Arsenic Compounds (in Italian), Chim. Ind., 48 (1966) 126-131.

[331] F.H. Wehmeier, R.A. Laudise, J.W. Shiever, The System Ag2S-As2S3 and the Growth of Crystals of Proustite, Smithite and Pyrargyrite, Mat. Res. Bull., 3 (1968) 767-777.

[332] I.S. Kovaleva, L.D. Popova, N.P. Luzhnaya, V.V. Sukhankina, L.I. Antonova, Reactions in the System Ag-As-S in the Region of Crystallization of Ag3AsS3 and AgAsS2, Inorg. Mater. (Engl. Transl.), 7 (1971) 1340-1344.

[333] R. Blachnik, U. Wickel, Phase Relations in the System Ag-As-S and Thermal Behaviour of Ag7MX6 Compounds, Zeitschrift für Naturforschung B, 35 (1980) 1268-1271.

[334] G W Roland, Phase relations below 575 degrees C in the system Ag-As-S, Economic Geology, 65 (1970) 241-252.

[335] G.W. Roland, R.G. Seidensticker, A coprecipitation mechanism to explain Ag7AsS6 inclusions in proustite (Ag3AsS3) crystals, Journal of Crystal Growth, 10 (1971) 213-217.

[336] G. Petzow, G. Effenberg, Ternary alloys. A comprehensive compendium of evaluated constitutional data and phase diagrams, VCH, Weinheim, 1988.

[337] B. Gather, R. Blachnik, Temperature-Composition Diagrams in the Ag2(VIb)-(Vb) Sections of the Ternary Ag-(Vb)-(VIb) Systems, Journal of Less-common Metals, 58 (1978) 7-12.

[338] I.S. Chaus, N.M. Kompanichenko, V.G. Andreichenko, A.G. Grishchuk, The Ag3AsS3-Ag System, Izv. Akad. Nauk SSSR, Neorg. Mater., 17 (1981) 2146-2149.

[339] A.M. Gaudin, D.W. McGlashan, Sulphide silver minerals; a contribution to their pyrosynthesis and to their identification by selective iridescent filming, Economic Geology, 33 (1938) 143-193.

[340] H. Sommerlad, On attempts to prepare sulphantimonites and sulfarsenites of silver, copper and lead by dry means, Zeitschrift für anorganische Chemie, 18 (1898) 420-447.

[341] Z.T. Gasanova, L.F. Mashadieva, V.P. Zlomanov, M.B. Babanly, Thermodynamic study of the Ag2S-As2S3-S system by EMF measurements with Ag4RbI5 as a solid electrolyte, Inorganic Materials, 50 (2014) 6-9.

[342] V.E. Gorbunov, K.S. Gavrichev, V.L. Zalukaev, M.L. Golovei, Heat capacity and thermodynamic properties of proustite, Ag3AsS3, in the 10-350 K range, Zh. Fiz. Khim., 56 (1982) 1121-1124.

[343] V.M. Gurevich, V.E. Gorbunov, K.S. Gavrichev, I.L. Khodakovsky, Low-Temperature Heat-Capacity of Proustite Ag3AsS3 and Smithite AgAsS2, Geokhimiya, 1 (1989) 132-139.

[344] A.A. Godovikov, N.A. Il'yasheva, R.G. Kuryayeva, S.N. Nenasheva, Z.N. Fedorova, Investigation of Dry Sulfide systems (in Russian), Novosibirsk,, 1975.

[345] Z.N. Fedorova, V.V. Gurov, R.G. Kuryaeva, I.V. Sinyakov, Dissociation Pressures of Solid Proustite ans Smithite, Izv. Akad. Nauk SSSR, Neorg. Mater., 13 (1977) 2220-2223.

[346] B. Lange, F. Scholz, H. Bautsch, F. Damaschun, G. Wappler, Thermodynamics of the xanthoconite-proustite and pyrostilpnite-pyrargyrite phase transition as determined by abrasive stripping voltammetry, Physics and Chemistry of Minerals, 19 (1993) 486-491.

[347] J. Wernick, New semiconducting ternary compounds, Journal of Physics and Chemistry of Solids, 3 (1957) 157-159.

[348] J.H. Wernick, S. Geller, K.E. Benson, Synthetic Proustite, Ag3AsS3, Analytical Chemistry, 30 (1958) 303.

[349] M.M. Faktor, R. Hanks, T.H. Lemon, Thermal analysis of proustite, Journal of Inorganic and Nuclear Chemistry, 30 (1968) 2077-2080.

[350] M.I. Golovei, G.N. Shpyrko, M.I. Gurzan, Enthalpy of Melting of Ag3AsS3 and Ag3SbS3, Inorg. Mater. (Engl. Trans.), 10 (1974) 307.

[351] N.A. Il'yasheva, B.G. Nenashev, Heat of Melting of Proustite (Ag3AsS3), Inorg. Mater. (Engl. Trans.), 13 (1977) 888-889.

[352] Z.N. Fedorova, V.V. Gurov, B.G. Nenashev, Determination of the Saturated Vapor Pressure over AgAsS2 Melt, Izv. Akad. Nauk SSSR, Neorg. Mater., 21 (1985) 14-16.

[353] R. Blachnik, B. Gather, Enthalpies of Melting of Some Ternary ABX2-Compounds (A =Cu, Ag, B = As, Sb, Bi, X = S, Se, Te) (in German), Z. Naturforsch. B,, B27 (1972) 1417-1418.

[354] G.V. Belov, G.F. Voronin, A.L. Emelina, Convex Envelope Algorithm for Phase Diagram Calculations and Its Software Implementation, Mat. Model, 18 (2006) 67-78.

[355] F. Liu, Q. Xu, H. Liang, H. Wan, C. Zhong, X. Min, L. Zhang, Stabilization mechanism of arsenic-sulfide slag by density functional theory calculation of arsenic-sulfide clusters, Journal of Hazardous Materials, 410 (2021) 124567.

[356] S. Tsuchihashi, Y. Kawamoto, Properties and structure of glasses in the system As-S, Journal of Non-Crystalline Solids, 5 (1971) 286-305.

[357] I. Barin, O. Knacke, O. Kubaschewski, Thermochemical properties of Inorganic Substances, Springer-Verlag, Berlin, Germany, 1977.

[358] D.D. Wagman, W.H. Evans, I. Halow, V.B. Parker, S.M. Bailey, R.H. Schumm, Selected Values of Chemical Thermodynamic Properties, National Bureau of Standards, U.S. Department of Commerce, Washington, 1968-1971.

[359] R. Sadanaga, S. Sueno, X-ray study on the α-β transition of Ag2S, Mineralogical Journal, 5 (1967) 124-143.

[360] S. Banerjee, S. Bhattacharya, D. Chakravorty, Resistivity hysteresis of Ag2S nanocomposites, The Journal of Physical Chemistry C, 111 (2007) 13410-13413.

[361] A.I. Gusev, S.I. Sadovnikov, Acanthite–argentite transformation in nanocrystalline silver sulfide and the Ag2S/Ag nanoheterostructure, Semiconductors, 50 (2016) 682-687.

[362] P. Waldner, Gibbs Energy Modeling of Digenite and Adjacent Solid-State Phases, Metallurgical and Materials Transactions B, 48 (2017) 2157-2166.

[363] R. Schmid-Fetzer, V. Tomashik, A. Watson, O. Bodak, W. Chong, Non-Ferrous Metal Systems. Part 1, Springer-Verlag Berlin Heidelberg2006.

[364] R.P. Elliott, Constitution of Binary Alloys, First Supplement McGraw-Hill1965.

[365] M.R. Baren, The Ag-As (silver-arsenic) system, Bulletin of Alloy Phase Diagrams, 11 (1990) 113-116.

[366] K.K. Kelley, G.S. Parks, H.M. Huffman, A New Method for Extrapolating Specific Heat Curves of Organic Compounds below the Temperatures of Liquid Air, The Journal of Physical Chemistry, 33 (1929) 1802-1805

[367] I. Barin, Thermochemical data of pure substances, VCH Publishers, Weinheim, 1989.

[368] A.T. Ward, Raman spectroscopy of sulfur, sulfur-selenium, and sulfur-arsenic mixtures, The Journal of Physical Chemistry, 72 (1968) 4133-4139.

[369] F.C. Lin, S.M. Ho, Chemical Durability of Arsenic-Sulfur-Iodine Glasses, Journal of the American Ceramic Society, 46 (1963) 24-28.

[370] M.J. Stashick, R.A. Marriott, Viscoelastic behavior corresponding to reptative relaxation times across the λ-transition for liquid elemental sulfur, The Journal of Chemical Physics, 152 (2020) 044503.

[371] A.V. Steblevskii, A.S. Alikhanyan, A.S. Pashinkin, V.A. Malyusov, Vapor composition in the arsenic-sulfur system, Zh. Neorg. Khim., 31 (1986) 2451–2456.

[372] Q. Dehaine, L.T. Tijsseling, H.J. Glass, T. Törmänen, A.R. Butcher, Geometallurgy of cobalt ores: A review, Minerals Engineering, 160 (2021) 106656.

[373] P.S. Hooda, Trace elements in soils, Wiley, Chichester, 2010.

[374] S.S. Afolabi, M.O. Zakariyah, M.H. Abedi, W. Shafik, A survey on cobalt metallurgical processes and its application, Journal of the Indian Chemical Society, 98 (2021) 100179.

[375] H. Abdollahi, R. Saneie, S.Z. Shafaei, M. Mirmohammadi, A. Mohammadzadeh, O.H. Tuovinen, Bioleaching of cobalt from magnetite-rich cobaltite-bearing ore, Hydrometallurgy, 204 (2021) 105727.

[376] H.A.E. Sayed, A.M.E. Naggar, B.H. Heakal, N.E. Ahmed, S. Said, A.A. Abdel-Rahman, Deep catalytic desulphurization of heavy gas oil at mild operating conditions using self-functionalized nanoparticles as a novel catalyst, Fuel, 209 (2017) 127-131.

[377] R.D. McKerracher, C.P.d. Leon, R.G.A. Wills, A.A. Shah, F.C. Walsh, A review of the iron–air secondary battery for energy storage, ChemPlusChem, 80 (2015) 323-335.

[378] M.Z. Abzalov, T.S. Brewer, L.I. Polezhaeva, Chemistry and distribution of accessory Ni, Co, Fe arsenic minerals in the Pechenga Ni-Cu deposits, Kola Peninsula, Russia, Mineralogy and Petrology, 61 (1997) 145.

[379] C.L. Corkhill, D.J. Vaughan, Arsenopyrite oxidation–A review., Applied Geochemistry, 24 (2009) 2342-2361.

[380] E.C.D. Santos, M.P. Lourenço, L.G. Pettersson, H.A. Duarte, Stability, structure, and electronic properties of the pyrite/arsenopyrite solid–solid interface–A DFT study, The Journal of Physical Chemistry C, 121 (2017) 8042-8051.

[381] G.M. Mudd, Z. Weng, S.M. Jowitt, I.D. Turnbull, T.E. Graedel, Quantifying the recoverable resources of by-product metals: The case of cobalt, Ore Geology Reviews, 55 (2013) 87-98.

[382] B. Pei, B. Björkman, B. Jansson, B. Sundman, Thermodynamic Assessment of the Fe-As System Using an Ionic Two-sublattice Model for the Liquid Phase, Z. Metallkd, 85 (1994) 171-177.

[383] M. Ohno, K. Yoh, Thermodynamic modeling of the system As–Fe combined with first-principles total energy calculations, Journal of Crystal Growth, 310 (2008) 2751-2759.

[384] Y. Xing, J. Brugger, A Tomkins, Y. Shvarov, Arsenic Evolution as a Tool for Understanding Formation of Pyritic Gold Ores, Geology 47 (2019) 335-338.

[385] P. Waldner, A.D. Pelton, Thermodynamic modeling of the Fe-S system, Journal of phase equilibria and diffusion, 26 (2005) 23-38.

[386] u.r. submitted in Journal of Phase Equilibria and diffusion.

[387] V.K. Friedrich, Equilibrium Diagram of the Cobalt-Arsenic Alloys, Metallurgie, 5 (1908) 150-157.

[388] U. Haschimoto, Relation Between the Allotropic Transformation of Cobalt and Some Additional Elements, J. Jpn. Inst. Met., 1 (1937) 177-190.

[389] W. Koster, W. Mulfinger, Die Systeme des Kobalts mit Bor, Arsen, Zirkon, Niob und Tantal, Z. Metallkunde, 38 (1938) 348-350.

[390] M.J. Kochner, Solid Solutions in the Cobalt-Arsenic System, Doklady Akad. Nauk S .S.S.R., 73 (1950) 1197-1199.

[391] M. Hino, T. Azakami, Arsenic Activity in the Molten Co-As System- Thermodynamic Study of Molten Arsenic Aloys (4th report), Resources and materials, 109 (1993) 785-790.

[392] R.D. Heyding, L.D. Calvert, Arsenides of Transition Metals: The Arsenides of Iron and Cobalt, Can. J. Chem., 55 (1957) 449-457.

[393] M. Ellner, E. Lukacevic, M. El-Borage, The Structure and Stability of Co5As2, J. Less-Common Met., 118 (1986) 327-333.

[394] A.K. Espeleta, K. Yamaguchi, K. Itagaki, Calorimetric Study of Some Arsenides and Antimonides (MxAsy and MxSby (M=Cu, Fe, Co, Ni)), Shigen-to-Soza, 107 (1991) 658-663.

[395] A. Nylund, A. Roger, J.P. Senateur, R. Fruchart, Structural transitions between phosphides, arsenides and arsenophoshides of the composition M 2 P, M 2 As and M 2 (P 1—x As x), Monatshefte für Chemie/Chemical Monthly, 102 (1971) 1631-1642.

[396] A. Kjekshus, K.E. Skaug, On the Phases Cr2As, Fe2As, Co2As and Rh2As, Acta Chem. Scand., 26 (1972) 2554-2556.

[397] K. Selte, A. Kjekshus, On Phase Transitions Between the MnP and NiAs Type Structures, Acta Chem. Scand., 27 (1973) 3195-3206.

[398] C. Griffin, A text-book of inorganic chemistry, 1917.

[399] J.C. Quesnel, R.D. Heyding, Transition Metal Arsenides: V. A Note on the Rhodium/Arsenic System and the Monoclinic Diarsenides of the Cobalt Family Canadian Journal of Chemistry, 40 (1962) 814-818.

[400] R. Darmon, M. Wintenberger, Structure cristalline de CoAs2, Bulletin de Minéralogie, 89 (1966) 213-215.

[401] A. Kjekshus, T. Rakke, High Temperature Studies of Marcasite and Arsenopyrite Type Compounds, Acta Chem. Stand. A,, 31 (1977) 517-529.

[402] T. Siegrist, F. Hulliger, High-temperature behavior of CoAs2 and CoSb2, Journal of Solid State Chemistry, 63 (1986) 23-30.

[403] N. Mandel, J. Donohue, The refinement of the crystal structure of skutterudite, CoAs3, Acta Crystallographica Section B: Structural Crystallography and Crystal Chemistry, 27 (1971) 2288-2289.

[404] S.E. Vaisburd, T.F. Remen, Activities of Components in Arsenide Melts of Irin, Cobalt and Nickel, Russian Journal of Physical Chemistry 42 (1968) 389-391.

[405] A.D. Niessen, F.R.D. Boer, R.D. Boom, P.F.D. Chatel, W.C.M. Mattens, A.R. Miedema, Model predictions for the enthalpy of formation of transition metal alloys II, Calphad, 7 (1983) 51-70.

[406] M.W. Hisham, S.W. Benson, Correlations of heats of formation of the different valency states of solid, polyvalent binary metal compounds, The Journal of Physical Chemistry, 89 (1985) 3417-3425.

[407] G.B. Naumov, I.L.v. Khodakovskii, B.N. Ryzhenko, Handbook of Thermodynamic Data, U.S. Geological Survey, Water Resources Division1974.

[408] C.J. Smithells, E.A. Brandes, Smithells metals reference book, Seventh edition ed.1992.

[409] M.I. Kochnev, Thermodynamic properties of cobalt arsenides Doklay Akademii nauk SSSR (Comptes rendus de l'Académie des sciences de l'URSS), 70 (1950) 433-435.

[410] J. Majzlan, S. Kiefer, K. Lilova, T. Subramani, A. Navrotsky, M. Tuhý, A. Vymazolova, D.A. Chareev, E. Dachs, A. Benisek, Calorimetric study of skutterudite (CoAs2. 92) and heazlewoodite (Ni3S2), American Mineralogist, 107 (2022) 22191-22225.

[411] W. Friedrich, W. Borchers, Eisen und Arsen, Metallurgie, 4 (1907) 129-137.

[412] H. Sawamura, T. Sakari, T. Inoue, M. Uematsu, Fe-As System in the Range of High Arsenic, Tetsu-to-Hagané, 39 (1953) 776-777.

[413] P. Oberhoffer, A. Gallaschik, Contribution to the Knowledge of Iron-Arsenic Alloys, Stahl Eisen, 43 (1923) 398-400.

[414] W.D. Jones, The influence of Diffusing Elements Upon the Alpha-Gamma Inversion of Iron, J. Iron Steel Inst., 130 (1934) 429-437.

[415] V.N. Svechnikov, V.N. Gridnev, Allotropic Transformation in Iron-Arsenic and Iron Antimony Alloys (in Russian), Metallurg, 13 (1938) 13-19.

[416] H. Sawamura, T. Mori, An Investigation of Equilibrium Diagram of Fe-As-C System, Department of metallurgy Kyoto University Japan, 1952, pp. 129-144.

[417] H. Sawamura, T. Mori, A supplement to Investigation of Equilibrium Diagram of Fe-As-C, Kyoto University Japan, 1954, pp. 182-189.

[418] V.N. Svchnikov, A.K. Shurin, A More Precise Determination of the Equilibrium Diagram of A Fe-As System, Ukrainian SSR, 1 (1957) 27-29.

[419] V.N. Svechnikov, V.M. Pan, A.K. Shurin, The effect of phosphorous and arsenic on the parameter of the crystal lattice and hardness of iron (in Russian), Fizika metallov i metallovedenie, 6 (1958) 662-664.

[420] B. Predel, M. Frebel, The precipitation behavior of α-mixed crystals of iron with arsenic and antimony (in German), Archiv für das Eisenhüttenwesen, 42 (1971) 365-373.

[421] B. Bozic, Equilibrium phase diagram for the iron-arsenic system (in Serbian), Srpska Akademija Nauka i Umetnosti, Odeljenje Tehnickih Nauka, 14 (1979) 1-16.

[422] V.F. Wever, Ueber den Einfluß der Elemente auf den Polymorphismus des Eisens, Archiv für das Eisenhüttenwesen, 2 (1929) 739-748.

[423] B.I. Bozic, R.J. Lucic, Martensitic Transformation in iron-arsenic alloys Journal od Materials Scieince, 12 (1977) 751-756.

[424] G. Hagg, Rontgenographische Studien uber die binaren Systeme von Eisen mit Phosphor, Arsen, Antimon und Wismut Z. Krist., 68 (1928) 470-471.

[425] G. Hagg, X-Ray Studies on the System Iron Arsenid, Zeitschr. Kristallographie, 71 (1929) 134-136.

[426] A. Seitkan, G.I. Lampronti, R.N. Widmer, N.P.M. Casati, S.A.T. Redfern, Thermal Behavior of Iron Arsenides Under Non-Oxidizing Conditions, ACS Omega, 5 (2020) 6423-6428.

[427] D. Gonzalez-Alvarez, F. Grønvold, B. Falk, W.J.E. F., B. R., K. G., FeAs: Heat capacity, enthalpy increments, other thermodynamic properties from 5 to 1350 K, and magnetic transition, The Journal of Chemical Thermodynamics, 21 (1989) 363-373.

[428] M.J. Buerger, The Crystal Structure of Lollingite: FeAs2, Zeitschr. Kristallographie, 82 (1932) 504-513.

[429] R.D. Heyding, L.D. Calvert, Arsenides of the Transition Metals III. A Note on the Higher Arsenides of Iron, Cobalt and Nickel Can. J. Chem., (1960) 313-316.

[430] M. Hino, T. Azakami, Activities of Molten Iron-Arsenic and Nickel-Arsenic Binary Alloys, Min. Met. Inst. Japan, 96 (1980) 553-558.

[431] R. Hultgren, P.D. Desai, D.T. Hawkins, M. Gleiser, K.K. Kelley, D.D. Wagman, Selected values of the thermodynamic properties of the elements, American Society of Metals OH, 1973.

[432] J. Botor, A. Zajaczkowski, L. Dziewidek, G.H. Siderov, The Arsenic Activity in the Liquid Z. Metallkde, 82 (1991) 304-309.

[433] Y. Dong, Y. Peng, S. Wei, Y. Zhu, Activity of Arsenic in Fe-As Melt, Iron and Steel(China), 21 (1986) 11-13.

[434] F. Tsukihashi, K. Kuroda, S. Arakawa, N. Sano, Activity coefficient of antimony and arsenic in molten iron and carbon saturated iron, Steel research, 65 (1994) 53-57.

[435] W. Yan, Y. Yang, W. Chen, M. Barati, A. McLean, Thermodynamic assessment of arsenic in iron and nickel alloys, Ironmaking & Steelmaking, 44 (2016) 220-226.

[436] J. Wypartowicz, K. Fitzner, O.J. Kleppa, Standard enthalpy of formation of Cu3As and heats of mixing in the liquid systems Cu-As and Fe-As by direct combination high temperature drop calorimetry, Journal of Alloys and Compounds, 217 (1995) 1-4.

[437] E. Perfetti, G.S. Pokrovski, K. Ballerat-Busserolles, V. Majer, F. Gibert, Densities and heat capacities of aqueous arsenious and arsenic acid solutions to 350 °C and 300 bar, and revised thermodynamic properties of As(OH)3°(aq), AsO(OH)3°(aq) and iron sulfarsenide minerals, Geochimica et Cosmochimica, 72 (2008) 713-731.

[438] T.A. Stolyarova, Enthalpies of formation of iron arsenides, Geokhimia, 7 (1977) 1095–1098.

[439] T.A. Stolyarova, The Enthalpy of Formation of Iron Arsenide (Fe2As), Russian Journal of Physical Chemistry. Translated from Zhurnal Fizichekoi Khimii, 52 (1978) 898.

[440] J. Klingbeil, R. Schmid-Fetzer, Interaction of metals with AlAs and InAs: estimation of ternary Al-As-M and in-As-M phase diagrams, Calphad, 13 (1989) 367-388.

[441] A.S. Pashinkin, V.A. Muratova, N.V. Moiseyev, J.V. Bazhenov, Heat capacity and thermodynamic functions of iron diarsenide in the temperature range 5 K to 300 K, The Journal of Chemical Thermodynamics, 23 (1991) 827-830.

[442] B. Jansson, Trita-Mac-234, Division of Physical Metallurgy, in: R.I.o. Technology (Ed.)Stockholm, Sweden, 1984.

[443] P.E. Blochl, Projector Augmented-wave method, Phys. Rev. B, 50 (1994).

[444] J.P. Perdew, K. Burke, M. Ernzerhof, Generalized gradient approximation made simple, Physical review letters, 77 (1996) 3865.

[445] T. Tanaka, N.A. Gokcen, Excess thermodynamic properties of dilute solutions, Journal of Phase Equilibria, 16 (1995) 10-15.

[446] V. Raghavan, Phase diagrams of ternary iron alloys. Part 2. Ternary systems containing iron and sulphur, ASM International, New Delhi, 1987.

[447] K. Nishihara, T. Izaki, Fundamental Studies on Spices (1st Report) Equilibrium Relations in the Fe2As-FeS System (in Japanese), Journal of the Mining and Metallurgical Society of Japan 78 (1962) 609-611.

[448] L. Clark, Year book. The Fe-As-S system, Carnegie Institution of Washington1958.

[449] H. McKinstry, Mineral assemblages in sulfide ores; the system Cu-Fe-As-S, Economic Geology, 58 (1963) 483-505.

[450] U. Kretschmar, S.D. Scott, Phase Relations Involving Arsenopyrite in the System Fe-As-S and their Application, Canadian mineralogist, 14 (1976) 364-386.

[451] S.R. Hem, E. Makovicky, F. Gervilla, Compositional trends in Fe, Co and Ni sulfarsenides and their crystal-chemical implications: Results from the Arroyo De La Cueva deposits, Ronda peridotite, Southern Spain, The Canadian Mineralogist, 39 (2001) 831-853.

[452] M. Wintenberger, Étude électrique et magnétique de composés sulfurés et arséniés d'éléments de transition. III. Propriétés électriques et magnétiques et liaisons dans l'arsénopyrite, la cobaltite et la loellingite, Bulletin de Minéralogie, 85 (1962) 107-119.

[453] N. Morimoto, L.A. Clark, Arsenopyrite crystal-chemical relations. American Mineralogist, Journal of Earth and Planetary Materials, 46 (1961) 1448-1469.

[454] D.D. Klemm, Synthesen und Analysen in den Dreiecksdiagrammen FeAsS-CoAsS-NiAsS und FeS2-CoS2-NiS2, Neues Jahrbuch für Mineralogie-Abhandlungen, 103 (1965) 205-255.

[455] G. Simon, S.E. Kesler, S. Chryssoulis, Geochemistry and textures of gold-bearing arsenian pyrite, Twin Creeks, Nevada; implications for deposition of gold in carlin-type deposits, Economic Geology, 94 (1999) 405-421.

[456] A.S. Stepanov, R.R. Large, E.S. Kiseeva, L.V. Danyushevsky, K. Goemann, S. Meffre, I. Zhukova, I. Belousov, Phase relations of arsenian pyrite and arsenopyrite, Ore Geology Reviews, 136 (2021) 104285.

[457] M. Reich, S.E. Kesler, S. Utsunomiya, C.S. Palenik, S.L. Chryssoulis, R.C. Ewing, Solubility of gold in arsenian pyrite, Geochimica et Cosmochimica Acta, 69 (2005) 2781-2796.

[458] M.A.A. Schoonen, H.L. Barnes, Reactions forming pyrite and marcasite from solution: I. Nucleation of FeS2 below 100 °C, Geochimica et Cosmochimica Acta, 55 (1991) 1495-1504.

[459] M.A.A. Schoonen, H.L. Barnes, Reactions forming pyrite and marcasite from solution: II. Via FeS precursors below 100 °C, Geochimica et Cosmochimica Acta, 55 (1991) 1505-1514.

[460] M.A.A. Schoonen, H.L. Barnes, Mechanisms of pyrite and marcasite formation from solution: III. Hydrothermal processes, Geochimica et Cosmochimica Acta, 55 (1991) 3491-3504.

[461] M.E. Fleet, A.H. Mumin, Gold-Bearing Arsenian Pyrite and Marcasite and Arsenopyrite from Carlin Trend Gold Deposits and Laboratory Synthesis, American Mineralogist, 82 (1997) 182-193.

[462] S.R. Hem, E. Makovicky, The system Fe–Co–Ni–As–SI Phase Relations in the (Fe, Co, Ni) As0.5 S1.5 Section at 650 and 500 C. , The Canadian Mineralogist, 42 (2004) 43-62.

[463] M. Reich, U. Becker, First-principles calculations of the thermodynamic mixing properties of arsenic incorporation into pyrite and marcasite., Chemical Geology, 225 (2006) 278-290.

[464] N.K. Foley, R.A. Ayuso., Mineral sources and transport pathways for arsenic release in a coastal watershed, USA, Geochemistry: Exploration, Environment, Analysis, 8 (2008) 59-75.

[465] V. Ettler, Z. Johan, Mineralogy of metallic phases in sulphide mattes from primary lead smelting, Comptes Rendus Geoscience, 335 (2003) 1005-1012.

[466] T. Mikuš, M. Chovan, O. Ponomarenko, S. Bondarenko, O. Grinchenko, Hydrothermal Nickel Mineralization from the Black Shales in Čierna Lehota, Mineralogical journal, 35 (2013) 27-32.

[467] M. Hino, Activities of Molten Cu-As, Cu-S-As and Fe-S-As Alloys, J. Min. Metall. Inst. Japan, 101 (1985) 543-548.

[468] A.S. Pahinkin, V.A. Muratova, A.M. Antukov, N.V. Moiseyev, Heat capacity and thermodynamic functiobs of arsenopyrite (in Russian), Neorg. Mater., 23 (1989) 221-224.

[469] P. Toulmin, P. Barton, A thermodynamic study of pyrite and pyrrhotite, Geochimica et Cosmochimica Acta, 28 (1964) 641-671.

[470] S. Fushimi, A.H. Webster, The Growth of Arsenopyrite Single Crystals by the Closed-tube Iodine Vapour Transport Technique, Department of Energy, Mines and Resources, Mines Branch, Ottawa, Canada, 1969.

[471] G.N. Zviadadze, V.G. Rtskhiladze, Thermodynamics of the dissociation of arsenopyrite (in Russian), Soobsch. Acad. Nauk Gruz. SSR, 33 (1964) 175–181.

[472] A.S. Pashinkin, V.A. Fedorov, G.N. Zviadidze, A.S. Malkova, A.P. Izergin, A.A. Izergin, S.A. Generalova, O.I. Dzhaparidze, L.A. Gelovani, Dissociation Pressure of Arsenopyrite and Ivestigation of the Fe-As-S System (in Russian), Zhur. Prikladnoi Khim. , 52 (1979) 1085-1091.

[473] K.I. Chudnenko, Thermodynamic Modeling in Geochemistry: Theory, Algorithms, Software, and Applications (in Russian), Novosibirsk, 2010.

[474] N.V. Vilor, L.A. Kaz'min, L.A. Pavlova, Aresenopyrite-Pyrite Paragenesis in Gold Deposits (Thermodynamic Modeling), Russian Geology and Geophysics, 55 (2014) 824-841.

[475] Y.V. Shvarov, HCh: New potentialities for the thermodynamic simulation of geochemical systems offered by Windows, Geochemistry International, 46 (2008) 834-839.

[476] A.S. Stepanov, Arsenic evolution as a tool for understanding formation of pyritic gold ores, Geology, 47 (2019) e491.

[477] M.E. Fleet, S.L. Chryssoulis, P.J. MacLean, R. Davidson, C.G. Weisener, Arsenian pyrite from gold deposits; Au and As distribution investigated by SIMS and EMP, and color staining and surface oxidation by XPS and LIMS, The Canadian Mineralogist, 31 (1993) 1-17.

[478] A.L. Foster, G.E. Brown, T.N. Tingle, G.A. Parks, Quantitative arsenic speciation in mine tailings using X-ray absorption spectroscopy, American Mineralogist, 83 (1998) 553-568.

[479] V.L. Tauson, Gold solubility in the common gold-bearing minerals; experimental evaluation and application to pyrite, European journal of mineralogy, 11 (1999) 937-947.

[480] G. Simon, H. Huang, J.E. Penner-Hahn, S.E. Kesler, L.S. Kao, Oxidation state of gold and arsenic in gold-bearing arsenian pyrite, American Mineralogist, 84 (1999) 1071-1079.

[481] K.S. Savage, T.N. Tingle, P A O'Day, G.A. Waychunas, D.K. Bird, Arsenic speciation in pyrite and secondary weathering phases, Mother Lode gold district, Tuolumne County, California, Applied Geochemistry, 15 (2000) 1219-1244.

[482] P. Le-Pape, M. Blanchard, J. Brest, J.C. Boulliard, M. Ikogou, L. Stetten, G. Landrot, G. Morin, Arsenic incorporation in pyrite at ambient temperature at both tetrahedral S–I and octahedral FeII sites: Evidence from EXAFS–DFT analysis, Environmental Science & Technology, 51 (2017) 150-158.

[483] F. Voute, S.G. Hagemann, N.J. Evans, C. Villanes, Sulfur isotopes, trace element, and textural analyses of pyrite, arsenopyrite and base metal sulfides associated with gold mineralization in the Pataz-Parcoy district, Peru: Implication for paragenesis, fluid source, and gold deposition mechanisms, Mineralium Deposita, 54 (2019) 1077-1100.

[484] A.P. Deditius, S. Utsunomiya, D. Renock, R.C. Ewing, C.V. Ramana, U. Becker, S.E. Kesler, A Proposed New Type of Arsenian Pyrite: Composition, Nanostructure and Geological Significance, Geochimica et Cosmochimica Acta, 72 (2008) 2919-2933.

[485] C. Kusebauch, M. Oelze, S.A. Gleeson, Partitioning of Arsenic Between Hydrothermal Fluid and Pyrite During Experimental Siderite Replacement, Chemical Geology, 500 (2018) 136-147.

[486] M. Blanchard, M. Alfredsson, J. Brodholt, K. Wright, C.R.A. Catlow, Arsenic Incorporation Into FeS2 Pyrite and Its Influence on Dissolution: a DFT Study, Geochimica et Cosmochimica Acta, 71 (2007) 624-630.

[487] G. Qian, J. Brugger, D. Testemale, W. Skinner, A. Pring, Formation of As (II)-pyrite During Experimental Replacement of Magnetite Under Hydrothermal Conditions, Geochimica et Cosmochimica Acta, 100 (2013) 1-10.

[488] P. Moller, G. Kersten, Electrochemical accumulation of visible gold on pyrite and arsenopyrite surfaces, Mineralium Deposita, 29 (1994) 404-413.

[489] P. Le-Pape, M. Blanchard, A. Juhin, J.-P. Rueff, M. Ducher, G. Morin, D. Cabaret, Local Environment of Arsenic in Sulfide Minerals: Insights from High-Resolution X-ray Spectroscopies, and First-Principles Calculations at the As K-edge, Journal of Analytical Atomic Spectrometry, 33 (2018) 2070-2082.

[490] H.W. Nesbitt, I.J. Muir, A.R. Prarr, Oxidation of arsenopyrite by air and air-saturated, distilled water, and implications for mechanism of oxidation, Geochimica et Cosmochimica Acta, 59 (1995) 1773-1786.

[491] J.A. Tossell, D.J. Vaughan, J.K. Burdett, Pyrite, marcasite, and arsenopyrite type minerals: Crystal chemical and structural principles, Physics and Chemistry of Minerals, 7 (1981) 177-184.

[492] J.M. Hartley, A.Z. Al-Bassam, R.C. Harris, G. Frisch, G.R. Jenkin, A.P. Abbott, Investigating the dissolution of iron sulfide and arsenide minerals in deep eutectic solvents, Hydrometallurgy, 198 (2020) 105511.

[493] B. Hyde, M. Okeeffe, Marcasite and pyrite (FeS2), Australian journal of chemistry, 49 (1996) 867-872.